MECHANICAL CONTROL OF HEART RATE: INVESTIGATING DETERMINANTS OF THE CHRONOTROPIC RESPONSE TO SINOATRIAL NODE STRETCH

by

Eilidh A. MacDonald

Submitted in partial fulfilment of the requirements
for the degree of Doctor of Philosophy

at

Dalhousie University
Halifax, Nova Scotia
November 2020

TABLE OF CONTENTS

LIST OF FIGURES

ABSTRACT

The sinoatrial node (SAN) is heavily regulated by multiple factors, including stretch, enabling adaptation of heart rate to changes in physiological demand. Right atrial distention, caused by an increase in venous return to the heart, increases heart rate. Thus, changes in mechanical load result in beat-by-beat adaptation of SAN function. Chronotropic responses to stretch have been demonstrated in transplanted and isolated hearts, in isolated SAN tissue, and even in single SAN cells, indicating that the stretch response is intrinsic to the SAN itself. However, mechanisms and determinants responsible for the SAN stretch response are incompletely understood.

The zebrafish represents an attractive alternative experimental model for the study of cardiac electrophysiological mechanisms, due to its many physiological similarities with human and the relative ease of its genetic manipulation. Thus, my first objective was to determine the response of the zebrafish isolated SAN to varying degrees of controlled stretch. Consistent with humans and most mammals studied, stretch of the zebrafish SAN results in increased beating rate (BR) in a magnitude-dependent manner. These studies also indicated that baseline force and the direction of stretch may play an important role in determining the magnitude of the chronotropic response. Further, these data demonstrate the viability of zebrafish as a model species for studying SAN stretch responses.

It is thought that the chronotropic response to SAN stretch is due to activation of cation non-selective stretch-activated channels (SAC_{NS}). As the reversal potential of SAC_{NS} is between the maximum diastolic and systolic potential of the SAN action potential (~ -10 mV), we predicted that SAN BR could be modulated through acute SAC_{NS} activation, resulting in an increase *or* decrease in BR depending on the timing of activation within the cardiac cycle. My second objective was to investigate the importance of activation timing and action potential morphology in the chronotropic response to SAN stretch. To test this, I utilised transgenic zebrafish and mice expressing a light-activated ion channel (channelrhodopsin-2), which passes a non-specific cation current with similar characteristics to SAC_{NS}, including reversal potential properties. In both species, and with all light intensities, an increase or a decrease in BR could be elicited, depending on the timing of light application within the SAN cycle. This was confirmed, and further explored, using rabbit and mouse SAN cell computational models. Finally, using a pharmacological intervention to manipulate the action potential duration of mouse SAN, we caused a shift in the change in BR, supporting the importance of the interaction between the SAC_{NS} reversal potential and action potential morphology for the SAN stretch response.

We also hypothesised that the magnitude of the response to SAN stretch is influenced by tissue mechanics. In my final objective I compared how the response of the isolated rabbit and mouse SAN relates to tissue stiffness and whether structural differences may account for observed responses. We measured applied force and tissue stiffness and compared this to chronotropic responsiveness and utilised second-harmonic generation imaging of stretched and unstretched SAN tissue to visualise changes in collagen crimp and alignment. We found differences in the relationship between SAN mechanical properties and the electrophysiological response to stretch between rabbit and mouse, as well as species-differences in SAN structure both at baseline and changes with stretch.

Overall, my thesis provides further insight into the electrophysiological and mechanical determinants of the control of SAN function by stretch, which is critical for a fundamental understanding of mechanically induced changes in cardiac rhythm.

LIST OF ABBREVIATIONS USED

4-AP – 4-aminopyridine

ACh – acetylcholine

AF – atrial fibrillation

ANOVA – analysis of variance

ANS – Autonomic Nervous System

AP – action potential

BR – beating rate

CL – cycle length

CNS – Central Nervous System

Ca^{2+} – calcium

ChR2 – channelrhodopsin-2

Cl^- – chloride

E_{ChR2} – reversal potential of ChR2

$E_{SAC,NS}$ – reversal potential of SAC_{NS}

E_{rev} – reversal potential

E_x – reversal potential of I_x

HCN – hyperpolarisation-activated cyclic nucleotide-gated

IBV – inter-beat variability

I_{CaL} – L-type Ca^{2+} current

$I_{CaL1.2}$ – L-type Ca^{2+} channel isoform $Ca_v1.2$ current

$I_{CaL1.3}$ – L-type Ca^{2+} channel isoform $Ca_v1.3$ current

I_{CaT} – T-type Ca^{2+} channel isoform $Ca_v3.1$ current

I_{ChR2} – channelrhodopsin-2 current

$I_{Cl,swell}$ – cell-volume activated Cl^- current

I_{K1} – inward rectifier K+ current

I_{KACh} – ACh-activated K+ current

I_{Kr} – rapid delayed rectifier K^+ current

I_{Ks} – slow delayed rectifier K^+ current

I_{Na} – fast Na^+ current

$I_{Na1.1}$ – fast Na^+ channel isoform $Na_v1.1$ current

$I_{Na1.5}$ – fast Na^+ channel isoform $Na_v1.5$ current

I_{NaCa} – Na^+/Ca^{2+} exchanger current

I_{NaK} – Na^+-K^+ pump current

$I_{SAC,NS}$ – cation non-selective SAC current

IVC – inferior *Venae cavae*

I_b – background current

$I_{b,Ca}$ – background Ca^{2+} current

$I_{b,NA}$ – background Na^+ current

$I_{b,K}$ – background K^+ current

I_{si} – slow inward current

I_{st} – Sustained inward Na^+ current

I_{sus} – Sustained component of 4-AP-sensitive currents

I_{to} – transient component of 4-AP-sensitive currents

I_{total} – total current

I_x – SAC_{NS}-like current

K^+ – potassium

MDP – maximum diastolic potential

MSP – maximum systolic potential

NCX – Na^+-Ca^{2+} exchanger

NT – normal Tyrode's

Na^+ – sodium

RSA – respiratory sinus arrhythmia

RyR – ryanodine receptor

SAC – stretch activated channels

SAC_{NS} – cation non-selective SAC

SAN – sinoatrial node

SDD – spontaneous diastolic depolarization

SDRR – standard deviation of cycle length

SEM – standard error of the mean

SERCA – sarco/endoplasmic reticulum Ca^{2+}-ATPase

SHGM – second-harmonic generation microscopy

SR – sarcoplasmic reticulum

SVC – superior *Venae cavae*

V_m – membrane potential

bpm – beats per minute

dV/dt – change in V_m as a function of time

g_x – conductance of I_x

ACKNOWLEDGEMENTS

I would like to begin by acknowledging that Dalhousie University, where we learn, work, and live, is in Mi'kma'ki – the traditional, unceded, and unsurrendered territory of the Mi'kmaq people. I believe it is incredibly important to acknowledge the harmful and ongoing impacts of colonisation and the attempted assimilation of Indigenous people. This has destructive impacts on the education, cultures, languages, health, child welfare, and prosperity of Indigenous people, and has resulted in genocide. Considering the ways in which we, as settlers, benefit from these oppressive systems and contribute to them, as well as taking constructive actions to work at deconstructing them are an essential steps towards reconciliation and must be done both in our individual lives and in the context of education, academia, and health. I would like to take this opportunity to commit myself to continually learning, listening, and actively working against these systems of oppression in all contexts of my life.

I am very grateful for the guidance and support I have received (and continue to receive) from many people throughout my studies. First and foremost, I would like to thank my supervisor, Alex Quinn, for taking a chance on me, and then for sharing his enthusiasm for science. I have always felt incredibly supported while simultaneously feeling encouraged to explore my own ideas and interests. He has provided me with many opportunities, and I could not have asked for a better supervisor and mentor. I have learned a wide variety of things from Alex – perhaps most importantly he taught me that even if I have no idea how to do something it does not mean that I can't do it… it just means that I don't know how *yet*. This approach has given me the confidence to have a go at things, no matter how inadequate I feel, which has been a wonderful gift.

I would like to extend my thanks to the members of my committee – Frank Smith, Robert Rose, and Sarah Wells – for their helpful insight, support, and guidance. They have each helped to guide my project by expanding my perspective, and then selflessly shared their time and expertise to teach me theoretical and technical approaches. I would also like to thank Teun de Boer for being my external examiner, and for helping in the conception of the glass hooks for stretching the zebrafish SAN. I am also grateful to the members of Alex's lab and to the other faculty, staff, and students from the Department of Physiology who have been kind, helpful, and supportive. In particular, I would like to thank Matthew Stoyek for his willingness to share his expertise and teach me the ways of the zebrafish.

Thank you to the funding bodies who have supported my work and the Quinn laboratory, including the National Science and Engineering Research Council of Canada, the Dalhousie Medical Research Foundation, Mitacs Canada, the Heart and Stroke Foundation, the Faculty of Medicine, and the Department of Physiology and Biophysics.

I am incredibly thankful for the exposure I have had to Peter Kohl and for the mentorship and support he has provided me. I am pretty sure Peter is a wizard – he's wise, insightful, creative, kind, and magical. He's my Dumbledore. I would also like to thank all of the members of the Institute for Experimental Cardiovascular Medicine for welcoming, supporting, and teaching me – both science things and how to eat lunch. So many students, scientific, and technical staff helped me and worked with me, for which I am very thankful. I would like to thank the section heads, for their time, expertise, and friendship, especially Eva Rog-Zielinska and Callum Zgierski-Johnston. I have been incredibly lucky to have been exposed to so many brilliant, inspiring, and kind people during my studies.

And finally, I would like to thank my family and friends for their ongoing support and belief in me. First, in my nine years in Nova Scotia I am lucky to have found a second family. Thank you for all the pints, yoga, laughs, tunes, and adventures. My extended family (aunts, uncles, cousins, and the Brown family) has been a mosh-pit of support, for which I am very grateful – what an intelligent, kind, and inspiring group of people to have hold you up. Big hugs and a thank you to Elspeth and Natalia. Thank you to my brothers, Ruaridh and Duncan, for being the GOAT and for their love and laughs. Thank you to my parents for believing in me and supporting me, for the cups of tea and sandwiches, and for answering my ridiculously frequent facetime calls. Hopefully a combination of Da's love for writing and Mum's passion for science has found its way into this document. And finally, biggest love and thank you to my Adam – you are the best.

CHAPTER 1: INTRODUCTION

Excitation of the heart, which results in its pumping action, begins within the organ itself. Each heartbeat is generated by the heart's natural pacemaker, known as the sinoatrial node (SAN). The intrinsic or 'myogenic' origin of cardiac rhythm generation was first identified nearly 140 years ago by Walter Gaskell (Gaskell, 1882). Its anatomical location within the heart – adjacent to the *crista terminalis* at the junction of the right atrium and the superior *vena cava* – was identified only a few decades later (Keith and Flack, 1907). Yet, even more than a century on, many questions remain unanswered regarding this extraordinary, sometimes curious, but clearly vital piece of tissue.

1.1. SINOATRIAL NODE AUTOMATICITY

What is clear is that the SAN region of the heart is composed of tissue containing pacemaker cells that spontaneously generate action potentials (AP) initiating each heartbeat. These AP are characterised by their spontaneous diastolic depolarisation (SDD) phase in which the membrane potential (V_m) gradually depolarises from its most negative value (maximum diastolic potential, MDP) towards the threshold required to generate an AP (Figure 1.1). The slope of SDD is a key determinant of the frequency of AP firing in the SAN, which determines heart rate (Mangoni and Nargeot, 2008).

A robust system of currents drives SDD (Figure 1.1). The specific ionic mechanisms that result in the spontaneous firing of the SAN, and their relative contribution, has been heavily debated and intensely investigated, predominantly in mammalian studies (Lakatta et al., 2010; Difrancesco and Noble, 2012; Maltsev and Lakatta, 2012; Rosen et al., 2012). Two main hypotheses have been demonstrated, specifically, that SDD is driven primarily by transmembrane currents known as the 'V_m clock'; or that SDD is driven by intracellular Ca^{2+} cycling, known as the 'Ca^{2+} clock' (Lakatta and DiFrancesco, 2009). Consensus has not been reached regarding the importance or predominance of either hypothesis, and in fact it has been shown that they work in conjunction and become mutually entrained (Lakatta et al., 2010), so from this point a distinction will not be made between the two 'clock' systems.

The inward depolarising 'funny' current (I_f) contributes to early SDD (Difrancesco, 2010). It is activated at V_m below ~ -40 mV and is carried by Na^+ through hyperpolarisation-activated cyclic nucleotide-gated (HCN) channels (Difrancesco, 2010). As the V_m becomes depolarised, inward Ca^{2+} currents become activated: initially

through $Ca_v3.1$, the transient T-type Ca^{2+} current (I_{CaT}); and then at a slightly higher threshold the long lasting L-type Ca^{2+} current (I_{CaL}) becomes activated, first through $Ca_v1.3$ and then at an even slightly higher threshold through $Ca_v1.2$ (Mesirca et al., 2015). Intracellular Ca^{2+} cycling has also been shown to be a fundamental contributor to SDD and automaticity (Lakatta et al., 2008). Local Ca^{2+} releases from the sarcoplasmic reticulum (SR) occur during SDD and are either spontaneously occurring and/or are triggered by $Ca_v1.3$ (Lakatta et al., 2010; Torrente et al., 2016). Ryanodine receptors (RyR), through which the Ca^{2+} from the SR is extruded, are situated in close proximity to the Na^+-Ca^{2+} exchanger (NCX) which (following the local Ca^{2+} releases) generates a depolarising current as it extrudes one Ca^{2+} ion in exchange for three Na^+ ions (Lakatta et al., 2008).

Once these depolarising currents cause the V_m to reach the threshold for $Ca_v1.2$, I_{CaL} generates the upstroke of the SAN AP, different from working cardiomyocytes in which the fast Na^+ current (I_{Na}) generates the AP upstroke through $Na_v1.5$ channels (Mangoni and Nargeot, 2008). Although $Na_v1.5$ channels may not necessarily contribute to pacemaking, they are heterogeneously expressed in the SAN and therefore can indirectly modulate AP firing rate (Lei et al., 2005). Other heterogeneously expressed currents may also contribute to pacemaking, such as a sustained inward current and currents passed by transient receptor potential-canonical channels (Zhang et al., 2002; Ju et al., 2007).

Repolarisation of V_m is driven by the inactivation of I_{CaL} and activation of repolarising currents. The primary repolarising currents in SAN myocytes are the rapid (I_{Kr}) and slow (I_{Ks}) delayed rectifier K^+ currents. At the end of the repolarisation, the decay of I_{Kr} and I_{Ks} allows for the inward currents, such as I_f, to cause SDD once again (Aziz et al., 2018). In primary SAN myocytes there is very little, heterogeneously expressed, inward rectifier K^+ current (I_{K1}), compared to working myocytes, in which I_{K1} stabilises the resting V_m, and therefore its absence in SAN cells contributes to the occurrence of SDD. Other K^+ currents may also contribute to repolarisation of the SAN, such as a current passing through TREK1, the ultra-rapid inwardly rectifying K^+ current, acetylcholine-activated K^+ current, and the adenosine triphosphate-sensitive K^+ current (Unudurthi et al., 2016; Aziz et al., 2018). Ca^{2+}-activated K^+ channels may also be important for reaching MDP, as their blockade can cause a decrease in AP firing rate (Weisbrod et al., 2016). An inwardly rectifying chloride current, which is activated during the upstroke, may also contribute to SAN repolarisation (Mangoni and Nargeot,

2008). And finally, the Na^+-K^+ ATPase generates an outward current because it extrudes three Na^+ ions in exchange for two K^+ ions, contributing to repolarisation and maintaining electrochemical homeostasis (Mangoni and Nargeot, 2008).

The combined, out-of-phase activity of these currents results in the oscillatory behaviour of the SAN, even though none of the currents are independently oscillatory. SAN automaticity continues even with the loss of one (or more) of the currents described above due to redundancy within the system, which is a protective mechanism important for ensuring that it continues to fire under widely varying conditions and circumstances (Irisawa et al., 1993). The many components of pacemaking are not only redundant but also mutually entrained. The coupling of the system occurs *via* effects of each component on the others resulting in the mutual entrainment of sarcolemmal ion channel activity and Ca^{2+} cycling by intracellular regulatory mechanisms (Lakatta et al., 2010). Not only are the pacemaking components within individual SAN cells mutually entrained, but the pacemaker cells within the SAN are also entrained with one another in order to fire synchronously (Jalife, 1984).

It is imperative for heart rate to be continuously adapting to the changing requirements of the body. SAN activity is therefore tightly controlled to maintain normal heart rhythm and to accommodate these changes in physiological demand. There are many factors that influence the currents that generate the SAN AP, and because the frequency of AP firing from the SAN determines beating rate (BR), these factors modulate BR. Modulation of BR generally occurs through activation of intracellular signalling pathways that alter AP parameters (*i.e.,* the slope of SDD, plateau length, or amplitude) all of which can change cycle length (Bartos et al., 2015). Activation of these intracellular pathways can occur a multitude of ways, predominantly through ligand stimulation of G-protein coupled receptors (Mangoni and Nargeot, 2008).

For example, SAN automaticity is influenced by biochemical signals from the autonomic nervous system (ANS) and by circulating peptides and hormones (MacDonald et al., 2020b). Catecholamines are released from the sympathetic branch of the ANS and bind to adrenergic receptors, increasing BR; and acetylcholine (ACh) from the parasympathetic branch of the ANS binds to cholinergic receptors to decrease BR (Gordan et al., 2015). They activate G-protein coupled receptors to initiate a cascade of signals that result in alterations in SDD and/or repolarisation that cause a change in BR (Brown et al., 1979; Bucchi et al., 2007). Endocrine, paracrine, and autocrine

hormones and peptides are also important modulators of BR (Beaulieu and Lambert, 1998). And finally, stretch of the SAN – resulting in an increase in its mechanical load – alters BR. The modulation of BR by stretch is the overall focus of this work.

1.2. The Chronotropic Response to SAN Stretch

The mechano-sensitivity of BR was established over a century ago in a study by Francis Bainbridge identifying that intravenous fluid injection, causing right atrial distention, causes an increase in BR in anesthetised dogs (Bainbridge, 1915). This is known as the 'Bainbridge response' (Figure 1.2) and has since been established in humans in a study in which investigators passively lifted the legs of healthy subjects, which resulted in increased venous pressure (without a simultaneous increase in arterial pressure, which would instead activate the dominating baroreceptor reflex, decreasing BR, Figure 1.3). This increase in venous pressure resulted in increased BR, consistent with what Bainbridge observed in dogs (Bainbridge, 1915; Roddie et al., 1957; Donald and Shepherd, 1978). Not only has this positive chronotropic response (*i.e.,* an increase in BR) to SAN stretch has been demonstrated in humans, it has also been shown in a multitude of animal models, including dogs, rabbits, cats, guinea pigs, and rats (Figure 1.4, Pathak, 1958; Lange et al., 1966; Quinn and Kohl, 2016). Interestingly, the chronotropic response to sustained SAN stretch is instead predominantly negative (*i.e.,* a decrease in BR) in the mouse (Figure 1.5, Cooper and Kohl, 2005).

The Bainbridge response is important under normal physiological conditions as the mechanical environment of the SAN within the body is constantly and cyclically changing throughout the cardiac cycle. During ventricular contraction, the atrio-ventricular valve-plane undergoes a basal to apical 'shift', causing stretch of the SAN, with maximal stretch occurring during SDD (Hales et al., 2012). Peak stretch levels coincide with SDD, which increases the slope of SDD *via* stretch-induced inward currents (Cooper et al., 2000), thus 'priming' SAN cells during the period in which their V_m moves towards the excitation threshold. This mechanical 'priming' of pacemaker cells is important as it allows for beat-by-beat adaptation of BR to mechanical load, such that greater venous return to the heart, resulting in greater SAN stretch, will cause faster firing of the very next beat (Quinn and Kohl, 2012). However, mechanical control of BR may only be functional within a range of mechanical loads, as excessive stretch can cause BR irregularities (Lange et al., 1966). Thus, SAN mechanosensitivity may also be relevant in cardiac pathologies resulting in changes in SAN stretch, such as

volume overload in the atria, resulting in increased SAN stretch; or with increased atrial stiffness from structural remodelling or fibrosis, resulting in reduced SAN stretch (Quinn and Kohl, 2020).

The chronotropic response to SAN stretch was initially presumed to be neurally-mediated, i.e., a Bainbridge reflex. Stretch-induced increases in BR, however, occur in the isolated heart (Blinks, 1956), in SAN tissue (Blinks, 1956; Deck, 1964; Cooper and Kohl, 2005), and in single SAN cells (Cooper et al., 2000) all of which are disconnected from the Central Nervous System (CNS), implicating that this response is intrinsic (at least in part) to the SAN itself, thus demonstrating the influence of a Bainbridge response, separate from autonomic influence. The SAN-stretch induced chronotropic response has been shown to be insensitive to pharmacological adrenergic and cholinergic blockade (Blinks, 1956; Pathak, 1958; Brooks et al., 1966; Lange et al., 1966; Brooks and Lange, 1977; Chiba, 1977; Bolter, 1994; Wilson and Bolter, 2002), pharmacological ablation of intracardiac neurons (Wilson and Bolter, 2002), and blockade of neuronal Na^+ channels (Chiba, 1977; Wilson and Bolter, 2002), which is further evidence that non-neuronal, myogenic mechanisms are involved in the chronotropic response to SAN stretch (Quinn and Kohl, 2012).

Yet, in contrast to these data, there is also evidence of an interaction between the control of BR by the ANS and SAN mechano-sensitivity. Vagal (parasympathetic) nerve stimulation (which causes a decrease in baseline BR) enhances the chronotropic response to SAN stretch (Brooks and Lange, 1977; Bolter, 1994; Wilson and Bolter, 2001). In other words, when the vagal nerve is stimulated the increase in BR caused by SAN stretch is greater than the stretch-induced increase in BR without nerve stimulation. Inversely, the chronotropic response to vagal nerve stimulation is diminished following SAN stretch (which causes an increase in baseline BR) both in SAN tissue preparations and in whole animals (Bolter and Wilson, 1999; Wilson and Bolter, 2001), which is at least partially explained by stretch inactivation of the ACh-activated K^+ current (I_{KACh}, Han et al., 2010). Pharmacological stimulation of the ANS similarly has been shown to modulate the change in BR with SAN stretch. Cholinergic stimulation (causing a decrease in baseline BR) enhances the chronotropic response to stretch whereas adrenergic stimulation (causing an increase in baseline BR) diminishes the chronotropic response to SAN stretch (Deck, 1964; Brooks and Lange, 1977; Rossberg et al., 1985; Bolter, 1996; Barrett et al., 1998; Wilson and Bolter, 2001; Han et al., 2010). And finally, interestingly, following a large increase in baseline BR due to

adrenergic overstimulation, the response to stretch in rat atria switches from an increase in BR to a decrease in BR (Barrett et al., 1998). It is difficult to conclude whether there is an interaction between the individual chronotropic responses to ANS signalling and to SAN stretch – it is possible that these data merely reflect the dependence of the magnitude of each response on baseline BR, which has been previously demonstrated (Coleridge and Linden, 1955; Cooper and Kohl, 2005).

Regardless, the combined influence of autonomics and mechanics on BR is evidenced by the variations in BR that coincide with the respiratory cycle: increased BR during inspiration and decreased BR during expiration (Ludwig, 1847). This is known as 'respiratory sinus arrhythmia' (RSA) and is considered to be an indicator of vagal tone (Yasuma and Hayano, 2004). RSA is not only the result of vagal inputs from the CNS, however, because it still exists (albeit to a lesser extent) in humans following heart transplantation (in which the heart is disconnected from the CNS) implicating that these respiration-related oscillations in BR may be in part due to the changing mechanical environment of the heart (Bernardi et al., 1989, 1990). It is also possible that local reflexes contribute to RSA through activation of the intracardiac nervous system. Specifically, respiration results in fluctuations in right atrial volume by reduced intra-thoracic and increased abdominal pressure during inspiration, favouring venous return, and impeded venous return during expiration. Even if there is an interaction between mechanical and autonomic contributions to RSA, these data confirm that the chronotropic response to SAN stretch is, at least in part, intrinsic to the heart itself.

1.3. Cellular Mechanisms of SAN Mechano-sensitivity

The cellular mechanisms evoking the chronotropic response to SAN stretch remain uncertain. There may be several mechanosensors within SAN cells – mechanosensitive enzymes, membrane domains, or structural linkage proteins – but it is most feasible that the acute response to stretch is due to the result of ion translocation through stretch-activated channels (SAC, Peyronnet et al., 2016) or perhaps due to the mechano-sensitivity of the pacemaking currents.

Many components of pacemaking have been shown to be mechanosensitive. The activation, deactivation, and current amplitude of HCN channels are altered by mechanical stimulation in cell expression systems (Calloe et al., 2005; Lin et al., 2007). When clamped to cyclic waveforms, stretch of these cells caused a frequency-dependent alteration of HCN channels such that at higher baseline frequencies stretch increases

rate and at lower baseline frequencies stretch decreases rate (Lin et al., 2007). This is different from the SAN stretch-induced chronotropic response which has a dependence on baseline BR, where greater increases in BR are observed at lower baseline BR (Coleridge and Linden, 1955; Cooper and Kohl, 2005). Further, in the HCN channel study, baseline frequency altered the *direction* of the response (increase *vs*. decrease), whereas in the SAN studies baseline frequency influences the *magnitude* of the response, rather than the *direction* (an exception being following adrenergic overstimulation in rat, as mentioned above, Barrett et al., 1998). It is unknown if HCN channel mechano-sensitivity is contributing to the SAN stretch-induced changes in BR. Regardless, these discrepancies suggest it may not be relevant.

Many other ion channels and transporters in the heart have been shown to be mechanically sensitive, including I_{NaCa}, I_{CaL}, I_{CaT}, I_{Kr}, and I_{Ks}, but they respond to cell volume manipulation (Baumgarten et al., 2011). Cell volume changes are mechanically different from stretch and therefore it is uncertain if these currents are stretch-sensitive (Quinn and Kohl, 2012). Stretch of single ventricular cells has demonstrated mechano-sensitivity of intracellular Ca^{2+} cycling, which may also be occurring in SAN cells. Specifically, axial stretch causes an increase in Ca^{2+} release from RyR in ventricular myocytes (Iribe et al., 2009). If this were to also occur in SAN cells it would likely result in increased BR. This again remains unknown, however, and requires targeted investigation. Despite these uncertainties, it has been shown that intracellular Ca^{2+} cycling contributes to the chronotropic response to SAN stretch, as the stretch response is altered by interventions that interfere with Ca^{2+} handling (Arai et al., 1996). Specifically, blocking reuptake of Ca^{2+} into the SR (by inhibiting sarco/endoplasmic reticulum Ca^{2+}-ATPase, SERCA), or by blocking Ca^{2+} release from the SR (by inhibiting RyR) reduces the increase in BR with SAN stretch without changing baseline BR (Arai et al., 1996). Despite these studies, it is still unclear how heavily the mechano-sensitivity of pacemaking currents and components contribute to the chronotropic response to SAN stretch.

Nevertheless, stretch-activated membrane channels have been shown to be involved as their pharmacological block causes a reversible reduction in the chronotropic response to SAN stretch (Cooper and Kohl, 2005). Microelectrode recordings in SAN tissue have demonstrated that stretch lowers the maximum systolic potential (MSP), and raises the MDP (Figure 1.6, Deck, 1964; Lange et al., 1966). From these data it can be inferred that the stretch response may in fact be due to a stretch-

activated ion channel with a reversal potential (E_{rev}) somewhere between MDP and MSP, which narrows the range of plausible candidates (Cooper et al., 2000). Both cell-volume activated Cl^- current ($I_{Cl,swell}$) and the current passed through cation non-selective SAC ($I_{SAC,NS}$) could, therefore, theoretically account for these stretch-induced changes in SAN firing.

Although $I_{Cl,swell}$ has an E_{rev} near 0 mV, these channels require an increase in cytosolic volume for their activation, and there is a lag (often exceeding 1 minute) before the activation of $I_{Cl,swell}$ (Hagiwara et al., 1992). This means its response is too slow to account for the near instantaneous nature of the chronotropic response to SAN stretch. A subsequent study reinforced that the SAN stretch response might be quite different from the response to cell volume changes, as hypoosmotic swelling actually caused a decrease in BR in rabbit SAN cells (Lei and Kohl, 1998). Further, cell swelling (in which cell diameter increases while length does not change) is mechanically different from axial stretch, which causes cell lengthening and a decrease in diameter, but no change in volume (Cooper et al., 2000).

Therefore, it is reasonable to hypothesise that SAC_{NS} activation may be the primary mediator of SAN stretch effects. $I_{SAC,NS}$ has an E_{rev} between 0 and -20 mV (Guharay and Sachs, 1984), and stretch of single rabbit SAN cells increases AP firing rate and elicits a current with an E_{rev} near -11 mV, which increases the likelihood of the possibility that $I_{SAC,NS}$ may be responsible, at least in part, for the stretch-induced chronotropic response (Figure 1.7, Cooper et al., 2000). Despite this, the molecular identity of SAC_{NS} has yet to be determined (Peyronnet et al., 2016) and whether it is the main mediator of SAN stretch effects remains unknown.

1.4. Goals and Objectives

It has been known for over a century that atrial distention results in an increase in BR, and it is well established that it is an important heart rate control mechanism. Despite this and the plethora of data demonstrating SAN mechano-sensitivity, mechanisms that elicit this change in BR are still incompletely understood. Identifying appropriate animal models, then utilising and integrating these various model systems for their specific and unique advantages allows for a greater understanding of the electrophysiological, temporal, structural, and mechanical determinants of the chronotropic response to SAN stretch. **Overall, the goal of my thesis was to**

investigate mechanisms and determinants driving the chronotropic response to SAN stretch.

Although the mouse is the primary genetically modifiable experimental model species utilised for cardiovascular investigations, it may not represent an appropriate species for the investigation of stretch-induced changes in SAN BR as stretch of the mouse SAN has been shown to cause a decrease (rather than an increase) in BR (Cooper and Kohl, 2005). An alternative genetically modifiable species may aid in defining the unknown mechanisms responsible for SAN stretch responses. The zebrafish is becoming an increasingly powerful and popular genetically modifiable experimental model for the study of cardiac electrophysiological mechanisms (Genge et al., 2007; Vornanen and Hassinen, 2016; Gut et al., 2017). **Thus, my first objective was to characterise the response of the zebrafish SAN to stretch in order to establish it as a potential model species for studying mechanisms driving the chronotropic response to stretch.**

It has been suggested that the stretch-induced increase in BR demonstrated in most species is the result $I_{SAC,NS}$ activation (Cooper and Kohl, 2005). Further, it is also theoretically possible that activation of $I_{SAC,NS}$ is responsible for the species-difference observed with stretch of the mouse SAN, in which BR decreases, rather than increases (Cooper and Kohl, 2005). This hypothesis would mean that the discrepancy is not due to a difference in cellular stretch-activated mechanism(s), but rather that the same underlying mechanism – activation of $I_{SAC,NS}$ – generates a different outcome in mice due to species-specific differences in background electrophysiology, specifically, differences in AP morphology (Cooper and Kohl, 2005). Activation of $I_{SAC,NS}$ causes the V_m to be pulled toward its E_{rev} ($E_{SAC,NS}$, between -20 and 0 mV), which will result in different effects depending on the phase of the cardiac cycle in which $I_{SAC,NS}$ is activated. Specifically, during phases in which the SAN V_m is spontaneously moving towards $E_{SAC,NS}$ (during SDD or early repolarisation), activation of $I_{SAC,NS}$ will aid the other active currents (contributing to SDD or early repolarisation), thus shortening the cycle length and increasing BR (Figure 1.8, green arrows). Conversely, during phases in which the V_m is spontaneously moving away from $E_{SAC,NS}$ (late AP upstroke, late repolarisation), $I_{SAC,NS}$ activation will oppose the other active currents (working against late upstroke or late repolarisation) causing lengthening of the cycle and decreasing BR (Figure 1.8, red arrows). Consequently, based on this theory, the chronotropic response to sustained SAN stretch would be the net effect of these competing phases, resulting

in either an increase, decrease, or no change in BR depending on AP morphology. Theoretically, in mouse there is a greater portion of the cardiac cycle during which sustained SAC_{NS} activation would cause a decrease in BR compared to human and other species, and thus in which AP should be preferentially shortened by sustained stretch, causing an increase in BR. Testing this requires activation of $I_{SAC,NS}$ during only specific phases of the cardiac cycle, rather than sustained activation. Rapid stretch to activate $I_{SAC,NS}$ during specific phases of the cardiac cycle is not feasible due to the viscoelastic nature of SAN tissue and is an uncontrolled approach for specifically testing the effects of $I_{SAC,NS}$ activation, as all mechanosensitive SAN components would become activated. A method to overcome these limitations is to utilise transgenic lines of zebrafish and mice expressing a light-activated ion channel (channelrhodopsin-2, ChR2), which passes a cation-non-selective current with similar characteristics to $I_{SAC,NS}$. Specifically, ChR2 has similar on-off kinetics, stimulation magnitude-dependence, and, most importantly an E_{rev} (between -20 and 0 mV) as with SAC_{NS} (Cooper et al., 2000; Bruegmann et al., 2010). By using ChR2 as a surrogate for SAC_{NS}, it becomes possible to determine whether BR can be both increased *and* decreased in each species depending on activation timing within the cardiac cycle. Further, it tests the feasibility of $I_{SAC,NS}$ activation as a mechanistic explanation for the observed species difference to sustained SAN stretch without activating other mechanosensitive components of the SAN. Through these experiments it can be established if AP morphology can determine the *direction* of the chronotropic response to sustained SAN stretch (positive; increase in BR, or negative; a decrease in BR). **This approach allowed the undertaking of my second objective, which was to investigate the importance of stimulus timing and action potential morphology for the chronotropic response to SAC_{NS}-like current activation.**

Previous studies have demonstrated an apparent dependence of the magnitude of the stretch-induced increase in BR on mechanical considerations. Specifically, some studies have proposed that strain is a key parameter (Sanders et al., 1979; Kamiyama et al., 1984), while others have suggested that stress levels (Brooks et al., 1966; Chiba, 1977; Arai et al., 1996) or a combination of both (Lange et al., 1966) determine the magnitude of the effect of stretch on BR. The importance of mechanical considerations on the stretch response was corroborated in my initial zebrafish experiments, as a lack of a controlled preload resulted in considerable variability in the magnitude of the chronotropic response, and therefore it became clear that mechanical parameters, such

as preload and tissue stiffness, might be important for dictating the degree of responsiveness. Mechanical parameters and structural properties of the SAN may influence how stress/strain is distributed throughout the tissue. This could alter which components of the SAN undergo the most stress/strain, potentially altering the magnitude of chronotropic responses. These structural properties may also differ between species and contribute to the species-specific responses to SAN stretch. This study aims to understand how mechanical parameters and structural characteristics of the SAN might influence the *magnitude* of the chronotropic response to SAN stretch. This has potentially important implications in SAN dysfunction, as mechanical and structural properties of the SAN and atria change under certain pathological conditions and could alter this important BR control mechanism. **Thus, my third objective was to investigate the structural and mechanical factors influencing the chronotropic response to SAN stretch**.

Figure 1.1. SAN cell APs and ion fluxes responsible for automaticity.

I_{CaL}, L-type Calcium (Ca^{2+}) currents; I_{CaT}, T-type Ca^{2+} current; I_f, funny current; $I_{Kr/s/Ca}$, rapid delayed rectifier / slow delayed rectifier / Ca^{2+}-activated potassium currents; I_{NaCa}, sodium-calcium exchanger current; MDP, maximum diastolic potential; MSP, maximum systolic potential; SR, sarcoplasmic reticulum; SDD, spontaneous diastolic depolarisation. Shaded regions indicate inward current (downward) and outward current (upward).

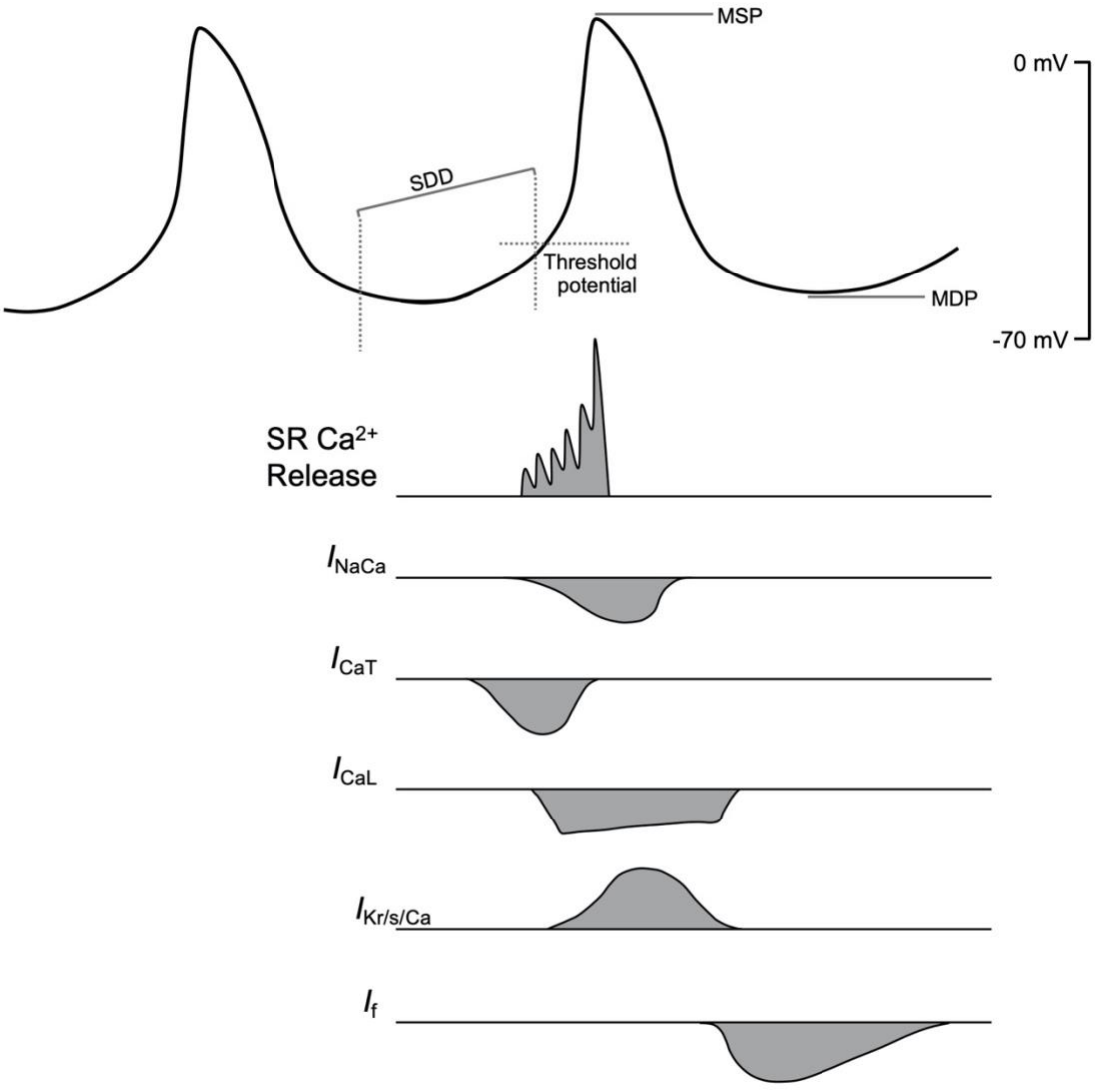

Figure 1.2. Chronotropic response to right atrial distention in dog.

An increase in heart rate (middle trace) observed following saline injection that causes an increase in venous pressure (top trace) and right atrial distention without a simultaneous increase in arterial blood pressure (bottom trace) in the anesthetised dog. BP, blood pressure; VP, venous pressure (From Bainbridge, 1915).

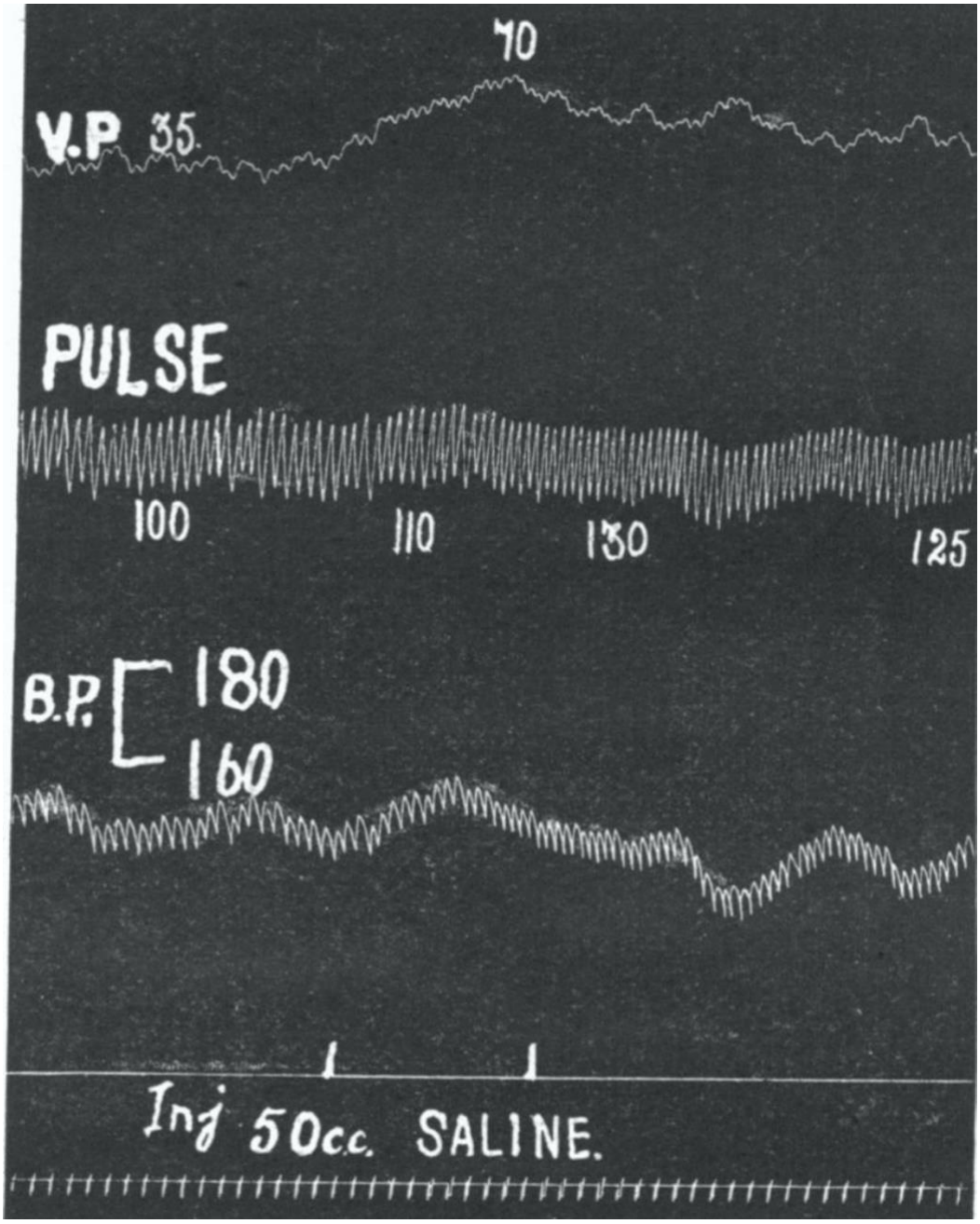

Figure 1.3. Chronotropic response to right atrial distention in human.

By passively lifting the legs of healthy human subjects, venous pressure increased without an increase in mean arterial pressure or pulse pressure and resulted in an increase in heart rate (From Donald and Shepherd, 1978).

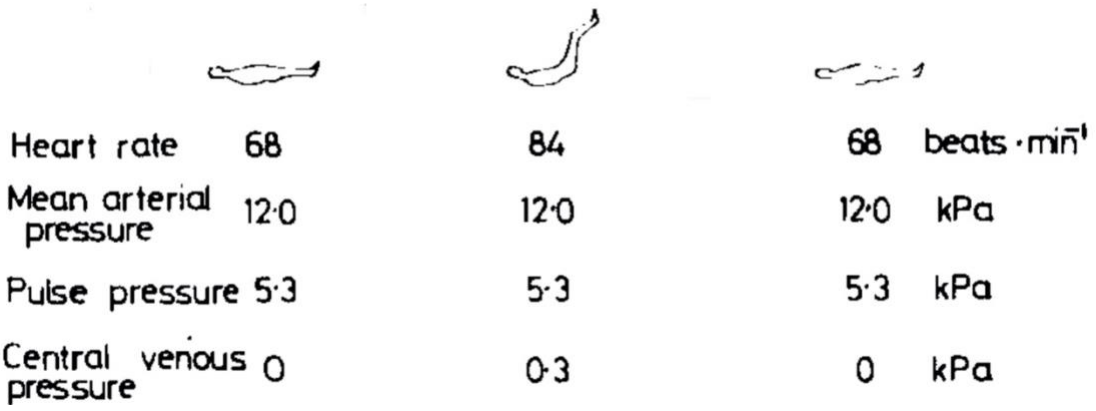

Figure 1.4. Chronotropic response to right atrial distention in mammals.

The positive chronotropic response observed with distention of the isolated right atria of rabbit, guinea pig and albino rats with increasing magnitudes of intraluminal pressures. (From Pathak 1958).

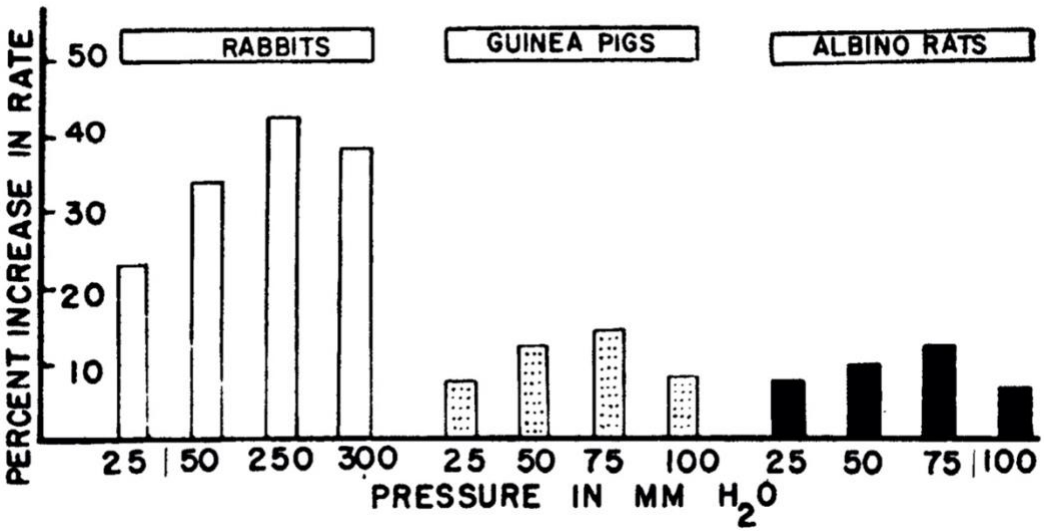

Figure 1.5. Chronotropic response to SAN stretch in the mouse.

(A) Representative mouse SAN stretch data. Top panel shows the change in passive tension with stretch and the lower panel demonstrates the simultaneous decrease in BR. (B) Summary of the stretch-induced change in BR in the mouse SAN at 27°C (grey circles) and 37°C (black circles) and in the guinea pig SAN (squares), plotted as a function of initial BR. (From Cooper and Kohl 2005).

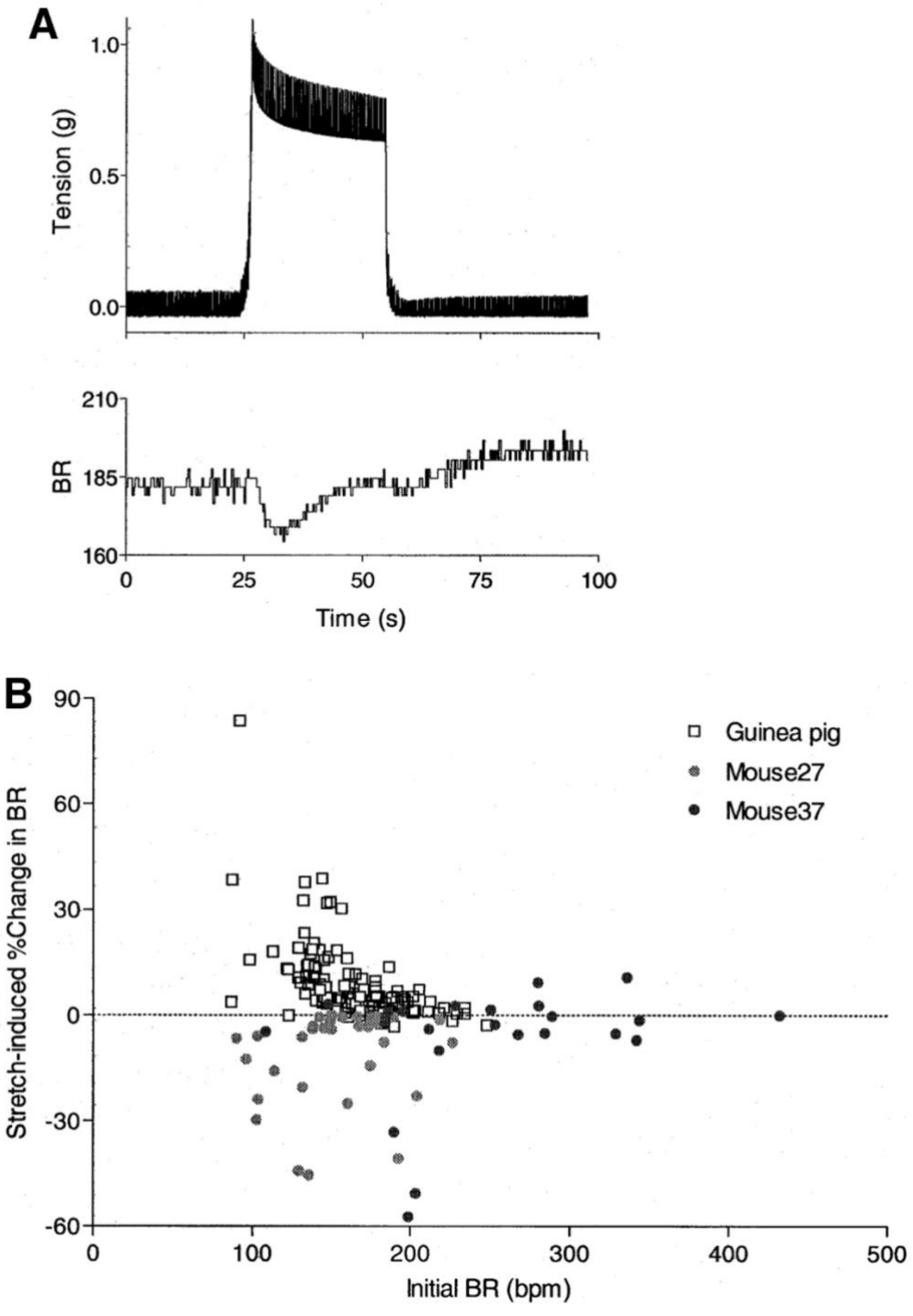

Figure 1.6. SAN stretch-induced changes in BR and V_m.

Microelectrode recording (top trace) of the spontaneously beating cat SAN before, during, and after 30% stretch. Bottom trace is of the echocardiogram. (From Deck, 1964).

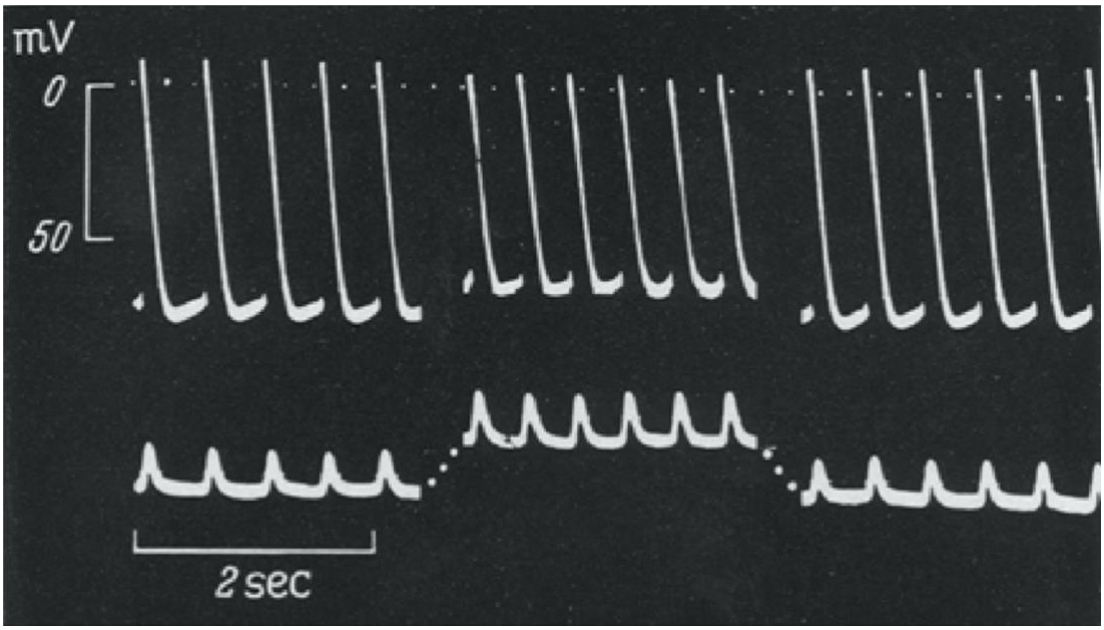

Figure 1.7. Stretch-induced changes in BR in the rabbit SAN cell.

(A) Stretch of a single rabbit SAN cell by 7% of resting length, applied using carbon fibres attached to opposite ends of the cell. (B) Recording of spontaneous SAN firing in an isolated rabbit SAN cell in unstretched (light curve) and stretched (dark curve) states (From Cooper et al., 2000).

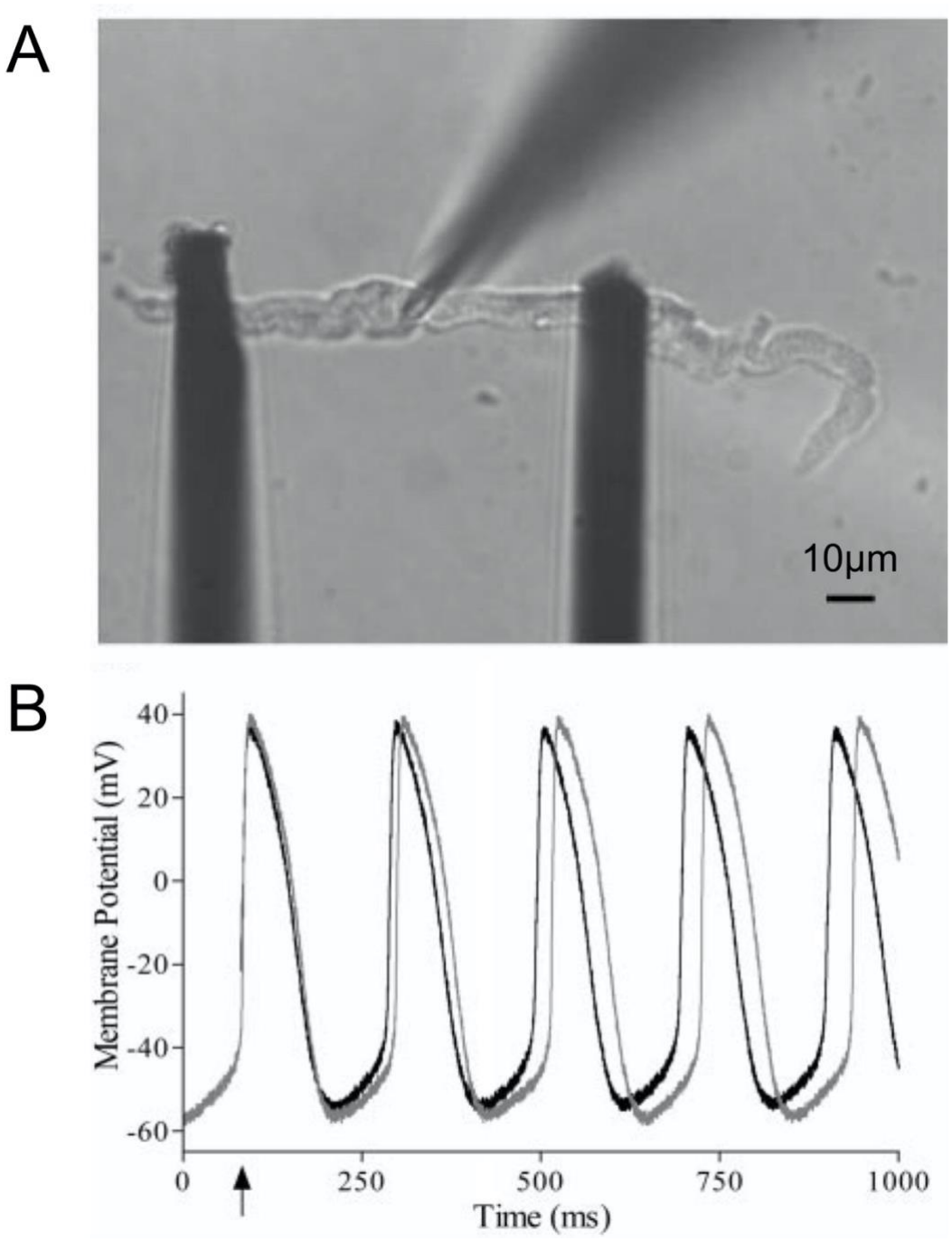

Figure 1.8. Schematic illustration of theoretical effects of SAC_{NS} on the SAN cell AP.

The dotted line represents the reversal potential of $I_{SAC,NS}$ ($E_{SAC,NS}$) and the arrows represent the direction of $I_{SAC,NS}$ at a given point in the AP. Green arrows represent phases in which $I_{SAC,NS}$ activation would increase BR. Red arrows represent phases in which $I_{SAC,NS}$ activation would decrease BR.

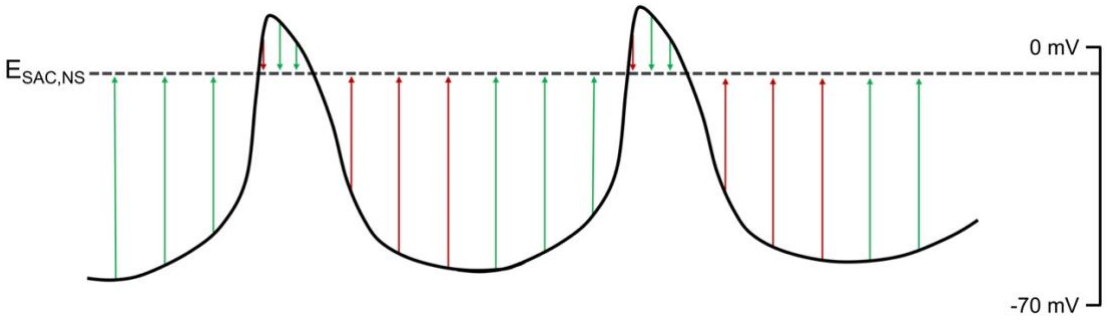

CHAPTER 2: ESTABLISHING THE ZEBRAFISH AS A MODEL FOR STUDYING THE CHRONOTROPIC RESPONSE TO SAN STRETCH

2.1. INTRODUCTION

Despite many years of study in various species, a multitude of questions remain unanswered regarding the SAN stretch response (Quinn and Kohl, 2020). Genetic modification of animal models has advanced the ability for specific interrogation of electrophysiological responses in the heart and may be an important next step in these investigations. However, genetically modified mice are the most commonly utilised model species for cardiac electrophysiological studies and they are not an optimal model for studies of SAN mechano-sensitivity as they have been shown to respond to SAN stretch with a decrease, rather than an increase, in BR (Cooper and Kohl, 2005). Thus, identification of a genetically modifiable model species that responds to SAN stretch with an increase in BR, consistent with humans, would be advantageous for enhancing our understanding of the SAN stretch response. Hence, in this study I examined the response of the zebrafish SAN to stretch.

2.1.1. The Zebrafish as a Model for the Study of Cardiovascular Electrophysiology

The zebrafish represents a new powerful and popular experimental model for cardiovascular research. Initially, the predominant experimental use of the zebrafish was for developmental research (including cardiovascular system development) due to the optical transparency of their embryos and larval stages, but in recent years their uses have broadened, becoming expansive (Gut et al., 2017). The zebrafish genome has been fully sequenced with ~70% of genes having a corresponding human gene encoding a protein with the same function, making it an increasingly useful vertebrate model for studying human physiology and disease (Howe et al., 2013). Morphological and systemic differences between zebrafish and mammalian hearts, such as its two- vs. four-chambered heart and its low vs. high blood pressure limits some uses of zebrafish as a cardiac model (Hu et al., 2001). Despite this, the zebrafish can be an extremely useful model for studying human cardiac electrophysiology and is, at least in some ways, an advantageous alternative to the mouse due to its fecundity, rapid breeding, efficient housing, the relative ease of its genetic manipulation using current techniques, and perhaps most importantly, its electrophysiological similarities to the human heart

(Rafferty and Quinn, 2018). Due to these assets, it is a useful model species for cardiac electrophysiological studies (Genge et al., 2007; Vornanen and Hassinen, 2016; Gut et al., 2017).

The heart rate of the zebrafish (~ 100 – 200 beats per minute, bpm) is somewhat comparable to human, especially in relation to the fast heart rate of the mouse (~ 500 – 700 bpm, Nemtsas et al., 2010; Kaese and Verheule, 2012). AP morphology in zebrafish ventricular, atrial, and SAN cells is also similar to human, most notably as the AP includes a more prominent plateau phase following the upstroke that is not consistently evident in mouse cells (Nemtsas et al., 2010; Tessadori et al., 2012; Vaidyanathan et al., 2013). Ionic current, channel, and intracellular Ca^{2+}-handling protein expression and function, as well as the gene products which sequence them, have all been characterised in zebrafish ventricular and atrial cells, identifying useful similarities and limiting differences compared to the human situation (Ravens, 2018; van Opbergen et al., 2018b). However, the ionic properties of SAN cells in the zebrafish are less well understood and require further investigation.

2.1.2. The Zebrafish as a Model for the Study of SAN Function

Consistent with mammals, electrical activity in the zebrafish is spontaneously initiated from pacemaker cells and propagates through the heart causing contraction (Stoyek et al., 2016). These pacemaker cells are organised in a ring-shaped structure at the sinoatrial valve, which is at the border between the sinus venosus and the atrium (Tessadori et al., 2012). SAN development in the zebrafish occurs from cardiac progenitor cells expressing the same transcription factors as mammals: T-box transcription factor 3 and Islet-1 (Tessadori et al., 2012). Most of the currents that drive SDD and automaticity in the mammalian SAN have not been characterised or identified in the zebrafish SAN. It has been demonstrated in the zebrafish, however, that a hyperpolarisation-activated inward current with the properties of I_f (denoted as I_h) is involved in generating SAN automaticity (Baker et al., 1997; Warren et al., 2001). This was determined by the discovery of a mutation (*slow mo*) that causes a reduction in I_h activity and, consequently, a reduction in BR (Baker et al., 1997; Warren et al., 2001). As previously described, another contributor to mammalian pacemaking is the decay of I_{Kr}, and this repolarising current has also been shown to contribute to pacemaking in the zebrafish (Baker et al., 1997). More recently it has been demonstrated that pharmacological block of HCN channels, or the combined inhibition of RyR and

SERCA, significantly reduces the maximal BR observed in response to acute warming, implicating a role for both I_f and intracellular Ca^{2+} handling in zebrafish pacemaker activity (Marchant and Farrell, 2019). Similarly, pharmacological inhibition of I_{Kr} or I_{CaL} results in reduced BR in the zebrafish, suggesting involvement of these currents in pacemaking (van Opbergen et al., 2018a).

Apart from these studies, characterisation of specific pacemaking mechanisms in the zebrafish is an area warranting further investigation. Nevertheless, many of the currents that contribute to pacemaking in mammals have been identified in the zebrafish atrium and/or ventricle, and thus it is conceivable that the ionic composition of the SAN does not vary greatly from that of the atria (Vornanen and Hassinen, 2016; Ravens, 2018). For example, I_h is present in working cardiomyocytes in the zebrafish, which differs from mammals, where the functional contribution of I_f is limited to the cardiac conduction system (Warren et al., 2001; Baruscotti et al., 2010; Vornanen and Hassinen, 2016). Further, I_{CaT}, which contributes to SDD in mammals (but is not prominent in working mammalian cardiomyocytes) is present and abundant in zebrafish working cardiomyocytes, contributing to their more neonatal-like phenotype (van Opbergen et al., 2018b). Similarly, components of intracellular Ca^{2+}-cycling, such as RyR, SERCA, and NCX are present and active in the zebrafish, but instead move Ca^{2+} into the SR and out of the cell at proportionately different magnitudes (van Opbergen et al., 2018b). Further studies must be conducted to gain a thorough understanding of the ionic currents involved in zebrafish SAN automaticity.

The autonomic control of zebrafish SAN function is comprised of neural pathways that regulate heart rate through adrenergic and cholinergic mechanisms in a similar manner to mammals (Stoyek et al., 2016). The small size of the zebrafish heart allows for both visualisation and access to the intracardiac nervous system, overcoming the limitations of larger animal models, making the zebrafish a powerful and novel model for gaining a comprehensive understanding of the autonomic control of SAN function (Stoyek et al., 2015). Not only has it been established that the zebrafish can be used to study autonomic SAN control, it has also been shown to be a useful model for studying contractility and mechano-electric coupling. Specifically, in single ventricular cells, contractile force regulation has many similarities to mammals making it an appropriate model for cardiac contractile biological experimentation (Dvornikov et al., 2014). Further, the zebrafish heart has been shown to be mechanosensitive, as ventricular stretch in the isolated embryo heart causes acute electrophysiological

changes (Werdich et al., 2012). In that study it was also anecdotally mentioned that stretch of the heart caused an increase in heart rate, suggesting perhaps an acute influence of stretch on SAN firing.

The ease of genetic modification, the breeding and housing advantages, and the SAN function comparable to mammals suggest the zebrafish may be an appropriate model for studying the chronotropic response to SAN stretch. It has advantages over the mouse, the most utilised genetically modifiable model for cardiovascular electrophysiology, because of its long AP plateau phase and its slower BR. While the mouse has been shown to respond to SAN stretch with a decrease in BR (Cooper and Kohl, 2005) compared to the increase in BR observed in all other species studied, the response in zebrafish has not been systematically studied. Thus, in order to justify the use of zebrafish as a model to study SAN mechano-sensitivity, the response to SAN stretch must first be characterised. Identifying a genetically modifiable species with a consistent chronotropic response to stretch compared to human would enhance the investigation of SAN stretch mechanisms by creating new avenues for investigation with genetic tools. Thus, as the chronotropic response to SAN stretch has not yet been systematically investigated in the zebrafish, my goal was to examine the effects of controlled, sustained stretch on the BR of the zebrafish isolated SAN in order to evaluate its utility as a novel model for the study of intrinsic mechanical SAN regulation. Based on the similar BR and AP morphology in the zebrafish compared to large mammals, I hypothesised that the zebrafish would respond to SAN stretch with an increase in BR.

2.2. METHODS

2.2.1. Animals

Adult (6 - 12 months post-fertilisation) wild-type (AB) zebrafish were used. All experimental procedures were approved by the Dalhousie University Committee for Laboratory Animals and followed the guidelines of the Canadian Council on Animal Care. Zebrafish were euthanised in Tris-buffered (pH 7.4; BP152, Fisher Scientific, Ottawa, Canada) tricaine (2 mM; E10521, Sigma-Aldrich, Oakville, Canada) in room temperature tank water until there was no response to fin pinch.

2.2.2. Zebrafish SAN Isolation

Once euthanised, zebrafish were placed into a Sylgard-lined dish (DC 170, Dow Corning, Midland, USA) filled with Krebs-Henseleit solution, containing, in mM: 120

NaCl, 4.7 KCl, 26 $NaHCO_3$, 1.4 NaH_2PO_4, 1.0 $MgCl_2$, 1.8 $CaCl_2$, 5.0 Glucose; with an osmolality of 300 ± 5 mOsm/kg and a pH of 7.40 ± 0.05. A ventral midline incision was made through the body wall, exposing the heart. Tissue encompassing the ventral aorta, ventricle, atrium, and sinus venosus was removed and placed in a separate dish. The ventricle was removed, and the atrium cut open and pinned flat exposing the SAN ring. A custom suction microelectrode (1.00/0.58 mm outer/inner diameter; 1B100 and MPH6R10, World Precision Instruments, Sarasota, USA) connected to an ECG amplifier (Animal Bio Amp, ADInstruments, Colorado Springs, USA) was positioned at the edge of the atrium. Suction was applied with a 1 ml syringe to measure the local ECG. The bath was bubbled with carbogen (95% O_2, 5% CO_2) and maintained at 28°C (physiological zebrafish temperature), which was measured using a thermocouple (T-type pod, ADInstruments) with a temperature-controlled (TC-344C, Warner Instruments, Hamden, USA), warmed platform (WP-16, Warner Instruments). Temperature and ECG signals were recorded at 2000 Hz using a data acquisition (DAQ) device (PowerLab, ADInstruments) controlled by LabChart (ADInstruments).

2.2.3. Zebrafish SAN Stretch

Piezoelectric linear translators for application of sub-nanometre resolution stretch (P-621.1CD, Physik Instrumente, Auburn, USA) were fixed to the stage on a rack and pinion track for coarse positioning (56798, Edmond Optics). Microelectrode holders (MPH110, World Precision Instruments) coupled to independent three-axis hydraulic micromanipulators (MHW-103, Narishige International, East Meadow, USA) were mounted onto the piezoelectric translators for fine positioning (Figure 2.1A) and held two custom-made micro-sized hooks (Figure 2.1B) built from single-barrel borosilicate glass capillaries (2.00/1.12 mm outer/inner diameter; 1B200F, World Precision Instruments) gently bent using a custom setup with a micromanipulator and a fire polisher. The hooks were carefully inserted into the oval-shaped SAN ring opposing each other in either the long- or short-axis direction (Figure 2.2A, n=13 for each). Hooks were positioned under an upright microscope (BX63, Olympus, Richmond Hill, Canada) with a 5× objective using the micromanipulators. The SAN tissue rested in the loops of the hooks without tissue puncture or damage. Piezoelectric position was controlled by a servo controller (E-665.CR, Physik Instrumente) driven by a DAQ device (USB-6361, National Instruments, Austin, USA) to apply precise magnitudes of

stretch (Figure 2.2B-C, 10, 25, or 50%) with custom routines developed in LabView (National Instruments).

2.2.4. Experimental Protocol

Once hooks were positioned in either the long- or short-axis direction, the SAN preparations were left to equilibrate for 30 min to ensure a stable baseline BR. Using the micromanipulators, the hooks were separated such that each hook just began to stretch the SAN without affecting BR. This distance between the hooks (inter-hook distance) in this pre-stretch position was then measured. The SAN ring was stretched 10% of the pre-stretch inter-hook distance by moving both piezoelectric translators apart and then after 30 s, back to the pre-stretch distance, moving in both directions at a rate of 1 mm/s. Following 120 s of rest, this same protocol was repeated three times, resulting in a total of four stretches at this length. Following this, this entire stretch procedure was repeated with 25 and 50% increases in pre-stretch distance for a total of 12 stretches per preparation. The position of the piezoelectric translators was recorded at 2000 Hz with the DAQ device.

2.2.5. Data Analysis and Statistics

Data were analysed using custom routines in Matlab (MathWorks, Natick, USA). The peaks of the ECG signal were used to calculate BR and stretch percentage was calculated from the positions of the two piezoelectric translators. Baseline BR was calculated as the average BR during the 120 s period of rest prior to each stretch. Average and peak BR during the stretch period were measured. Average BR was measured over the entire 30 s stretch period. Peak BR was averaged over five beats on either side of the shortest cycle length for a total of eleven beats. The time to peak response was calculated by measuring the time when stretch began to the time at which the shortest CL began. Inter-beat variability (IBV) was calculated as the standard deviation of BR during both the baseline and stretch periods.

Statistical analysis was performed in SPSS (IBM, Armonk, USA). Values are presented as mean ± standard error of the mean (SEM) and were considered significant with a p-value < 0.05. Three variables relating to the stretch response were examined: (1) stretch magnitude (10 vs. 25 vs. 50%), (2) temporal response (average vs. peak change in BR), and (3) direction of stretch (long- vs. short-axis). Two-way repeated-measures analysis of variance (ANOVA) was used to assess these variables.

Specifically, the effect of stretch magnitude was determined by comparing baseline, average, and peak BR with each increasing strain magnitude. The temporal response was established by comparing the average change in BR with the peak change in BR for each stretch magnitude. And finally, IBV was compared at baseline and with stretch at each stretch magnitude in both the long- and short-axis direction. The influence of stretch direction was evaluated using two-way mixed ANOVA to compare the peak percentage change in BR for long- and short-axis stretch at each stretch magnitude. One-way repeated measures ANOVA was used to compare the time to peak BR in both directions and at all stretch magnitudes. Significant main effects were analysed by Bonferroni post hoc tests, and when the interaction effect was significant, simple effects were analysed by Student's t-test. SAN ring diameter and average time to peak BR for both directions of stretch were compared by two-tailed, unpaired Student's t-test. The initial and final temperature was compared by two-tailed, paired Student's t-test. The relationship between baseline BR and the peak change in BR was assessed by linear regression.

2.3. RESULTS

All SAN preparations displayed regular spontaneous beating (137 ± 8.30 bpm; $n = 26$). The inter-hook distance was 220 μm before both long- and short-axis stretch (220 ± 11 μm; 220 ± 13 μm respectively, $p = 0.989$). There was no change in baseline BR or temperature throughout the stretch protocol (initial: 28.4 ± 0.2 °C, final: 27.9 ± 0.2 °C, $p = 0.18$), and the peak change in BR was not related to baseline BR (all R^2-values < 0.1).

2.3.1. Direction and Magnitude of Stretch

Peak BR with stretch was greater than baseline BR for both stretch directions and at all stretch magnitudes (Figures 2.3, 2.4). Average BR with stretch was greater than baseline BR with all stretch magnitudes in the short-axis direction, but only with 50% stretch in the long-axis direction (Figure 2.4). With short-axis stretch, peak BR was greater at 50% stretch than at 10 or 25% stretch, displaying the dependence of responsiveness on stretch magnitude (Figure 2.4). The direction-stretch magnitude interaction was significant ($p = 0.013$), such that there was a greater peak percentage change in BR with 25% short-axis stretch compared to 25% long-axis stretch (Figure 2.5).

2.3.2. Temporal Response

BR began to increase immediately with long-axis stretch, reaching a peak on average after 15.6 ± 1 s, which remained consistent across all stretch magnitudes (10%: 14.8 ± 1.5 s; 25%: 16.5 ± 1.7 s; 50%: 15.6 ± 2.0 s; n = 13, p = 0.68). The time to peak BR was also not dependent on stretch magnitude with short-axis stretch (10%: 17.8 ± 1.5 s; 25%: 19.8 ± 1.6 s; 50%: 18.3 ± 2.0 s; n = 13, p = 0.62), although the average time to peak BR (18.6 ± 1.0 s) was longer than for long-axis stretch (p = 0.03). Upon release, BR began to immediately decrease, returning to baseline over a similar time course as the increase with stretch. With short-axis stretch, the peak percentage change in BR was greater than average change at all stretch magnitudes reflecting the gradual (not immediate) increase in rate during the stretch period (Figure 2.6).

2.3.3. Interdependence of Stretch Magnitude, Timing, and Direction

For both long- and short-axis stretch, the interaction of the temporal effect (peak vs. average) and stretch magnitude (10, 25, or 50%) on BR was significant (p = 0.042 and 0.021, respectively). Figure 2.7 shows the absolute peak and average change in BR for long- and short-axis stretch, demonstrating this temporal- (average vs. peak) and stretch direction- (long- vs. short-axis) dependence of stretch effects. For comparison, changes in BR were normalised to the pre-stretch value by calculating the percentage change in BR. The temporal effect-stretch magnitude interaction on percentage change in BR was significant for short-axis stretch only (p = 0.039)

2.3.4. Inter-beat Variability

IBV was measured by the standard deviation of BR. The interaction effect of IBV with stretch and stretch magnitude was significant for both long- and short-axis stretch (p = 0.003 and 0.016, respectively). IBV decreased with 10% stretch in both the long- and short-axis direction and increased with 50% stretch in the long-axis direction (Figure 2.8).

2.4. Discussion

The present study is a systematic investigation of the chronotropic response to varying degrees of controlled SAN stretch in the zebrafish. An immediate and continuous increase in BR was observed, gradually reaching a maximum part way through a period

of sustained stretch. Both the direction and magnitude of stretch influence the responsiveness of the SAN. This increase in BR observed is consistent with the chronotropic response to SAN stretch that has been demonstrated in most mammals, apart from mice. This indicates that the zebrafish may indeed represent an innovative experimental model species to study mechanisms involved in the chronotropic response to changes in mechanical load.

2.4.1. Advantages and Limitations of the Zebrafish as a Model for SAN Stretch

Perhaps most importantly, the zebrafish responds to SAN stretch with an increase in BR, consistent with most mammals studied, including human (Quinn and Kohl, 2012). This indicates that this important SAN control mechanism may be highly conserved across the ancestral vertebrate spectrum. Also consistent with other species is the time-, magnitude-, and direction-dependence of the chronotropic response to SAN stretch (Quinn and Kohl, 2012). One limitation in the study of mechanical regulation of the SAN has been the lack of genetically modifiable model species with comparable responses to SAN stretch as in the human. The zebrafish has now been identified as a novel genetically modifiable model species for studying SAN mechano-sensitivity.

It has been proposed that due to the relationship between $E_{SAC,NS}$ and SAN AP morphology, activation of SAC_{NS} by SAN stretch can account for the species-specific changes in BR that occur (Cooper et al., 2000). The SAN stretch-induced increase in BR observed in this study further supports this concept as the zebrafish has a slower BR at baseline and a longer plateau phase compared to the mouse (Nemtsas et al., 2010). This variation in AP morphology between the two species could potentially result in the differences in their chronotropic responses to SAN stretch. Although this theoretical explanation is conceivable, and perhaps even probable, it requires experimental validation. One major limitation for this, however, is that although many candidates exist, the molecular identity of SAC_{NS} remains unknown (Peyronnet et al., 2016). As it has now been established that SAN-stretch responses are present in zebrafish, and many genetically engineered zebrafish lines and powerful techniques for their creation exist, they may represent an innovative model for discovering the identity of SAC_{NS}. Further, studying the effect of SAN stretch on AP morphology, Ca^{2+} handling, and SAN excitation patterns is possible in the zebrafish by employing previously established fluorescent-based optical mapping or optogenetic techniques. This further enhances its utility as a model species for investigating SAN mechano-sensitivity.

A potentially important consequence of SAN stretch is impacts on IBV, which are also present in the zebrafish. Both in humans with pulmonary hypertension and in anesthetised pigs, SAN stretch causes a reduction in IBV (Horner et al., 1996; McGowan et al., 2009). Reduced IBV is associated with an increased risk for sudden cardiac death and arrythmia, and may in part be the result of the atrial distention present with certain pathologies (Horner et al., 1996; McGowan et al., 2009). In agreement with these studies, 10% stretch in both directions also resulted in a reduction in IBV in the zebrafish. 50% stretch in the short-axis direction, however, resulted in an increase in IBV. This discrepancy may be the result of experimental differences, such as intact heart vs. isolated atrial preparations, or long vs. short stretch durations. Alternatively, this difference could be because 50% stretch of the SAN is bordering on a pathophysiological level of stretch in the zebrafish, resulting in irregular rhythms that increase IBV. Finally, it is possible that this difference is simply due to species differences.

Although this study suggests the zebrafish may be a useful and powerful model for studying mechanical regulation of the SAN, there are limitations to its utility. Determining the mechanical parameters that influence the magnitude of the chronotropic response to SAN stretch is important not only for our understanding of the role of mechanical SAN regulation under normal physiological conditions, but also its contribution to pathophysiological conditions and SAN dysfunction. The zebrafish heart possesses many electrophysiological similarities to the mammalian heart, yet structurally they are very different. The zebrafish SAN is a ring shape at the border between the sinus venosus and the atrium that forms the sinoatrial valve (Tessadori et al., 2012). Thus, its mechanical environment within the heart and the experimental stretch conditions are both very different than for that of the mammalian SAN, restricting the viability of the zebrafish for the study of the mechanical determinants of the chronotropic response to SAN stretch.

2.4.2. Determinants of the Chronotropic Response to SAN Stretch

In this work, we have shown that the SAN stretch induced increase in BR in zebrafish is time-, magnitude-, and direction-dependent. The temporal nature of the stretch response is demonstrated in the time to peak response. Even though BR immediately increased with SAN stretch in the zebrafish, there was a delay to the peak response. After stretch is released, the SAN returns to baseline BR over a similar timescale.

Although time to peak was not reported in previous studies, in the representative figures the peak response appears to occur immediately upon SAN stretch in the guinea pig, rabbit, and dog (Figure 2.9, Brooks et al., 1966; Chiba, 1977; Kamiyama et al., 1984; Cooper and Kohl, 2005). This discrepancy may point to the involvement of a slowly activating second messenger system provoking the chronotropic response to SAN stretch in the zebrafish that requires time to reach maximal response and time for its removal after a return to baseline tissue length. Alternatively, this could potentially be explained by the mechanical properties of the zebrafish SAN. Its ring shape may alter the dispersion of strain throughout the pacemaker compared to stretch of the sheet-like structure of the mammalian SAN. Due to these structural differences, in this way the zebrafish is a disadvantageous model species for studying the mechanical determinants of SAN stretch.

The temporal-dependence of the response also identifies further areas for investigation and highlights the importance of stretch timing. It has been shown in ventricular myocytes that stretch effects are AP phase-dependent (Hansen et al., 1990; Calkins et al., 1991; Franz et al., 1992; Nishimura et al., 2008). In the rabbit isolated SAN it has also been shown that sinusoidal stretching, rather than sustained stretch, can result in frequency- and timing-dependent changes in SAN firing (Ushiyama and Brooks, 1977). This is undoubtedly more physiologically relevant than sustained activation, as *in situ* the SAN is stretched only during atrial filling, which is a transient, non-sustained event. Under normal conditions, SAN stretch will be greatest during SDD, when SAN cells are moving towards AP initiation, 'mechanically priming' them (Quinn and Kohl, 2012) to adjust to diastolic load on a beat-by-beat basis. This facilitates the ability of the heart to match cardiac output (BR x stroke volume) to venous return. On the contrary, in pathophysiological conditions that involve dyssynchronous contraction, systolic or early diastolic stretch could occur, affecting cell repolarisation and thus potentially slowing BR or destabilising function. Despite this, most SAN stretch studies (including the present study) have utilised sustained and sometimes excessive stretch. Because the timing of stretch application is important, experiments seeking to understand SAN stretch mechanisms would optimally be controlled to mimic physiological and/or pathophysiological states. Studies investigating the effects of cardiac cycle-synchronised stretch are required to understand the importance of phase timing for the chronotropic response to SAN stretch. Thus, the aim of my second objective was to investigate this by utilising the

zebrafish, as it has now been established here as a useful model to study SAN stretch mechanisms.

It has been previously established in other species that chronotropic responsiveness is stretch-magnitude dependent, with larger stretches causing greater increases in BR (Quinn and Kohl, 2012). This magnitude-dependence remains consistent with stretch of the zebrafish SAN. Beyond this, the mechanical parameter(s) dictating chronotropic responsiveness are still unknown. Specifically, if the SAN is preferentially responding to strain (stretch) or stress (tension) remains uncertain and challenging to disentangle. Some previous studies have applied constant strain to the SAN (Deck, 1964; Kamiyama et al., 1984) whereas others have applied constant stress (Brooks et al., 1966; Chiba, 1977; Arai et al., 1996; Cooper and Kohl, 2005), and both result in positive chronotropic changes in BR. In the zebrafish, the direction of stretch also determined chronotropic responsiveness, with stretch in the short-axis direction resulting in greater increases in BR than stretch in the long-axis direction. Previously it has been shown that there is an effect of the spatial nature of stretch in the rabbit SAN, in which concentric stretch resulted in a greater chronotropic response than linear stretch (Deck, 1964). It is possible that the dependence on the direction of stretch in the zebrafish may reflect an influence of anisotropic tissue properties, which could affect the spatial distribution of stress and/or strain across the pacemaker. Despite the same baseline inter-hook length in both the short- and long-axis direction and the consistent stretch magnitudes, the SAN ring may have been experiencing different baseline and applied forces.

To address this, in my third objective I apply a consistent preload and measure the applied force in further zebrafish SAN stretch experiments in an attempt to reduce the considerable inter-subject variability of the stretch-induced change in BR recorded in my initial experiments. Further, this approach is replicated in the rabbit and mouse SAN in order to understand the structural and mechanical factors influencing the chronotropic response to SAN stretch due to the limitations of the disadvantageous morphology of the zebrafish SAN for mechanical studies. Force measurements and structural imaging during SAN stretch experiments in mammalian species helps provide insight into these unanswered questions regarding the mechanical parameters that determine the magnitude of the stretch-induced change in BR.

2.5. CONCLUSION

The zebrafish responds to sustained SAN stretch with an increase in BR, which is consistent with the response in humans and most mammals. Mechanical regulation of the SAN is an important BR control mechanism, allowing adaptation of the heart to changes in venous return on a beat-by-beat basis. Although it has been known for over a century that changes in mechanical loading of the right atrium results in alterations in BR, mechanisms eliciting this response remain unknown. A contributing factor to this may be the lack of an appropriate genetically modifiable model species. Due to its functional and genetic similarities to human, the relative ease of its genetic modification, and – as determined in this work – its conserved response to SAN stretch, the zebrafish is an innovative and advantageous model for studying the molecular and electrophysiological mechanisms underlying this important physiological phenomenon.

Figure 2.1. Zebrafish isolated SAN stretch experimental setup.

(A) Three-axis micromanipulators mounted on piezoelectric linear translators to allow for the positioning and manipulation of micro-sized glass hooks into the zebrafish isolated SAN ring. ECG measured using a suction microelectrode. Experiments performed in a heated and bubbled bath under an upright microscope. (B) Custom-made micro-sized glass hooks constructed from single-barrel borosilicate glass capillaries. (From MacDonald et al., 2017).

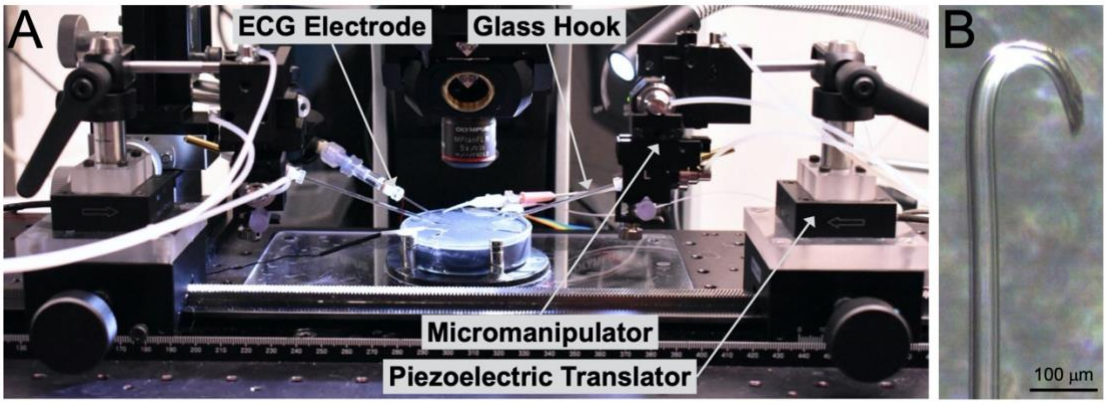

Figure 2.2. Zebrafish isolated SAN stretch representative preparation.

(A) Isolated zebrafish atrium pinned flat exposing the oval SAN ring (outlined by pink dashed line), in which glass hooks were inserted opposing each other in the long- or short-axis direction (long-axis: red dashed line; short-axis: red solid line) and separated to the pre-stretch position, with ECG measured by a suction microelectrode. (B) 25% and (C) 50% short-axis SAN stretch. (Adapted from MacDonald et al., 2017).

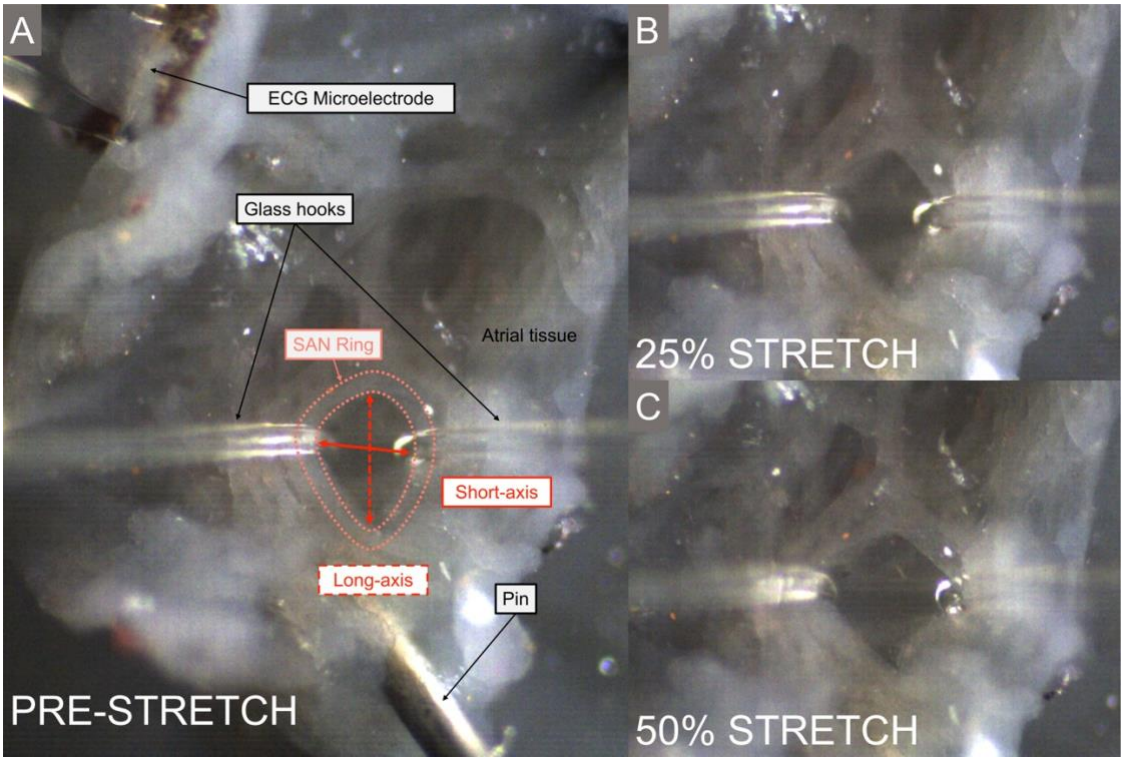

Figure 2.3. Zebrafish isolated SAN stretch representative data.

ECG temperature, BR, and stretch magnitude signals for four repetitions of 25% short-axis stretch. (From MacDonald et al., 2017).

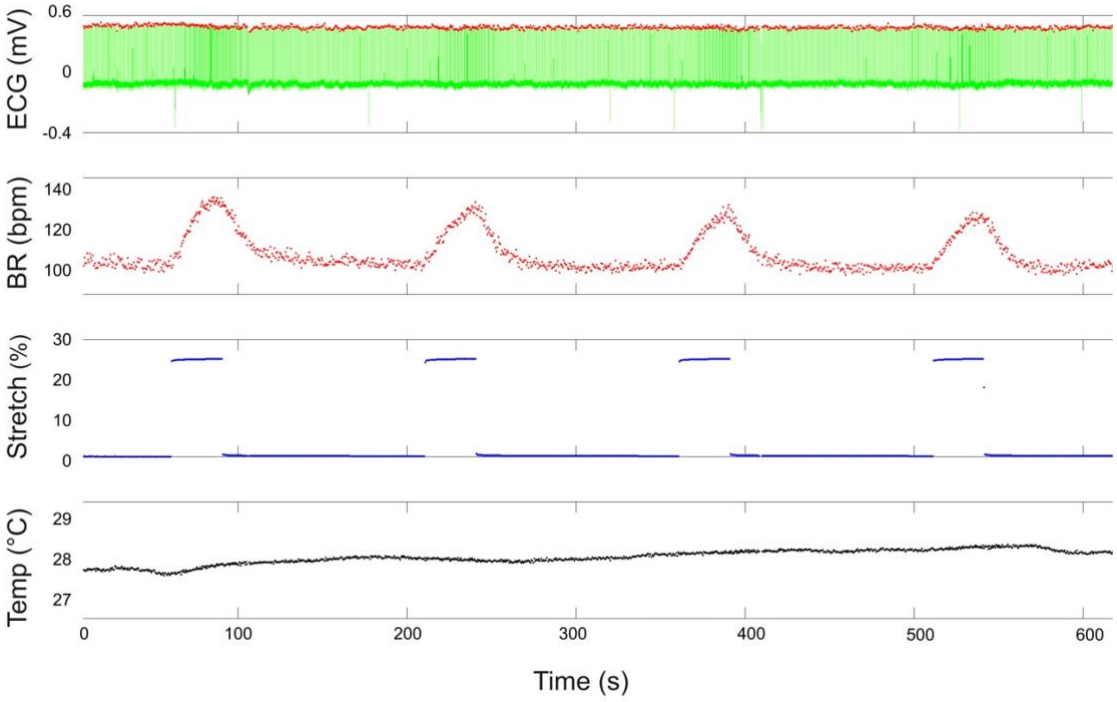

Figure 2.4. Stretch-induced changes in beating rate with zebrafish SAN stretch. Baseline, average, and peak BR for 10, 25, and 50% stretch in the (A) long-axis and (B) short-axis direction. *p<0.05 for average vs. baseline and #p<0.05 for 50% vs. 10 or 25%. (Adapted from MacDonald et al., 2017).

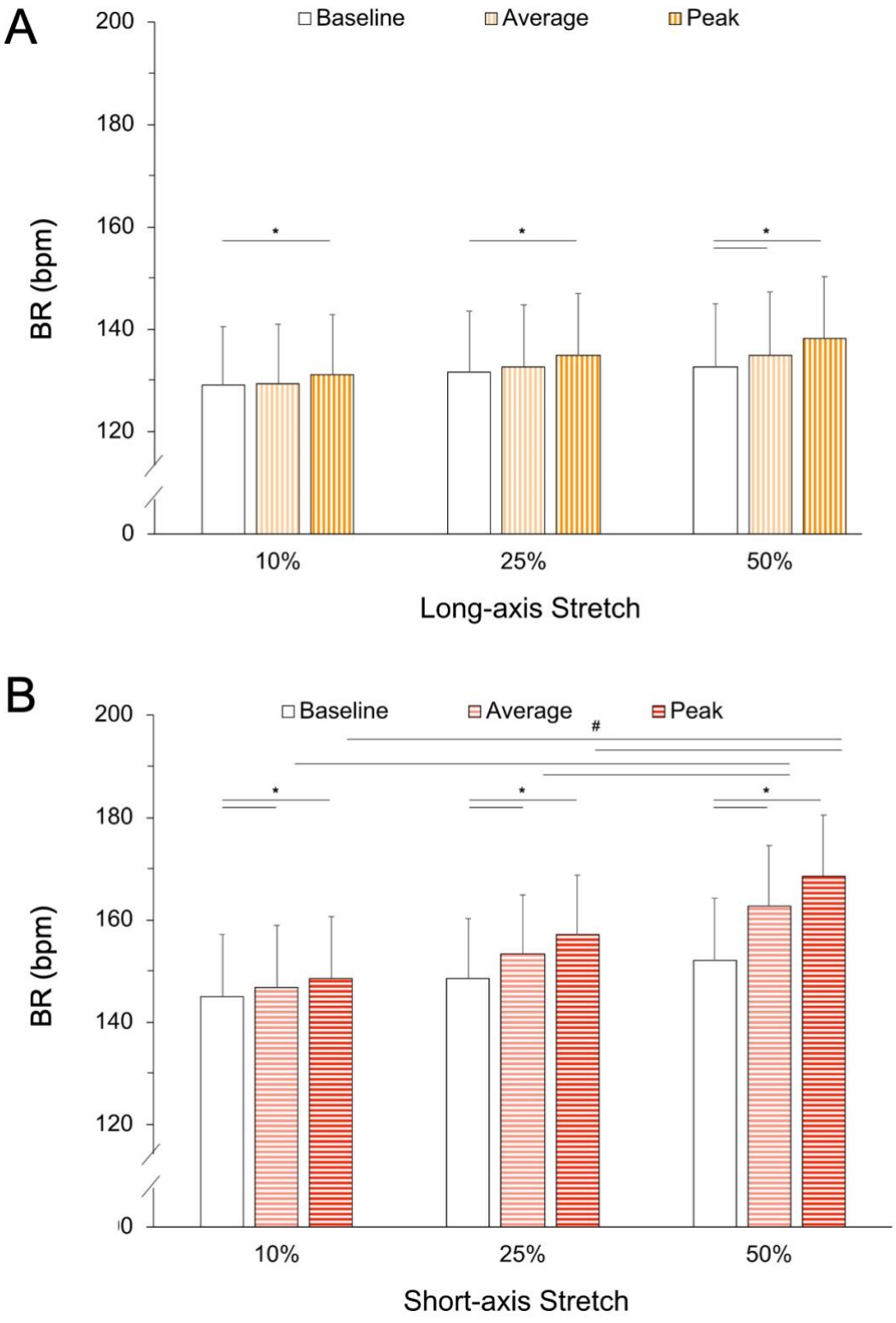

Figure 2.5. Directional dependence of the chronotropic response to zebrafish SAN stretch.

Peak percentage change in BR for 10, 25, and 50% stretch in the long-axis (orange, vertical stripes) compared to the short-axis (red, horizontal stripes) direction. *p<0.05 for short-axis vs. long-axis. (Adapted from MacDonald et al., 2017).

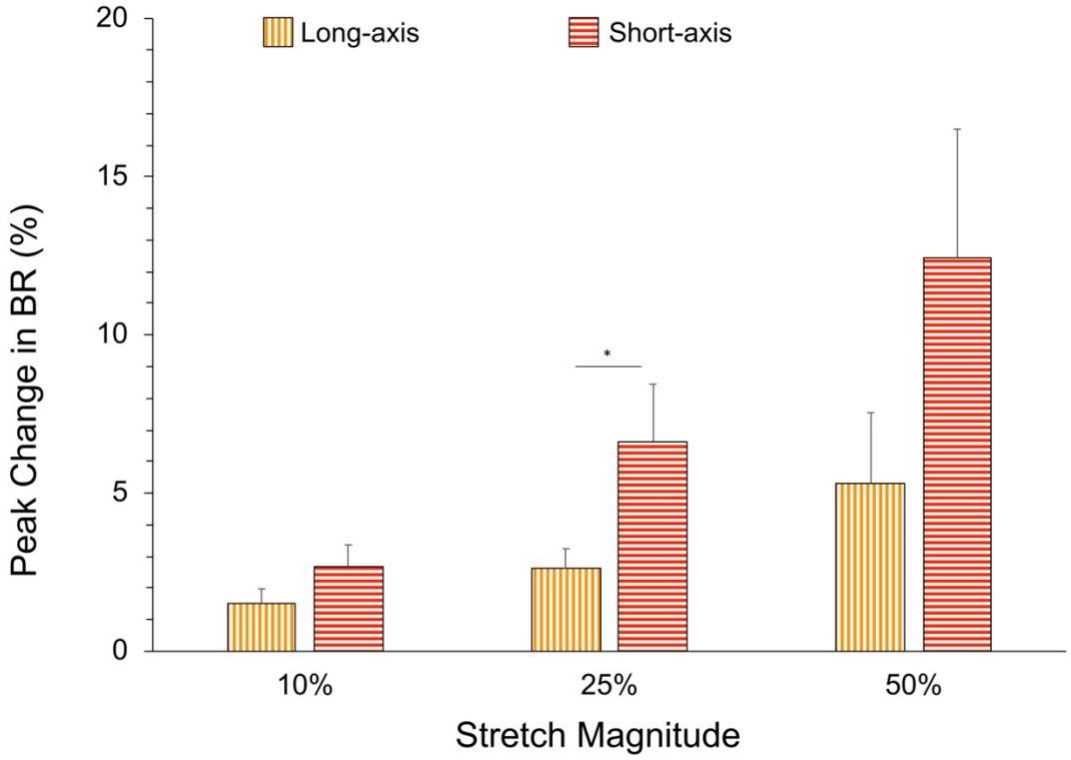

Figure 2.6. Temporal dependence of the chronotropic response to zebrafish SAN stretch.

Average and peak percentage change in BR for 10, 25, and 50% stretch in the (A) long-axis and (B) short-axis direction. *p<0.005 for peak vs. average. (Adapted from MacDonald et al., 2017).

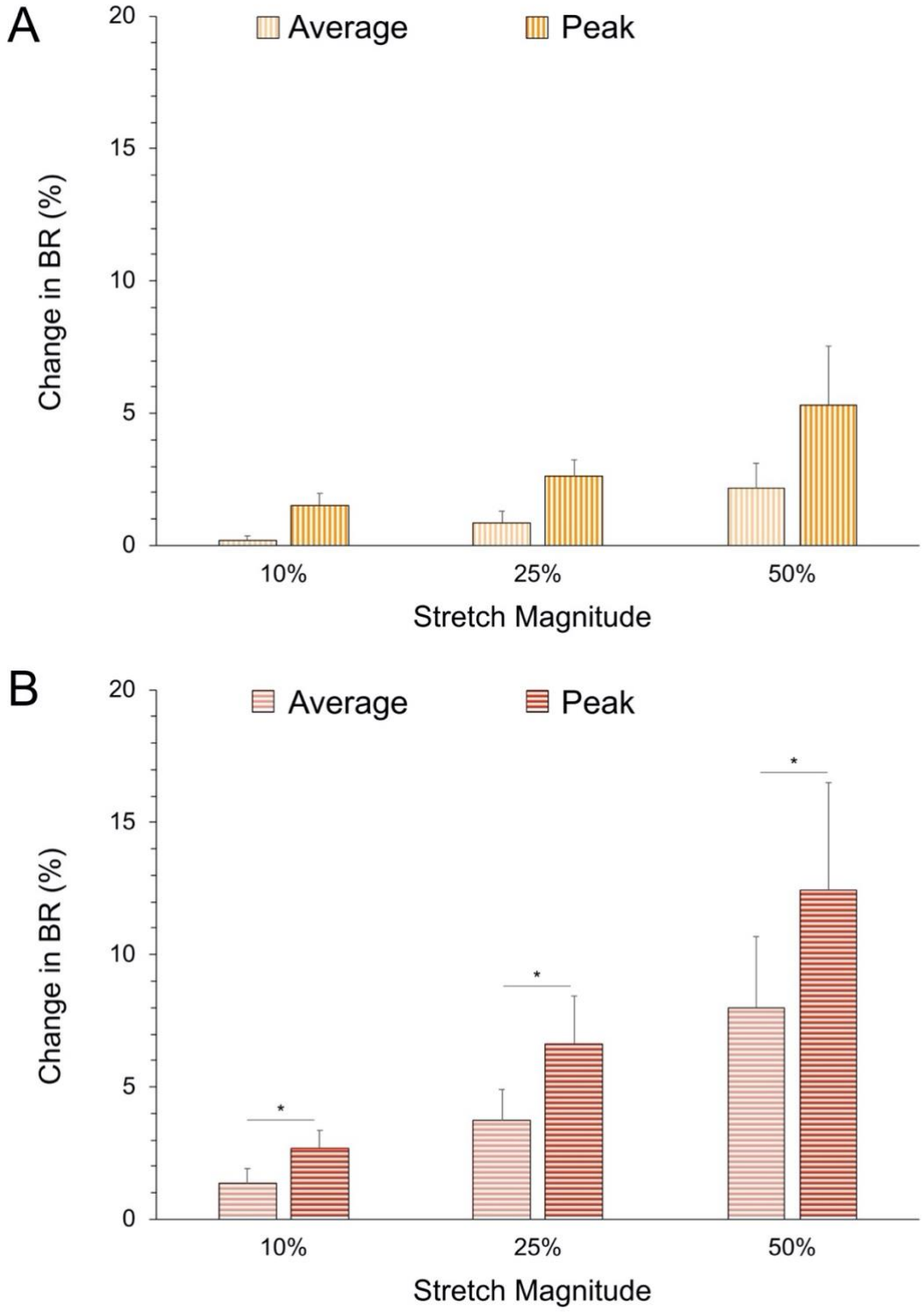

Figure 2.7. Chronotropic response to zebrafish SAN stretch.

Absolute average (small squares) and peak (large squares) change in BR for 10, 25, and 50% stretch in the long-axis (orange) and short-axis (red) direction. (Adapted from MacDonald et al., 2017).

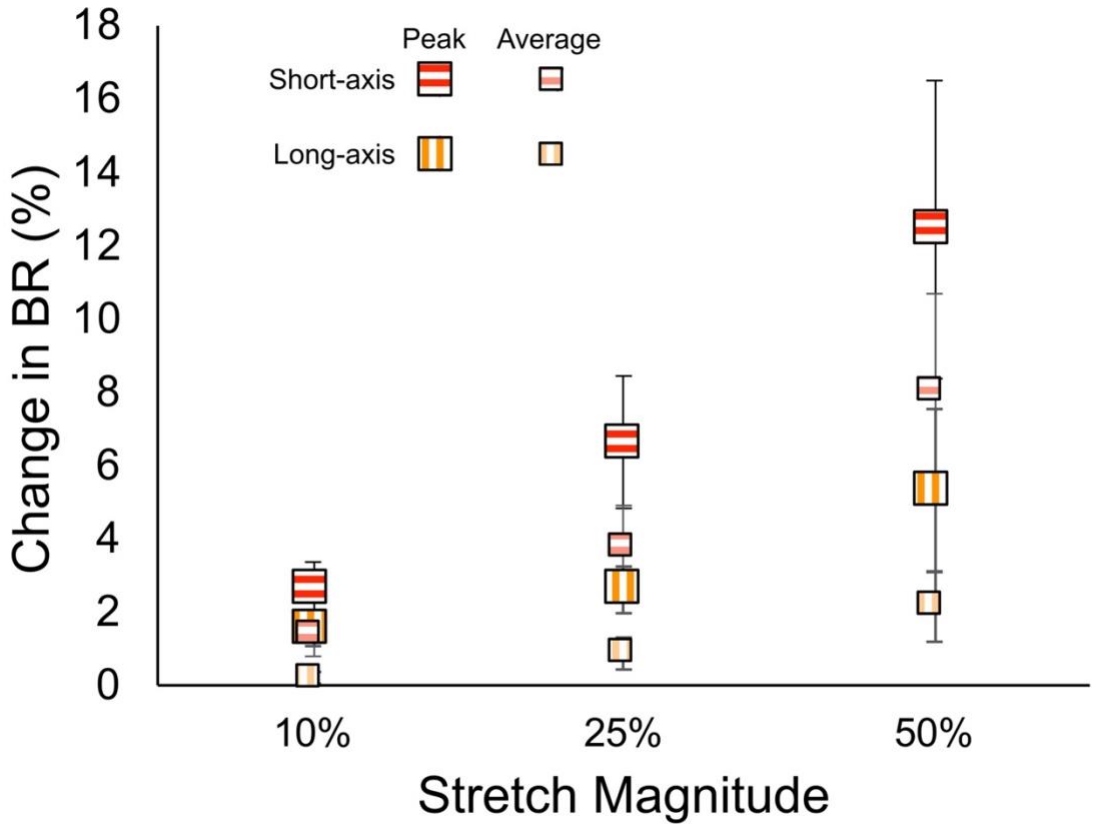

Figure 2.8. Inter-beat variability with zebrafish SAN stretch.

Standard deviation (SD) of BR at baseline and during 10, 25, and 50% stretch in the (A) long-axis and (B) short-axis direction. *p<0.05 for stretch vs. baseline. (Adapted from MacDonald et al., 2017).

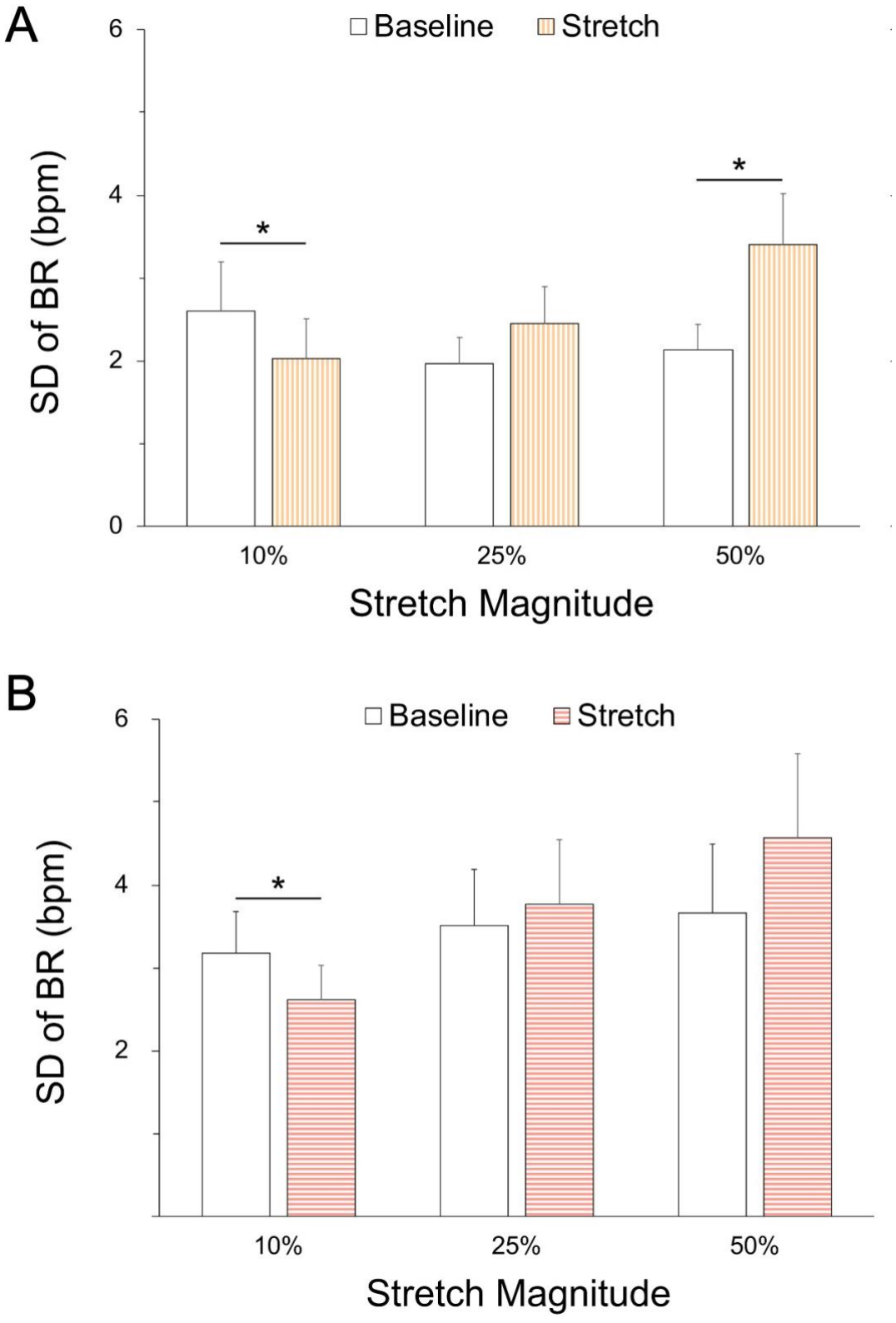

Figure 2.9. Zebrafish and rabbit isolated SAN stretch representative data.
Examples of the change in BR observed in the rabbit (A) and zebrafish (B) following SAN tension/stretch application. (Data in A from Cooper and Kohl, 2005).

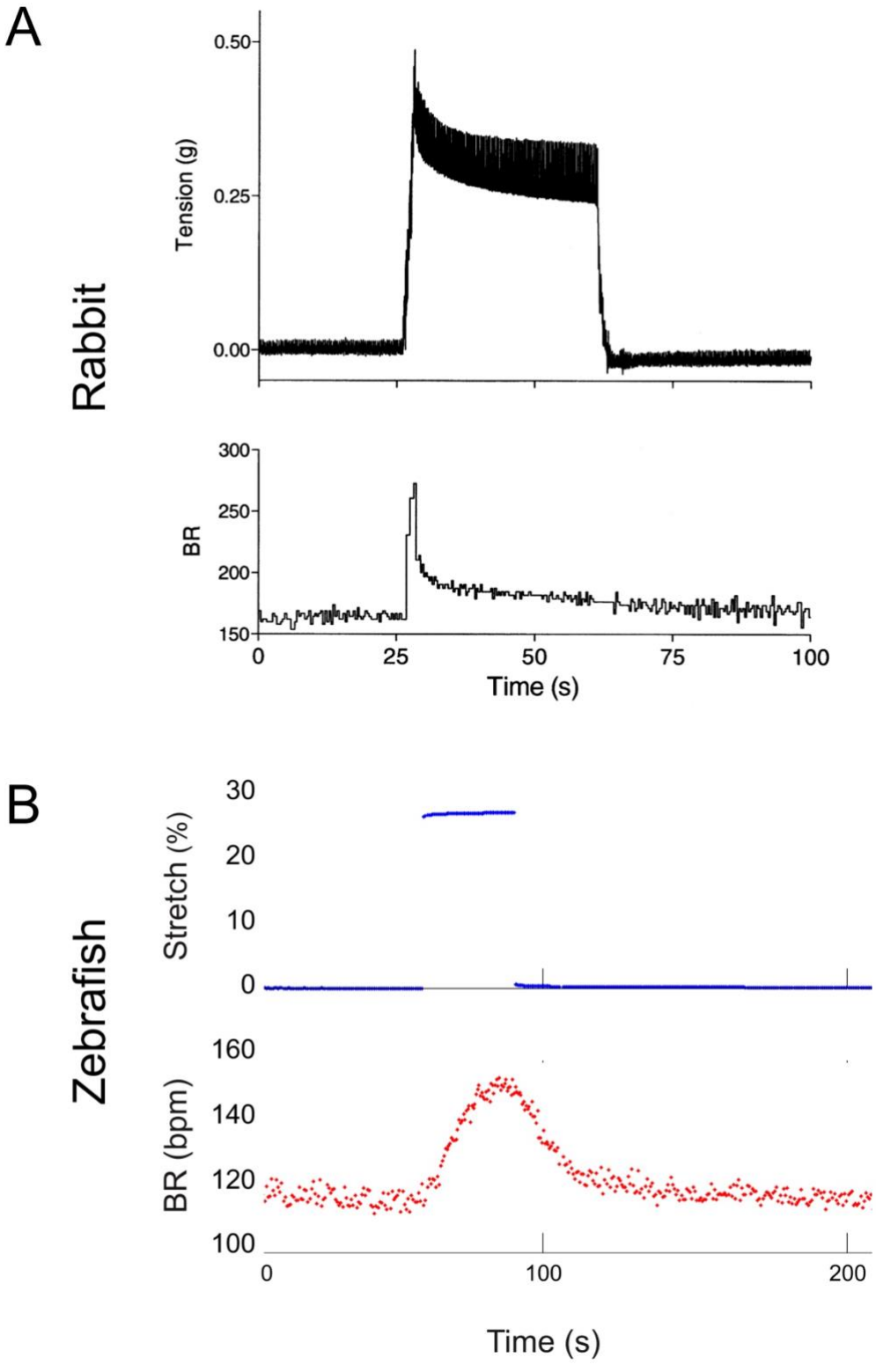

CHAPTER 3: INVESTIGATIONS REGARDING THE IMPORTANCE OF ACTION POTENTIAL MORPHOLOGY AND CHANNEL ACTIVATION TIMING FOR THE CHRONOTROPIC RESPONSE TO SAN STRETCH

3.1. INTRODUCTION

With the zebrafish newly identified as a useful genetically modifiable model species for studies of SAN stretch responses, determining how to best utilise the zebrafish for these investigations became the next step. It has been suggested that $I_{SAC,NS}$ may be responsible for the chronotropic response to SAN stretch and thus genetically targeting the channel(s) passing this current would be a logical approach. However, the molecular identity of the channel(s) passing $I_{SAC,NS}$ are unknown, making this approach currently unachievable (Peyronnet et al., 2016). To overcome this constraint, I instead employed an optogenetic approach, using a light-activated channel as a surrogate for $I_{SAC,NS}$, to interrogate the possible contribution of $I_{SAC,NS}$ in the chronotropic response to SAN stretch, and the importance of AP morphology and channel activation timing in this response.

3.1.1. Optogenetics for Cardiac Electrophysiological Investigations

Optogenetic techniques are an elegant methodology for the precise observation or control of the biological function of cells, tissues, or organs (isolated or *in vivo*) using genetically-expressed proteins that respond to light (Deisseroth et al., 2006). Some photo-sensitive proteins fluoresce in response to changes in biochemical or electrical parameters, such as membrane voltage, ion concentration, or pH, allowing one to observe changes in cellular states through changes in fluorescent signals. Control of cellular activity is also possible with light-activated channels, transporters, or enzymes, and began with the discovery of channelrhodopsins: light-gated cation channels from green algae (Nagel et al., 2002). Although originally a tool for neurobiological research, in the past decade optogenetic techniques have been effectively transferred to the heart and have become a powerful and innovative tool for cardiovascular research. They are commonly utilised and have many applications, including both for visualisation and control of cardiac activity (as reviewed by Schneider-Warme, 2018; Ferenczi et al., 2019; Joshi et al., 2020) with some examples to follow.

Optogenetic approaches have been successfully employed many times for visualisation of electrophysiological changes within the heart. For instance, utilising a

line of transgenic zebrafish expressing both voltage and Ca^{2+} sensors allowed for spatiotemporal electrophysiological measurements of BR, electrical activity, and Ca^{2+} handling, in both *in vivo* embryo hearts and isolated adult hearts, at baseline and in response to pharmacological agents (van Opbergen et al., 2018a). Not only do optogenetic approaches allow for visualisation of the heart, they have also been utilised to control cardiomyocyte excitability. Specifically, Bruegmann et al. employed a transgenic mouse model expressing channelrhodopsin-2 (ChR2) in cardiomyocytes, enabling them to depolarise the tissue with blue light pulses, stimulate APs, and pace the heart from the right atrium, ventricles, or the septum (Bruegmann et al., 2010). Arrenberg et al. optically paced or transiently arrested zebrafish hearts with blue or orange light pulses using two transgenic strains: one expressing ChR2 and the other a light-activated chloride pump (Arrenberg et al., 2010). These studies were the first examples of optogenetic approaches successfully overtaking cardiac electrophysiology to either pace or silence the heart. This has also been accomplished in a ChR2 expressing mouse SAN preparation optically paced with concurrent Ca^{2+} and voltage optical mapping (Dong et al., 2019).

Subsequently, optogenetic control of cardiomyocytes has been utilised to moderately manipulate APs. In a study using neonatal rat cardiomyocytes expressing ChR2, blue light pulses were able to increase AP duration by lengthening the repolarisation phase (Park et al., 2014), demonstrating the ability to subtly alter cellular electrophysiology, rather than simply overtaking or silencing its activity. The inverse – subtle manipulation of V_m resulting in decreased AP duration by shortening the repolarisation phase – was demonstrated a few years later with green light pulses activating an anion channelrhodopsin expressed in neonatal rat cardiomyocytes (Govorunova et al., 2016), which was replicated in the intact and whole zebrafish heart (Kopton et al., 2018). Controlling cardiac activity can also be achieved with optogenetic manipulation of non-cardiomyocyte cells types in the heart. For example, in a transgenic mouse line expressing ChR2 in parasympathetic neurons, illumination of the epicardium in the SAN region allowed for temporally-controlled cholinergic-mediated slowing of BR (Moreno et al., 2019).

Optogenetic termination of atrial fibrillation (AF) has been demonstrated in ChR2 mice and in an *in silico* human model in the hope of generating a potentially pain-free and less harmful approach for defibrillation compared to electrical cardioversion (Boyle et al., 2018; Bruegmann et al., 2018). Specifically, in mice expressing both ChR2 and

an AF-promoting mutation, epicardial blue light illumination of the atria terminated AF episodes in both *in vivo* and explanted hearts (Bruegmann et al., 2018). In the computational study, by using models of human hearts that included ChR2, they were able to reliably terminate atrial tachycardia with endocardial illumination (Boyle et al., 2018). Similar experimental strategies have been conducted in the ventricle, with optogenetic stimulation terminating ventricular arrhythmias in mouse, rat, and simulated human hearts (Bruegmann et al., 2016; Nyns et al., 2017; Funken et al., 2019).

As these examples demonstrate, in both zebrafish and mice, optogenetic techniques are a useful tool for visualising changes and overtaking, or silencing electrophysiological activity, both in physiological and pathophysiological settings. They have also been used to precisely and moderately adjust electrophysiological activity, rather than fully controlling it. In combination with computational simulations and pharmacological investigations, the present study utilises precisely timed ChR2 activation to manipulate SAN function.

3.1.2. Computational Modelling for Cardiac Electrophysiological Investigations

The first cardiac computational cell model was developed by Denis Noble in 1960 building on the seminal Hodgkin-Huxley concepts to reproduce a Purkinje cell AP in a mathematical formulation consisting of three ion fluxes (Noble, 1960). Since then, cardiac computational models have become much more sophisticated based upon decades of interactive iteration between experiment and theory (Noble and Rudy, 2001). Current theoretical models, built and validated using experimental data, have utility for integrating and expanding our knowledge base in order to generate new hypotheses, make predictions, and test their plausibility, which can result in future experimental aims (Quinn and Kohl, 2013) and clinically predictive power (Trayanova et al., 2012).

Shortly following his original Purkinje cell model, Noble modified his original model to replicate pacemaker cell activity (Noble, 1962). This model, however, had many limitations (such as the absence of a Ca^{2+} current). A subsequent iteration that he and his colleagues produced (based upon voltage clamp analysis of single cells) was greatly enhanced, containing a Ca^{2+} current and the presence of an AP without rapidly activated Na^{+} currents (McAllister et al., 1975). These advances continued, resulting in the development of increasingly complex and highly detailed single SAN pacemaker cell models, generated from the extensive experimental progress made in cardiac cellular electrophysiology (Wilders, 2007). Although these computational models had

become more comprehensive, they remained limited as they did not adequately represent the complexities of intracellular Ca^{2+} handling or autonomic responses (Wilders, 2007). More recently, models of mouse (Kharche et al., 2011), guinea pig (Himeno et al., 2008), and rabbit (Maltsev and Lakatta, 2009; Severi et al., 2012) single SAN pacemaker cells have incorporated both detailed Ca^{2+} handling dynamics and autonomic inputs, resulting in models that more accurately represents reality. A lack of experimental data has hindered the development of a human SAN cell model, but this has been recently overcome using available human data and either animal experimental data or theoretical assumptions for the parameters for which human data was not available (Pohl et al., 2016; Fabbri et al., 2017).

Computational modelling of the SAN has provided important insights, including into the response of SAN cells to stretch. Specifically, sustained stretch results in an increase in MDP and a reduction in MSP and an increase in BR without an increase in the slope of SDD, which is both consistent with the experimental data and is compatible with the computationally-derived hypothesis that the response is the result of SAC_{NS} activation (Cooper et al., 2000). Thus, under the appropriate circumstances, implementation of computational modelling can enhance and expand experimental investigations. In the present study, in an attempt to investigate the potential role of SAC_{NS} in the SAN stretch-induced chronotropic response, both optogenetic and computational approaches are employed.

3.1.3. SAC_{NS} and AP Morphology

The relationship between the $E_{SAC,NS}$ (the reversal potential of $I_{SAC,NS}$) and the SAN AP is an essential consideration when considering the effects of stretch on BR. Because $E_{SAC,NS}$ is between -20 and 0 mV, it is also in-between the MDP and MSP of the SAN AP (Guharay and Sachs, 1984; Cooper et al., 2000). Therefore, the direction of the cation current passing through SAC_{NS} will switch depending on the V_m, such that in some phases $I_{SAC,NS}$ will be an inward, depolarising current whereas in others it will be an outward, repolarising current (Figure 1.8). If $I_{SAC,NS}$ is activated throughout the SAN AP, the net effect of its activation should be proportionate to the phases in which it aids the active pacemaking currents (SDD, early repolarisation) *vs*. the phases in which it counteracts them (late upstroke, late repolarisation). Accordingly, the net effect should be dependent on AP morphology.

Due to distinct ion channel expression, SAN AP morphology has species-specific differences (Nemtsas et al., 2010; Kalyanasundaram et al., 2019). Within each species, the SAN is electrophysiologically heterogenous, with variations in ion channel expression across the node and, consequentially, differences in AP morphology throughout (Opthof et al., 1987a; Monfredi et al., 2018). Further, AP morphology in individual SAN cells varies or changes when intracellular signalling pathways become activated or inactivated (Bucchi et al., 2007). Therefore, it would be overly simplistic to assert that the SAN AP morphology for each species has one specific, distinctive shape. With this caveat in mind, there are general differences in the AP morphology between species that can be noted (especially in primary pacemaker cells), and thus may alter the net effect of sustained $I_{SAC,NS}$ activation.

For instance, the rabbit SAN AP is characterised by a relatively long period of SDD (~50% of the cycle length) and a prominent plateau phase (~25% of the cycle length, Opthof et al., 1987b), resulting in a greater proportion of the SAN cycle (~ 75%) during which $I_{SAC,NS}$ activation would aid the active pacemaking currents, rather than hinder them, such that the net effect should be an increase in BR. In zebrafish, there is also a greater proportion of the SAN AP during which $I_{SAC,NS}$ activation would shorten the cycle length (~ 70%), and increase BR (Tessadori et al., 2012). Conversely, in the mouse SAN, SDD and the AP plateau are proportionately shorter, and the net effect of $I_{SAC,NS}$ activation is more closely balanced between increasing (~ 55%) or decreasing (~ 45%) BR (Verheijck et al., 2001). This conceptual explanation (Figure 3.1) supports the suggestion that the chronotropic response to SAN stretch is mediated by $I_{SAC,NS}$ activation and, as a result, sustained stretch causes an increase in BR in most species but a decrease in the mouse, because of differences in AP morphology (Cooper et al., 2000). Although this is a feasible theory, it requires further investigation and experimental validation.

Once the zebrafish was identified as a useful model for studying mechanisms eliciting SAN mechano-sensitivity, the next target became testing the feasibility that SAC_{NS} activation elicits the SAN stretch response. The zebrafish is an advantageous model for this because BR increases in response to stretch (as it does in humans), and it is genetically modifiable. However, because the molecular identity of SAC_{NS} is unknown, there is no specific gene to target. There are a multitude of possible candidates (Peyronnet et al., 2016), but generating a multitude of zebrafish lines in hopes of identifying one is outside of our scope and expertise. Further, $I_{SAC,NS}$ may in

fact be the result of ions flowing through more than one stretch-sensitive channel, therefore individually targeting single molecular candidates could be misleading or could result in only partial understanding. Therefore, to address this question an unconventional approach was pursued.

Conveniently, the current passed by ChR2 (I_{ChR2}) has very similar characteristics to $I_{SAC,NS}$. Most importantly, the E_{rev} of I_{ChR2} (E_{ChR2}) in cardiac myocytes, like $E_{SAC,NS}$, is also between -20 and 0 mV (Bruegmann et al., 2010), which is the characteristic of $I_{SAC,NS}$ critical for our hypothesis (Figure 3.2 A). Further, the current-voltage (I/V) relationships of both $I_{SAC,NS}$ and I_{ChR2} myocytes are linear over the voltages of the SAN AP (Cooper et al., 2000; Bruegmann et al., 2010), the on-off kinetics of both currents are relatively fast, and they have similar current to stimulus magnitude (*i.e.,* light intensity or pressure) relationships (Drs. Remi Peyronnet and Franziska Schneider-Warme, IEKM, Germany; personal communication, data not shown). Because the molecular identity of SAC_{NS} is unknown and thus cannot be genetically targeted, the similarities between these currents suggest that ChR2 can be utilised as a surrogate for SAC_{NS} to investigate its effect on the SAN AP and BR. Thus, ChR2 provides a non-invasive approach for stimulating a "SAC_{NS}-like" current at different time points within the cardiac cycle. This approach enables testing of the feasibility that a SAC_{NS}-like current (I_x) could be responsible for the species differences observed with sustained stretch and allows for investigations into the hypothesis that the relationship between E_{rev} and AP morphology influences the response to current activation. This is an advantageous approach compared to rapid SAN stretches as the light pulses can be easily manipulated and can be very short in duration (which is problematic for stretch due to cell viscoelasticity). Further, this is a cleaner, more controlled approach to understanding the specific effects of SAC_{NS}-like current activation as other mechanosensitive components of the SAN (such as the pacemaking components described in the Introduction) will not be activated. This simplified model is therefore an appropriate and useful tool for understanding this complex system.

Thus, my aim was to use an optogenetic approach in the zebrafish to gain further understanding into how the chronotropic response to activation of a SAC_{NS}-like current varies depending on activation timing and AP morphology. This was combined with a similar approach in the mouse, for comparison of the response to I_x activation and to determine if I_x activation could account for species differences in the response to sustained SAN stretch. The experimental results were then confirmed and recapitulated

at a cellular level and translated to the rabbit using computational modelling. Finally, this theory was tested by applying sustained stretch to the mouse SAN before and after pharmacologically lengthening the AP to observe if changes in AP morphology alter the chronotropic response to stretch.

3.2. METHODS

3.2.1. Animals

Adult transgenic zebrafish (6 - 12 months post-fertilisation) with cardiac myocyte-specific expression of humanised ChR2 (hChR2) on a *casper* background were generated using the tol2 transposase system by Sarah Rafferty. The necessary expression plasmid was created by combining hChR2 fused to an eYFP reporter (pME-hChR2(H134R)-eYFP, which was extracted from pAAV.CaMKIIa.hChR2(H134R)-eYFP, courtesy of Dr. Karl Deisseroth, Stanford), a cardiac myosin light chain-2 (cmlc2) promotor (p5E-cmlc2, courtesy of Dr. Ian Scott, University of Toronto) and p3E-polyA and pDestTol2 (courtesy Dr. Jason Berman, Dalhousie University) with LR clonase enzyme and injected into *casper* zebrafish embryos along with Tol2 transposase mRNA at the one cell stage. Injected embryos were screened for YFP fluorescence in the heart, tested for a functional response to light stimulation (an increase in heart rate), grown up, and incrossed for two generations before use.

Adult transgenic mice (8 - 12 weeks) with cardiac myocyte-specific expression of hChR2 on a C57BL/6J background were bred by crossing mice with Cre-recombinase under the control of the αMHC (alpha-myosin heavy chain) promotor (αMHC-Cre, The Jackson Laboratory Stock No. 011038) with mice with floxed hChR2 fused to an eYFP reporter (Ai32(RCL-ChR2(H134R)/EYFP, The Jackson Laboratory Stock no. 024109), such that ~ 25% of offspring had ChR2 targeted to cardiomyocytes (αMHC-ChR2). PCR of genomic DNA from ear tissue samples was used to genotype mice and experiments were run on adult female double-positive offspring and age-matched litter mates not expressing ChR2 for the control groups. This transgenic line was generated by the technical team at the Institute for Experimental Cardiovascular Medicine (IEKM) at the University of Freiburg, Germany.

The Dalhousie University Committee for Laboratory Animals approved all experimental procedures for the zebrafish experiments, which followed the guidelines of the Canadian Council on Animal Care. The local Institutional Animal Care and Use Committee in Freiburg, Germany (Regierungspraesidium Freiburg, X-16/10R)

approved the experimental procedures for the mice experiments, which followed the German animal welfare laws and guidelines (TierSchG and TierSchVersV), compatible with Directive 2010/63/EU of the European Parliament on the protection of animals used for scientific purposes.

3.2.2. Experimental Protocols: Zebrafish

Zebrafish atrial preparations exposing the SAN ring were isolated, as described in my first objective, from adult ChR2 transgenic zebrafish (6 - 12 months and pinned flat in a 28 °C bath containing normal Tyrode's solution (NT, containing in mM: 140 NaCl, 5.4 KCl, 1.8 CaCl2, 1 MgCl2, 5 HEPES, 11 Glucose; pH 7.4 adjusted with NaOH). SAN preparations were positioned under an upright microscope (BX63, Olympus, Richmond Hill, Canada) with a 20× water-immersion objective (XLUMPLFLN 20XW, Olympus). For ChR2 activation, the SAN ring was illuminated with a spot of blue light, delivered by a fluorescence light source (U-HGLGPS, Olympus) through a 470/20 nm excitation filter (ET470/20x, Chroma Technology; Bellows Falls, United States) and a 50/50 dichroic mirror (21000 - 50/50 Beamsplitter, Chroma Technology). YFP expression was collected with a 500/60 nm excitation (HQ500/60M-2P Chroma), a 562 nm dichroic (FF562-Di03, Semrock; Rochester, USA), and a 578/21 nm emission (FF01-578/21-25, Semrock) filter. The microscope was set at the smallest aperture producing a 0.16 mm^2 spot that was focused onto the SAN ring. Light application was either sustained or pulsed and experiments were run in completely dark conditions. Temperature, ECG, and LED-trigger system signals were continuously recorded using the same set-up that was used during the stretch experiments in my first objective. Light intensities were measured using a USB power meter (PM16-120, Thorlabs; Newton, United States).

For the zebrafish sustained light experiments (n = 8), sustained stretch experiments from my first objective were mimicked. The SAN ring was illuminated with a blue spot of light (6.1 $\mu W/mm^2$) such that only the SAN region was illuminated for 30 s followed by 120 s in complete darkness. This was then repeated. Next, the entire procedure was repeated with increasing light intensities of: 24.3, 41.1, 58.1, and 73.8 $\mu W/mm^2$ for a total of five light intensities.

For the zebrafish pulsed light experiments (n = 8) the following eight light intensities were used: 2.3, 6.7, 7.5, 14.1, 32.4, 113.2, 270.4, and 465.3 $\mu W/mm^2$. A custom-made electrical triggering device (Nova Scotia Product Design and

Development Centre; Halifax, Canada) detected the peak of the atrial ECG activation spike and – following a specified "delay" time from the spike – triggered a 50 ms light pulse from a LED triggering system (developed in collaboration with Dr. Illija Uzelac and Dr. Flavio Fenton from the Department of Physics, Georgia Institute of Technology, USA). Thus, the light pulse occurred within a similar phase of the cardiac cycle on each beat despite any beat-to-beat variability in cycle length. The experimental protocol (Figure 3.3) began with pulsing of the lowest light intensity for 20 s at a delay time 25 ms shorter than the full spontaneous cycle length (rounded to the nearest multiple of 25). Following a 30 s rest period, the light pulse delay timing was decreased by 25 ms and again the lowest light intensity was pulsed for 20 s at the new delay time. For example, if a SAN preparation had a baseline cycle length of 305 ms, the first delay was set to 275 ms. For 20 s, a 50 ms light pulse would begin 275 ms after the ECG spike for each beat. Then the preparation would rest for 30 s. After rest, light would again pulse for 20 s, this time at a delay time of 250 ms. This protocol was repeated until a delay of 1 ms was reached (as a 0 ms delay was not technically feasible). Then the entire protocol was again repeated at each of the seven remaining light intensities with at least 3 minutes of rest between each light intensity.

3.2.3. Experimental Protocols: Mouse

Adult female ChR2 transgenic mice were sacrificed by cervical dislocation and hearts were rapidly excised and placed in a bath with NT solution, in which the atria were isolated from the ventricles and pinned down in a Sylgard-lined dish (DC 170; Dow Corning, Midland, MI). The endocardial side of the SAN was exposed by making incisions along the front surface of the superior and inferior *Venae cavae* (SVC, IVC). Excess fat and pericardial tissue were removed from the underside of the SAN. The corner edges of the SVC and IVC were pinned to leave the SAN flat against the bottom of the water-jacketed bath which was heated to 37°C and bubbled with 100% O^2. ChR2 was excited using a blue LED through a 470/20 nm excitation filter underneath a macroscope (MVX10, Olympus, Tokyo, Japan) creating a 6.2 mm^2 spot that illuminated the SAN region. Temperature, ECG (*via* a suction microelectrode), and LED-trigger system signals were recorded using the same set-up as the zebrafish experiments.

The ChR2 mouse experiments followed the same protocol as the zebrafish experiments with the following differences: (i) only three light intensities were used: 8.0, 15.1, and 30.9 $\mu W/mm^2$; (ii) light pulse duration was 10ms (rather than 50 ms) (iii)

and light pulse delay timing decreased by 10 ms each step (rather than 25 ms). Once this was completed with all three light intensities the entire protocol was repeated with 25 ms light pulse durations and 25 ms delay-step decreases.

3.2.4. SAC_{NS}-like Current Activation in SAN Cell Simulations

These simulations were performed in collaboration with the computational modelling team at the IEKM and were implemented in Matlab (MathWorks, Natick, USA) by Robin Moss. Specifically, previously optimised, publicly available rabbit (Severi et al., 2012) and mouse (Kharche et al., 2011) SAN single cell models were exported to MatLab using OpenCOR (https://opencor.ws) and were modified to include an additional "SAC_{NS}-like" current (I_x) with E_{rev} = -20 mV. The added current was limited in that it did not include dynamic on/off activation kinetics and when activated or inactivated was immediately fully activated or inactivated producing square current responses. The equation for this additional current was a Hodgkin-Huxley formulation:

$$I_x = g_x * (V_m - E_x)$$

where g_x represents the conductance of I_x and E_x represents the E_{rev} of I_x. Simulations were run to mimic sustained and pulsed light experimental work. Five different current amplitudes were utilised (4, 8, 12, 16, and 20 pS/pF) to emulate the increasing light intensities or stretch magnitudes used experimentally. I_x was active for 10 ms pulses (to reflect the shortest experimental light pulse time) and the delay time was decreased by 10 ms steps. The delay prior to I_x activation was triggered when the V_m became greater than -10 mV. The V_m was determined using the following equations:

$$dV/dt = -(I_{total})/\text{cell capacitance}$$

$$\text{mouse: } I_{total} = I_{Na1.1} + I_{Na1.5} + I_{CaL1.2} + I_{CaL1.3} + I_{CaT} + I_{Kr} + I_{Ks} + I_f + I_{to} + I_{sus} + I_{K1} + I_{st} + I_{NaK} + I_{NaCa} + I_{b,Na} + I_{b,K} + I_{b,Ca} + I_x$$

$$\text{rabbit: } I_{total} = I_f + I_{Kr} + I_{Ks} + I_{to} + I_{NaK} + I_{NaCa} + I_{Na} + I_{CaL} + I_{CaT} + I_{K,ACh} + I_x$$

where dV/dt represents the change in V_m as a function of time, I_{total} represents the total current, and all other currents are defined in the Abbreviations section.

3.2.5. Pharmacological Modulation of Mouse SAN AP During Stretch

A detailed description of the mouse SAN isolation procedure and stretch method are described in my third objective, but briefly, following cervical dislocation, the heart was rapidly excised from adult female mice (C57BL/6J, 8 - 12 weeks, n=6) and placed in a bath of NT solution. The ventricles were removed, and the atria isolated. An insect pin was gently woven through the SVC at the top of the SAN region and through the IVC at the bottom of the SAN region. The top pin was attached to a clip hanging from an isometric force transducer (PY2 72-4491, Harvard Apparatus, Holliston, MA), while a second clip, attached to a computer-controlled linear DC-servomotor (LM 1247-02-01; FAULHABER MICROMO, Clearwater, FL), was clipped to the bottom pin, allowing for precise stretch of the SAN. For this study, the SAN preparations were subjected to two 30 s periods of 40% stretch, interspersed with 120 s of rest. 4-aminopyridine (4-AP), a blocker of potassium currents important for repolarisation in mouse SAN cells, (275875; Sigma-Aldrich, St. Louis, MO; made freshly from a 25 mM stock solution in distilled water and pH titrated to 7.4 using HCl) was added to the water-jacketed chamber containing Krebs-Henseleit solution bubbled with carbogen at 37°C measured at final concentrations of 50, 100 and 500 μM, which have been shown to increase mouse SAN AP duration (by ~20%, 30% and 50%, respectively) by lengthening the plateau phase (Gonotkov and Golovko, 2013; Golovko et al., 2015). Each 4-AP concentration was incubated for two minutes before being subjected to two rounds of 40% stretch. Then, following a 20-min-washout, the 40% stretch protocol was repeated.

3.2.6. Data Analysis and Statistics

BR was determined by calculating the average over the 30 s period of sustained light or stretch; the 20 s period of pulsed light; or the 30 or 120 s periods of rest. Light intensities that caused pacing during pulsed light experiments were omitted in order to evaluate the changes with subthreshold light levels. Data are presented as mean ± SEM. One-way ANOVA was used for comparison of BR in the sustained light experiments. Two-way ANOVA was used to assess differences in BR for the pulsed light experiments based on two variables: delay time and light intensity. *Post hoc* comparisons were done using Sidak's (for sustained) or Tukey's (for pulsed) multiple comparison tests. Comparison of the absolute changes in BR at all delays for 10 vs. 25 ms light pulse duration in the mouse SAN were compared for each light intensity by unpaired Student's t-test. Changes in BR with 4-AP application were assessed with mixed-effects

analysis. A p-value of less than 0.05 was considered to indicate a statistically significant difference.

3.3. RESULTS

3.3.1. Sustained Light or Stretch: Experiments and Simulations

Sustained light activation of ChR2 in the zebrafish SAN caused an increase in BR with light intensities of 24.3 μW/mm^2 and greater (Figure 3.4). Sustained ChR2 activation in the mouse SAN also caused an increase in BR with 30.9 μW/mm^2 of light (Figure 3.5). In the rabbit SAN cell model, activation of a SAC_{NS}-like current caused an increase in AP firing rate with all current densities (Figure 3.6). In the mouse SAN cell model, however, the lowest two current densities (4 and 8 pS/pF) caused a slight decrease in BR whereas the higher three densities caused an increase in BR (Figure 3.7). In both the rabbit and mouse simulations, sustained I_x activation causes a current density-dependent reduction in AP amplitude, by way of an increased MDP and a decreased MSP.

3.3.2. Pulsed Light or Stretch: Experiments

Baseline BR did not change throughout the experiments in either species (Figure 3.8). Activation of ChR2 in both the zebrafish and mouse SAN by short, cardiac-cycle time specific light pulses, caused chronotropic changes. At high light intensities, if the light pulses paced the SAN those changes in BR were eliminated such that only changes with subthreshold light levels were evaluated (Figure 3.9). BR was dependent upon both light intensity and light pulse timing. Consistent with sustained ChR2 activation, the *magnitude* of the change in BR was dependent on light intensity, such that greater chronotropic changes occurred at higher light intensities. BR was also dependent on light pulse timing as it determined the *direction* of the chronotropic response. Pulsed light at longer delay timings resulted in an increase in BR, whereas shorter delays timings elicited a decrease in BR (Figure 3.10 and 3.11). These responses are consistent in both species (Figure 3.12). Further, light pulse duration also influenced the magnitude of the change in BR, such that a longer (25 ms) light pulse duration caused larger changes in BR than the shorter (10 ms) duration pulse (as demonstrated in the mouse SAN; Figure 3.13).

3.3.3. Pulsed Light or Stretch: Simulations

The cell-level computational modelling largely corroborated the experimental results (albeit using a rabbit SAN model in place of the zebrafish, as a zebrafish SAN model is not currently available). The change in BR elicited by I_x activation was current density-dependent, such that greater current magnitudes caused larger chronotropic changes (Figure 3.14). Also consistent with experimental data, when I_x was activated at longer delay timings it caused an increase in BR whereas at shorter delay timings it caused a decrease in BR (Figure 3.14). In both species, V_m depolarised when I_x was activated. Following depolarisation when I_x was activated at longer delay timings, SDD continued as normal, only from a higher V_m. Cycle length was shorter due to the earlier depolarisation, which resulted in an increase in BR (Figure 3.15). When activated at shorter delay timings, I_x depolarised the V_m during the "on" pulse, however, following this depolarisation V_m began to repolarise again, or "re-repolarise", from the slightly increased V_m; consequently the cycle length became longer than the uninterrupted cycle length, thus slowing BR. This slight "backtracking" induced by I_x activation caused a repolarisation delay resulting in lengthening of the cycle length, and therefore a decrease in BR (Figure 3.16). Unlike with sustained I_x activation, AP amplitude, MDP, and MSP were not affected by pulsed I_x activation.

Although in the SAN cell simulations both species responded with a decrease in BR with short light pulses and an increase with long light pulses, there are some species differences in response characteristics. The magnitude of the chronotropic response to I_x activation was much larger in the mouse simulation in both directions (40% peak decrease and 25% peak increase in BR) compared to the rabbit simulation (6% peak decrease and 11% peak increase in BR, Figure 3.17). Not only is the chronotropic response much greater in the mouse simulations compared to the rabbit simulations, it is also a much larger magnitude than the response in the mouse SAN experimentally (4% peak decrease and 8% peak increase in BR) with the same light pulse duration (10 ms). Interestingly, however, when the light pulse duration was reduced from 10 ms to 5 ms in the computational mouse model, the magnitude of the change in BR (11% peak decrease and 15% peak increase) was more comparable to the rabbit simulation and the mouse experimental data (Figure 3.18).

It is also interesting to observe that in both species only a 5 ms difference in delay time results in a switch in the direction of the chronotropic response, *i.e.,* I_x activation at a delay time of 110 ms (mouse) or 210 ms (rabbit) resulted in increased BR, whereas 115 ms (mouse) or 215 ms (rabbit) delays caused decreased BR (Figure 3.17). In the

mouse, the peak changes in BR occured at nearly the same delay times (peak decrease: 110 ms, peak increase: 125 ms) as the change from increased to decreased BR (Figure 3.17). This is not the case in the rabbit, in which the delay times that cause the peak increase (255 ms) or decrease (170 ms) in BR are not the same as the transition delay times (Figure 3.17).

Although these data support our hypothesis that activation timing contributes to determining the direction of the chronotropic response, they also demonstrate that the E_{rev} of I_x does not (at least exclusively) dictate the direction of the response. For instance, as I_x activation causes the V_m to move towards the E_{rev}, we predicted its activation would increase BR during early SDD, yet during early SDD the I_x induced depolarisation is not sufficient to increase BR and instead results in decreased BR. Visualising the effects of I_x activation on the individual currents in the model may provide insight into mechanisms driving the bi-phasic chronotropic response. The non-linear interdependence of ionic currents in SAN cells, and their strong dependence on V_m, makes determining the specific effects of I_x activation that may result in a chronotropic change difficult to clearly discern, however visualising the changes in each current with I_x activation at a delay time resulting in increased BR compared to a delay resulting in decreased BR may help distinguish this difference based on the behaviour of the current during I_x activation, and immediately after it is turned off.

Specifically, looking at the relative effects of I_x on mouse SAN cell currents from the simulations at and following the time I_x is turned off – when V_m diverges in cells whose BR increases (increasing V_m) or decreases (decreasing V_m; Figure 3.19A) – provides insight into which currents appear to contribute to (Figure 3.19B) or oppose (Figure 3.19D) the difference in the change in BR, or those which do not seem to be contributing but rather are simply following the change in V_m (Figure 3.19C). The peak increase in BR occurs when I_x is pulsed with a delay of 115 ms, after which I_{Na} is nearly three times that of I_{Na} with a stimulation delay of 110 ms (Figure 3.19B), contributing to a greater depolarising current with a delay of 115 ms. The difference in depolarising current is further enhanced by effects on I_{CaT}, as in the same time period I_{CaT} density is greater and increasing with a 115 ms delay but lower and decreasing with a 110 ms delay (Figure 3.19B). Concurrently, I_{K1} begins to decrease and becomes lower with a 115 ms delay, while it is increasing and becomes higher with a 100 ms delay, which would result in a greater repolarising current with a delay of 100 ms (Figure 3.19B). Interestingly, in the same period, I_{Kr} is increasing to a greater extent with a 115 ms

delay, which would in fact oppose the observed difference in the change in BR, but the difference in currents is much smaller than that of I_{K1} (Figure 3.19D). Overall, the result of the pulsed I_x in the region in which the V_m diverges is a whole cell inward (negative), depolarising current with a 115 ms delay, resulting in an increase in BR, and an outward (positive), repolarising current with a 110 ms delay, resulting in a decrease in BR (Figure 3.19E).

In the rabbit simulations the change in currents when comparing delay times that cause the peak increase or decrease in BR are not as apparent as in the mouse, making it less clear which currents are contributing, opposing, or not contributing to the change in BR. However, reviewing the currents during the time in which the V_m diverges from the unperturbed V_m after I_x turns off (Figure 3.20A) provides some suggestions about the contributing currents. It appears that I_{Na} and I_{CaT} may also be contributing to the difference in the chronotropic response with different stimulation delays in the rabbit, as they increase compared to the unperturbed V_m (Figure 3.20C, E). Perhaps simulations utilising a longer pulse duration or magnitude to create larger discrepancies between the currents with each delay or considering individual current densities and their interactions would provide greater clarity. Additional computational studies could provide further insight and a more thorough understanding.

3.3.4. Pharmacological Modulation of the Mouse SAN Action Potential

Linear stretch of the isolated mouse SAN by 40% of its baseline length resulted in variable chronotropic responses such that BR increased in half of the SAN tested and decreased in the other half (Figure 3.21). With application of 500 μM 4-AP there was a positive shift in the stretch-induced change in BR without an underlying shift in baseline BR (Figure 3.21). The magnitude of the stretch-induced changes in BR was not related to baseline BR before stretch (Figure 3.21C).

3.4. Discussion

This study investigates the feasibility of a SAC_{NS}-like current eliciting the SAN stretch-induced chronotropic response by using optogenetic, computational, and pharmacological approaches. Sustained activation of ChR2 increased BR in transgenic zebrafish and mice, as did SAC_{NS}-like current activation in rabbit and mouse SAN cell computational models (apart from the lowest current densities in the mouse computational model, in which a decrease in BR occurred). Pulsed activation of ChR2

caused an increase or a decrease in BR depending on light pulse timing within the cardiac cycle in both transgenic species, implicating that the direction of the chronotropic response is determined by the timing of ChR2 activation within the cardiac cycle, and therefore it may depend upon AP morphology. This was recapitulated in the SAN cell computational simulations, substantiating the experimental findings both at a cellular level and in a larger mammalian species. Finally, these theories were translated back to SAN stretch, by demonstrating that pharmacological manipulation of AP morphology can alter the chronotropic response to sustained stretch.

3.4.1. Sustained Light or Stretch Predominantly Increases BR

Sustained activation of ChR2 in the transgenic zebrafish SAN elicits a light intensity-dependent increase in BR, mimicking the response evoked by zebrafish SAN stretch. Sustained activation of ChR2 in the transgenic mouse also causes an increase in BR. When considering ChR2 as a surrogate for SAC_{NS}, this result is incompatible with the previously reported reduction in BR induced by stretch of the mouse SAN (Cooper and Kohl, 2005). This inconsistency may be due to a different underlying stretch mechanism in the mouse SAN compared to other species, or, it could implicate that $I_{SAC,NS}$ density is reduced in mice and therefore I_{ChR2} density in these experiments does not correspond with $I_{SAC,NS}$ density in the previous experiments. Computational approaches were utilised to investigate this discrepancy.

Although the computational cell simulations with sustained I_x activation predominantly resulted in faster SAN cell firing, the lowest two current densities slightly slowed BR in the mouse cell model. Thus, it is possible that the inward current elicited by sustained stretch is considerably smaller than most of the inward ChR2 currents generated in this study. Interestingly, at the lowest light intensity in the transgenic zebrafish, sustained ChR2 activation elicited a decrease in BR in some animals, consistent with the response in the mouse simulation.

Although the ChR2 mice did not respond to sustained light of any intensity with a reduction in BR, the variable and predominantly negative response observed with SAN stretch in the mouse (Cooper and Kohl, 2005) is more comparable with the variable chronotropic response in the simulation, and thus perhaps the direction of the chronotropic response to stretch is dependent on, or at least related to, current density. The sustained I_x simulations in mouse caused an increase in MDP from baseline regardless of the chronotropic response. An increase in MDP from baseline was also

observed with I_x activation in the rabbit SAN cell simulations, which is consistent with both a previous computational study of stretch and with experimentally observed stretch-induced currents, both of which also resulted in an increase in MDP (Cooper et al., 2000). In this study and in other previous reports, none of the current densities or stretch magnitudes resulted in a reduction in BR in the rabbit SAN (Quinn and Kohl, 2016). The current density-dependence of the direction of the change in BR in the mouse simulations could thus be related to differences in ion channel expression between mouse and rabbit, which would also result in the observed differences in AP morphology. It is possible that the direction of the stretch-induced chronotropic changes are dependent upon the interaction between current density, AP morphology, and $E_{SAC,NS}$. Sustained activation of I_x results in a current density-dependent depolarisation of the V_m, which will alter the activation or inactivation of voltage-dependent pacemaker currents. Regardless, cyclic SAN stretch, rather than sustained stretch is potentially more physiologically relevant, and therefore the response to acute cycle-time specific ChR2 activation required investigation.

3.4.2. Cycle Time Dependence of Light or Stretch Application in the Chronotropic Response

Pulsed activation of ChR2 induced a change in BR in both transgenic species, the direction of which depended upon light pulse timing. With high light intensities, pulsed ChR2 stimulation paced both the zebrafish and mouse heart, which is consistent with what has been previously demonstrated (Arrenberg et al., 2010; Bruegmann et al., 2010; Cheng et al., 2019). It is interesting to note that in a previous experiment with transgenic zebrafish it was demonstrated that when cardiomyocyte-specific ChR2 was activated with pulsed light at frequency near to the normal BR, BR slowed (although no explanation was given, Arrenberg et al., 2010). In the current study, the focus was to modulate BR (rather than overdrive pace the heart) using subthreshold levels of light. Fascinatingly, although sustained ChR2 activation results in increased BR, pulsed activation with subthreshold light levels could elicit an increase or a decrease in BR depending on light pulse timing. Specifically, ChR2 stimulation at longer delay timings caused increases in BR, whereas at shorter delay timings ChR2 stimulation decreased BR. This data demonstrates the ability of a channel with a reversal potential between the MDP and MSP to either increase or decrease BR, depending on the timing of its

activation. Therefore, it is possible that cardiac-cycle timed activation of $I_{SAC,NS}$ would also elicit the same response.

These results were reproduced in both a mouse and rabbit SAN cell computational model with an added SAC_{NS}-like current activated at various delay timings. Although the response was generally the same as the experimental data (increased BR with longer delay timings and decreased BR with shorter delay timings) there was a difference in the response between the species in the simulations. The peak changes in BR in the mouse computational model were much greater than the rabbit simulation (as well as those seen experimentally). This most likely relates to the fact that any given duration of light pulse in the mouse constitutes a larger portion of the total cycle length (and of the AP) compared to the rabbit, supported by the finding that a change in light pulse duration itself altered the magnitude of the response. Of course even with the same pulse duration of 10 ms, a greater response was seen in the mouse SAN model compared to the experiments, but this may relate to a mismatch between the magnitude of actual ChR2 current and the simulated SAC_{NS}-like current, or perhaps differences between tissue (experiments) and single cell (simulations) responses. Interestingly, though, the magnitude of the response was similar to the mouse experiments when a light pulse duration of 5 ms was applied to the mouse simulation.

The peak changes in BR in the mouse were caused by the same delay timings that result in a transition from decreased to increased BR, whereas in the rabbit the delays resulting in peak changes in BR are not at the transition delay timings. The simulations are powerful in that they allow us to investigate if the V_m is expected to be changing with I_x activation as hypothesised. When I_x is activated at longer delay timings (during SDD) it immediately depolarises the V_m, causing the cell to reach the upstroke threshold more quickly. When I_x is activated at shorter delay times (during late repolarisation) again the V_m immediately depolarises, however, when I_x is turned off, repolarisation "resets" and continues from the depolarised position and thus the cycle length is increased. This response was consistent in both species. What was not consistent, however, was the relationship between the peak change in BR and the delay timings over which the chronotropic response transitioned from an increase to a decrease in BR. This difference may be due to species-specific differences in ionic currents. Based on the response of the ionic currents to I_x activation it is reasonable to hypothesise the effect of I_x on I_{Na}, I_{CaT}, and I_{K1} may be responsible for the chronotropic response in mouse, whereas in the rabbit it is less clear, although I_{Na} and I_{CaT} may also

be contributing. This requires further investigation in experimental preparations using pharmacological interventions and in the computational model. Either way, as the proposed hypothesis suggested (Cooper and Kohl, 2005), specifically timed activation of I_x resulted in increased or decreased BR. However, the computational results did not match the prediction regarding the specific phases in the AP that would increase or decrease BR. For instance, during early SDD we hypothesised BR would increase due to I_x-induced depolarisation, yet BR decreased. Our hypothesis did not take into consideration effects on other currents, so although I_x caused depolarisation, its activation was not sufficient to overcome effects on other currents, which overall elicited a decrease in BR.

Interestingly, the present data resemble a previously reported phenomenon known as "phase-resetting", by which injection of a subthreshold depolarising current pulse into spontaneously beating cardiac cells causes a timing-dependent change in BR. This has been demonstrated in spontaneously beating rabbit SAN tissue preparations, in which they also showed that the phase-setting response is not neurally-mediated, as it is present during inhibition of sympathetic or parasympathetic receptors. (Sano et al., 1978). Phase-resetting behaviour is not only present in multicellular preparations and computational simulations, but also with subthreshold current pulses in individual isolated rabbit SAN cells (Anumonwo et al., 1991). In general, past phase-resetting studies, including experimental studies in SAN tissue strips (Sano et al., 1978; Jalife and Antzelevitch, 1979) and computational studies in single SAN cells (Reiner and Antzelevitch, 1985; Coster and Celler, 2003), are consistent with what we see both in our simulations and with ChR2 activation, as depolarising pulses can increase or decrease cycle length based on their timing, magnitude, and duration. Another phase-resetting characteristic comparable to our data, shown in a rabbit single SAN cell simulation, is that with low depolarising current amplitudes the transition from increased to decreased cycle length is smooth, whereas with larger current amplitudes the transition is abrupt (Tsalikakis et al., 2007b), which we observed with increasing light intensities in the ChR2 zebrafish and mouse experiments, and with increasing current densities in the simulations. It has also been shown that differences in ionic current densities between peripheral and central node cells results in a difference in phase-resetting behaviour (Tsalikakis et al., 2007b, 2007a). Specifically, a higher stimulus amplitude is required to cause a change in cycle length in peripheral cells, likely because of their larger I_{Na} density (Tsalikakis et al., 2007b). This supports our

prediction that I_{Na} is contributing to the chronotropic response in mouse, and also may help explain why in the computational mouse cell simulations we saw much greater magnitudes of chronotropic responses than in the experimental mouse SAN tissue preparations. Other computational phase-resetting studies have suggested which combination of current(s) may be responsible for the chronotropic change based on individual current plots or block of currents in the model. One study suggested: I_f, slow inward current (I_{si}; perhaps representative of I_{CaL} and I_{CaT}), and delayed rectifier K^+ currents (Reiner and Antzelevitch, 1985), while another suggested I_{si} and background current (I_b), and to a lesser extent 'the' K^+ current (Guevara and Jongsma, 1990). The contribution of I_{si} may reflect our I_{CaT} prediction, and the prediction that K^+ currents contribute to the change in BR is also consistent with our data. However, Guevara and Jongsma described that I_f and/or I_{Na} could be removed from the model with little consequence on phase-resetting behaviour, which is a direct contradiction to Reiner and Antzelevitch's and our assessment that I_f and/or I_{Na} may be predominant contributors. Finally, it has been proposed that phase-resetting properties of the SAN are essential for rhythmic coordination of SAN cells, allowing pacemaker cells to become stably and mutually entrained, such that they respond to each other or external stimuli without firing (Jalife and Antzelevitch, 1979; Ypey et al., 1982; Anumonwo et al., 1991; Verheijck et al., 1998b). For instance, it may be what allows inhomogeneous vagal innervation to slow the entire SAN and not just the regions which are innervated (Jalife and Antzelevitch, 1979). It has also been suggested that the mutual entrainment of SAN cells by phase-resetting properties may help prevent a group of irregularly fast or arrhythmic cells taking over pacemaking, by resetting their activity (Ypey et al., 1982). Thus, perhaps SAN stretch is an important and protective heart rate control mechanism because it aids in the mutual entrainment of SAN cells *via* phase-resetting responses to stretch, as well as causing BR to adapt to changes in venous return.

This ability to increase or decrease BR with ChR2 not only provides experimental validation that $I_{SAC,NS}$ may be eliciting the chronotropic response to stretch, it also holds an exciting translational potential as a therapeutic pacing technique. Currently available electronic-based pacing technologies do not allow for subtle changes in BR but instead can only overdrive sinus rate. Optogenetic approaches for pacing have previously been considered, and limitations identified (Bruegmann and Sasse, 2015). However, one major advantage, identified in this study, is that pulsed, cycle-synchronized subthreshold activation of ChR2 would allow for the fine-tuning of heart rate by subtle

modulation of the SAN, rather than over-drive pacing. Overall, this work explores fundamental physiological questions while simultaneously discovering potential translational and therapeutic advances.

3.4.3. Translating Simulations and Surrogates back to Stretch and SAC_{NS}

This combined optogenetic and computational approach offers a unique strategy for understanding the potential contribution of SAC_{NS} to the SAN stretch response. However, a SAC_{NS} surrogate and simulations can only test feasibility and generate predictions. Thus, it is important to translate these insights back to the context of SAN stretch. The difference in the chronotropic response of the SAN to stretch in mouse (a varied response, often including a decrease in BR rather than a consistent increase) can be theoretically explained by differences in the relationship between $E_{SAC,NS}$ and the disparate SAN AP shape in mouse compared to rabbit. Following that logic, an increase in the length of the plateau of the SAN AP in mouse would be expected to cause a positive shift in the stretch-induced change in BR as it increases the proportion of time that $I_{SAC,NS}$ activation would shorten cycle length. Application of concentrations of 4-AP previously shown to lengthen the plateau phase in the mouse SAN AP by ~20-50% *via* block of repolarising potassium currents (Gonotkov and Golovko, 2013; Golovko et al., 2015) consistently caused increases in BR with SAN stretch, rather than a variable response or a decrease in BR. After washout there was a negative shift in the stretch-induced chronotropic response. This result strongly supports the critical importance of AP morphology for the chronotropic response of the SAN to stretch, relating the ChR2 data and the simulations to the SAN stretch response.

3.5. Conclusion

It has been known for over a century that SAN stretch causes a change in BR, yet mechanisms underlying this response have remained elusive. It has been hypothesised that SAC_{NS} elicits this BR response, but it has been challenging to investigate this possibility because its molecular identity is unknown. Although this study does not directly investigate SAC_{NS}, the combined optogenetic, computational, and pharmacological approaches together develop our understanding of the chronotropic response to SAC_{NS}-like current activation. In both the transgenic and computational models, BR could be increased or decreased with brief ChR2 or I_x activation depending on activation timing, and pharmacologically lengthening the AP positively shifted the

chronotropic response to SAN stretch in the mouse. Taken together, these data demonstrate the importance of both AP morphology and SAC_{NS}-like current activation timing to the chronotropic response to SAN stretch.

Figure 3.1. Theoretical effects of SAC_{NS} on the SAN AP of rabbit, mouse, and zebrafish.

Experimental membrane potential recordings from each species show the relation of electrophysiological parameters and SAC_{NS} reversal potential ($E_{SAC,NS}$). The time periods during which SAC_{NS} activity would either accelerate (green) or slow (red) BR are indicated. In rabbit and zebrafish, SAC_{NS} would accelerate changes in V_m during most of the action potential, while in mouse there is a greater proportion of time in which $I_{SAC,NS}$ activation would cause slowing. (Adapted from MacDonald et al., 2017).

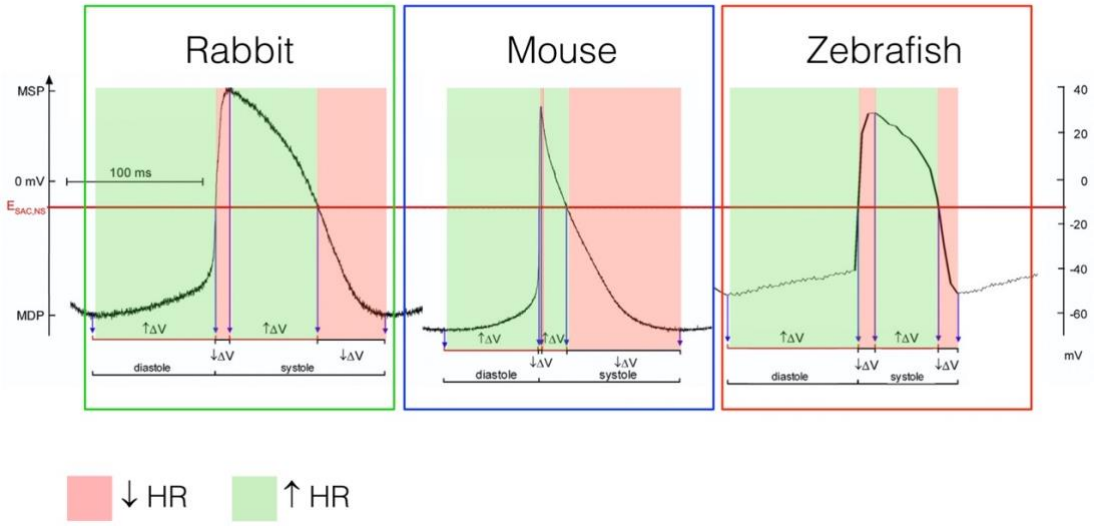

Figure 3.2. Comparison between $I_{SAC,NS}$ and I_{ChR2} characteristics.

Current-voltage relationship for each current demonstrating reversal potentials between -20 and 0 mV. (From Cooper et al., 2000 and Bruegmann et al., 2010).

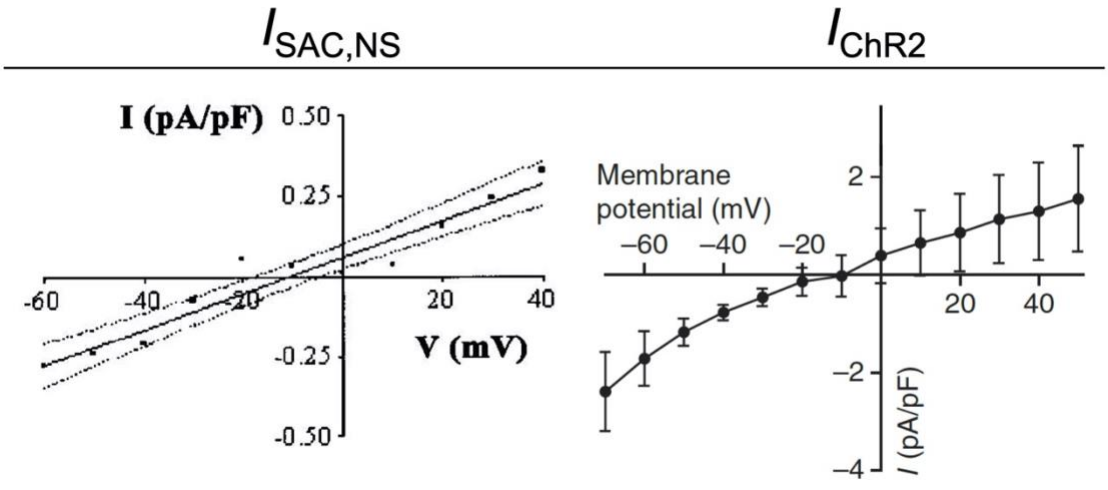

Figure 3.3. Experimental protocol for zebrafish pulsed light experiments.

(A) Light pulses of 50 ms duration and at the lowest light intensity (LI) occur following the ECG activation spike after Delay 1 (D1), a delay 25 ms shorter than the intrinsic cycle length (CL) rounded to the nearest multiple of 25. Light is pulsed at D1 for 20 s, followed by 30 s rest. (B) Light pulsed at Delay 2 (D2) which is a delay 25 ms shorter than D1. (C) This procedure is repeated multiple times with the delay time decreasing by 25 ms each step, until a delay of 1 ms is reached. (D) Following a 3-minute rest period, the entire protocol is repeated with each LI, beginning with D1 and ending with delay = 1 ms for each.

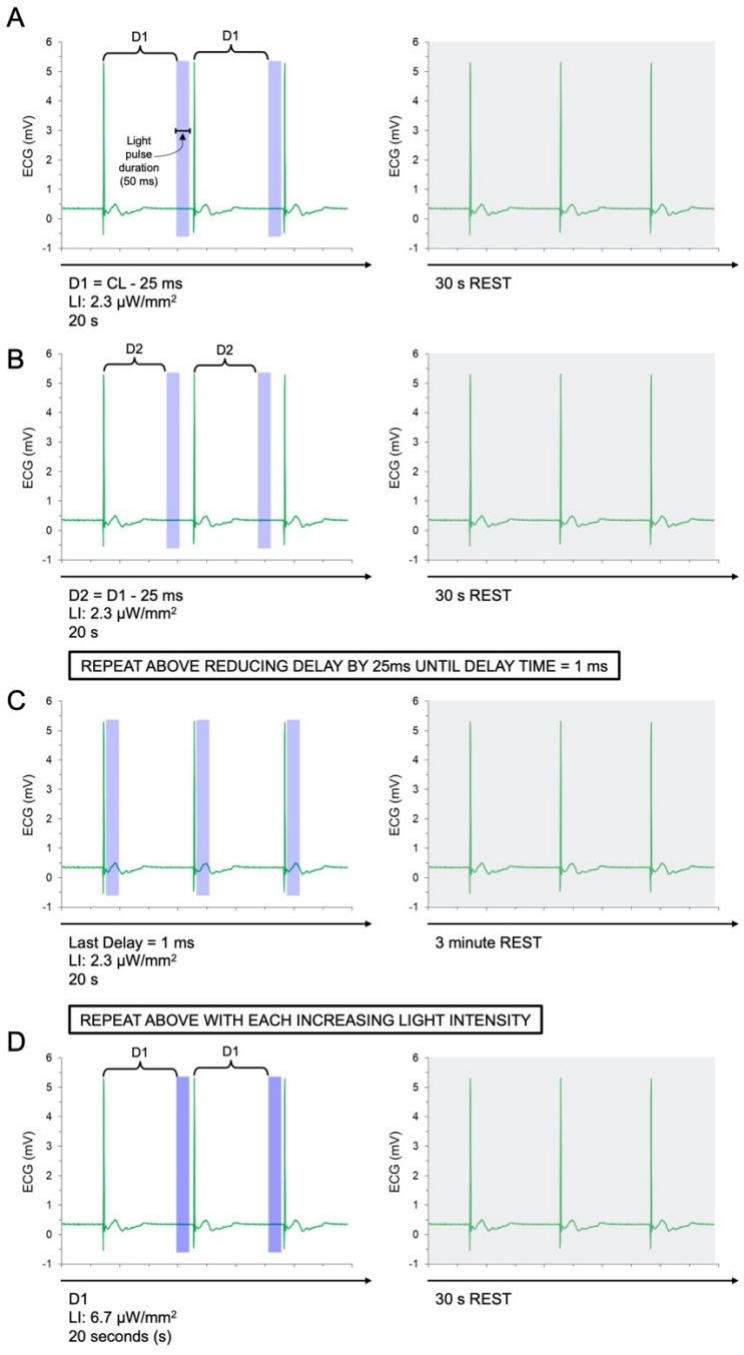

Figure 3.4. Chronotropic effect of sustained ChR2 activation in the zebrafish SAN. (A) BR and (B) percentage change in BR with sustained light stimulation of increasing intensity in the SAN from transgenic zebrafish expressing channelrhodopsin-2. *p<0.05 compared to baseline and #p<0.05 compared to 6.1μW/mm^2.

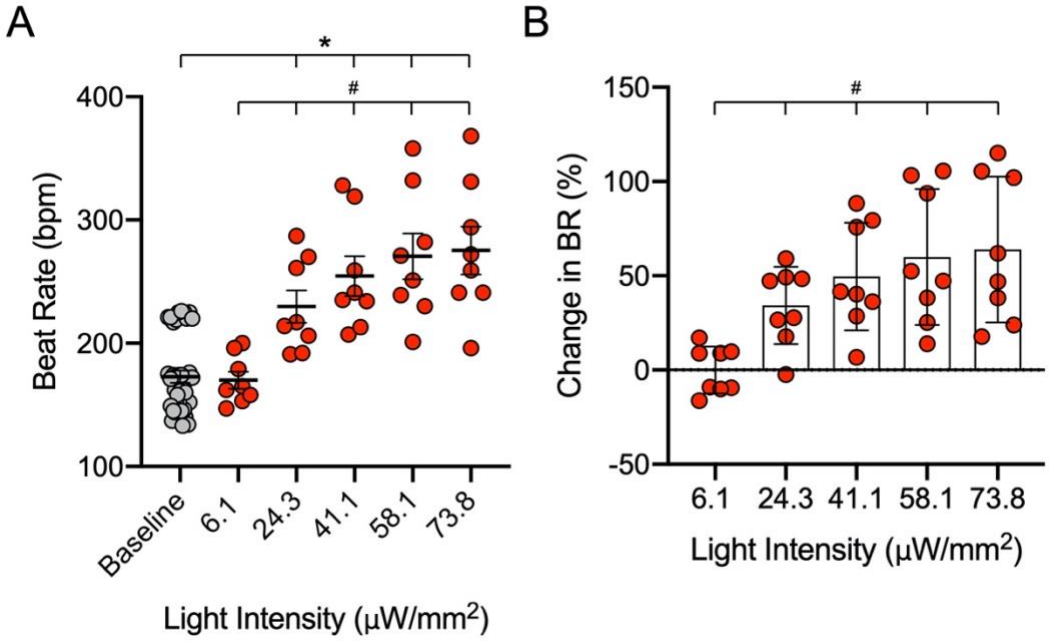

Figure 3.5. Chronotropic effect of sustained ChR2 activation in the mouse SAN. (A) BR and (B) percentage change in BR with sustained light stimulation of increasing intensity in the SAN from transgenic mouse expressing channelrhodopsin-2. *p<0.05 compared to baseline, #p<0.05 compared to 8.0 μW/mm^2, and **p<0.05 compared to 15.1 μW/mm^2.

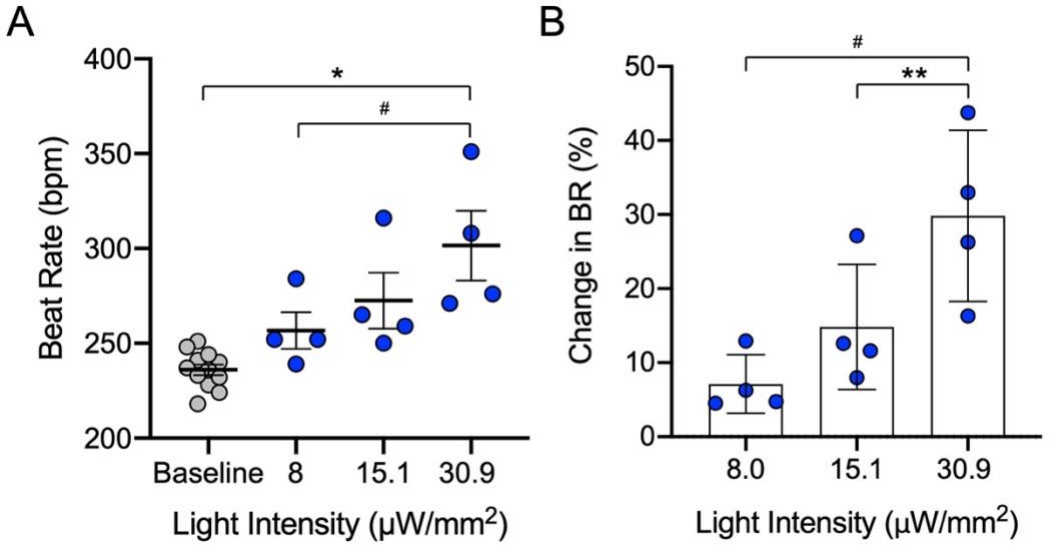

Figure 3.6. Effect of sustained I_x activation on BR and V_m in rabbit SAN cell simulations.

V_m and BR (green BR indicates increased compared to baseline) at baseline and with I_x activation with increasing current densities in rabbit SAN cell simulations.

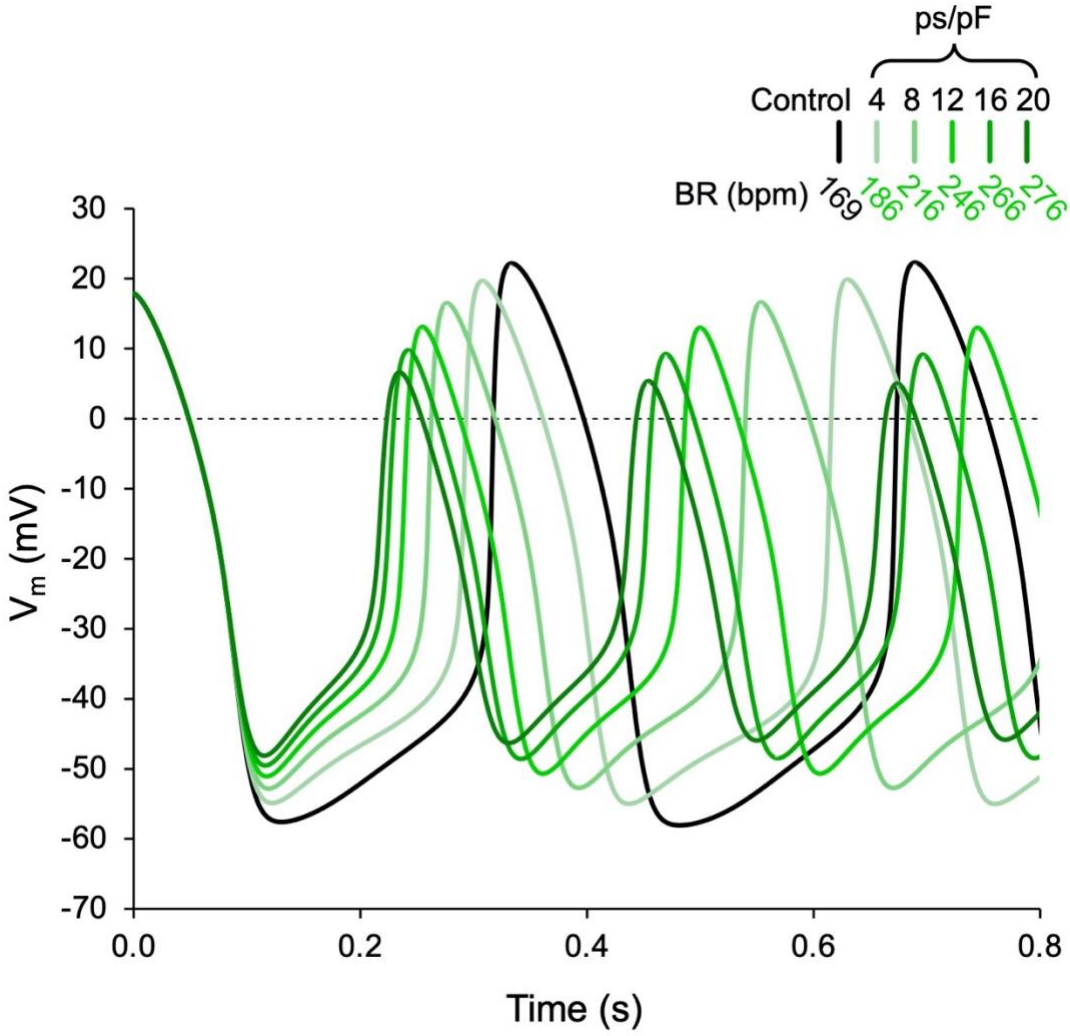

Figure 3.7. Effect of sustained I_x activation on BR and V_m in mouse SAN cell simulations.

V_m and BR (red BR indicates decreased compared to baseline; green BR indicates increased compared to baseline) at baseline and with activation of I_x with increasing current densities in mouse SAN cell simulations.

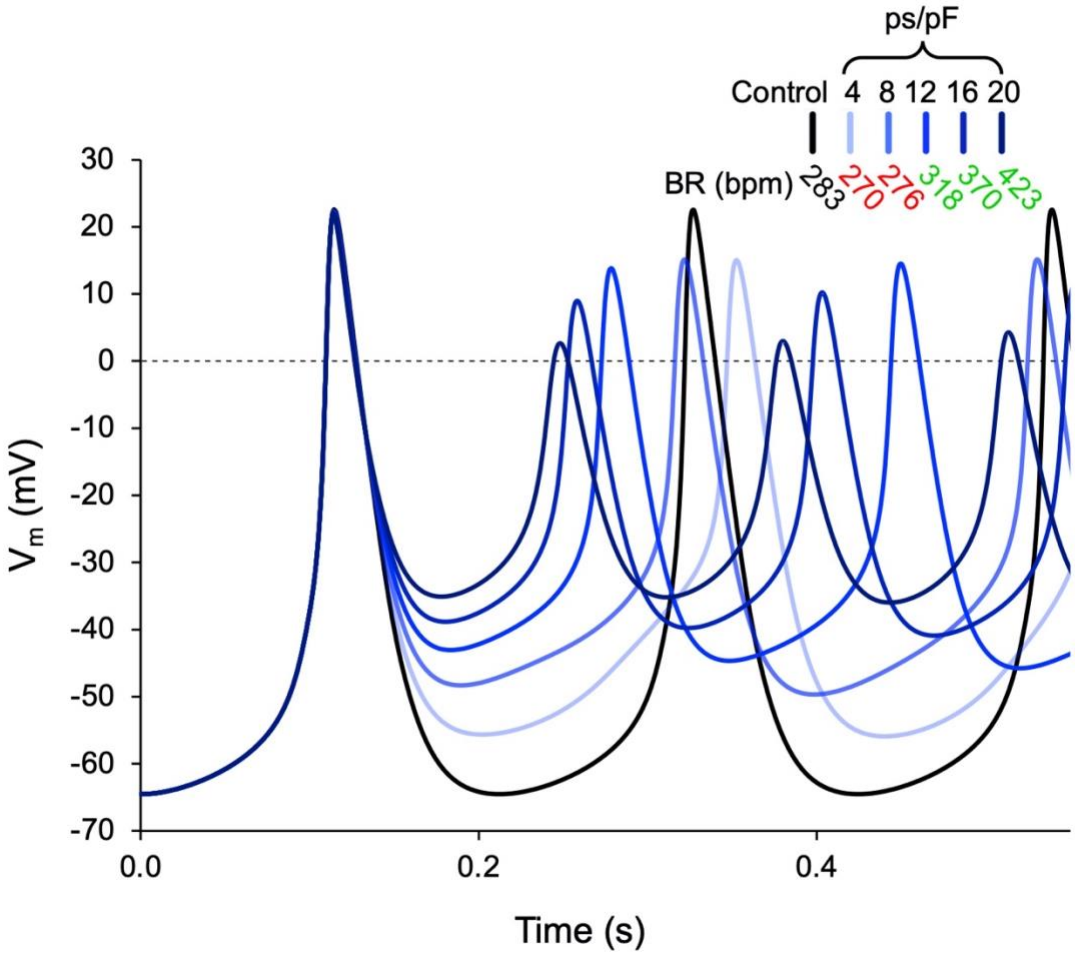

Figure 3.8. Baseline BR during pulsed ChR2 activation protocols.

BR throughout the experimental protocols with increasing light intensities in the SAN of transgenic zebrafish (A) and mouse (B) expressing ChR2.

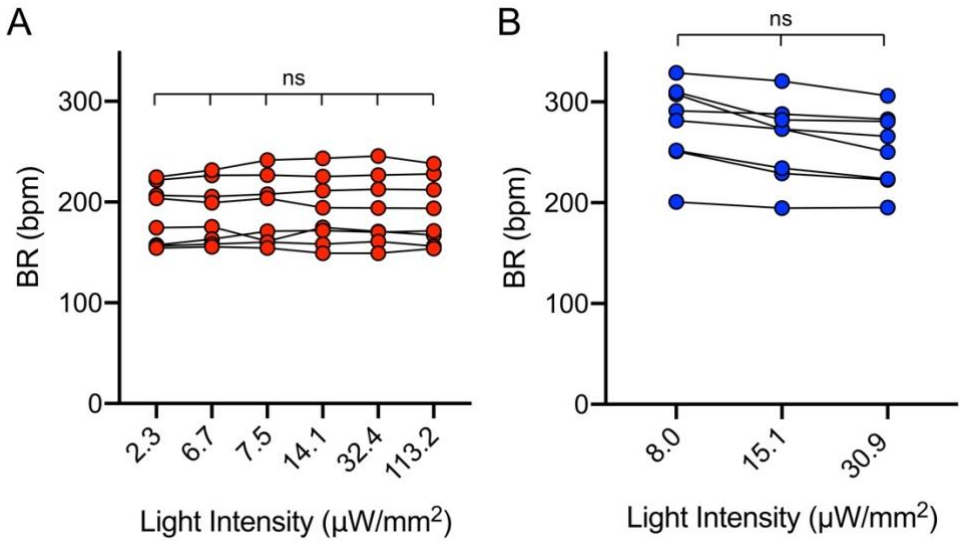

Figure 3.9. Representative data from pulsed ChR2 experiment in the zebrafish SAN.

BR as a function of stimulus delay timing shown as a percentage of the baseline cycle length (CL – grey dotted line). Solid grey line represents the theoretical pacing rates. Blue oval contains the changes in BR with subthreshold light levels.

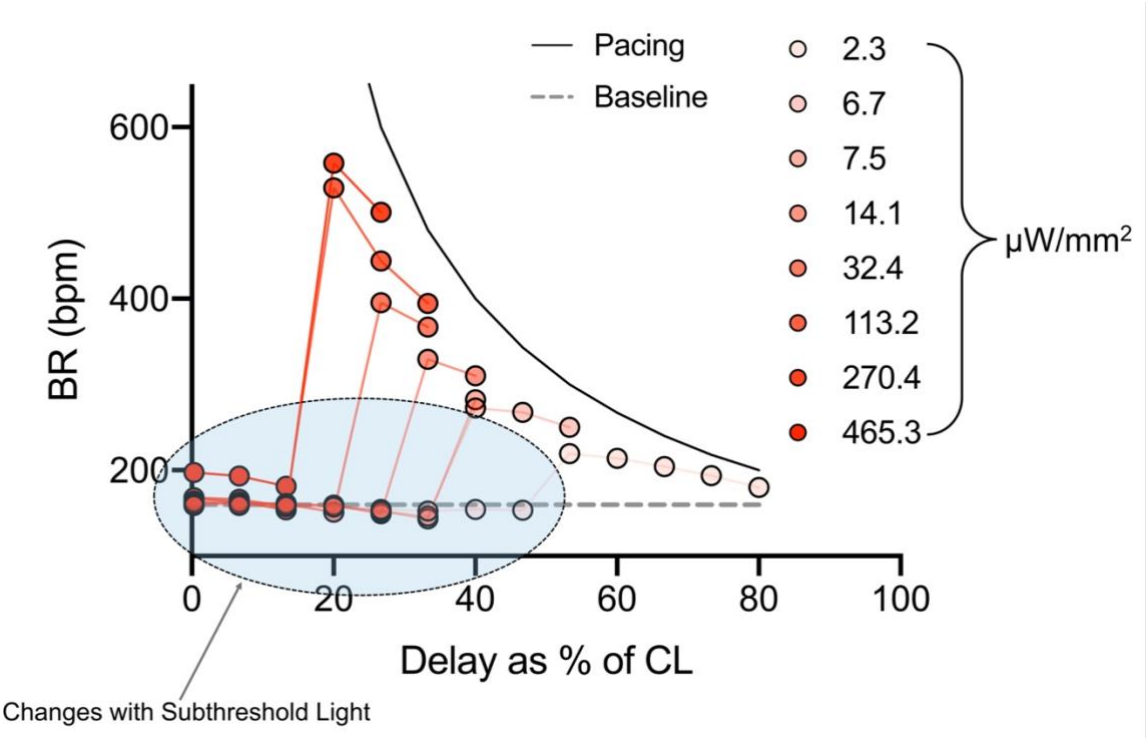

Figure 3.10. Chronotropic response to pulsed ChR2 activation in the zebrafish SAN.

Percentage change in BR as a function of delay timing shown as a percentage of the baseline cycle length (CL). (B) Change in BR with increasing light intensities at 30% and 75% of the CL. *p<0.05 across the group by two-way ANOVA, #p<0.05 compared to 2.3 μW/mm^2, and **p<0.05 compared to 6.7 μW/mm^2.

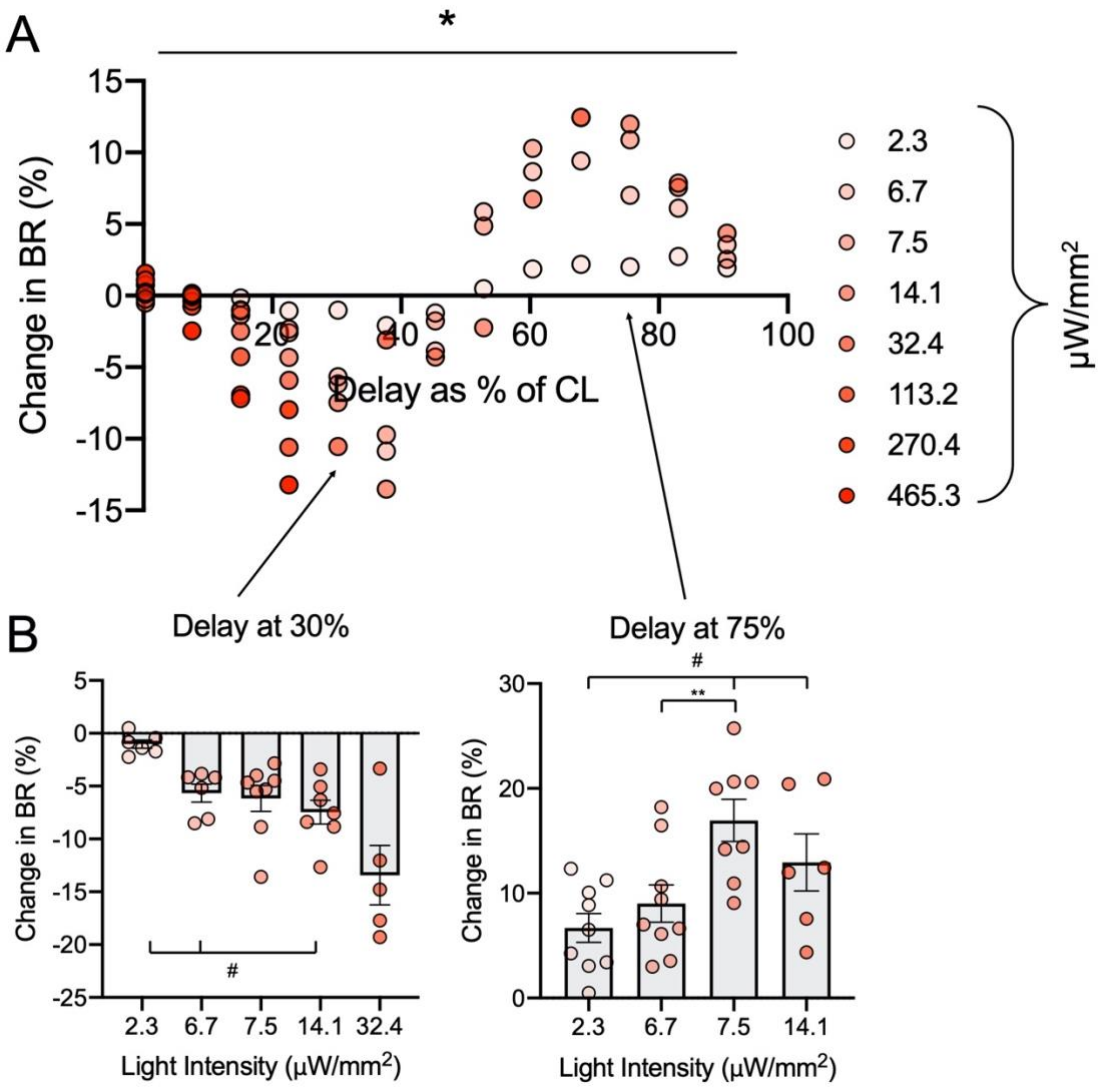

Figure 3.11. Chronotropic response to pulsed ChR2 activation in the mouse SAN. Percentage change in BR as a function of delay timing shown as a percentage of the baseline cycle length (CL). (B) Change in BR with increasing light intensities at 25% and 50% of the CL. *p<0.05 across the group by two-way ANOVA and #p<0.05 compared to 8.0 μW/mm^2.

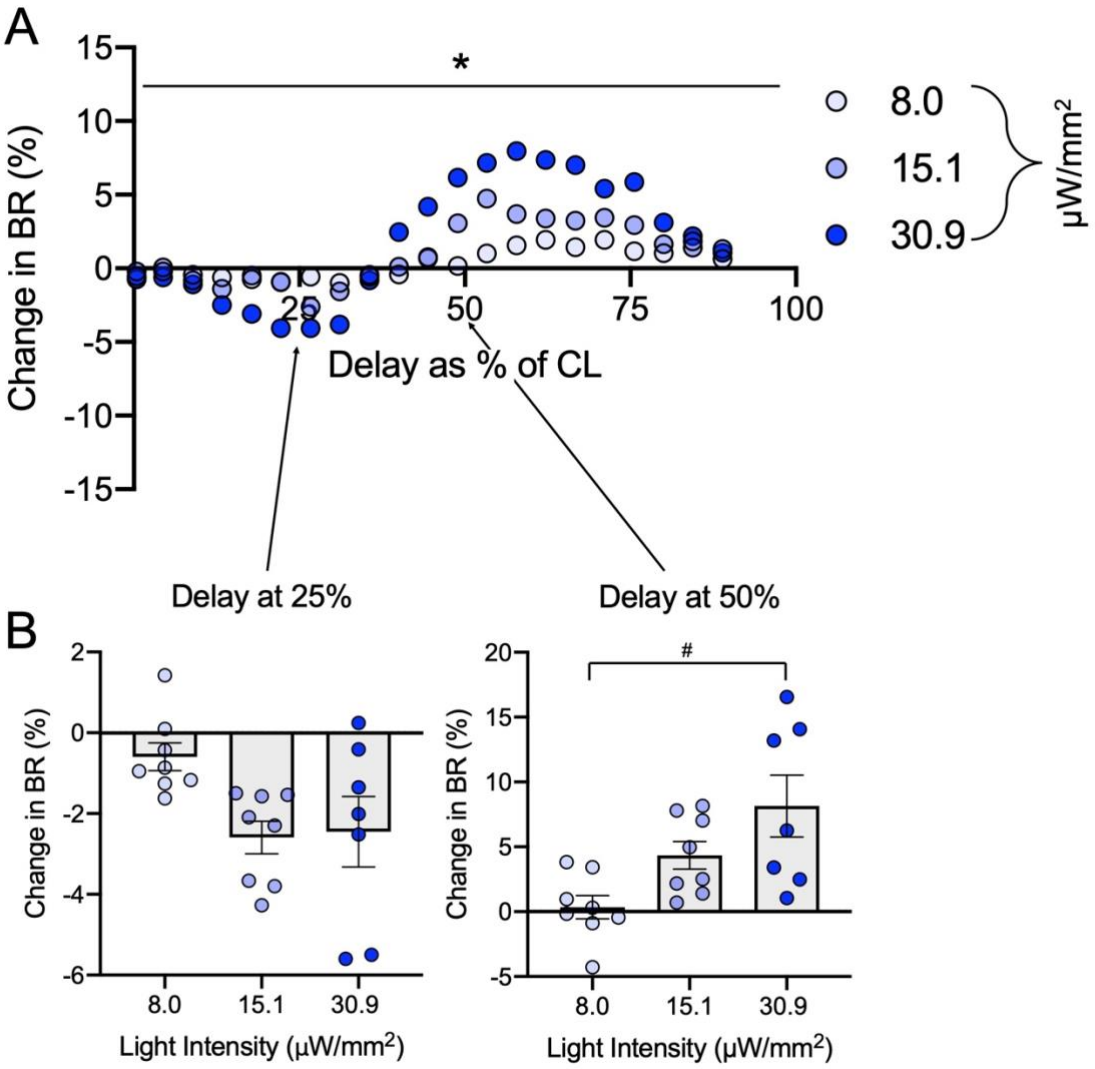

Figure 3.12. Chronotropic response to pulsed ChR2 activation in the zebrafish and mouse SAN.

Percentage change in BR as a function of pulsed light delay timing shown as a percentage of the baseline cycle length (CL) in the ChR2 mouse (blue) and zebrafish (red) SAN.

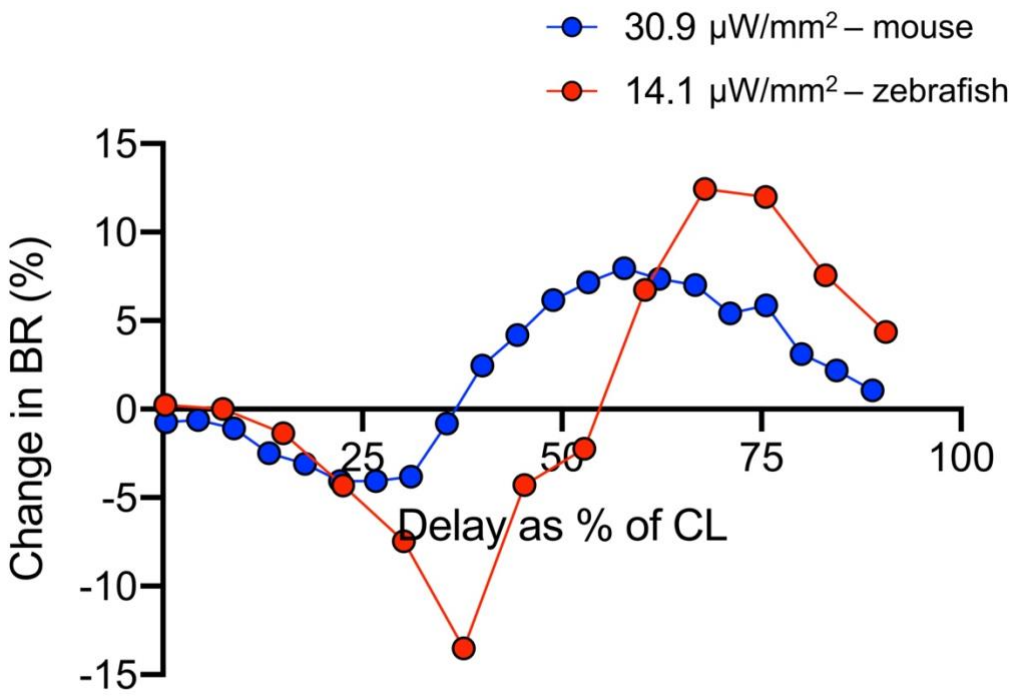

Figure 3.13. Importance of light pulse duration for the chronotropic response to ChR2 activation in the mouse SAN.

Percentage change in BR as a function of delay timing shown as a percentage of the baseline cycle length (CL) with a 10 ms and 25 ms duration light pulse with a low light intensity (A, 8.0 μW/mm^2), a medium light intensity (B, 15.1 μW/mm^2), and a high light intensity (C, 30.9 μW/mm^2). *p<0.05 for absolute changes in BR compared to 10 ms duration by unpaired Student's t-test for each light intensity.

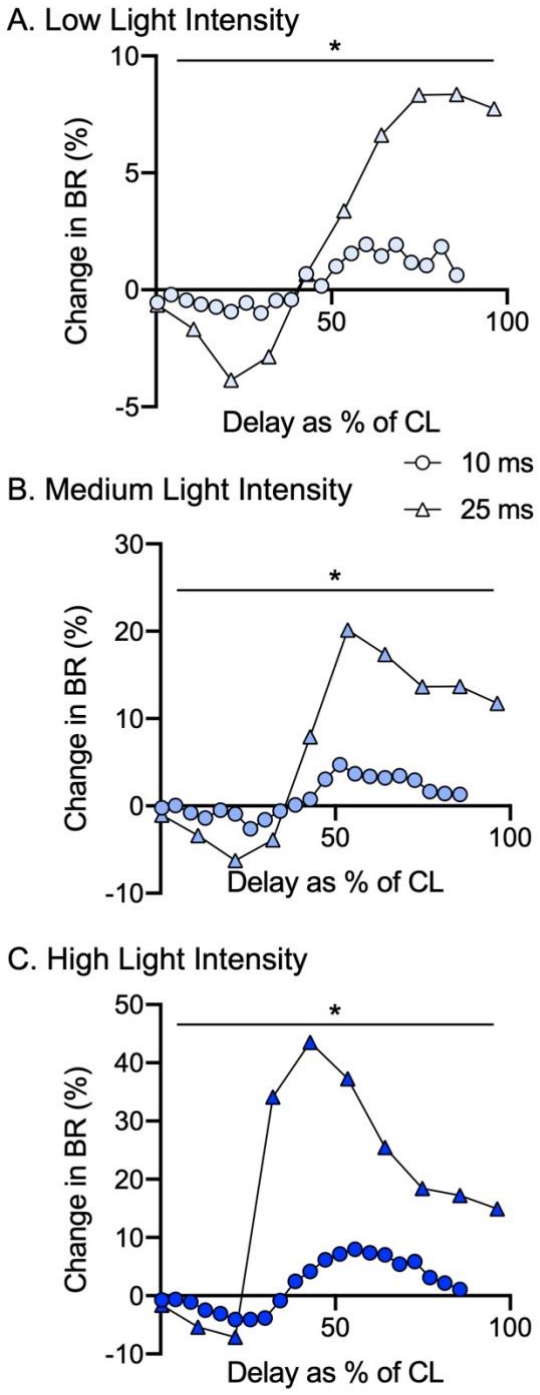

Figure 3.14. Chronotropic response to pulsed I_x activation in rabbit and mouse SAN cell simulations.

The change in BR elicited by pulsed (10 ms duration) I_x activation at varying delay times in single SAN cell computational simulations from the rabbit (A) and mouse (B).

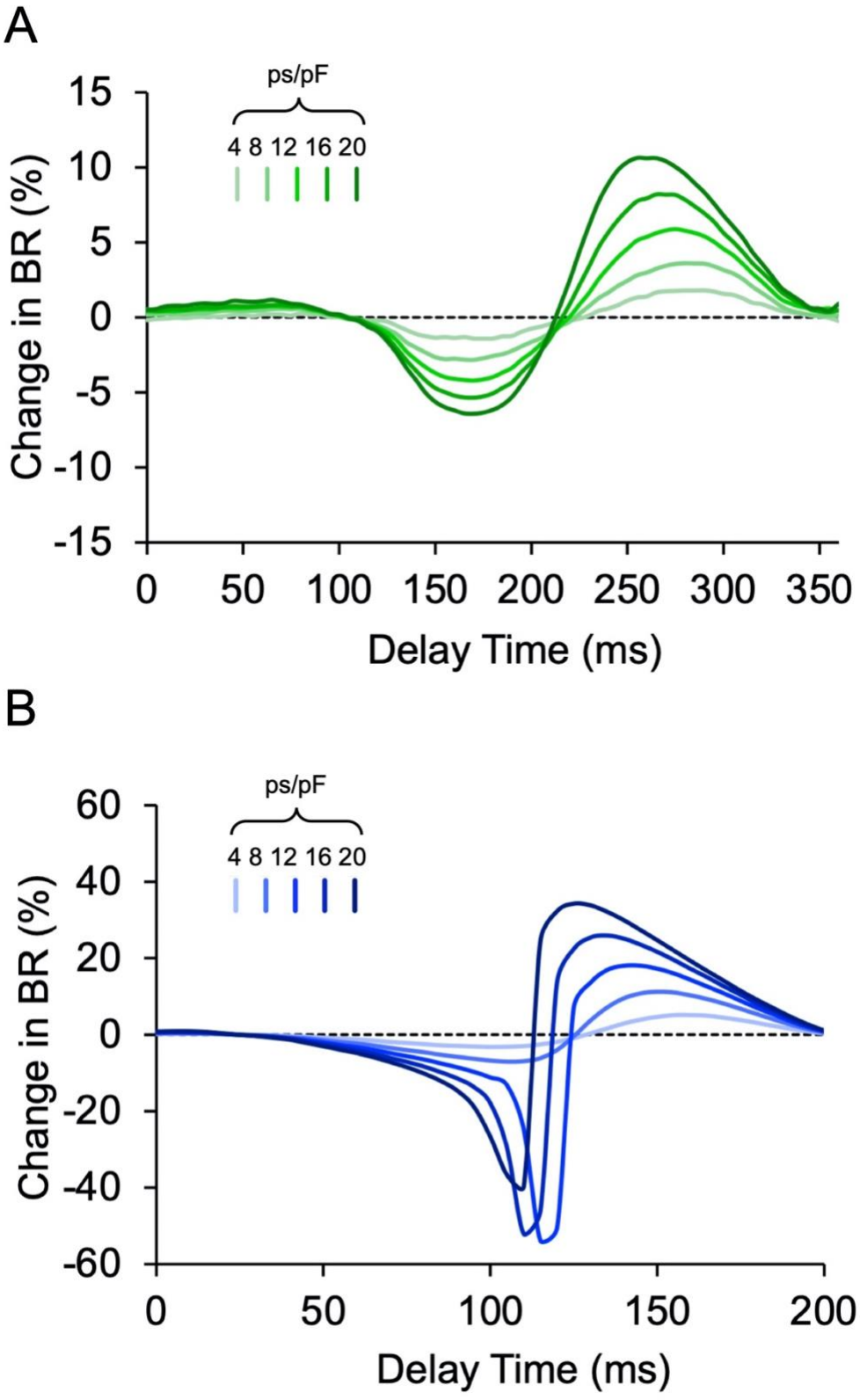

Figure 3.15. Increased BR from pulsed I_x activation in rabbit and mouse SAN cell simulations.

An increase in BR caused by pulsed I_x activation at longer delay times. The change in V_m elicited by I_x activation in the rabbit (A) and mouse (B) computational SAN cell simulations.

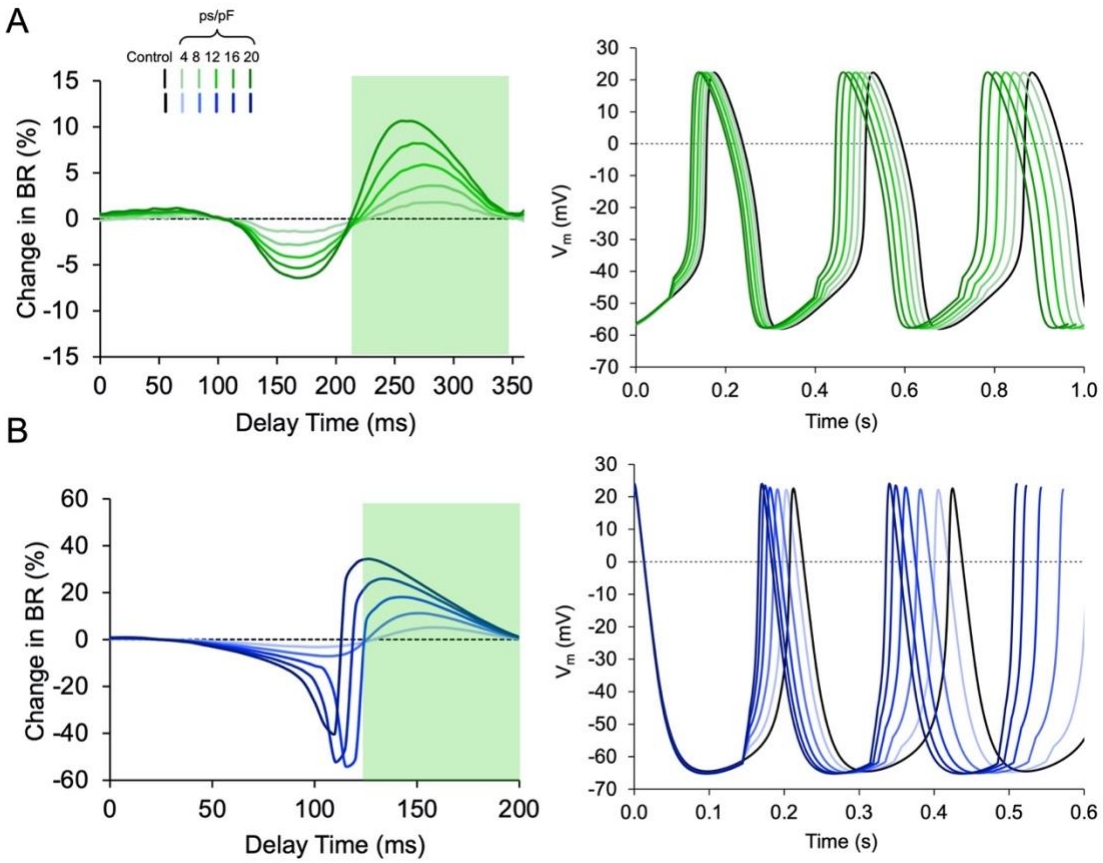

Figure 3.16. Decreased BR from pulsed I_x activation in rabbit and mouse SAN cell simulations.

A decrease in BR caused by pulsed I_x activation at shorter delay times. The change in V_m elicited by I_x activation in the rabbit (A) and mouse (B) computational SAN cell simulations.

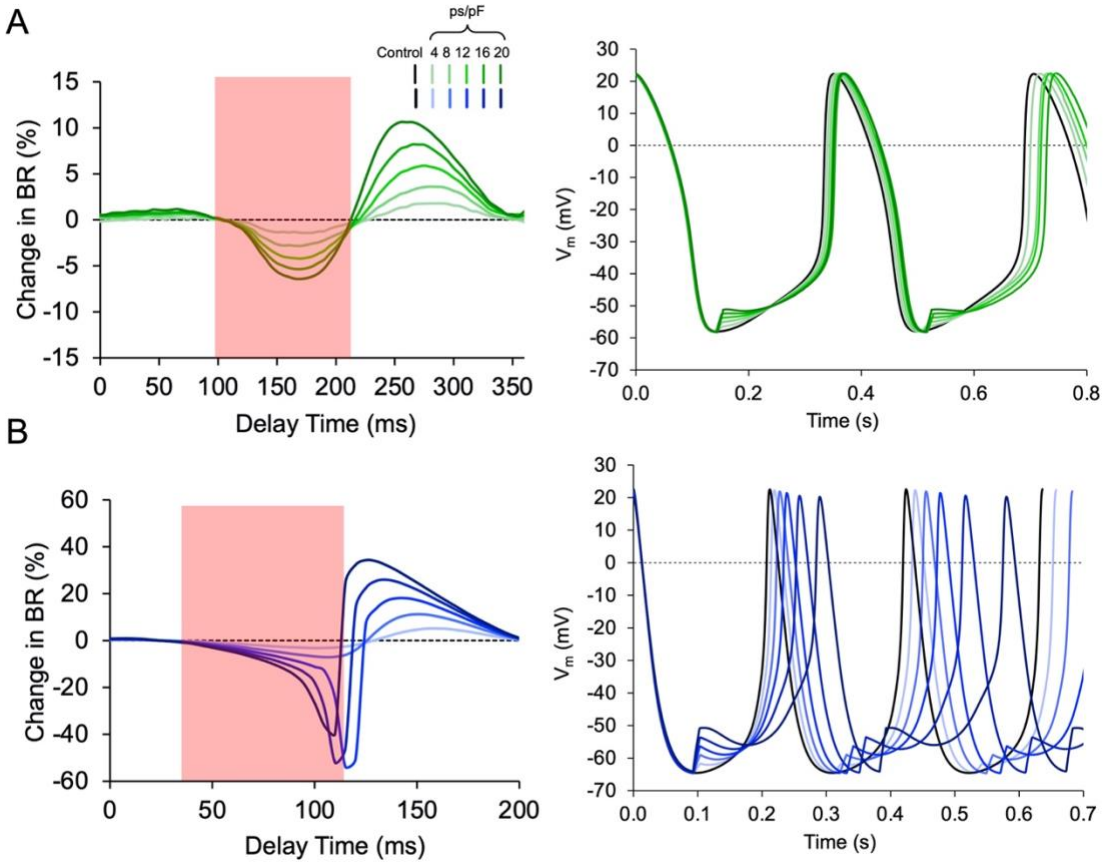

Figure 3.17. Delay times which elicit peak changes in BR and transitions from increased to decreased BR.

Changes in V_m and BR elicited by pulsed I_x activation at delay times which result in peak changes in BR (%) and over which the transition between decreased and increased BR occurs in rabbit (A) and mouse (B) computational SAN cell simulations.

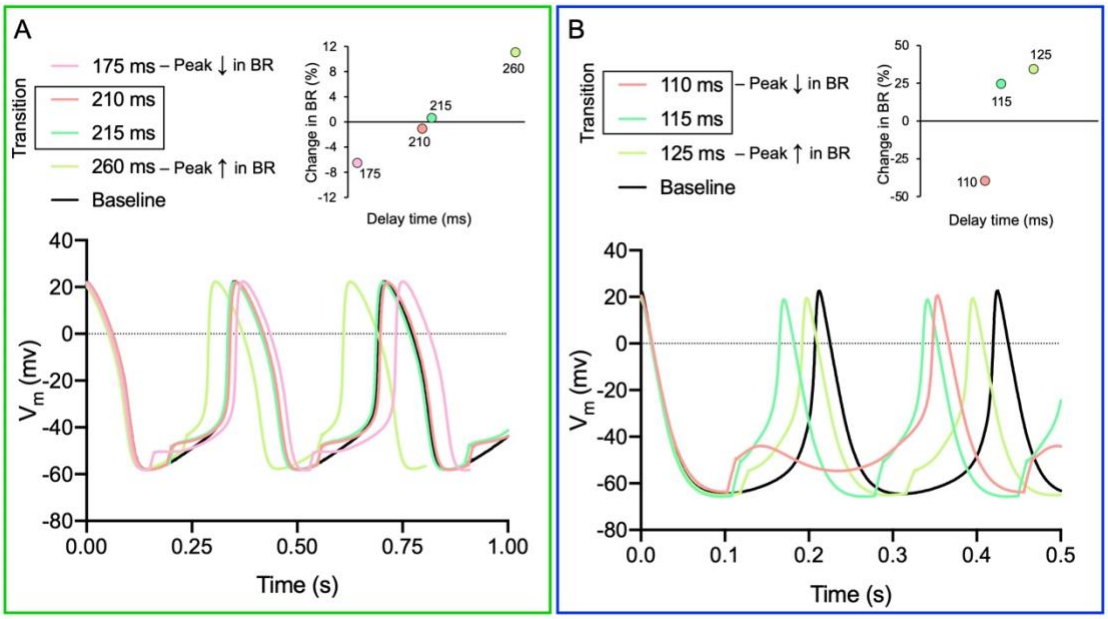

Figure 3.18. Importance of light pulse duration for the chronotropic response to ChR2 activation in rabbit and mouse SAN cell simulations.

The change in BR elicited by pulsed (5 ms duration) I_x activation at varying delay times in single SAN cell computational simulations from the rabbit (A) and mouse (B).

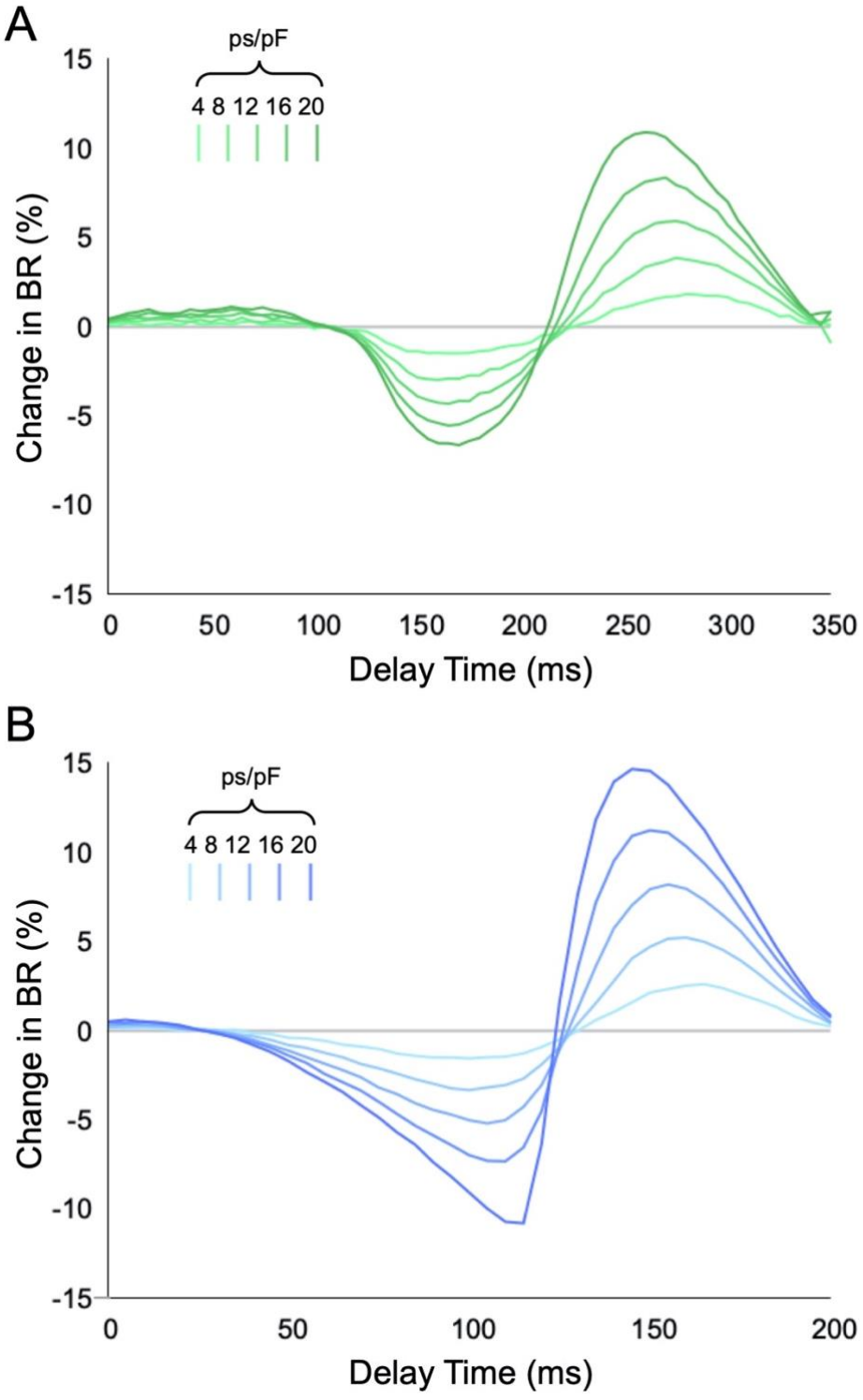

Figure 3.19. Changes in V_m and pacemaker currents in the mouse SAN cell simulations with pulsed I_x activation.

Changes in V_m (A) and in currents contributing to the difference in the chronotropic response (B), currents following V_m but not contributing to the difference (C), currents opposing the difference (D), and the total current (E) with time in an unperturbed mouse SAN simulation (Baseline) and with pulsed 10 ms I_x activation at a delay of 110 ms (pink), which results in decreased BR, and 115 ms (green), which results in increased BR. The vertical pink and green dashed lines indicate when I_x is turned off for the delay of 110 ms and 115 ms, respectively. The yellow section indicates the period in which V_m diverges between the two delays.

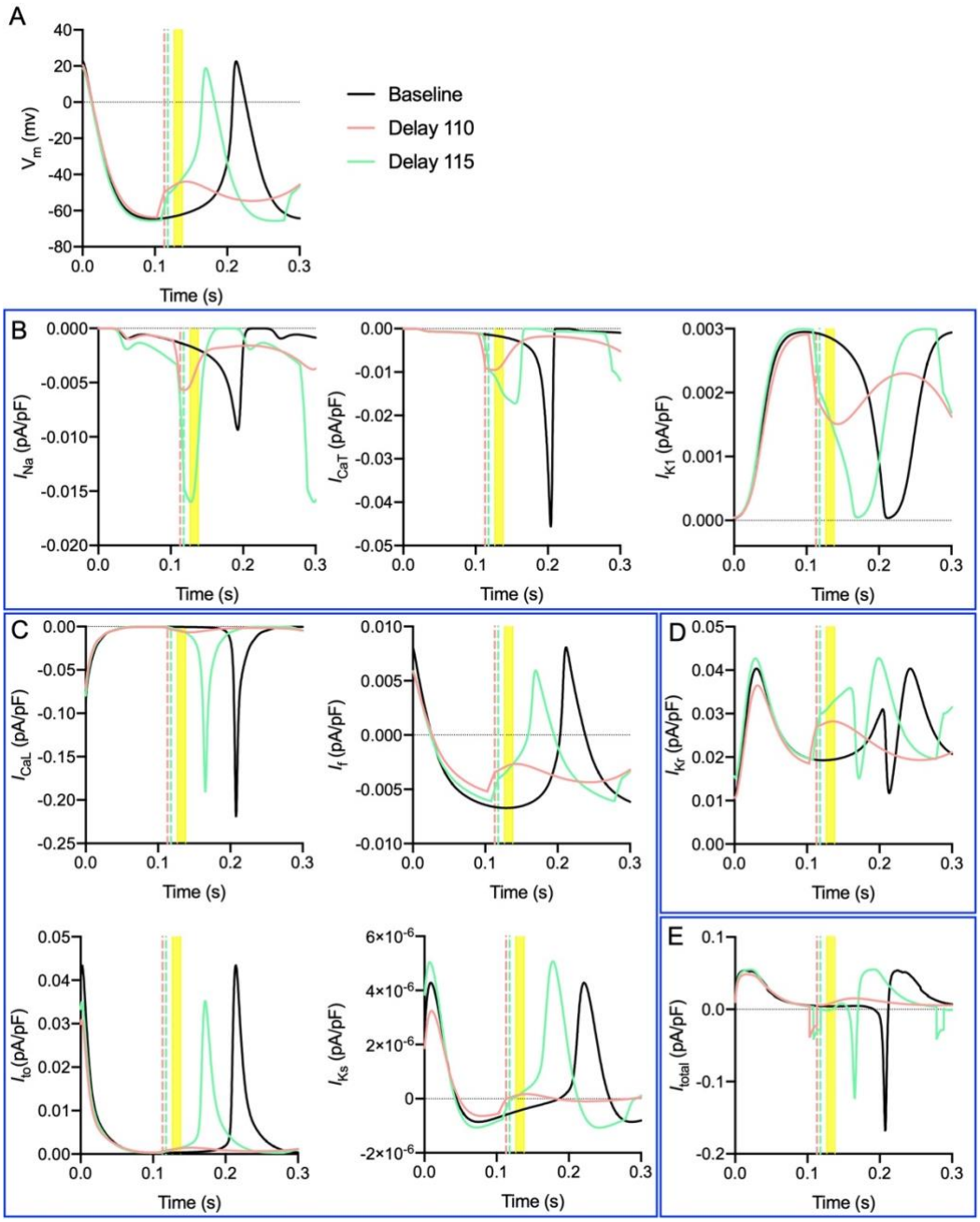

Figure 3.20. Changes in V_m and pacemaker currents in the rabbit SAN cell simulations with pulsed I_x activation.

Changes in V_m (A) and I_f (B) I_{CaT}, I_{CaL} (C) I_{Na} (D) I_{Kr}, I_{Ks}, I_{to} (E, G) and I_{tot} (F) with time in an unperturbed rabbit SAN simulation (Baseline) and with pulsed I_x activation at a delay of 175 ms (pink), which results in the peak decrease in BR, and 260 ms (green), which results in the peak increase in BR. The vertical pink and green dashed lines indicate when I_x is turned off, while the pink and green highlighted sections denote when V_m diverges from the unperturbed V_m, following an I_x pulse with a 175 or 260 ms delay, respectively.

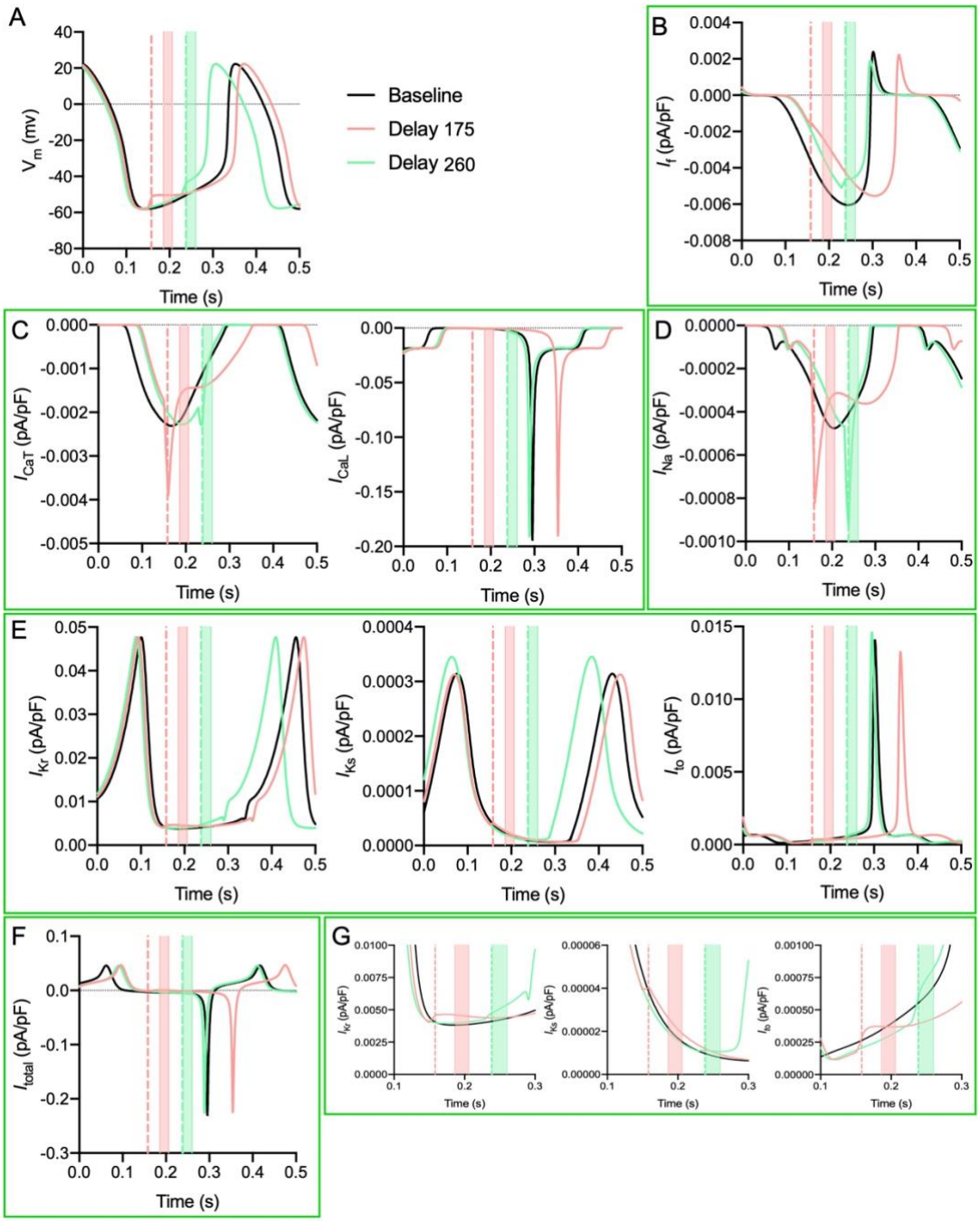

Figure 3.21. Effect of 4-AP on the chronotropic response to mouse SAN stretch. Pharmacological modification in action potential morphology resulting in a shift in the chronotropic response to SAN stretch. (A) Theoretical mouse SAN AP before (control) and with 4-aminopyridine (4-AP) application resulting in different proportions of the cycle during which activation of the stretch activated current ($I_{SAC,NS}$) would result in an increase (green) or a decrease (red) in BR. (B) The SAN stretch-induced change in BR observed at control, with 4-AP application, and after washout in the isolated mouse SAN. *p<0.05 compared to control. (C) The relationship between baseline BR and the change in BR with stretch. Adapted from MacDonald et al., 2020).

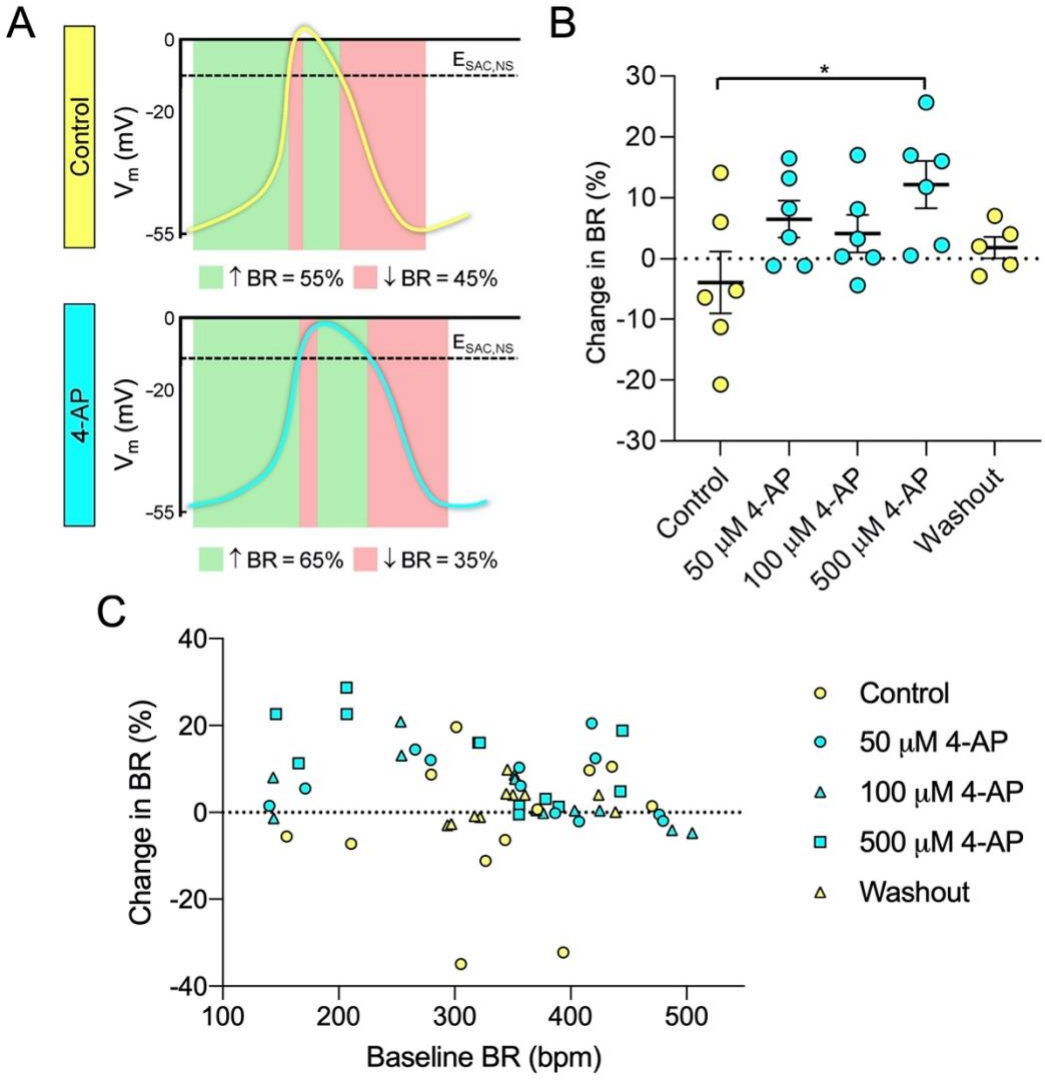

CHAPTER 4: UNDERSTANDING STRUCTURAL AND MECHANICAL FACTORS INFLUENCING THE CHRONOTROPIC RESPONSE TO SAN STRETCH

4.1. INTRODUCTION

Understanding that AP morphology and SAC_{NS}-like current activation timing can influence whether BR increases or decreases is important when considering the control of the SAN by stretch. In a normal physiological context, the SAN is stretched during atrial filling and therefore stretch occurs at the same time as SDD. Based on the theory that activation of $I_{SAC,NS}$ by stretch is the cause of the stretch-induced chronotropic response, stretch during SDD would be expected to increase BR in all species. This implicates that the Bainbridge response could be active in the mouse despite the previously observed reduction in BR in response to sustained stretch of the isolated SAN. If the mechanical and electrical synchrony of the heart become disrupted and stretch occurs during other phases of the AP, the Bainbridge response could be altered or absent, potentially contributing to electrical dysfunction or detrimental chronotropic changes in the SAN. Not only is the direction of the Bainbridge response important, but the magnitude of the response has important implications. Even if stretch is physiologically timed within the cardiac cycle (occurring during SDD) the magnitude of the response can vary. In the zebrafish SAN stretch study from my first objective both the amount of stretch and the direction of stretch affected the magnitude of the change in BR (MacDonald et al., 2017). Thus, for a more complete understanding of SAN mechano-sensitivity and its impacts on BR, investigations regarding the mechanical and structural determinants of the chronotropic response to stretch are essential, and the focus of this chapter.

4.1.1. SAN Composition, Structure, and Stretch

The structure of the SAN is complex and consists of pacemaker cells embedded in a fibrous connective tissue matrix consisting predominantly of collagen and elastin interspersed with fibroblasts (Monfredi et al., 2018). It extends perpendicularly to the *crista terminalis* between the SVC and IVC (Ho and Sánchez-Quintana, 2016). In order for the small SAN to overcome the source-sink mismatch to excite surrounding atrial tissue, the SAN is structurally isolated in a fibrous network, and the electrical signal propagates by way of specialised conduction pathways (Kalyanasundaram et al., 2019).

The pacemaker cells within the SAN are electrophysiologically and morphologically heterogeneous, with variable ion current densities and cell sizes and shapes (Boyett et al., 2000; Monfredi et al., 2018). Further, the composition and organisation of the SAN changes both with age and pathology (Csepe et al., 2015). Collagen content more than doubles from infancy to adulthood in humans (Alings et al., 1995), and pathological upregulation of fibrosis in the SAN is correlated with arrhythmias, SAN dysfunction, myocardial infarction, and heart failure (Csepe et al., 2015). Overall, the SAN is heterogeneous in structure and highly variable throughout life, age, and disease and thus, if structural and mechanical factors influence the magnitude of Bainbridge response, its contribution may vary between people and in different conditions or stages of life.

Not only is the SAN itself complex and heterogeneous, its structure and composition are highly variable across species (Opthof et al., 1987b; Boyett et al., 2000). For example, cell alignment in both the central SAN and in the transition from SAN to atrial tissue is disparate between species, as is the proportionate connective tissue content, ranging from ~25 – 90% of SAN volume (Opthof, 1988; Boyett et al., 2000; Glukhov et al., 2015; Kalyanasundaram et al., 2019). SAN cell volume also varies between species, although in all species SAN myocytes tend to be smaller and contain more abundant caveolae than the surrounding atrial myocytes (Boyett et al., 2000). The numerous caveolae in the SAN contribute to automaticity and SAN regulation through spatial compartmentalisation of G-protein coupled receptors, ion channels, and other protein complexes (Lang and Glukhov, 2018). In some species, myofilaments are sparse and poorly organised (not organised into myofibrils but instead running in all directions) whereas other species have more myofibrils, which are well organised into myofilaments (Boyett et al., 2000).

In all mammals studied, apart from the mouse, SAN stretch results in an increase in BR (Quinn and Kohl, 2012) and this response remains consistent despite the differences in SAN structure between species. Further, many different experimental approaches have been utilised to study SAN stretch, such as: increased venous return to the heart *via* bolus fluid injection in an *in vivo* intact heart (Bainbridge, 1915; Coleridge and Linden, 1955; Hashimoto et al., 1967; Bolter, 1994); attachment to and stretch of the epicardial surface of the SAN in the *in vivo* intact heart (Brooks et al., 1966; Brooks and Lange, 1977; Horner et al., 1996); right atrial inflation in the isolated Langendorff perfused heart (Eijsbouts et al., 2003) or in the isolated right atrium (Himmel and

Rossberg, 1983; Rossberg et al., 1985; Bolter, 1996; Barrett et al., 1998; Bolter and Wilson, 1999; Wilson and Bolter, 2002; Han et al., 2010); concentric stretch of isolated right atrial or SAN preparations (Deck, 1964); or linear SAN stretch either perpendicular (Arai et al., 1996; Cooper and Kohl, 2005) or parallel (Lange et al., 1966; Golenhofen and Lippross, 1969; Chiba, 1977; Kamiyama et al., 1984) to the *crista terminalis*. Interestingly, despite these vastly different experimental approaches and species differences in SAN structure, stretch consistently causes a positive chronotropic response (apart from in the mouse). This demonstrates that variable stretch techniques and SAN substrates do not alter mechanotransduction in a way that alters the *direction* of the chronotropic response. Nevertheless, it is possible that these variations in SAN stretch techniques and species-differences in SAN structure could influence mechanotransduction in such a way that the *magnitude* of the chronotropic response to stretch is altered. This is suggested by the fact that greater magnitudes of stretch or larger tensions result in greater increases in BR. Similarly, pathological changes in SAN structure and mechanics that may disrupt or change mechanotransduction (such as increased fibrosis) and thus impede the mechanical control of SAN function, may contribute to electrical disturbances and SAN dysfunction (Csepe et al., 2015).

In the zebrafish SAN stretch experiments from my first objective, and in preliminary mammalian experiments, it became evident that differences in preload may influence the magnitude of the chronotropic response, as without a set baseline force there was substantial variability in responsiveness (Figure 4.1). Specifically, the Coefficient of Variation of the change in BR was an average of 109 ± 9% for each stretch magnitude. Based on this, I hypothesised that SAN structure and mechanical parameters influence the magnitude of the chronotropic response to stretch. My final aim was to test this by studying some of the structural and mechanical factors that may influence SAN stretch, and the relationship of these factors to chronotropic responsiveness. Specifically, this study began by investigating the importance of baseline and applied force for determining the magnitude of the chronotropic response to SAN stretch in the zebrafish. Following this were investigations regarding the structural and mechanical differences between the mouse and rabbit SAN both at baseline and with stretch, and how these properties may influence chronotropic responsiveness. To test this, changes in BR and force with sustained SAN stretch of increasing magnitudes were measured and compared to SAN stiffness. Second-harmonic generation microscopy (SHGM) was then utilised to visualise collagen in the

SAN at baseline or with 40% stretch in order to investigate structural differences between species and change in SAN structure with stretch.

4.1.2. Rabbit and Mouse SAN Comparability

Although it was still possible to test the mechanical parameters of the stretch-induced increase in BR in the zebrafish, it was not an advantageous model for studying changes in structure with stretch due to the ring-shape structure of the SAN. The rabbit is a useful pre-clinical model for cardiac electrophysiological studies and is the species that has been most widely employed for investigating the mechanical control of BR (Quinn and Kohl, 2016). Therefore, this, and the flat, sheet-like nature of the rabbit SAN made the rabbit an appropriate model for this study. Although the mouse has been shown to respond to stretch with a decrease in BR (Cooper and Kohl, 2005), my second objective demonstrated that this may be the result of the same mechanism that elicits the increase in BR in most species, namely activation of $I_{SAC,NS}$. Therefore, this made it possible to determine if, as well as stimulation timing and AP morphology, mechanical and structural parameters influence the direction of the chronotropic response to stretch, or if these parameters only influence the magnitude of the response. Comparing the rabbit and mouse SAN is favourable because they both have thin endo- and epi-cardial layers made up of connective tissue, and most of the thickness (between the outer layers) is composed of pacemaker cells and connective tissue (Opthof et al., 1987b; Verheijck et al., 2001), whereas larger animals have thicker endo- and epi-cardial connective tissue layers (Kalyanasundaram et al., 2019).

The volume of the rabbit SAN is ~ 50% comprised of pacemaker cells and ~ 50% of extracellular matrix and fibroblasts (Bleeker et al., 1980; Opthof et al., 1987b). Pacemaker cells in the rabbit SAN have diverse morphologies, volumes, and ion current densities (Verheijck et al., 1998a; Monfredi et al., 2018). Small, spindle-shaped pacemaker cells are densely packed and inter-woven in a collagen network in the central region of the rabbit SAN, whereas in more peripheral regions cells are more ordered, less dense, and oriented parallel to the *crista terminalis* (Bleeker et al., 1980).

The central region of the mouse SAN is also densely packed with pacemaker cells, however, unlike in the rabbit, they are generally well-aligned, oriented perpendicularly to the *crista terminalis*, and there is proportionately less extracellular matrix and fewer fibroblasts, comprising ~ 25% of the volume, compared to ~ 50% in the rabbit SAN (Liu et al., 2007; Hao et al., 2011; Glukhov et al., 2015). The periphery of the mouse

SAN is comparable to the rabbit in that cells are more loosely packed and are arranged parallel to the *crista terminalis* (Liu et al., 2007).

4.2. METHODS

4.2.1. Animals

Adult female rabbits (New Zealand White, 2.1 ± 0.2 kg), adult female mice (C57BL/6J, 8 - 12 weeks), and adult wild-type zebrafish (AB, 6 - 12 months post-fertilisation) were used in this study. The Dalhousie University Committee for Laboratory Animals, or the local Institutional Animal Care and Use Committee in Freiburg, Germany (Regierungspraesidium Freiburg, X-16/10R) approved all experimental procedures, and followed the guidelines of the Canadian Council on Animal Care or German animal welfare laws and guidelines (TierSchG and TierSchVersV), compatible with Directive 2010/63/EU of the European Parliament on the protection of animals used for scientific purposes.

4.2.2. Force and Zebrafish SAN Stretch

The zebrafish SAN was isolated as described in my first objective in a carbogen-bubbled bath with Krebs-Henseleit solution maintained at 28°C. The stretch set-up for the ring-like zebrafish SAN was adapted from the previous zebrafish SAN stretch experiments from my first objective to allow for simultaneous force measurements. Specifically, one of the custom-made glass hooks remained attached to a piezoelectric linear translator for application of stretch, while the other hook was attached to an isometric force transducer and was stationary. In the initial experiments in this study, the same qualitative approach to determine baseline inter-hook distance was utilised from my first objective, in which hooks were separated to a point at which each hook appeared to begin to stretch the SAN ring. Once this position was reached, inter-hook distance was measured. The same sustained stretch protocol was repeated with 10, 25, and 50% stretch in the short-axis direction except with additional simultaneous baseline and applied force measurements. Short-axis stretch was chosen due to the greater responsiveness observed with short-axis stretch compared to stretch in the long-axis direction in the previous study. The relationship between baseline or applied force and the change in BR with stretch was then evaluated. Based on these data, the subsequent experiments were modified so that inter-hook or pre-stretch distance was set quantitatively rather than qualitatively by applying a pre-determined preload of ~ 5mg

both in the long- and short-axis direction. From this baseline, 25% stretch was applied twice for 30 s with 120 s rest in between stretches and temperature, force, and ECG signals were continuously recorded. In a final set of experiments, a preload of ~ 2 mg was applied in the short axis-direction prior to stretch application and utilised the same protocol as the mammalian stretch experiments in order to compare results across species.

4.2.3. Mammalian SAN Isolation

Rabbits were euthanised by ear vein injection of pentobarbital (140 mg/kg), followed by rapid heart excision, aortic cannulation and Langendorff perfusion (20 mL/min) with Krebs-Henseleit solution at 37°C containing, in mM: 120 NaCl, 4.7 KCl, 24 NaHCO3, 1.4 NaH2PO4, 1.0 MgCl2, 1.8 CaCl2, and 10 Glucose, with an osmolality of 300 ± 5 mOsm and a pH of 7.40 ± 0.05 and bubbled with carbogen (95% O2, 5% CO_2). The atria were carefully removed from the heart and placed in a bubbled bath of Krebs-Henseleit solution. Mice were sacrificed by cervical dislocation and hearts were rapidly excised and placed in a bath with Krebs-Henseleit solution, in which atria were isolated from the ventricles.

For both mammalian species, the outermost edge of each atrial appendage was pinned down in a Sylgard-lined dish (DC 170; Dow Corning, Midland, MI), taking care to not strain tissue beyond its inherent dimensions, such that the bottom of the atrial appendages (which normally rest against the ventricles) were face up. The endocardial side of the SAN was exposed by making incisions along the front surface of SVC and IVC. Excess fat and pericardial tissue were removed from the underside of the preparation carefully, so as to not pull, stretch, or damage the tissue. The rabbit (but not the mouse) SAN was then dissected along the medial edge of the *crista terminalis* and the interatrial septum. The mouse SAN has previously been shown to have irregularities in BR when cut along the medial limb of the CT (Verheijck et al., 2001), therefore for the mouse preparations the atrial appendages were left attached to the exposed SAN.

4.2.4. Mammalian SAN Stretch

For the mammalian preparations, insect pins were gently woven through the SVC (top) and IVC (bottom) edges of the SAN. In the mouse, although the atrial appendages were still attached to the SAN, they remained free from the pins. A clip was attached to the SVC pin at the top of the SAN preparation and was hung from an isometric force

transducer (PY2 72-4491, Harvard Apparatus, Holliston, MA). A second clip, which was adhered to a computer-controlled linear DC-servomotor (LM 1247-02-01; FAULHABER MICROMO, Clearwater, FL), was attached to the IVC pin at the bottom of the SAN prep. This allowed for simultaneous stretch and force measurements in a water-jacketed imaging chamber containing Krebs-Henseleit solution bubbled with carbogen and maintained at 37°C measured using a thermocouple (T-type pod; ADInstruments). The unstretched SAN was lengthened with 10 μm steps of the linear motor until a step resulted in a change in force. From there, again 10 μm steps were used to lengthen the SAN until a preload of ~ 200 mg for rabbit and ~ 50 mg for mouse was applied to the tissue. These values were based on preliminary experiments and previous studies (Kamiyama et al., 1984; Cooper and Kohl, 2005). The baseline tissue length (the distance between the SVC and IVC pins) was measured from video images (DMK 23UP1300; The Imaging Source, Charlotte, NC) with custom routines in Matlab (MathWorks, Natick, MA).

4.2.5. Experimental Protocol

The SAN was stretched by 10% of baseline tissue length at a rate of 25 mm/s with the linear motor in the mammalian preparations (Figure 4.2), and the zebrafish SAN was stretched to 10% of the inter-hook distance with the piezoelectric translator at a rate of 1mm/s. Stretch was sustained for 30 s before the SAN was returned to baseline length at the same rate. Each SAN was left at baseline for 120 s of rest before 10% stretch was once again applied for 30 s. Following these two stretches of 10%, the entire stretch procedure was repeated with larger stretches in steps of 10% until 50% stretch was applied or until BR became unstable. BR was calculated from the peaks of the electrical signals recorded. They were recorded from bipolar electrodes on either side of the mammalian SAN tissue connected to an ECG amplifier (Animal Bio Amp; ADInstruments, Colorado Springs, CO) or by using a custom suction microelectrode for the zebrafish SAN as previously described. Stretch was converted to strain by dividing the stretched length by the baseline length or inter-hook distance. An index of tissue stiffness (β) was calculated from the stress-strain data for each SAN by fitting the relationship: stress = $\alpha \times e^{\beta \times strain}$. Passive force was measured in diastole and was converted to stress in the mammals by dividing by the cross-sectional area of each SAN. The cross-sectional area was measured as SAN width multiplied by the average SAN

thickness for each species (294 μm for rabbit, 191 μm for mouse) such that the cross-section was perpendicular to the stretch direction in each SAN (rabbit = 1.45 ± 0.09 mm^2, mouse = 0.28 ± 0.01 mm^2). Temperature, force, and ECG signals were continuously recorded at 2 kHz using a data acquisition device (PowerLab) controlled by LabChart (ADInstruments).

4.2.6. SAN Collagen Imaging and Quantification

The isolated SAN from rabbit and mouse, as prepared above, were fixed either at baseline or 40% stretch. This was done with 4% paraformaldehyde in phosphate-buffered saline and left for 1 hour. Collagen was visualised using two-photon SHGM on an upright microscope (TCS SP8 DIVE; Leica Microsystems, Wetzlar, Germany) using a 25×, 1.0 NA, water immersion objective (IRAPO L 25x/1.00 W; Leica Microsystems) with 920 nm illumination from a pulsed laser (InSight X3 Dual; Spectra-Physics, Santa Clara, CA). The structure of collagen allows it to emit SHG light, thus excitation of collagen with two-photon lasers generates a signal distinguishable from the excitation wavelengths. Tiled z-stacks (442.9 × 442.9 μm in x-y, between 100 and 200 μm in z, with 6 to 9 tiled z-stacks per SAN) were recorded for 3D imaging and were stitched together and processed using Leica LAS-X (Leica Microsystems). The SHGM imaging and image processing was done by Dr. Eva Rog-Zielinska and Dr. Josef Madl at the IEKM in Freiburg, Germany.

In order to quantify species differences in collagen and its changes with stretch, collagen crimp and fibre alignment was measured. For characterisation of collagen crimp, wavelength (or period) and tortuosity (or 'waviness') were measured in a blinded manner using ImageJ (Schneider et al., 2012). Eight period measurements were made in each of three SHGM images for each layer (surface or middle), for a total of 48 measurements per preparation (unstretched or stretched, in mouse or rabbit). Tortuosity was calculated as the ratio of the collagen path length traced along the fibre from points "A" to "B", divided by the direct straight-line distance between points "A" and "B", which takes into consideration both crimp wavelength and amplitude, resulting in a measure of 'waviness'. Three tortuosity indexes were calculated in 3 images for each layer, for a total of 9 measurements per preparation.

Collagen orientation was characterised by Dr. Eva Rog-Zielinska and Joachim Greiner. This was done in the central SAN at the epicardial surface and in the middle

layer of SAN tissue by tracing the skeleton of 50 representative fibres in images from the acquired SHGM stacks, using the 'Simple Neurite Tracer' (Longair et al., 2011) within Fiji (Schindelin et al., 2012). To enable interactive tracing, the image stacks were laterally binned four times before tracing. In order to quantify the direction of each individual fibre, they performed principal component analysis of each to determine the principal eigenvector which represents the direction that best fits all points in the data, becoming the value for the fibre direction. Polar orientation plots, which demonstrate both the orientation of the fibre and the fraction of fibres at each orientation, were generated using the python package matplotlib (Hunter, 2007).

4.2.7. Data Analysis and Statistics

Data are presented as mean ± SEM. Mixed-effects analysis or one-way ANOVA was used for comparison of means where appropriate, and *post hoc* comparisons were done using Sidak's multiple comparison tests rather than Tukey's because Sidak's allows for missing values. Linear regression was used to assess the relationship between variables. A p-value of less than 0.05 was considered to indicate a statistically significant difference.

4.3. RESULTS

4.3.1. Force and the Zebrafish SAN Stretch Response

Using the modified experimental setup which enabled simultaneous force measurements, stretch of the zebrafish SAN again resulted in an increase in BR with all magnitudes of stretch. In these experiments (n = 10), in which a qualitative approach was utilised for determining baseline inter-hook distance (as before), there was large variability in preload. In these experiments there was a positive correlation between preload and peak percentage change in BR with 10% and 25% stretch but not with 50% stretch (Figure 4.3A: 10%: $R^2 = 0.5524$, $p = 0.0138$; 25%: $R^2 = 0.7249$, $p = 0.0018$; 50%: $R^2 = 0.2741$, $p = 0.1204$). Interestingly, the inverse was true regarding the relationship between applied force and peak percentage change in BR, such that there was a positive correlation with 50% stretch but not with 10% or 25% stretch (Figure 4.3B 10%: $R^2 = 0.004941$, $p = 0.8470$; 25%: $R^2 = 0.1703$, $p = 0.2359$; 50%: $R^2 = 0.6995$, $p = 0.0026$).

In the subsequent experiments (with stretch in the long-axis (n=5) or short-axis (n=5) direction), a controlled baseline force of ~ 5 mg (long axis: 5.65 ± 0.54 mg; short-

axis 4.67 ± 0.62 mg) resulted in a difference in baseline inter-hook separation distance (long-axis: 652 ± 91 µm *vs*. short-axis: 394 ± 45 µm, p = 0.03), suggesting the zebrafish SAN is more compliant in the long-axis direction (Figure 4.4). Further, with a controlled preload, the Coefficient of Variation of the change in BR was significantly reduced (69 ± 4% compared to 109 ± 9%, p = 0.0059) demonstrating that the variable responsiveness was likely the result of an uncontrolled preload. The difference in responsiveness previously observed with 25% stretch in the long- and short-axis direction was eliminated with a controlled preload, as there was no longer a difference in the peak percentage increase in BR between the groups (Figure 4.5, long-axis: 4.44 ± 0.92%; short-axis: 3.59 ± 0.49%; p = 0.2172).

4.3.2. The Species-Specific SAN Stretch Response and its Relation to SAN Stiffness

The rabbit (n = 9), mouse (n = 8), and zebrafish (n = 8) isolated SAN preparations demonstrated regular, spontaneous beating (rabbit: 189 ± 3 bpm; mouse: 401 ± 11 bpm; zebrafish: 148 ± 7 bpm) following baseline force application (rabbit: 210 ± 20 mg; mouse: 70 ± 10 mg; zebrafish: 2.2 ± 0.2 mg). Stretch caused a magnitude-dependent increase in BR in both the rabbit (Figure 4.6A) and zebrafish (Figure 4.6C) SAN with strain levels of 20% or greater ($p < 0.05$, by mixed-effects analysis in rabbit and one-way ANOVA in zebrafish) with BR returning to baseline each time stretch was released. Conversely, stretch of the mouse SAN resulted in a variable chronotropic response (Figure 4.6B). In three mice BR increased, in one mouse BR decreased, and in four mice responses varied between increasing and decreasing at different strains. In the rabbit and mouse there was no correlation between chronotropic responsiveness and baseline BR before stretch (Figure 4.7A – B: rabbit R^2-values < 0.3; $p > 0.1$; mouse R^2-values < 0.1, $p > 0.5$) whereas in the zebrafish there was an inverse relationship, with a lower baseline BR correlating with a greater increase in BR with 50% stretch (Figure 4.7C: 10%: $R^2 = 0.1897$, $p = 0.2807$; 20%: $R^2 = 0.3276$, $p = 0.1382$; 30%: $R^2 = 0.3254$, $p = 0.1398$; 40%: $R^2 = 0.3966$, $p = 0.0943$; 50%: $R^2 = 0.7710$, $p = 0.0041$).

In the rabbit, the baseline tissue length was 12.1 ± 0.6 mm and in the mouse it was 2.7 ± 0.2 mm. In both species, tissue stress at each strain was determined by dividing the measured diastolic force by the baseline SAN cross-sectional area (perpendicular to the direction of stretch), from which individual stress-strain curves were generated (Figure 4.8A – B). On average there was no difference in stress between

rabbit and mouse (Figure 4.9). Due to the divergent morphology of the zebrafish SAN, an applied force-strain curve was instead generated (Figure 4.8C).

To determine the relationship between the overall chronotropic responsiveness to stretch and SAN stiffness, the largest percentage change in BR from each preparation was plotted against an index of tissue stiffness, generated from the stress- or force-strain relations. In the mouse, absolute values of percentage change in BR were used to represent responsiveness, as in some mice the largest chronotropic change was negative, while for others it was positive. Interestingly, in both the mouse and zebrafish there was a positive correlation between chronotropic responsiveness to stretch and SAN stiffness, whereas in the rabbit this relationship was inversely correlated (Figure 4.10: rabbit: $R^2 = 0.4577$, $p = 0.0454$; mouse: $R^2 = 0.5541$, $p = 0.0341$; zebrafish: $R^2 = 0.7035$, $p = 0.0047$).

4.3.3. Collagen Alignment and Crimp with Stretch

Collagen was visualised with SHGM imaging in the SAN of rabbit and mouse at baseline and with 40% stretch (Figure 4.11). In the dense surface layers of unstretched SAN, collagen fibre alignment differed between rabbit and mouse (Figure 4.12). Fibres were aligned parallel to the crista terminalis in the rabbit but were randomly oriented in the mouse. Stretched preparations of both the rabbit and mouse, however, had collagen fibres that were more aligned parallel to the crista terminalis. In both species, collagen fibres were tightly crimped (as indicated by wavelength) and tortuous in the surface layer (Figure 4.13). There was no difference in crimp wavelength in stretched SAN from either species or in tortuosity in SAN from mouse, but tortuosity was lower in stretched rabbit SAN.

In the less-dense middle layers of unstretched SAN from both species, collagen fibres were randomly oriented, tortuous, and crimped (Figure 4.12 and 4.13). In stretched SAN preparations, collagen fibres were more aligned parallel to the crista terminalis and were less tortuous than in unstretched SAN preparations in both species. Crimp wavelength, however, was not different between stretched and unstretched SAN of the mouse but was larger in stretched compared to unstretched rabbit SAN.

4.4. Discussion

These experiments examine the importance of mechanical parameters, such as stretch direction, baseline and applied force, and tissue stress and stiffness to the magnitude of

the SAN stretch-induced change in BR. In experiments with an uncontrolled preload before stretch of the zebrafish SAN, there is a positive correlation between preload and chronotropic responsiveness. When preload is controlled, however, the dependence is instead on the applied force. Further, a controlled preload results in a difference in inter-hook distance in the long- vs. short- axis, implicating the SAN ring is mechanically anisotropic. Controlled baseline force also eliminates the previously observed stretch direction-dependence of the magnitude of the increase in BR. In the rabbit, sustained stretch causes a magnitude-dependent increase in BR, which is not the case in the mouse. The magnitude of the stretch-induced change in BR has a dependence on tissue stiffness in all species. Specifically, there is a positive correlation between stiffness and change in BR in the mouse and zebrafish, but an inverse relationship in the rabbit. This study shows species differences in SAN collagen characteristics and their change with stretch. The chronotropic response to SAN stretch is influenced by tissue mechanics, such that the magnitude of the change in BR is dependent on strain, baseline or applied load, and tissue stiffness.

4.4.1. Baseline or Applied Force Alters Chronotropic Responsiveness in Zebrafish

In the experiments characterising the response to stretch in the zebrafish SAN in my first objective there was a consistent increase in BR, however, there was a large inter-subject variability in the magnitude of the chronotropic response. Further, the dependence on stretch direction – a greater increase in BR with stretch in the short-axis direction compared to the long-axis direction – may reflect an influence of anisotropic tissue properties. This could affect the spatial distribution of stress and/or strain across the SAN ring. These factors demonstrated the need for simultaneous force measurements with strain so that the importance of a consistent preload could be determined.

The qualitative approach for determining inter-hook distance (as used in my first objective) resulted in a variable baseline force. In this case, the magnitude of the peak change in BR with 10% and 25% stretch was positively correlated with baseline force (but not with applied force), such that SAN preparations under a greater preload exhibited greater increases in BR with stretch. Interestingly, the magnitude of the peak change in BR with 50% stretch was instead positively correlated with applied force but not baseline force. However, in nine of the ten zebrafish, the relationship between

baseline force and time was significant (R^2-values > 0.7; $p < 0.005$), which is likely reflective of a gradual, time-dependent deformation of the tissue. It is possible that 50% stretch was dependent on applied force rather than baseline force due to the time-dependent change in baseline force, as 50% stretch was always applied near the end of the protocol. Further studies with a reversed or randomised order of stretch magnitudes would be required to address this. Regardless, it became apparent that using a quantifiable, controlled baseline load decreases the inter-subject variability in responsiveness and could account for the dependence in stretch direction observed between long- and short-axis stretch under uncontrolled baseline conditions.

When the baseline force was controlled, the pre-stretch inter-hook distance was larger in the long-axis direction (652 ± 91 μm) compared to the short axis direction (394 ± 45 μm), whereas in the initial study, inter-hook distance was the same in both directions (220 ± 11 μm and 220 ± 13 μm, respectively). This demonstrates that the zebrafish SAN ring may have anisotropic tissue properties such that the SAN is more compliant in the long-axis direction and stiffer in the short-axis direction. Interestingly, controlling the baseline force eliminated the direction-dependence in the chronotropic response. Although in my first objective 25% stretch in the short-axis direction resulted in a greater increase in BR than in the long-axis direction, there was no difference in the stretch-induced increase in BR between long- *vs*. short-axis stretch when baseline force was controlled. Interestingly, in the first objective there was no difference in inter-hook distance between long- and short-axis, whereas with controlled preload the long-axis inter-hook distance was larger than in the short-axis direction. This indicates that the difference in responsiveness observed in the previous study between the two directions likely arises from different preloads rather than direction-dependent differences in mechanotransduction.

4.4.2. Tissue Stiffness and the SAN Stretch-Induced Change in BR

The stretch-induced increase in BR in the rabbit SAN elicited in this study is consistent with previous reports from many groups using a multitude of distinctive experimental approaches (Deck, 1964; Golenhofen and Lippross, 1969; Ushiyama and Brooks, 1977; Kamiyama et al., 1984; Arai et al., 1996). Only one previously published study investigated the chronotropic response to SAN stretch in the mouse, and they showed a variable change in BR that was on average a decrease (Cooper and Kohl, 2005). Interestingly, although the data in this study do not show an overall decrease in BR in

response to stretch, this may be reflective of the different baseline BRs measured in this study compared to the previous report. When scaled to fit on the same axis, the response between the two studies is consistent, as the large decreases in BR were observed at lower baseline BRs than any of the preparations in this study displayed (Figure 4.14).

In all three species the magnitude of the chronotropic response to stretch is dependent on tissue stiffness. Surprisingly, in the rabbit this is a negative relationship – less stiff SANs are more responsive – while in the mouse and zebrafish the opposite is true and stiffer SANs are more responsive. Little is known regarding the mechanical parameters that determine the magnitude of the stretch-induced chronotropic response, and previous (non-murine) studies have varying suggestions regarding the key mechanical parameter. Some have proposed that the amplitude of the stretch-induced increase in BR is determined by the amount of tissue stretch (Kamiyama et al., 1984), while others have instead suggested it is determined by tissue tension (Chiba, 1977; Arai et al., 1996), or a combination of both (Pathak, 1958; Lange et al., 1966). The dependence of BR responsiveness on SAN stiffness may indicate that the mouse and zebrafish SAN respond predominantly to stress (rather than strain). Stress will be higher at the same strain in stiffer SAN preparations, so the greater change in BR would correspond to a stress response. The response in rabbit, contrarily, may not be stress-dependent, as the response magnitude was not positively correlated to tissue stiffness, yet still greater strain resulted in a greater increase in BR. In this study strain was the controlled variable, and therefore in order to more thoroughly determine the contribution of strain, controlled stresses would instead need to be applied to the tissue. The effect of mechanical loading on BR may depend on the mode of load application – controlled strain *vs*. controlled force – perhaps explaining the lack of agreement between previous experimental studies.

Although disentangling stress and strain is not straight-forward, it would provide an understanding of what stimuli the SAN is responding to during stretch. It is conceivable that the rabbit is more sensitive to strain whereas the mouse and zebrafish are more sensitive to stress, or, instead it is possible that mechanotransduction is differently distributed or transmitted to the stretch-sensitive components of the SAN. Differences in underlying tissue structure may result in different structural adaptations to stress/strain, changing mechanotransduction and therefore altering the responsiveness of the SAN to stretch.

4.4.3. Species Differences in SAN Structure and Changes in Structure with Stretch

Mechanical considerations that may be important for determining the magnitude of the SAN stretch-induced chronotropic response include differences in SAN structure at baseline or changes in structure with stretch, and in the current study both were observed. Due to the drastically different morphology of the zebrafish SAN compared to the mammalian SAN, only mammalian SAN samples were utilised in these experiments.

At baseline, the surface layers of the rabbit SAN contained dense, well-organised collagen fibres running parallel to the *crista terminalis*, which is consistent with previous work (Opthof et al., 1987b). In the stretched surface layer of the rabbit SAN there was a reduction in crimp tortuosity compared to baseline. Collagen appeared to be less dense in the surface layers of the mouse SAN compared to the rabbit at baseline, which has been shown in previous studies (Hao et al., 2011; Glukhov et al., 2015). Unlike the rabbit SAN, surface collagen was randomly oriented in the unstretched mouse SAN. However, when stretched, collagen fibres in the mouse SAN were aligned in the direction of stretch, parallel to the *crista terminalis* with no change in crimp characteristics. Thus, based on previous work and new data from this study, it seems the surface layers of the mouse and rabbit SAN differ at baseline (aligned, dense collagen in rabbit and poorly aligned collagen in mouse) and respond differently to stretch (reduced tortuosity in rabbit and realignment in mouse). Interestingly, even with these structural differences in the dense surface of the SAN, there was no difference in the stiffness of rabbit and mouse SAN.

In the middle layers of the rabbit SAN, collagen appeared to be less dense than in the surface and collagen fibres were randomly oriented, again in agreement with previous reports (Bleeker et al., 1980). The middle layers in the mouse were consistent with the rabbit in which collagen appeared less dense than in the surface layers and was irregularly oriented. For both species, in the stretched middle SAN layer there was a reduction in collagen crimp tortuosity and collagen fibres were aligned in the direction of stretch.

The reduction in collagen crimp (which may result in greater cell stretch (Rego et al., 2016), suggests that, because this is happening in both layers, the rabbit SAN may be suited for large strains. This is further supported at the cellular level, as rabbit SAN cells have more caveolae at baseline than mouse SAN cells, and the rabbit also has

greater incorporation of caveolae into the cell membrane, relieving membrane stress (MacDonald et al., 2020a). In contrast, with stretch, mouse SAN surface collagen fibres maintain their crimp and instead re-align in the direction of stretch. And, as they have fewer caveolae at baseline, mouse SAN cells may be less able to relieve cell membrane tension by incorporation of caveolae compared to rabbit cells, in which caveolae may act as a sarcolemmal surface reserve (MacDonald et al., 2020a). These differences could be a mechanistic explanation regarding the correlation between responsiveness in the mouse SAN – but not the rabbit SAN – to stress. If this were the case it could theoretically account for the observation in the present study that less stiff rabbit SAN preparations have greater chronotropic responses to stretch, while for the mouse the opposite is true.

Alternatively, this species-dependence of the relation between SAN stiffness and responsiveness could be the result of differences in the transduction of mechanical load to embedded pacemaker cells or other mechanosensitive SAN components, such as fibroblasts (Kohl et al., 1994). The degree of mechanical coupling between cells and collagen could contribute to the stiffness-dependent response. If cells are poorly coupled, then in a stiffer SAN (due to dense or stiffer collagen) less tension or stretch may be transmitted to pacemaker cells, essentially 'isolating' them from the external mechanical load and reducing the response. Contrarily, if there is strong coupling between collagen and SAN cells, then in a stiffer SAN more load may be transmitted to the pacemaker cells, increasing the response. If this were true, then perhaps in the rabbit cells are poorly coupled to collagen whereas the mouse they are not, explaining the disparate relationship between stiffness and chronotropic responsiveness in the two species. Interestingly, in a study on biomechanical properties and extracellular matrix in decellularized porcine SAN and left ventricular preparations it was found that the extracellular matrix in the SAN was different in composition and stiffer than in the left ventricle (Gluck et al., 2017). Further, they showed that the extracellular matrix in the SAN may serve as a protective scaffolding for pacemaker cells, reducing the stress they experience with stretch (Gluck et al., 2017). These data corroborate the idea that mechanical coupling between extracellular matrix and pacemaker cells may contribute to the dependence of chronotropic responsiveness on stiffness. The SAN of larger mammals (including pigs or humans) may be less responsive to stretch if stiffer, like in the rabbit, because the pacemaker cells are protected from stress by extracellular matrix.

This may have important implications for humans in ageing and disease, because under these circumstances the SAN can become more fibrotic and stiff (Kalyanasundaram et al., 2019). The human SAN, much like the rabbit, consists of pacemaker cells embedded in an extensive collagen network (Csepe et al., 2015). If the responsiveness of the human SAN to stretch is also inversely correlated with stiffness (as in the rabbit), then this could contribute to SAN dysfunction *via* a reduced chronotropic response to stretch with changes in tissue structure. Alternatively, if the opposite were true, it could contribute to SAN dysfunction *via* increased mechano-sensitivity. Either way, disruption of this important BR control mechanism may have pathological consequences.

The relative alignment of collagen and cells in the SAN may also be an important factor for mechanotransduction. Collagen is well aligned and arranged parallel to the *crista terminalis* in the rabbit SAN surface but randomly oriented in the mouse SAN surface. Cells are randomly arranged and embedded in the rabbit SAN (Bleeker et al., 1980), whereas in the mouse SAN they are arranged perpendicularly to the *crista terminalis* in the centre and parallel in the periphery (Liu et al., 2007). These distinct and specific arrangements and interactions of collagen and cells may result in differences in mechanotransduction, and therefore responsiveness, potentially contributing to the stiffness-dependence of the response. The importance of SAN tissue architecture was demonstrated as early as 1964, in a study in which concentric stretch caused greater increases in BR than linear stretch in the rabbit and cat SAN (Deck, 1964), and remains an area warranting further investigation.

4.5. Conclusion

This study demonstrates the importance of structural and mechanical SAN properties on the chronotropic response to stretch. In the zebrafish, responsiveness is dependent on either baseline or applied force, and stiffer SAN preparations result in larger increases in BR. Similarly, in the mouse stiffer SAN preparations also result in greater chronotropic changes, however, the direction of the response is variable. Interestingly, in the rabbit, less stiff SAN preparations result in greater increases in BR. The observed structural differences between the rabbit and mouse SAN at baseline, and their structural adaptations with stretch, may contribute to the difference in mechanical parameters demonstrated in this study. Mechano-sensitivity of the SAN is an important BR control mechanism, and its dysfunction – due to changes in SAN structural properties – may

contribute to arrhythmias. Therefore, further studies investigating this physiological mechanism may have important implications for understanding SAN dysfunction and treatment.

Figure 4.1. Variability of the chronotropic response to zebrafish SAN stretch. Change in BR with 10, 25, and 50% stretch of the zebrafish SAN from the 26 experiments in my first objective.

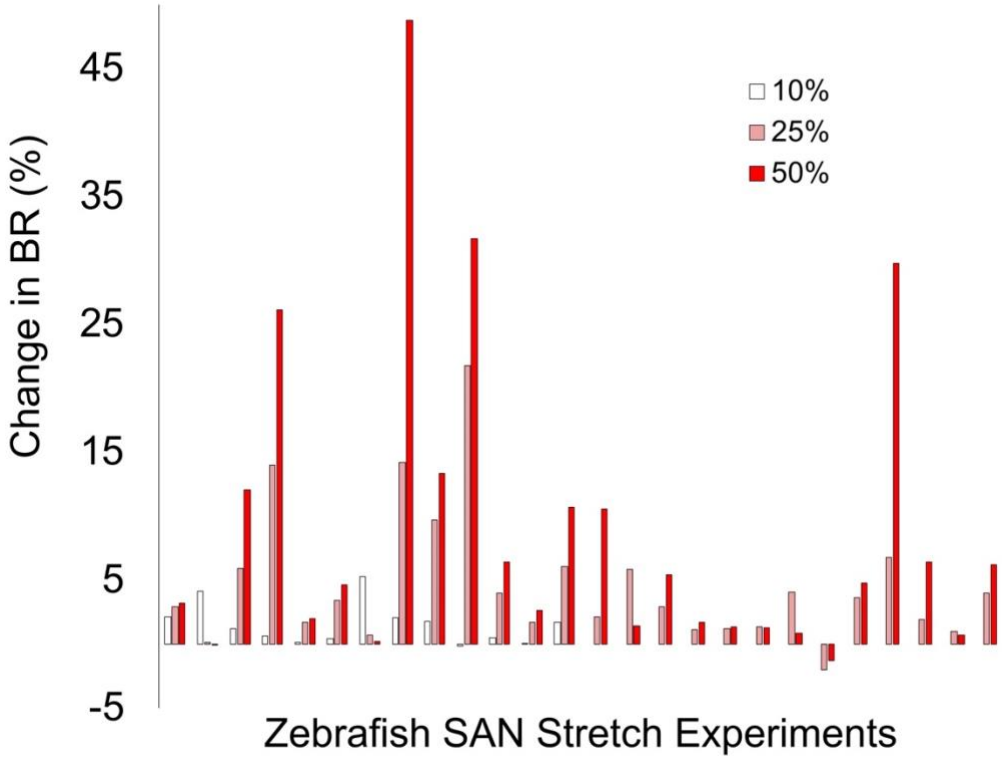

Figure 4.2. Mammalian isolated SAN stretch representative preparations.
Rabbit (A) and mouse (B) SAN preparations at baseline and with stretch. IVC, inferior *vena cava*; SVC, superior *vena cava*. (Adapted from MacDonald et al., 2020).

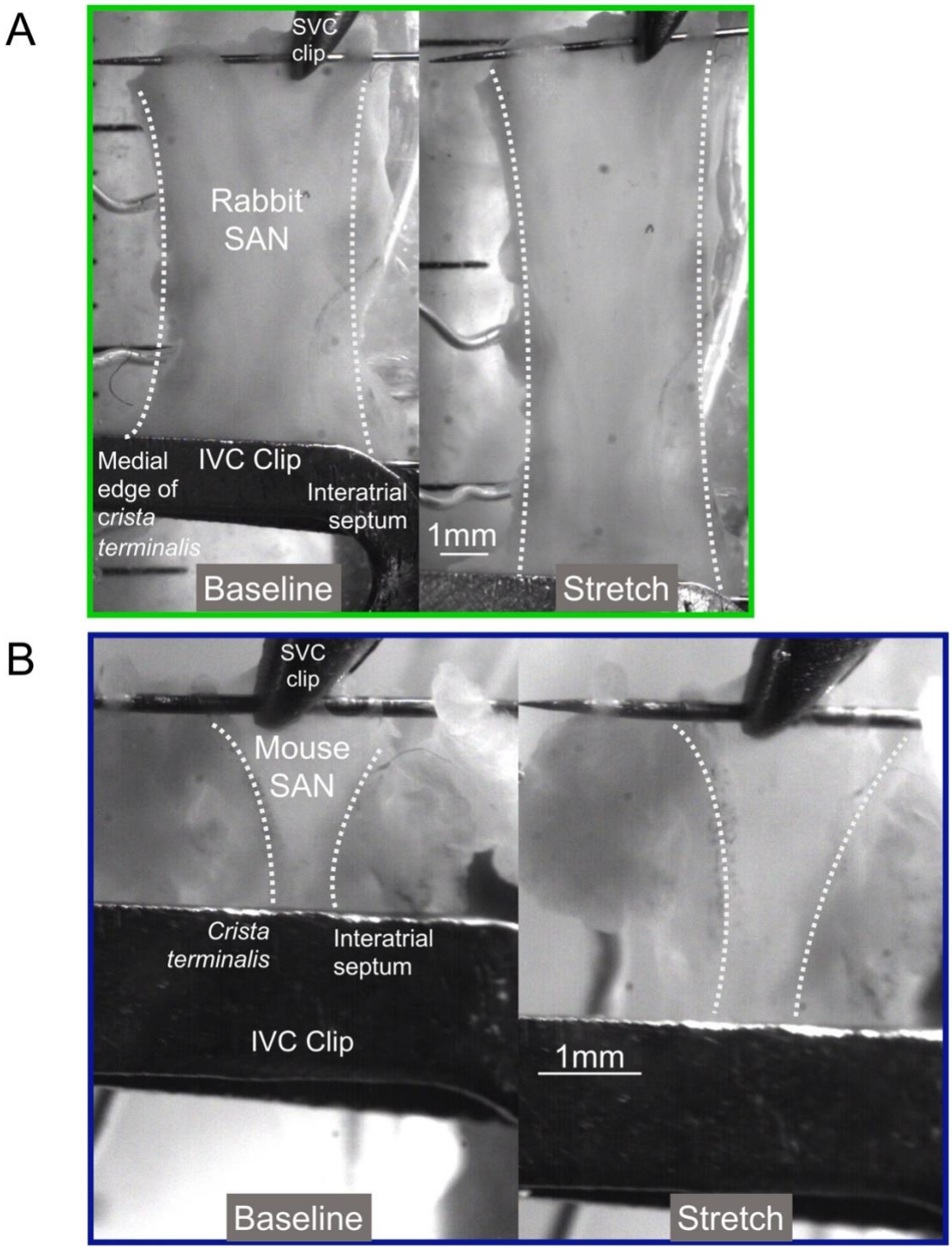

Figure 4.3. Relationship between chronotropic responsiveness and preload or applied force.

Peak change in BR as a function of baseline force (A) and applied force (B) in the zebrafish SAN. *p<0.05 when the relation significantly deviated from zero.

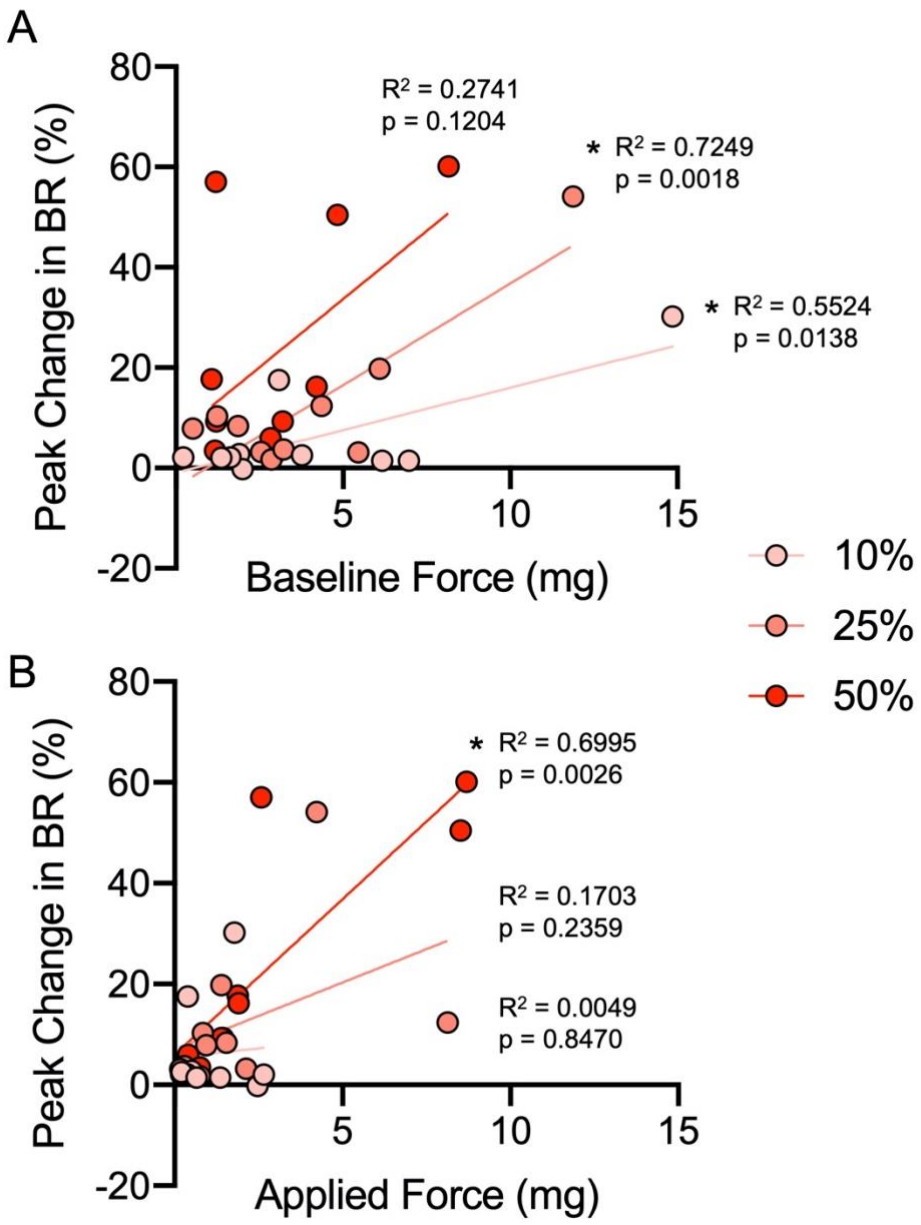

Figure 4.4. Inter-hook distance in long- and short-axis zebrafish SAN.

Inter-hook distance prior to stretch in the zebrafish sinoatrial node with a consistent baseline force (~ 5 mg) in the long- and short-axis direction. *p<0.05 by unpaired student t-test.

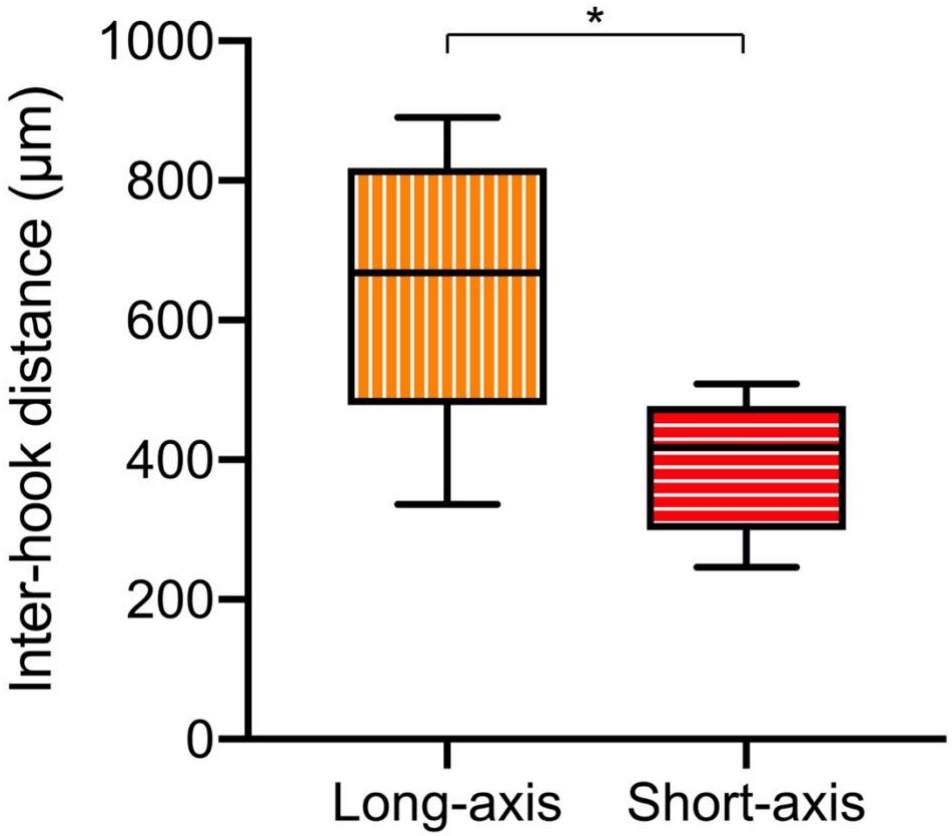

Figure 4.5. Long- or short-axis SAN stretch response with controlled or uncontrolled preload.

Peak percentage change in BR with stretch of the zebrafish SAN in the long- and short-axis direction with an uncontrolled baseline force (left) and with a consistent baseline force (~ 5 mg, right). *p<0.05 by unpaired student t-tests.

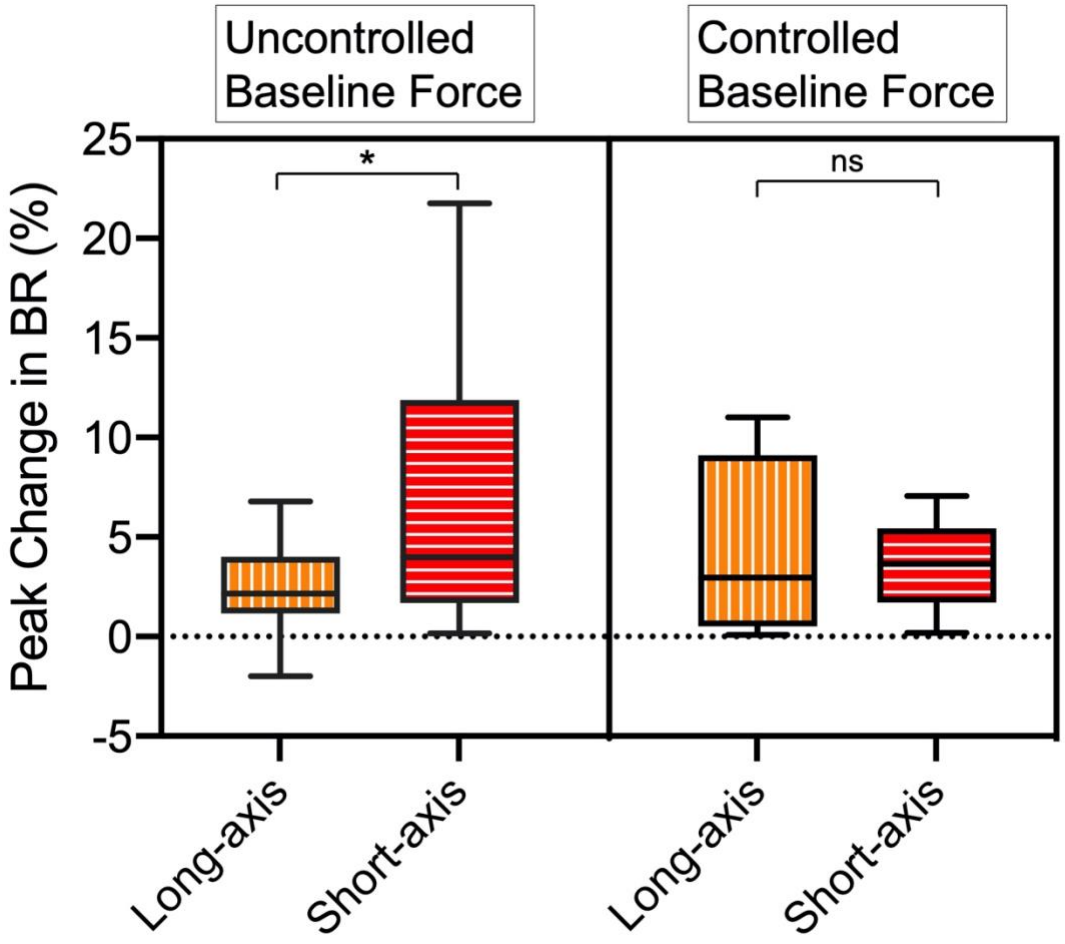

Figure 4.6. Chronotropic response to SAN stretch in the rabbit, mouse, and zebrafish.

SAN stretch-induced changes in BR Average percentage change in BR with increasing magnitudes of strain of the rabbit (A), mouse (B), and zebrafish (C) SAN. *p<0.05 by mixed-effects analysis and one-way ANOVA. (Adapted from MacDonald et al., 2020).

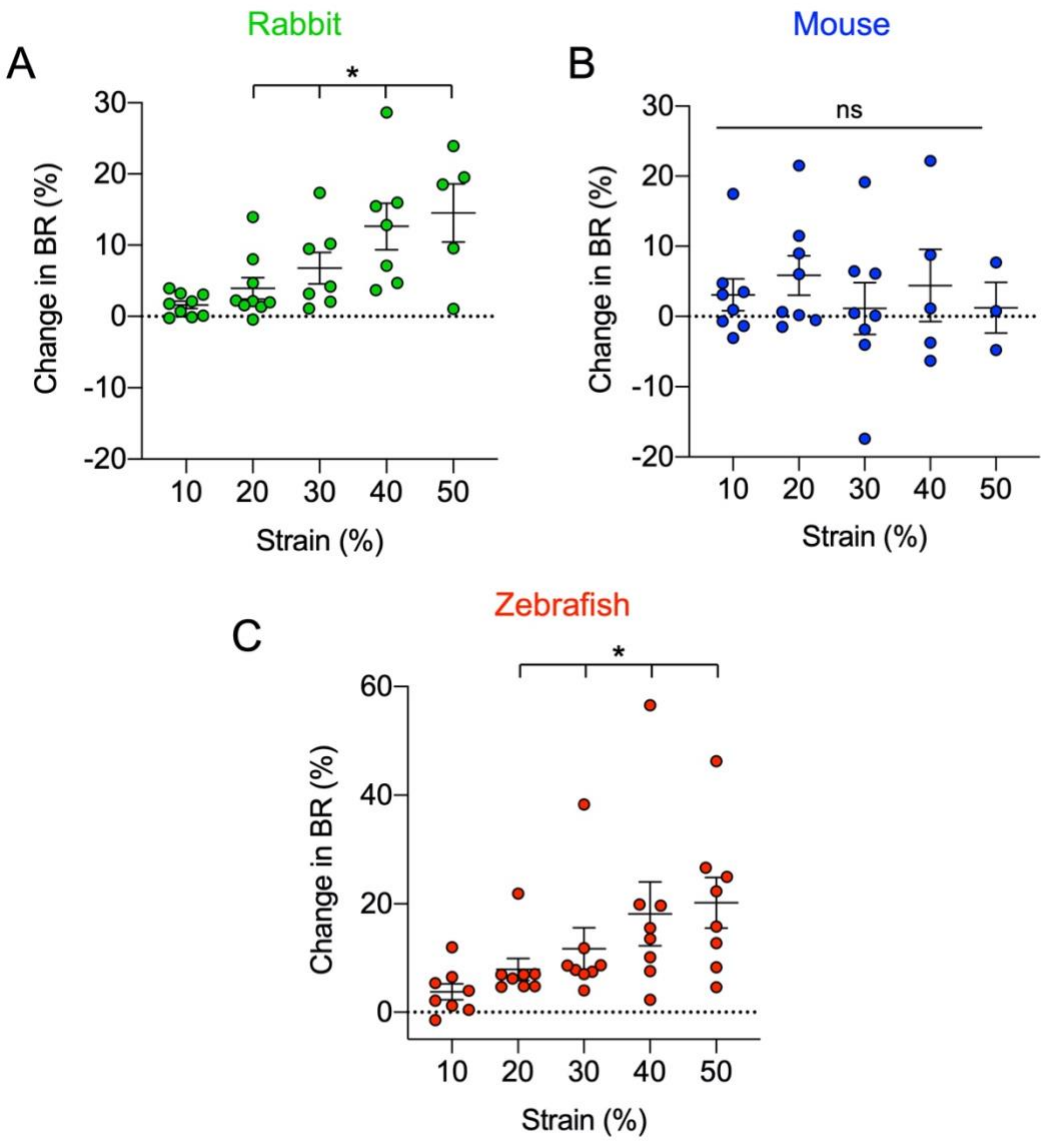

Figure 4.7. Relationship between chronotropic responsiveness and baseline BR. The change in BR as a function of baseline BR before stretch in the rabbit (A), mouse (B), and zebrafish (C) SAN with application of stretch of increasing magnitudes and the *p<0.05 when the relation significantly deviated from zero. (Adapted from MacDonald et al., 2020).

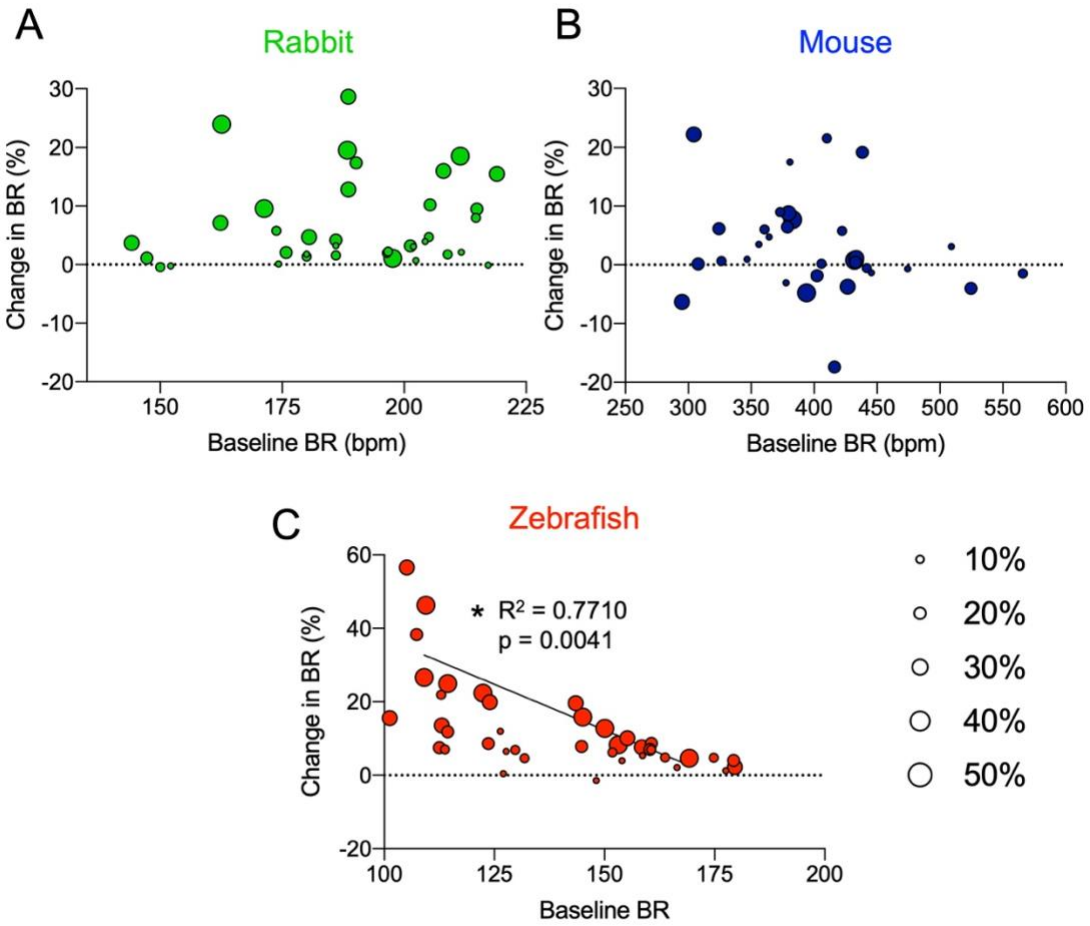

Figure 4.8. Rabbit, mouse, and zebrafish stress-strain curves.

Stress as a function of strain from each individual rabbit (A) and mouse (B) SAN stretch experiment. Applied force as a function of strain from each individual zebrafish (C) SAN stretch experiment. (Adapted from MacDonald et al., 2020).

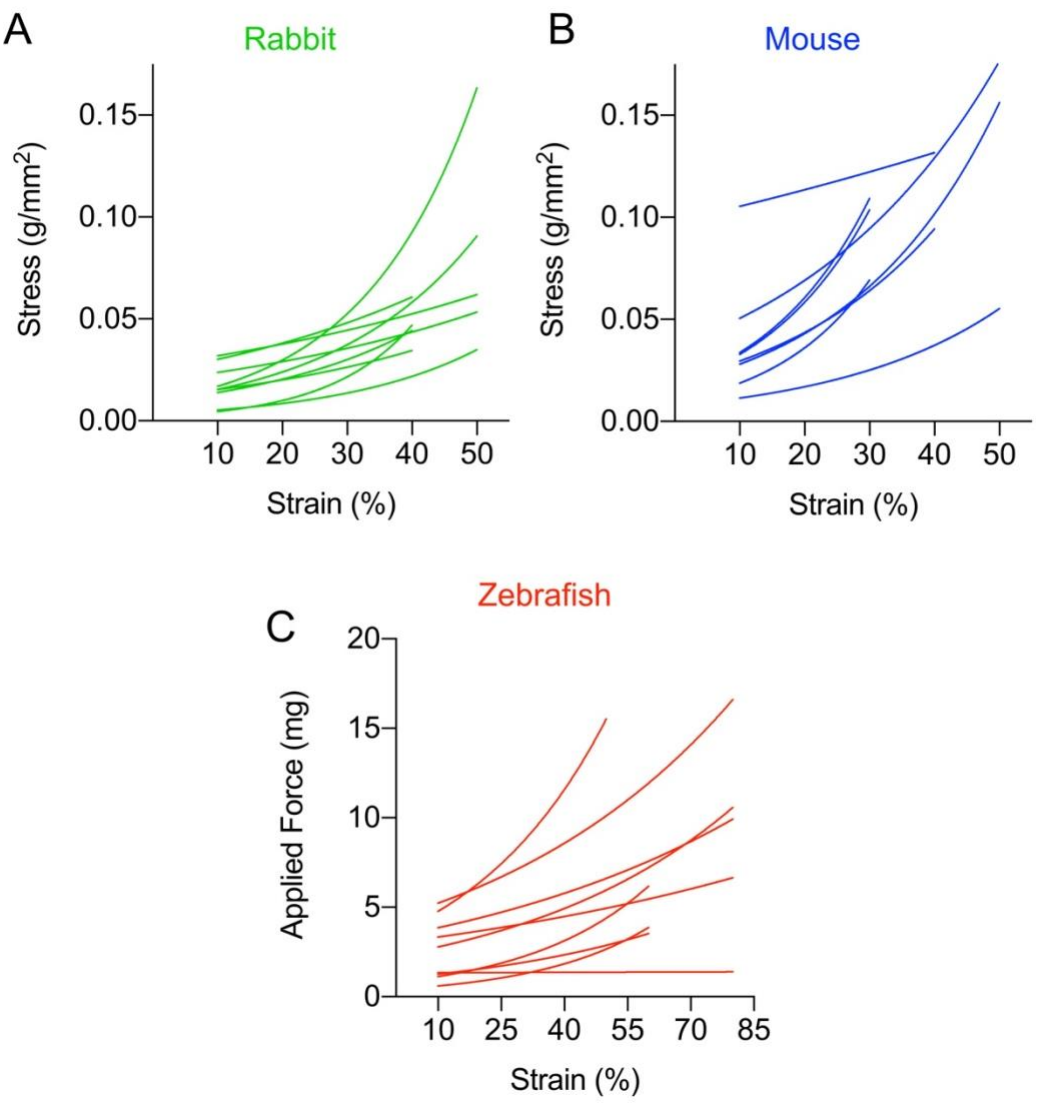

Figure 4.9. Average rabbit and mouse stress-strain curves.

Stress as a function of strain on average from rabbit (green) and mouse (blue) SAN stretch experiments. (Adapted from MacDonald et al., 2020).

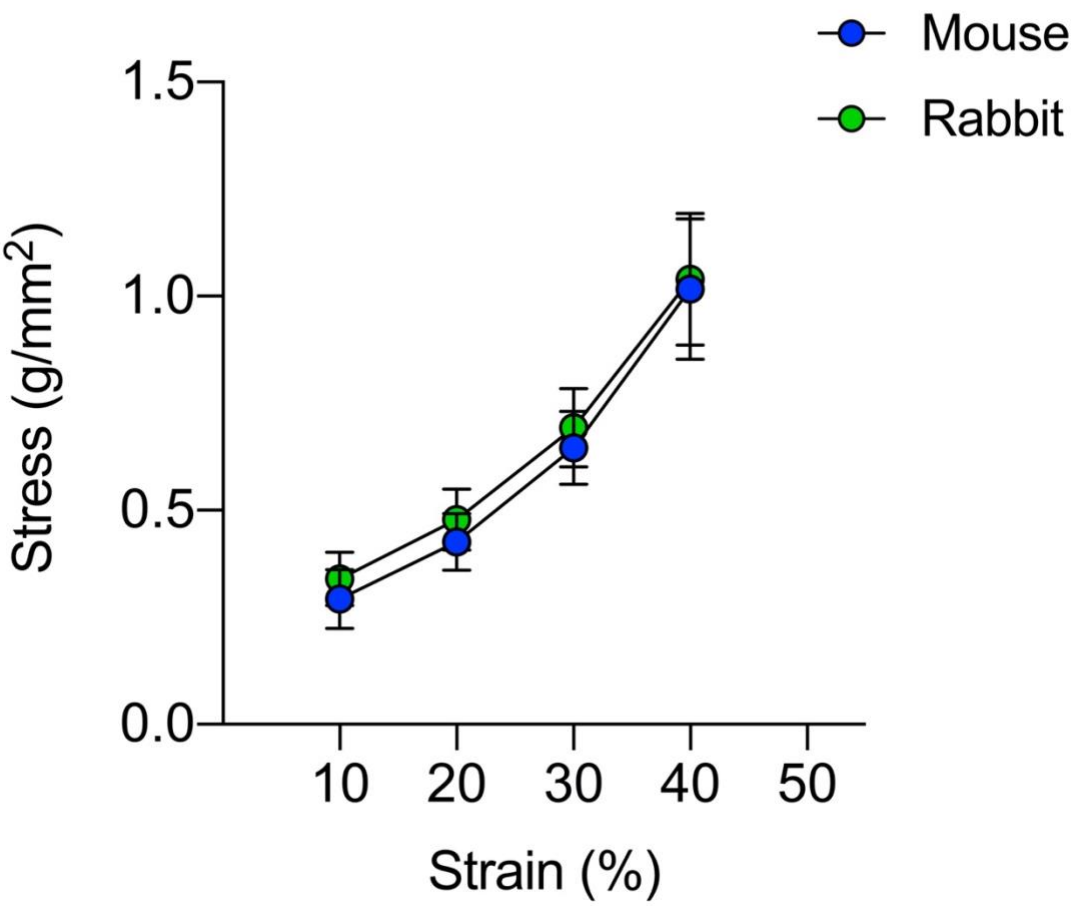

Figure 4.10. Relationship between chronotropic responsiveness and tissue stiffness.

The largest absolute percentage change in BR observed with SAN stretch as a function of tissue stiffness (β) for each individual rabbit (A), mouse (B), and zebrafish (C) SAN studied. (Adapted from MacDonald et al., 2020).

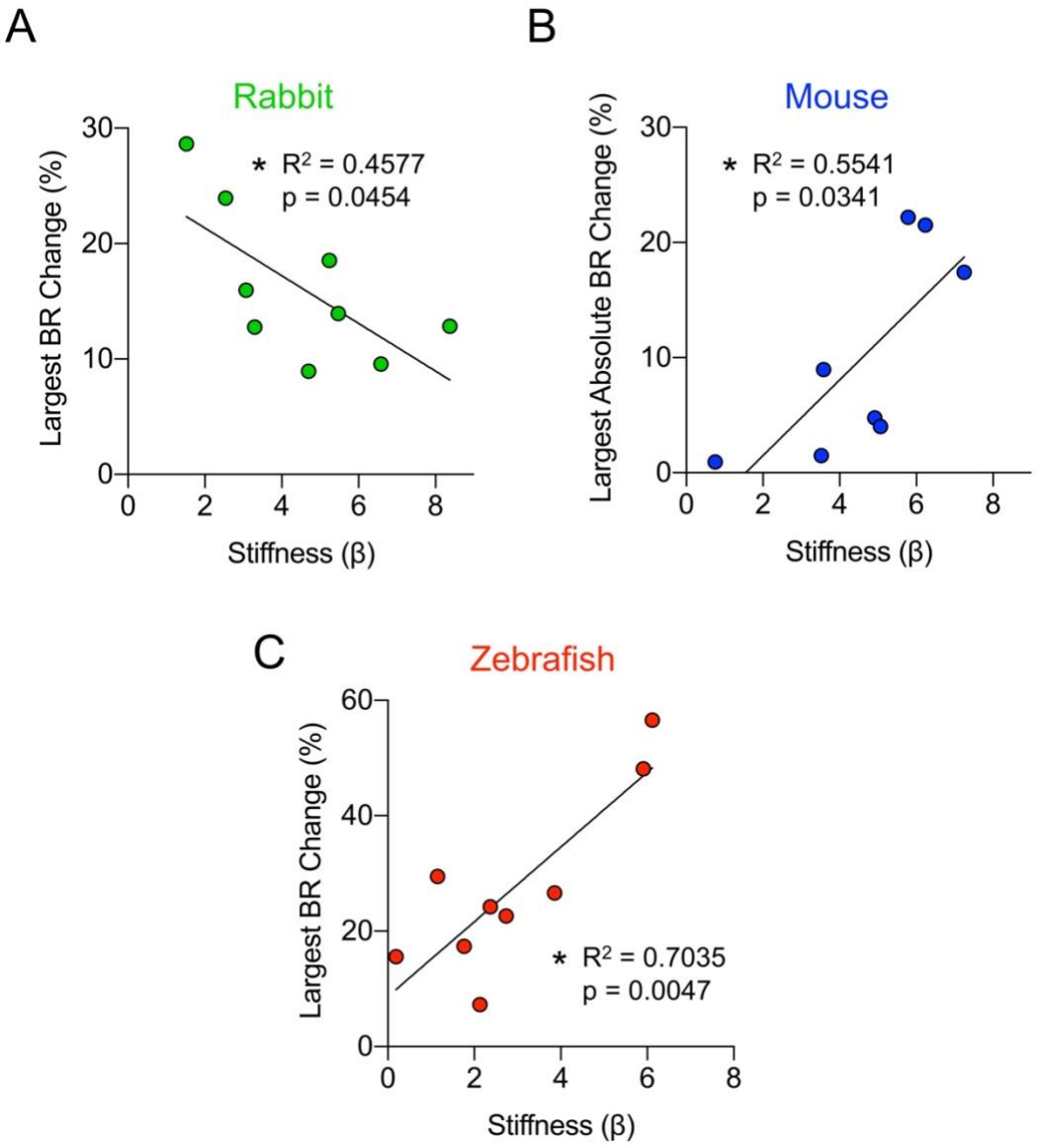

Figure 4.11. Structural changes with rabbit and mouse SAN stretch.

Representative second-harmonic generation images of collagen at the epicardial surface and in the middle layers of the central SAN of rabbit (left) and mouse (right), at baseline and during 40% stretch. (Adapted from MacDonald et al., 2020).

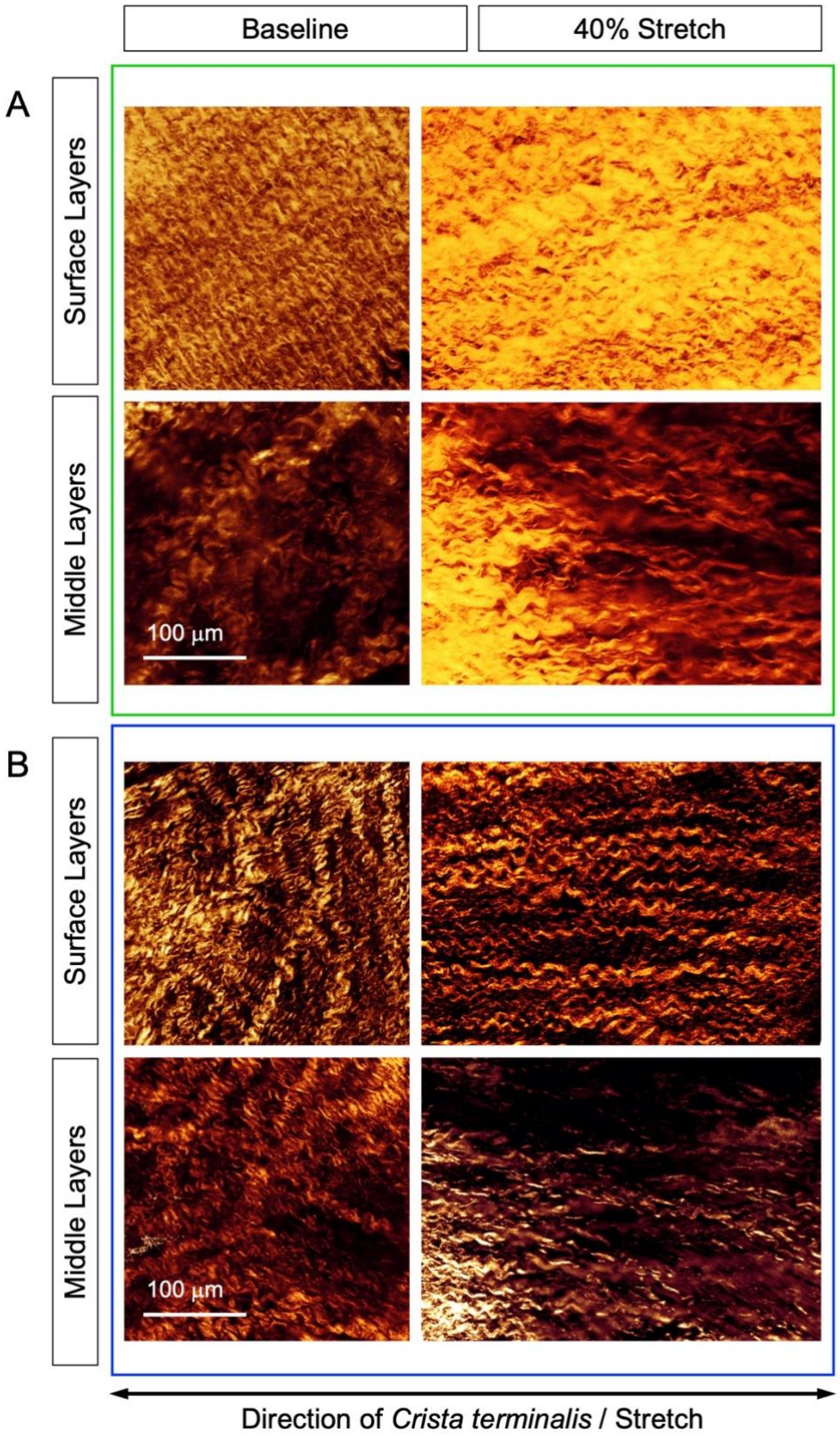

Figure 4.12. Changes in SAN collagen orientation with stretch.

Analysis of collagen orientation from SHGM images for rabbit (A) and mouse (B), unstretched and stretched samples (n=3 for each). Black bars represent the fraction of fibres averaged across all samples and coloured outlines represent the average fraction of fibres from individual samples. (Adapted from MacDonald et al., 2020).

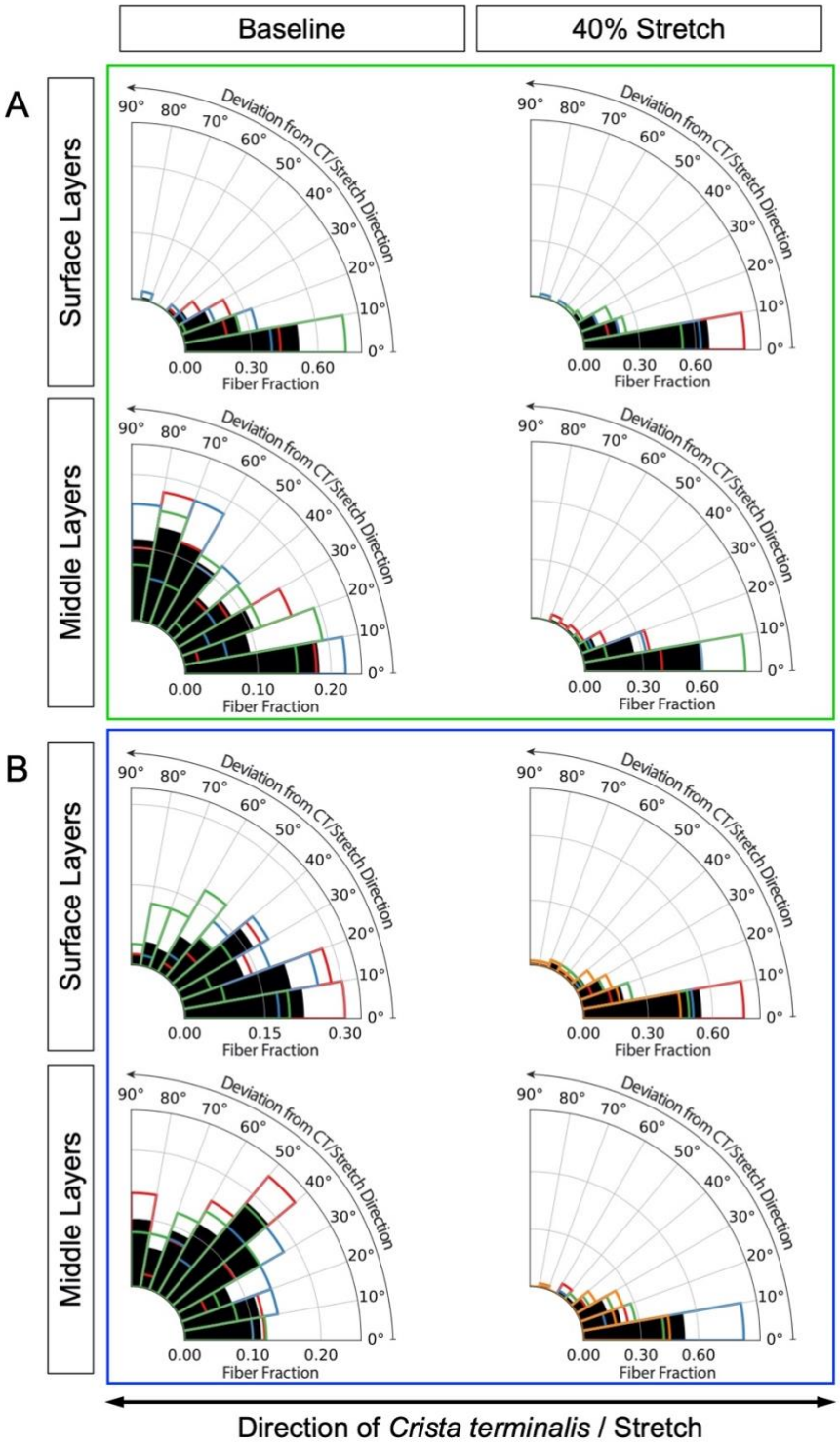

Figure 4.13. Changes in SAN collagen crimp with stretch.

Collagen crimp characteristics in the unstretched and stretched SAN from the mouse (blue) and rabbit (green). (A) Crimp tortuosity ratio and (B) crimp period length. (Adapted from MacDonald et al., 2020).

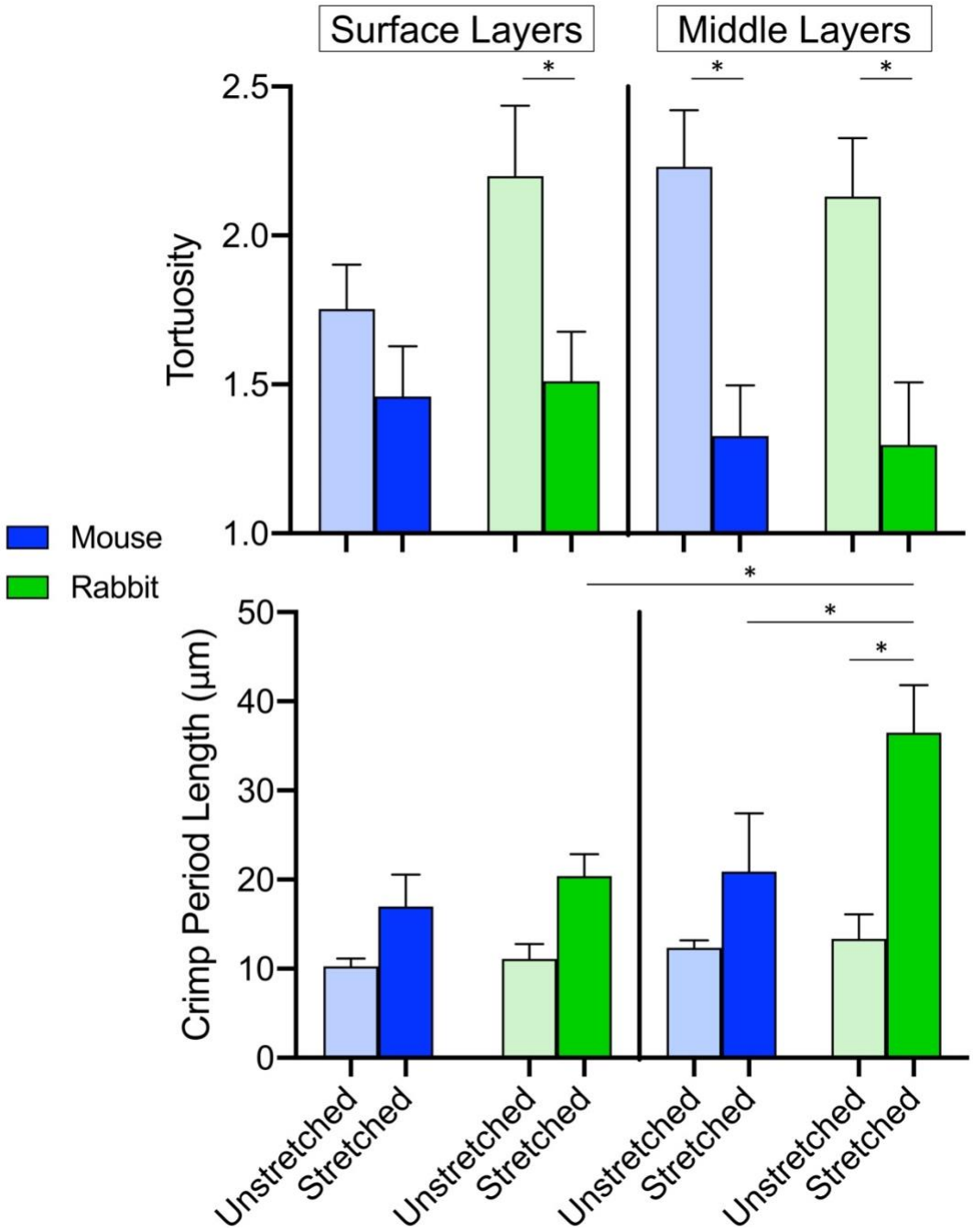

Figure 4.14. Relationship between chronotropic responsiveness and baseline BR in the mouse SAN.

Summary of the stretch-induced change in BR in the mouse SAN at 27°C (grey circles) and 37°C (black circles) and in the guinea pig SAN (squares), plotted as a function of initial BR (from Cooper and Kohl 2005) compared to the stretch-induced change in BR from the mouse SAN as a function of baseline BR in the current study. (Adapted from MacDonald et al., 2020).

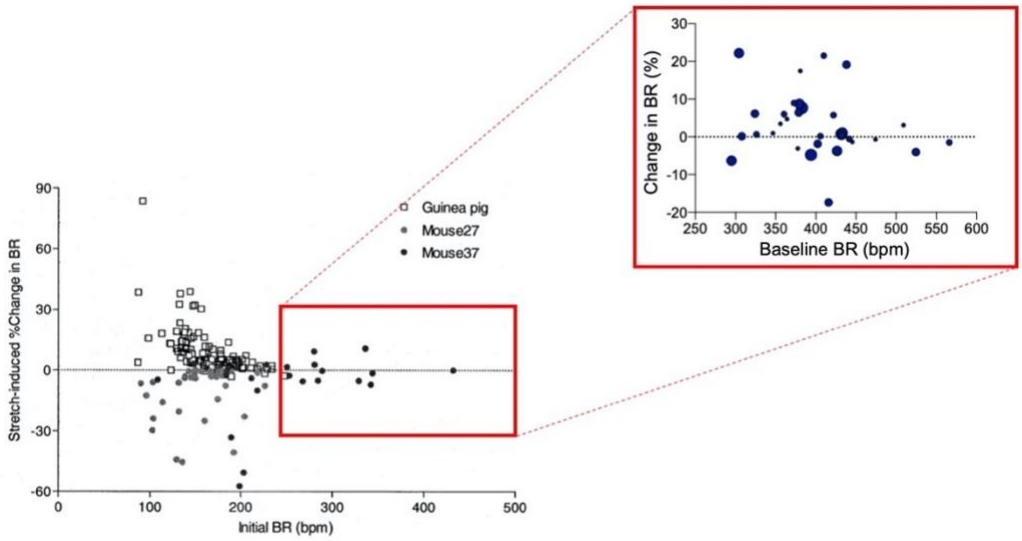

CHAPTER 5: DISCUSSION

5.1. ZEBRAFISH AS A MODEL FOR SAN STRETCH INVESTIGATIONS

This work provides further insight into the electrophysiological, mechanical, and structural determinants of the regulation of SAN function by stretch. It began by establishing the zebrafish as an innovative model for the study of SAN stretch mechanisms. The zebrafish is an advantageous model to investigate SAN mechano-sensitivity due to the ease of its genetic modification, its similarities in cardiac electrophysiology and extrinsic SAN control to humans, and most importantly – as established here – the similar response to SAN stretch (Vornanen and Hassinen, 2016; Gut et al., 2017; MacDonald et al., 2017). The positive chronotropic response to stretch in zebrafish is consistent with the response to SAN stretch in humans and most mammals. In contrast, the chronotropic response to sustained SAN stretch in the mouse is variable, positioning the zebrafish as a useful genetically modifiable model species for SAN stretch research. Like any model, the zebrafish has limitations. Its small, two-chambered heart experiences much lower physiological pressures than mammals and its ring-shaped SAN is morphologically dissimilar from the mammalian SAN. Yet despite its limitations, the zebrafish appears to be a useful and exciting model for mechano-electric coupling pacemaker studies, particularly when used in conjunction with other model systems.

5.2. AN OPTOGENETIC, COMPUTATIONAL, AND PHARMACOLOGICAL APPROACH FOR UNDERSTANDING SAC_{NS}-LIKE CURRENT ACTIVATION

My studies continued using this newly identified model to investigate the importance of timing and AP morphology for SAN stretch responses. This was initially pursued, paradoxically, without stretching the SAN. Instead, using light-activated ChR2 as a surrogate for SAC_{NS} provided a controlled and consistent technique for rapidly eliciting a 'SAC_{NS}-like' current. Brief light pulses activating ChR2 in the zebrafish SAN at different phases of the cardiac cycle caused varied chronotropic responses depending on the timing of the light pulse. This was intriguing because it demonstrated a systematic and reproducible way to increase or decrease BR using subthreshold activation rather than overdrive pacing. Previously, SAN stretch or ChR2 activation had only been shown to elicit chronotropic changes in one direction, unlike the newfound ability to systematically cause chronotropic changes in both directions (speed up or slow

down BR) based on stimulation timing. These zebrafish studies were replicated in the mouse SAN and a similar response was observed. The response in the mouse SAN was particularly exciting as its response to sustained stretch is inconsistent, whereas with cycle-timed activation a consistent increase or decrease was elicited. These responses also occurred in the computational simulations of rabbit and mouse single SAN cells that included a SAC_{NS}-like current. The advantage of this approach was the ability to investigate how V_m changes may be driving the increase or decrease in BR. Finally, pharmacological manipulation of AP morphology in the mouse positively shifted the chronotropic response to stretch, further supporting the notion that the interaction between $I_{SAC,NS}$ and the AP is a key determinant in the direction of the change in BR in the stretch response. Overall, this study emphasises the importance of stimulus timing and AP morphology in determining the direction of the chronotropic response to SAC_{NS}-like current activation.

5.3. Influence of SAN Structural and Mechanical Parameters on the Magnitude of Stretch-Induced Chronotropy

My final goal was to gain a better understanding of the variables that determine the magnitude of the chronotropic response to SAN stretch. In the zebrafish, when baseline force was not controlled, the magnitude of the change in BR was correlated with baseline force. When baseline force was controlled, the applied force instead was correlated with chronotropic responsiveness. These data make it unsurprising that in the zebrafish, stiffer SAN preparations result in larger increases in BR with stretch. This is also true in the mouse; however, the direction of the change in BR is inconsistent. Intriguingly the inverse is true in the rabbit, such that stiffer SAN preparations are less responsive to stretch. This species-difference may be due to the differences in structure between the rabbit and mouse unstretched SAN changes in structure with stretch. In the mouse SAN, surface collagen is randomly oriented and with stretch it becomes aligned to the crista terminalis. Conversely, surface collagen is already aligned in the unstretched rabbit SAN and instead becomes less tortuous with stretch. In the middle layers of both species, collagen is randomly oriented in the unstretched SAN and becomes oriented parallel to the crista terminalis and less tortuous with stretch. Although the specifics of how stretch mechanotransduction influences responsiveness remain uncertain, these studies do clearly demonstrate that SAN structure and mechanics influence the magnitude of the chronotropic response to stretch. Mechano-

sensitivity is an important SAN control mechanism, and alterations *via* changes in SAN structural properties may contribute to SAN dysfunction and arrhythmias.

5.4. Limitations and Future Directions

Combining various animal model systems and experimental approaches is a powerful strategy in that the specific advantages of each model can be maximised; however, acknowledging their limitations and the necessary assumptions for their utility is imperative. The rabbit heart is both electrophysiologically and morphologically similar to the human heart and is a common experimental model, including for mechano-electric coupling studies (Quinn and Kohl, 2016). Unlike the rabbit, mice and zebrafish are advantageous because of the ease of their genetic modification, but they have limitations. As previously described, certain electrophysiological characteristics of the mouse heart are considerably different from human and morphologically the zebrafish heart is quite distinct from the human heart. The biophysically-based mathematical models of single SAN cells used in this work are imperfect representations of reality, with specific limitations in part because they are based upon variable experimental results. For example, intracellular Ca^{2+} handling is more intricate than the rabbit SAN cell model depicts, and it is based on an assumption that early SDD is crucially dependent on I_f activation (Severi et al., 2012). The rabbit SAN cell model does not consider the two distinctive L-type Ca^{2+} current isoforms, but instead only one I_{CaL} is represented. The mouse model does have both $Ca_v1.2$ and 1.3 components but is limited in other ways. For example, block of I_{Kr} in the model does not change BR, which is contradictory to experimental I_{Kr} block, and some experimental data used to parameterise the model was taken from other species or cell types (Kharche et al., 2011). But still, it is important to remember that all models are simplified depictions of reality, appropriate for specific applications, and when used in combination with experimental studies result in a more comprehensive and cohesive investigation. This approach was successful in this work and generated additional hypotheses to be experimentally tested. Thus future work is required, including SAN stretch studies using larger animal model species in which the SAN structure differs from that of the zebrafish, mouse, or rabbit and more closely reflects human SAN structure (Kalyanasundaram et al., 2019).

Although my studies provide valuable new insight into SAN stretch-sensitivity, there is still a great deal about this important heart rate control mechanism that remains elusive. This work focuses on the contribution of SAN pacemaker cells for eliciting the

chronotropic response to stretch, where other mechanosensitive cell types in the SAN may be involved. For instance, fibroblasts in the SAN have been shown to be mechanosensitive and may also contribute to the stretch-induced change in BR (Kohl et al., 1994). The contribution of fibroblasts, and other mechanosensitive elements of the SAN, such as the intracardiac nervous system, may be important contributors to the response and warrant further investigation. The unknown identity of SAC_{NS} limits our ability to investigate the molecular mechanisms that elicit the chronotropic response to stretch. Identifying the molecular identity of SAC_{NS} – or identifying the contributing channels if $I_{SAC,NS}$ is based on the activity of multiple known channels – would provide a pharmacological and/or genetic target facilitating further research and potentially identifying a therapeutic target.

Insights extracted from the simulations can be translated back to additional experimental investigations because the chronotropic response observed in the optogenetic studies was reproduced in the computational models. The influence of I_x activation on individual pacemaking currents in the simulation can be visualised and effected currents can then be pharmacologically targeted experimentally either with optogenetic or stretch studies. The single-cell simulations do not, of course, take into consideration the complexities and effects of SAN structure, thus further simulations in a SAN tissue model could be valuable.

A multitude of factors have been shown to influence the chronotropic response to SAN stretch. For instance, the direction of stretch application has been shown to be important, both in the present study in the zebrafish and in previous work in the cat and rabbit SAN, in which concentric stretch caused a greater increase in BR than linear stretch (Deck, 1964). In the present work the importance of timing was demonstrated with ChR2 activation. This is consistent with a study that showed that sinusoidal stretch synchronised SAN cell firing and caused greater increases in BR than sustained stretch (Ushiyama and Brooks, 1977). The speed of stretch has also been shown previously to alter responsiveness (Lange et al., 1966; Arai et al., 1996). Finally, it was shown here that SAN mechanics, specifically stiffness, alters the chronotropic response to stretch. Examining how these factors intersect in a normal physiological context and how they change with age and disease is a crucial next step. Application of cyclic, oscillatory SAN stretch and simultaneous manipulation of these factors and parameters would provide greater insight into this control mechanism, as well as which factors predominantly dictate the chronotropic response magnitude.

For example, stretching the SAN from aged or diseased models (which are generally more fibrotic) could provide insight into how SAN mechano-sensitivity is altered with changes in SAN structure. In this work I identified that stiffness correlates with the chronotropic responsiveness to stretch. It has been shown that with age and certain pathologies (including heart failure, SAN ischemia, and inflammatory conditions) the SAN undergoes changes in structure, including an increase in fibrosis (Kistler et al., 2004; Morris and Kalman, 2014; Csepe et al., 2015). Therefore, it is reasonable to hypothesise that these changes in SAN structure will change stiffness and, consequently, responsiveness. Further, pathological changes in the SAN are correlated with an increased incidence of arrhythmias, especially atrial fibrillation (Csepe et al., 2015). It is interesting to consider if the electrical disturbances or arrhythmias associated with SAN structural changes are the consequence of alterations in mechanosensitive control of the SAN. If so, the contribution of changes in SAN mechano-sensitivity to SAN dysfunction is an area warranting further investigation and could potentially reveal mechanisms and generate therapeutic targets. Anecdotally, I found that an irregularly beating SAN would often beat more regularly upon stretch application (Figure 5.1A). This is consistent with previous observations in the cat SAN in which irregularities in BR disappeared following moderate stretch (Figure 5.1B, Lange et al., 1966). I confirmed these findings with a systematic evaluation of BR stability before and after application of preload in the zebrafish and rabbit SAN based on my data from the experiments in objective three. Specifically, by measuring the standard deviation of each cycle length (SDRR), I found that BR was unstable and became more stable with application of baseline tension in both species (Figure 5.2). This may be because the Bainbridge response is not engaged without baseline tension, or perhaps BR instability is due to a lack of stretch-induced mutual entrainment *via* phase-resetting behaviour. Regardless, this demonstrates the importance of SAN mechano-sensitivity as a BR control mechanism, as alterations in baseline load in pathological conditions may cause BR instability, which could be arrhythmogenic.

Finally, this work may provide important translation for therapeutic approaches and techniques. For instance, considering the importance of mechanics in the development of bio-artificial pacemakers may be essential, if not at least beneficial. Insights from this work also support the potential utility of optogenetic pacemaking. Artificial pacemakers currently only have the ability to overtake the natural system and increase BR. This work demonstrates the possibility for BR manipulation with

subthreshold levels of light such that BR could be increased or decreased depending on physiological demand. It is also interesting to consider the possibility of optogenetic control of the SAN as a replacement for mechanosensitive regulation in situations where the mechanical environment is altered or compromised. Specifically, in a SAN that is not experiencing or responding to stretch, perhaps cyclic activation of ChR2 during diastole could be a therapeutic approach for replacing regular mechanical control of the SAN.

5.5. CONCLUSION

It has been known for over a century that the chronotropic response to SAN stretch allows BR to be tuned to changes in haemodynamic load on a beat-by-beat basis. In my thesis I have utilised many new techniques and methodologies to explore this concept. The zebrafish, a contemporary model species for cardiovascular electrophysiological studies, responds to SAN stretch with an increase in BR consistent with most mammals and humans. With an optogenetic approach, specifically using ChR2 as a surrogate for SAC_{NS}, the importance of stimulation timing was identified, such that BR could be modulated – *i.e.,* increased or decreased – with a SAC_{NS}-like current depending on stimulation timing. This was explored more deeply using single SAN cell computational modelling. And finally, a multispecies approach identified the contribution of stiffness to the chronotropic response to stretch, and subsequent SHGM imaging of collagen in mammalian SAN preparations demonstrated a species difference in SAN collagen characteristics both at baseline and with stretch. While much is understood about SAN mechano-sensitivity, many questions remain unanswered regarding its physiological and pathophysiological importance and contribution, thus warranting further investigation.

Figure 5.1. Recovery of irregular BR by SAN stretch.

(A) An unstable rhythm is restored with 50% stretch (red box) of the zebrafish SAN, and BR becomes unstable again once stretch is released. (B) Unstable BR in the cat SAN is restored by stretch (indicated by lower line). BR once again becomes unstable when stretch is released (From Lange et al., 1966).

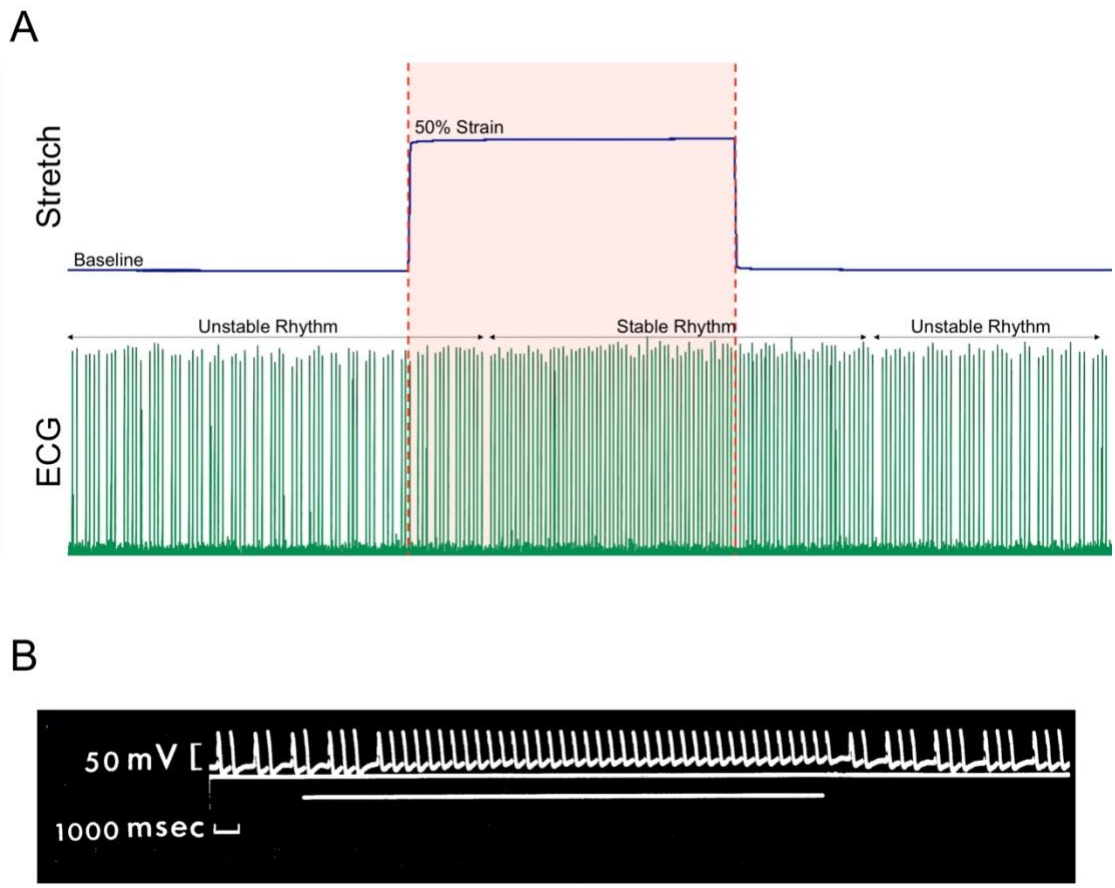

Figure 5.2. Importance of SAN baseline tension for stability of BR.

Representative ECG and the BR over time from zebrafish (A,C) and rabbit (B,D) SAN, slack and following application of baseline tension. Change in BR and SDRR from zebrafish (E) and rabbit (F) SAN preparations, slack and with baseline tension. *p<0.05 compared to slack by paired Student's t-test.

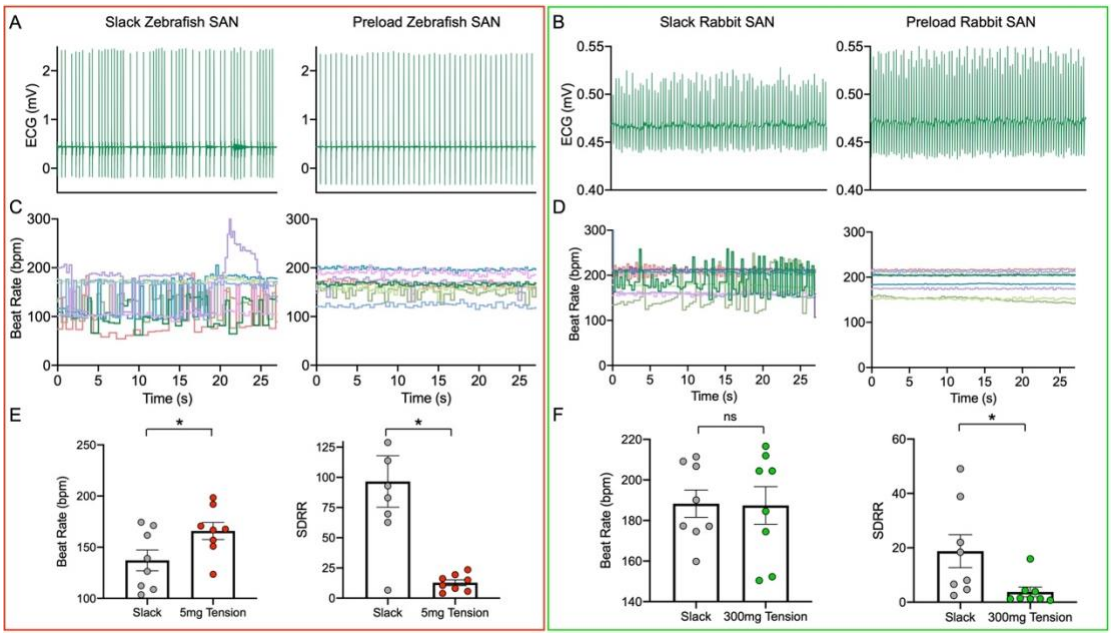

REFERENCES

Alings, A. M. W., Abbas, R. F., and Bouman, L. N. (1995). Age-related changes in structure and relative collagen content of the human and feline sinoatrial node: A comparative study. *Eur. Heart J.* 16, 1655–1667. doi:10.1093/oxfordjournals.eurheartj.a060792.

Anumonwo, J. M. B., Delmar, M., Vinet, A., Michaels, D. C., and Jalife, J. (1991). Phase resetting and entrainment of pacemaker activity in single sinus nodal cells. *Circ. Res.* 68, 1138–1153. doi:10.1161/01.RES.68.4.1138.

Arai, A., Kodama, I., and Toyama, J. (1996). Roles of Cl^- channels and Ca^{2+} mobilization in stretch-induced increase of SA node pacemaker activity. *Am. J. Physiol. - Hear. Circ. Physiol.* 270. 1736-1720. doi:10.1152/ajpheart.1996.270.5.h1726.

Arrenberg, A. B., Stainier, D. Y. R., Baier, H., and Huisken, J. (2010). Optogenetic control of cardiac function. *Science* 330, 971–974. doi:10.1126/science.1195929.

Aziz, Q., Li, Y., and Tinker, A. (2018). Potassium channels in the sinoatrial node and their role in heart rate control. *Channels* 12, 356–366. doi:10.1080/19336950.2018.1532255.

Bainbridge, F. A. (1915). The influence of venous filling upon the rate of the heart. *J. Physiol.* 50, 65–84. doi:10.1113/jphysiol.1915.sp001736.

Baker, K., Warren, K. S., Yellen, G., and Fishman, M. C. (1997). Defective "pacemaker" current (Ih) in a zebrafish mutant with a slow heart rate. *Proc. Natl. Acad. Sci. U. S. A.* 94, 4554–4559. doi:10.1073/pnas.94.9.4554.

Barrett, C. J., Bolter, C. P., and Wilson, S. J. (1998). The intrinsic rate response of the isolated right atrium of the rat, Rattus norvegicus. *Comp. Biochem. Physiol. A. Mol. Integr. Physiol.* 120, 391–397. doi:10.1016/s1095-6433(98)10077-6.

Bartos, D. C., Grandi, E., and Ripplinger, C. M. (2015). Ion channels in the heart. *Compr. Physiol.* 5, 1423–1464. doi:10.1002/cphy.c140069.

Baruscotti, M., Barbuti, A., and Bucchi, A. (2010). The cardiac pacemaker current. *J. Mol. Cell. Cardiol.* 48, 55–64. doi:10.1016/j.yjmcc.2009.06.019.

Baumgarten, C. M., Deng, W., and Raucci, F. J. (2011). "Cell volume-sensitive ion channels and transporters in cardiac myocytes," in *Cardiac Mechano-Electric Coupling and Arrhythmias* (Oxford University Press), 27–34. doi:10.1093/med/9780199570164.003.0004.

Beaulieu, P., and Lambert, C. (1998). Peptidic regulation of heart rate and interactions with the autonomic nervous system. *Cardiovasc. Res.* 37, 578–585. doi:10.1016/S0008-6363(97)00305-2.

Bernardi, L., Keller, F., Sanders, M., Reddy, P. S., Griffith, B., Meno, F., et al. (1989). Respiratory sinus arrhythmia in the denervated human heart. *J. Appl. Physiol.* 67, 1447–55. doi:10.1152/jappl.1989.67.4.1447.

Bernardi, L., Salvucci, F., Suardi, R., Soldá, P. L., Calciati, A., Perlini, S., et al. (1990). Evidence for an intrinsic mechanism regulating heart rate variability in the transplanted and the intact heart during submaximal dynamic exercise? *Cardiovasc. Res.* 24, 969–981. doi:10.1093/cvr/24.12.969.

Bleeker, W. K., Mackaay, A. J. C., Masson-Pevet, M., Bouman, L. N., and Becker, A. E. (1980). Functional and morphological organization of the rabbit sinus node. *Circ. Res.* 46, 11–22. doi:10.1161/01.RES.46.1.11.

Blinks, J. R. (1956). Positive chronotropic effect of increasing right atrial pressure in the isolated mammalian heart. *Am. J. Physiol.* 186, 299–303. doi:10.1152/ajplegacy.1956.186.2.299.

Bolter, C. P. (1994). Intrinsic cardiac rate regulation in the anaesthetized rabbit. *Acta Physiol. Scand.* 151, 421–428. doi:10.1111/j.1748-1716.1994.tb09764.x.

Bolter, C. P. (1996). Effect of changes in transmural pressure on contraction frequency of the isolated right atrium of the rabbit. *Acta Physiol. Scand.* 156, 45–50. doi:10.1046/j.1365-201X.1996.430151000.x.

Bolter, C. P., and Wilson, S. J. (1999). Influence of right atrial pressure on the cardiac pacemaker response to vagal stimulation. *Am. J. Physiol. Integr. Comp. Physiol.* 276, R1112–R1117. doi:10.1152/ajpregu.1999.276.4.R1112.

Boyett, M. R., Honjo, H., and Kodama, I. (2000). The sinoatrial node, a heterogeneous pacemaker structure. *Cardiovasc. Res.* 47, 658–687. doi:10.1016/S0008-6363(00)00135-8.

Boyle, P. M., Murphy, M. J., Karathanos, T. V., Zahid, S., Blake, R. C., and Trayanova, N. A. (2018). Termination of re-entrant atrial tachycardia via optogenetic stimulation with optimized spatial targeting: insights from computational models. *J. Physiol.* 596, 181–196. doi:10.1113/JP275264.

Brooks, C. M., and Lange, G. (1977). Interaction of myogenic and neurogenic mechanisms that control heart rate. *Proc. Natl. Acad. Sci. U. S. A.* 74, 1761–1692. doi:10.1073/pnas.74.4.1761.

Brooks, C. M., Lu, H. H., Lange, G., Mangi, R., Shaw, R. B., and Geoly, K. (1966). Effects of localized stretch of the sinoatrial node region of the dog heart. *Am. J. Physiol.* 211, 1197–1202. doi:10.1152/ajplegacy.1966.211.5.1197.

Brown, H., Difrancesco, D., and Noble, S. (1979). Cardiac pacemaker oscillation and its modulation by autonomic transmitters. *J. Exp. Biol.* 81, 175–204.

Bruegmann, T., Beiert, T., Vogt, C. C., Schrickel, J. W., and Sasse, P. (2018). Optogenetic termination of atrial fibrillation in mice. *Cardiovasc. Res.* 114, 713–723. doi:10.1093/cvr/cvx250.

Bruegmann, T., Boyle, P. M., Vogt, C. C., Karathanos, T. V., Arevalo, H. J., Fleischmann, B. K., et al. (2016). Optogenetic defibrillation terminates ventricular arrhythmia in mouse hearts and human simulations. *J. Clin. Invest.* 126, 3894–3904. doi:10.1172/JCI88950.

Bruegmann, T., Malan, D., Hesse, M., Beiert, T., Fuegemann, C. J., Fleischmann, B. K., et al. (2010). Optogenetic control of heart muscle in vitro and in vivo. *Nat. Methods* 7, 897–900. doi:10.1038/nmeth.1512.

Bruegmann, T., and Sasse, P. (2015). Optogenetic cardiac pacemakers: Science or fiction? *Trends Cardiovasc. Med.* 25, 82–83. doi:10.1016/j.tcm.2014.10.016.

Bucchi, A., Baruscotti, M., Robinson, R. B., and DiFrancesco, D. (2007). Modulation of rate by autonomic agonists in SAN cells involves changes in diastolic depolarization and the pacemaker current. *J. Mol. Cell. Cardiol.* 43, 39–48. doi:10.1016/j.yjmcc.2007.04.017.

Calkins, H., Levine, J. H., and Kass, D. A. (1991). Electrophysiological effect of varied rate and extent of acute in vivo left ventricular load increase. *Cardiovasc. Res.* 25, 637–644. doi:10.1093/cvr/25.8.637.

Calloe, K., Elmedyb, P., Olesen, S. P., Jorgensen, N. K., and Grunnet, M. (2005). Hypoosmotic cell swelling as a novel mechanism for modulation of cloned HCN2 channels. *Biophys. J.* 89, 2159–2169. doi:10.1529/biophysj.105.063792.

Cheng, Y., Li, H., Lei, H., Jiang, C., Rao, P., Wang, L., et al. (2019). Flexible and precise control of cardiac rhythm with blue light. *Biochem. Biophys. Res. Commun.* 514, 759–764. doi:10.1016/j.bbrc.2019.05.035.

Chiba, S. (1977). Pharmacologic analysis of stretch-induced sinus acceleration of the isolated dog atrium. *Jpn. Heart J.* 18, 398–405. doi:10.1536/ihj.18.398.

Coleridge, J. C., and Linden, R. J. (1955). The effect of intravenous infusions upon the heart rate of the anaesthetized dog. *J. Physiol.* 127, 31P. doi:10.1113/jphysiol.1955.sp005308.

Cooper, P. J., and Kohl, P. (2005). Species- and preparation-dependence of stretch effects on sino-atrial node pacemaking. *Ann. N. Y. Acad. Sci.* 1047, 324–335. doi:10.1196/annals.1341.029.

Cooper, P. J., Lei, M., Cheng, L. X., and Kohl, P. (2000). Selected contribution: axial stretch increases spontaneous pacemaker activity in rabbit isolated sinoatrial node cells. *J. Appl. Physiol.* 89, 2099–104. doi:10.1152/jappl.2000.89.5.2099.

Coster, A. C. F., and Celler, B. G. (2003). Phase response of model sinoatrial node cells. *Ann. Biomed. Eng.* 31, 271–283. doi:10.1114/1.1553455.

Csepe, T. A., Kalyanasundaram, A., Hansen, B. J., Zhao, J., and Fedorov, V. V. (2015). Fibrosis: A structural modulator of sinoatrial node physiology and dysfunction. *Front. Physiol.* 6, 1–8. doi:10.3389/fphys.2015.00037.

Deck, K. A. (1964). Dehnungseffekte am spontanschlagenden, isolierten sinusknoten. *Pflugers Arch. Gesamte Physiol. Menschen Tiere* 280, 120–130. doi:10.1007/BF00363751.

Deisseroth, K., Feng, G., Majewska, A. K., Miesenböck, G., Ting, A., and Schnitzer, M. J. (2006). Next-generation optical technologies for illuminating genetically targeted brain circuits. *J. Neurosci.* 26, 10380–10386. doi:10.1523/JNEUROSCI.3863-06.2006.

Difrancesco, D. (2010). The role of the funny current in pacemaker activity. *Circ. Res.* 106, 434–446. doi:10.1161/CIRCRESAHA.109.208041.

Difrancesco, D., and Noble, D. (2012). The funny current has a major pacemaking role in the sinus node. *Heart Rhythm.* 9, 299–301. doi:10.1016/j.hrthm.2011.09.021.

Donald, D. E., and Shepherd, J. T. (1978). Reflexes from the heart and lungs: Physiological curiosities or important regulatory mechanisms. *Cardiovasc. Res.* 12, 449–469. doi:10.1093/cvr/12.8.449.

Dong, R., Mu-u-min, R., Reith, A. J. M., O'Shea, C., He, S., Duan, K., et al. (2019). A protocol for dual calcium-voltage optical mapping in murine sinoatrial preparation with optogenetic pacing. *Front. Physiol.* 10. 954. doi:10.3389/fphys.2019.00954.

Dvornikov, A. V., Dewan, S., Alekhina, O. V., Pickett, F. B., and De Tombe, P. P. (2014). Novel approaches to determine contractile function of the isolated adult zebrafish ventricular cardiac myocyte. *J. Physiol.* 592, 1949–1956. doi:10.1113/jphysiol.2014.270678.

Eijsbouts, S. C. M., Majidi, M., Van Zandvoort, M., and Allessie, M. A. (2003). Effects of acute atrial dilation on heterogeneity in conduction in the isolated rabbit heart. *J. Cardiovasc. Electrophysiol.* 14, 269–278. doi:10.1046/j.1540-8167.2003.02280.x.

Fabbri, A., Fantini, M., Wilders, R., and Severi, S. (2017). Computational analysis of the human sinus node action potential: model development and effects of mutations. *J. Physiol.* 595, 2365–2396. doi:10.1113/JP273259.

Ferenczi, E. A., Tan, X., and Huang, C. L. H. (2019). Principles of optogenetic methods and their application to cardiac experimental systems. *Front. Physiol.* 10. doi:10.3389/fphys.2019.01096.

Franz, M. R., Cima, R., Wang, D., Profitt, D., and Kurz, R. (1992). Electrophysiological effects of myocardial stretch and mechanical determinants of stretch-activated arrhythmias. *Circulation* 86, 968–978. doi:10.1161/01.CIR.86.3.968.

Funken, M., Malan, D., Sasse, P., and Bruegmann, T. (2019). Optogenetic hyperpolarization of cardiomyocytes terminates ventricular arrhythmia. *Front. Physiol.* 10. doi:10.3389/fphys.2019.00498.

Gaskell, W. H. (1882). Preliminary observations on the innervation of the heart of the tortoise. *J. Physiol.* 3, 369–379. doi:10.1113/jphysiol.1882.sp000110.

Genge, C. E., Lin, E., Lee, L., Sheng, X., Rayani, K., Gunawan, M., et al. (2007). The zebrafish heart as a model of mammalian cardiac function. *Rev. Physiol. Biochem. Pharmacol.* 171, 99–136. doi:10.1007/112_2016_5.

Gluck, J. M., Herren, A. W., Yechikov, S., Kao, H. K. J., Khan, A., Phinney, B. S., et al. (2017). Biochemical and biomechanical properties of the pacemaking sinoatrial node extracellular matrix are distinct from contractile left ventricular matrix. *PLoS One* 12, e0185125. doi:10.1371/journal.pone.0185125.

Glukhov, A. V., Kalyanasundaram, A., Lou, Q., Hage, L. T., Hansen, B. J., Belevych, A. E., et al. (2015). Calsequestrin-2 deletion causes sinoatrial node dysfunction and atrial arrhythmias associated with altered sarcoplasmic reticulum calcium cycling and degenerative fibrosis within the mouse atrial pacemaker complex. *Eur. Heart J.* 36, 686-697a. doi:10.1093/eurheartj/eht452.

Golenhofen, K., and Lippross, H. (1969). Der Effekt dynamischer und statischer Dehnung auf die Spontanfrequenz des isolierten Herzschrittmachers. *Pflügers Arch. Eur. J. Physiol.* 309, 145–158. doi:10.1007/BF00586964.

Golovko, V., Gonotkov, M., and Lebedeva, E. (2015). Effects of 4-aminopyridine on action potentials generation in mouse sinoauricular node strips. *Physiol. Rep.* 3, 1–8. doi:10.14814/phy2.12447.

Gonotkov, M. A., and Golovko, V. A. (2013). Aminopyridine lengthened the plateau phase of action potentials in mouse sinoatrial node cells. *Bull. Exp. Biol. Med.* 156, 4–6. doi:10.1007/s10517-013-2263-5.

Gordan, R., Gwathmey, J. K., and Xie, L.-H. (2015). Autonomic and endocrine control of cardiovascular function. *World J. Cardiol.* 7, 204. doi:10.4330/wjc.v7.i4.204.

Govorunova, E. G., Cunha, S. R., Sineshchekov, O. A., and Spudich, J. L. (2016). Anion channelrhodopsins for inhibitory cardiac optogenetics. *Sci. Rep.* 6, 1–8. doi:10.1038/srep33530.

Guevara, M. R., and Jongsma, H. J. (1990). Phase resetting in a model of sinoatrial nodal membrane: Ionic and topological aspects. *Am. J. Physiol. - Hear. Circ. Physiol.* 258, 734–747. doi:10.1152/ajpheart.1990.258.3.h734.

Guharay, F., and Sachs, F. (1984). Stretch-activated single ion channel currents in tissue-cultured embryonic chick skeletal muscle. *J. Physiol.* 352, 685–701. doi:10.1113/jphysiol.1984.sp015317.

Gut, P., Reischauer, S., Stainier, D. Y. R., and Arnaout, R. (2017). Little fish, big data: Zebrafish as a model for cardiovascular and metabolic disease. *Physiol. Rev.* 97, 889–938. doi:10.1152/physrev.00038.2016.

Hagiwara, N., Masuda, H., Shoda, M., and Irisawa, H. (1992). Stretch-activated anion currents of rabbit cardiac myocytes. *J. Physiol.* 456, 285–302. doi:10.1113/jphysiol.1992.sp019337.

Hales, P. W., Schneider, J. E., Burton, R. A. B., Wright, B. J., Bollensdorff, C., and Kohl, P. (2012). Histo-anatomical structure of the living isolated rat heart in two contraction states assessed by diffusion tensor MRI. *Prog. Biophys. Mol. Biol.* 110, 319–330. doi:10.1016/j.pbiomolbio.2012.07.014.

Han, S., Wilson, S. J., and Bolter, C. P. (2010). Tertiapin-Q removes a mechanosensitive component of muscarinic control of the sinoatrial pacemaker in the rat. *Clin. Exp. Pharmacol. Physiol.* 37, 900–904. doi:10.1111/j.1440-1681.2010.05408.x.

Hansen, D. E., Craig, C. S., and Hondeghem, L. M. (1990). Stretch-induced arrhythmias in the isolated canine ventricle. Evidence for the importance of mechanoelectrical feedback. *Circulation* 81, 1094–1105. doi:10.1161/01.CIR.81.3.1094.

Hao, X., Zhang, Y., Zhang, X., Nirmalan, M., Davies, L., Konstantinou, D., et al. (2011). TGF-β1-mediated fibrosis and ion channel remodeling are key mechanisms in producing the sinus node dysfunction associated with SCN5A deficiency and aging. *Circ. Arrhythmia Electrophysiol.* 4, 397–406. doi:10.1161/CIRCEP.110.960807.

Hashimoto, K., Tanaka, S., Hirata, M., and Chiba, S. (1967). Responses of the sino-atrial node to change in pressure in the sinus node artery. *Circ. Res.* 21, 297–304. doi:10.1161/01.RES.21.3.297.

Himeno, Y., Sarai, N., Matsuoka, S., and Noma, A. (2008). Ionic mechanisms underlying the positive chronotropy induced by β1-adrenergic stimulation in guinea pig sinoatrial node cells: A simulation study. *J. Physiol. Sci.* 58, 53–65. doi:10.2170/physiolsci.RP015207.

Himmel, W., and Rossberg, F. (1983). Effekt von verapamil auf die chronotrope autoregulation des kaninchenvorhofes. *Res. Exp. Med.* 183, 233–236. doi:10.1007/BF01855646.

Ho, S. Y., and Sánchez-Quintana, D. (2016). Anatomy and pathology of the sinus node. *J. Interv. Card. Electrophysiol.* 46, 3–8. doi:10.1007/s10840-015-0049-6.

Horner, S. M., Murphy, C. F., Coen, B., Dick, D. J., Harrison, F. G., Vespalcova, Z., et al. (1996). Contribution to heart rate variability by mechanoelectric feedback: Stretch of the sinoatrial node reduces heart rate variability. *Circulation* 94, 1762–1767. doi:10.1161/01.CIR.94.7.1762.

Howe, K., Clark, M. D., Torroja, C. F., Torrance, J., Berthelot, C., Muffato, M., et al. (2013). The zebrafish reference genome sequence and its relationship to the human genome. *Nature.* 496, 498–503. doi:10.1038/nature12111.

Hu, N., Joseph Yost, H., and Clark, E. B. (2001). Cardiac morphology and blood pressure in the adult zebrafish. *Anat. Rec.* 264, 1–12. doi:10.1002/ar.1111.

Iribe, G., Ward, C. W., Camelliti, P., Bollensdorff, C., Mason, F., Burton, R. A. B., et al. (2009). Axial stretch of rat single ventricular cardiomyocytes causes an acute and transient increase in Ca^{2+} spark rate. *Circ. Res.* 104, 787–795. doi:10.1161/CIRCRESAHA.108.193334.

Irisawa, H., Brown, H. F., and Giles, W. (1993). Cardiac pacemaking in the sinoatrial node. *Physiol. Rev.* 73, 197–227. doi:10.1152/physrev.1993.73.1.197.

Jalife, J. (1984). Mutual entrainment and electrical coupling as mechanisms for synchronous firing of rabbit sino-atrial pace-maker cells. *J. Physiol.* 356, 221–243. doi:10.1113/jphysiol.1984.sp015461.

Jalife, J., and Antzelevitch, C. (1979). Phase resetting and annihilation of pacemaker activity in cardiac tissue. *Science (80-.).* 206, 695–697. doi:10.1126/science.493975.

Joshi, J., Rubart, M., and Zhu, W. (2020). Optogenetics: background, methodological advances and potential applications for cardiovascular research and medicine. *Front. Bioeng. Biotechnol.* 7. doi:10.3389/fbioe.2019.00466.

Ju, Y. K., Chu, Y., Chaulet, H., Lai, D., Gervasio, O. L., Graham, R. M., et al. (2007). Store-operated Ca^{2+} influx and expression of TRPC genes in mouse sinoatrial node. *Circ. Res.* 100, 1605–1614. doi:10.1161/CIRCRESAHA.107.152181.

Kaese, S., and Verheule, S. (2012). Cardiac electrophysiology in mice: A matter of size. *Front. Physiol.* 3, 345. doi:10.3389/fphys.2012.00345.

Kalyanasundaram, A., Li, N., Hansen, B. J., Zhao, J., and Fedorov, V. V. (2019). Canine and human sinoatrial node: differences and similarities in the structure, function, molecular profiles, and arrhythmia. *J. Vet. Cardiol.* 22, 2–19. doi:10.1016/j.jvc.2018.10.004.

Kamiyama, A., Niimura, I., and Sugi, H. (1984). Length-dependent changes of pacemaker frequency in the isolated rabbit sinoatrial node. *Jpn. J. Physiol.* 34, 153–165. doi:10.2170/jjphysiol.34.153.

Keith, A., and Flack, M. (1907). The Form and Nature of the Muscular Connections between the Primary Divisions of the Vertebrate Heart. *J. Anat. Physiol.* 41, 172–89. Available at: http://www.ncbi.nlm.nih.gov/pubmed/17232727 [Accessed January 6, 2020].

Kharche, S., Yu, J., Lei, M., and Zhang, H. (2011). A mathematical model of action potentials of mouse sinoatrial node cells with molecular bases. *Am. J. Physiol. - Hear. Circ. Physiol.* 301. doi:10.1152/ajpheart.00143.2010.

Kistler, P. M., Sanders, P., Fynn, S. P., Stevenson, I. H., Spence, S. J., Vohra, J. K., et al. (2004). Electrophysiologic and electroanatomic changes in the human atrium associated with age. *J. Am. Coll. Cardiol.* 44, 109–116. doi:10.1016/j.jacc.2004.03.044.

Kohl, P., Kamkin, A., Kiseleva, I., and Noble, D. (1994). Mechanosensitive fibroblasts in the sino-atrial node region of rat heart: interaction with cardiomyocytes and possible role. *Exp. Physiol.* 79, 943–956. doi:10.1113/expphysiol.1994.sp003819.

Kopton, R. A., Baillie, J. S., Rafferty, S. A., Moss, R., Zgierski-Johnston, C. M., Prykhozhij, S. V., et al. (2018). Cardiac electrophysiological effects of light-activated chloride channels. *Front. Physiol.* 9, 1806. doi:10.3389/fphys.2018.01806.

Lakatta, E. G., and DiFrancesco, D. (2009). What keeps us ticking: a funny current, a calcium clock, or both? *J. Mol. Cell. Cardiol.* doi:10.1016/j.yjmcc.2009.03.022.

Lakatta, E. G., Maltsev, V. A., and Vinogradova, T. M. (2010). A coupled SYSTEM of intracellular Ca^{2+} clocks and surface membrane voltage clocks controls the timekeeping mechanism of the heart's pacemaker. *Circ. Res.* 106, 659–73. doi:10.1161/CIRCRESAHA.109.206078.

Lakatta, E. G., Vinogradova, T. M., and Maltsev, V. A. (2008). The missing link in the mystery of normal automaticity of cardiac pacemaker cells. *Ann. N. Y. Acad. Sci.* 1123, 41–57. doi:10.1196/annals.1420.006.

Lang, D., and Glukhov, A. V. (2018). Functional microdomains in heart's pacemaker: a step beyond classical electrophysiology and remodeling. *Front. Physiol.* 9, 1686. doi:10.3389/fphys.2018.01686.

Lange, G., Lu, H. H., Chang, A., and Brooks, C. M. (1966). Effect of stretch on the isolated cat sinoatrial node. *Am. J. Physiol.* 211, 1192–1196. doi:10.1152/ajplegacy.1966.211.5.1192.

Lei, M., Goddard, C., Liu, J., Léoni, A. L., Royer, A., Fung, S. S. M., et al. (2005). Sinus node dysfunction following targeted disruption of the murine cardiac sodium channel gene Scn5a. *J. Physiol.* 567, 387–400. doi:10.1113/jphysiol.2005.083188.

Lei, M., and Kohl, P. (1998). Swelling-induced decrease in spontaneous pacemaker activity of rabbit isolated sino-atrial node cells. *Acta Physiol. Scand.* 164, 1–12. doi:10.1046/j.1365-201X.1998.00390.x.

Lin, W., Laitko, U., Juranka, P. F., and Morris, C. E. (2007). Dual stretch responses of mHCN2 pacemaker channels: Accelerated activation, accelerated deactivation. *Biophys. J.* 92, 1559–1572. doi:10.1529/biophysj.106.092478.

Liu, J., Dobrzynski, H., Yanni, J., Boyett, M. R., and Lei, M. (2007). Organisation of the mouse sinoatrial node: structure and expression of HCN channels. *Cardiovasc. Res.* 73, 729–738. doi:10.1016/j.cardiores.2006.11.016.

Longair, M. H., Baker, D. A., and Armstrong, J. D. (2011). Simple Neurite Tracer: open source software for reconstruction, visualization and analysis of neuronal processes. *Bioinformatics* 27, 2453–4. doi:10.1093/bioinformatics/btr390.

Ludwig, C. (1847). Beitrage zur kenntniss des einflusses der respriations bewegungen auf den blutlauf im aortensysteme. *Arch. Anat. Physiol.* 13, 242–302.

MacDonald, E. A., Madl, J., Greiner, J., Ramadan, A. F., Wells, S. M., Torrente, A. G., et al. (2020a). Sinoatrial node structure, mechanics, electrophysiology and the chronotropic response to stretch in rabbit and mouse. *Front. Physiol.* 11, 1–15. doi:10.3389/fphys.2020.00809.

MacDonald, E. A., Rose, R. A., and Quinn, T. A. (2020b). Neurohumoral control of sinoatrial node activity and heart rate: insight from experimental models and findings from humans. *Front. Physiol.* 11. doi:10.3389/fphys.2020.00170.

MacDonald, E. A., Stoyek, M. R., Rose, R. A., and Quinn, T. A. (2017). Intrinsic regulation of sinoatrial node function and the zebrafish as a model of stretch effects on pacemaking. *Prog. Biophys. Mol. Biol.* 130, 198–211. doi:10.1016/j.pbiomolbio.2017.07.012.

Maltsev, V. A., and Lakatta, E. G. (2009). Synergism of coupled subsarcolemmal Ca^{2+} clocks and sarcolemmal voltage clocks confers robust and flexible pacemaker function in a novel pacemaker cell model. *Am. J. Physiol. - Hear. Circ. Physiol.* 296, 594–615. doi:10.1152/ajpheart.01118.2008.

Maltsev, V. A., and Lakatta, E. G. (2012). The funny current in the context of the coupled-clock pacemaker cell system. *Hear. Rhythm* 9, 302–307. doi:10.1016/j.hrthm.2011.09.022.

Mangoni, M. E., and Nargeot, J. (2008). Genesis and regulation of the heart automaticity. *Physiol. Rev.* 88, 919–982. doi:10.1152/physrev.00018.2007.

Marchant, J. L., and Farrell, A. P. (2019). Membrane and calcium clock mechanisms contribute variably as a function of temperature to setting cardiac pacemaker rate in zebrafish Danio rerio. *J. Fish Biol.* 95, 1265–1274. doi:10.1111/jfb.14126.

McAllister, R. E., Noble, D., and Tsien, R. W. (1975). Reconstruction of the electrical activity of cardiac Purkinje fibres. *J. Physiol.* 251, 1–59. doi:10.1113/jphysiol.1975.sp011080.

McGowan, C. L., Swiston, J. S., Notarius, C. F., Mak, S., Morris, B. L., Picton, P. E., et al. (2009). Discordance between microneurographic and heart-rate spectral indices of sympathetic activity in pulmonary arterial hypertension. *Heart* 95, 754–758. doi:10.1136/hrt.2008.157115.

Mesirca, P., Torrente, A. G., and Mangoni, M. E. (2015). Functional role of voltage gated Ca2+ channels in heart automaticity. *Front. Physiol.* 6, 19. doi:10.3389/fphys.2015.00019.

Monfredi, O., Tsutsui, K., Ziman, B., Stern, M. D., Lakatta, E. G., and Maltsev, V. A. (2018). Electrophysiological heterogeneity of pacemaker cells in the rabbit intercaval region, including the SA node: Insights from recording multiple ion currents in each cell. *Am. J. Physiol. - Hear. Circ. Physiol.* 314, H403–H414. doi:10.1152/ajpheart.00253.2016.

Moreno, A., Endicott, K., Skancke, M., Dwyer, M. K., Brennan, J., Efimov, I. R., et al. (2019). Sudden heart rate reduction upon optogenetic release of acetylcholine from cardiac parasympathetic neurons in perfused hearts. *Front. Physiol.* 10, 1–11. doi:10.3389/fphys.2019.00016.

Morris, G. M., and Kalman, J. M. (2014). Fibrosis, electrics and genetics - Perspectives on sinoatrial node disease -. *Circ. J.* 78, 1272–1282. doi:10.1253/circj.CJ-14-0419.

Nagel, G., Ollig, D., Fuhrmann, M., Kateriya, S., Musti, A. M., Bamberg, E., et al. (2002). Channelrhodopsin-1: A light-gated proton channel in green algae. *Science (80-.).* 296, 2395–2398. doi:10.1126/science.1072068.

Nemtsas, P., Wettwer, E., Christ, T., Weidinger, G., and Ravens, U. (2010). Adult zebrafish heart as a model for human heart? An electrophysiological study. *J. Mol. Cell. Cardiol.* 48, 161–171. doi:10.1016/j.yjmcc.2009.08.034.

Nishimura, S., Seo, K., Nagasaki, M., Hosoya, Y., Yamashita, H., Fujita, H., et al. (2008). Responses of single-ventricular myocytes to dynamic axial stretching. *Prog. Biophys. Mol. Biol.* 97, 282–297. doi:10.1016/j.pbiomolbio.2008.02.011.

Noble, D. (1960). Cardiac action and pacemaker potentials based on the Hodgkin-Huxley equations. *Nature.* 188, 495–7. doi:10.1038/188495b0.

Noble, D. (1962). A modification of the Hodgkin-Huxley equations applicable to Purkinje fibre action and pacemaker potentials. *J. Physiol.* 160, 317–352. doi:10.1113/jphysiol.1962.sp006849.

Noble, D., and Rudy, Y. (2001). Models of cardiac ventricular action potentials: iterative interaction between experiment and simulation. *Philos. Trans. R. Soc. London. Ser. A Math. Phys. Eng. Sci.* 359, 1127–1142. doi:10.1098/rsta.2001.0820.

Nyns, E. C. A., Kip, A., Bart, C. I., Plomp, J. J., Zeppenfeld, K., Schalij, M. J., et al. (2017). Optogenetic termination of ventricular arrhythmias in the whole heart: Towards biological cardiac rhythm management. *Eur. Heart J.* 38, 2132–2136. doi:10.1093/eurheartj/ehw574.

Opthof, T. (1988). The mammalian sinoatrial node. *Cardiovasc. Drugs Ther.* 1, 573–597. doi:10.1007/BF02125744.

Opthof, T., Cgvanginneken, A., Bouman, L., and Jongsma, H. (1987a). The intrinsic cycle length in small pieces isolated from the rabbit sinoatrial node. *J. Mol. Cell. Cardiol.* 19, 923–934. doi:10.1016/S0022-2828(87)80621-1.

Opthof, T., de Jonge, B., Jongsma, H. J., and Bouman, L. N. (1987b). Functional morphology of the mammalian sinuatrial node. *Eur. Heart J.* 8, 1249–1259. doi:10.1093/oxfordjournals.eurheartj.a062200.

Park, S. A., Lee, S.-R., Tung, L., and Yue, D. T. (2014). Optical mapping of optogenetically shaped cardiac action potentials. *Sci. Rep.* 4. doi:10.1038/srep06125.

Pathak, C. L. (1958). Effects of changes in intraluminal pressure on inotropic and chronotropic responses of isolated mammalian hearts. *Am. J. Physiol.* 194, 197–9. doi:10.1152/ajplegacy.1958.194.1.197.

Peyronnet, R., Nerbonne, J. M., and Kohl, P. (2016). Cardiac mechano-gated ion channels and arrhythmias. *Circ. Res.* 118, 311–329. doi:10.1161/CIRCRESAHA.115.305043.

Pohl, A., Wachter, A., Hatam, N., and Leonhardt, S. (2016). A computational model of a human single sinoatrial node cell. *Biomed. Phys. Eng. Express* 2, 035006. doi:10.1088/2057-1976/2/3/035006.

Quinn, T. A., and Kohl, P. (2012). Mechano-sensitivity of cardiac pacemaker function: Pathophysiological relevance, experimental implications, and conceptual integration with other mechanisms of rhythmicity. *Prog. Biophys. Mol. Biol.* 110, 257–268. doi:10.1016/j.pbiomolbio.2012.08.008.

Quinn, T. A., and Kohl, P. (2013). Combining wet and dry research: Experience with model development for cardiac mechano-electric structure-function studies. *Cardiovasc. Res.* 97, 601–611. doi:10.1093/cvr/cvt003.

Quinn, T. A., and Kohl, P. (2016). Rabbit models of cardiac mechano-electric and mechano-mechanical coupling. *Prog. Biophys. Mol. Biol.* 121, 110–122. doi:10.1016/j.pbiomolbio.2016.05.003.

Quinn, T. A., and Kohl, P. (2020). Cardiac mechano-electric coupling: acute effects of mechanical stimulation on heart rate and rhythm. *Physiol. Rev.* doi:10.1152/physrev.00036.2019.

Rafferty, S. A., and Quinn, T. A. (2018). A beginner's guide to understanding and implementing the genetic modification of zebrafish. *Prog. Biophys. Mol. Biol.* 138, 3–19. doi:10.1016/j.pbiomolbio.2018.07.005.

Ravens, U. (2018). Ionic basis of cardiac electrophysiology in zebrafish compared to human hearts. *Prog. Biophys. Mol. Biol.* 138, 38–44. doi:10.1016/j.pbiomolbio.2018.06.008.

Rego, B. V., Wells, S. M., Lee, C.-H., and Sacks, M. S. (2016). Mitral valve leaflet remodelling during pregnancy: insights into cell-mediated recovery of tissue homeostasis. *J. R. Soc. Interface* 13, 20160709. doi:10.1098/rsif.2016.0709.

Reiner, V. S., and Antzelevitch, C. (1985). Phase resetting and annihilation in a mathematical model of sinus node. *Am. J. Physiol. Hear. Circ. Physiol.* 18. doi:10.1152/ajpheart.1985.249.6.h1143.

Roddie, I. C., Shepherd, J. T., and Whelan, R. F. (1957). Reflex changes in vasoconstrictor tone in human skeletal muscle in response to stimulation of receptors in a low-pressure area of the intrathoracic vascular bed. *J. Physiol.* 139, 369–76. doi:10.1113/jphysiol.1957.sp005897.

Rosen, M. R., Nargeot, J., and Salama, G. (2012). The case for the funny current and the calcium clock. *Hear. Rhythm* 9, 616–618. doi:10.1016/j.hrthm.2011.10.008.

Rossberg, F., Seim, H., and Strack, E. (1985). Chronotropic effects of the reversed carboxyl (RC) analogue of acetylcholine (β-homobetaine methylester) at defined intraluminal pressures on isolated right rabbit atria. *Res. Exp. Med.* 185, 139–144. doi:10.1007/BF01854899.

Sanders, R., Myerburg, R. J., Gelband, H., and Bassett, A. L. (1979). Dissimilar length-tension relations of canine ventricular muscle and false tendon: electrophysiologic alterations accompanying deformation. *J. Mol. Cell. Cardiol.* 11, 209–19. doi:10.1016/0022-2828(79)90465-6.

Sano, T., Sawanobori, T., and Adaniya, H. (1978). Mechanism of rhythm determination among pacemaker cells of the mammalian sinus node. *Am. J. Physiol. Hear. Circ. Physiol.* 4. doi:10.1152/ajpheart.1978.235.4.h379.

Schindelin, J., Arganda-Carreras, I., Frise, E., Kaynig, V., Longair, M., Pietzsch, T., et al. (2012). Fiji: an open-source platform for biological-image analysis. *Nat. Methods* 9, 676–82. doi:10.1038/nmeth.2019.

Schneider-Warme, F. (2018). The power of optogenetics: Potential in cardiac experimental and clinical electrophysiology. *Herzschrittmacherther. Elektrophysiol.* 29, 24–29. doi:10.1007/s00399-017-0545-8.

Schneider, C. A., Rasband, W. S., and Eliceiri, K. W. (2012). NIH Image to ImageJ: 25 years of image analysis. *Nat. Methods* 9, 671–675. doi:10.1038/nmeth.2089.

Severi, S., Fantini, M., Charawi, L. A., and Difrancesco, D. (2012). An updated computational model of rabbit sinoatrial action potential to investigate the mechanisms of heart rate modulation. *J. Physiol.* 590, 4483–4499. doi:10.1113/jphysiol.2012.229435.

Stoyek, M. R., Croll, R. P., and Smith, F. M. (2015). Intrinsic and extrinsic innervation of the heart in zebrafish (Danio rerio). *J. Comp. Neurol.* 523, 1683–1700. doi:10.1002/cne.23764.

Stoyek, M. R., Quinn, T. A., Croll, R. P., and Smith, F. M. (2016). Zebrafish heart as a model to study the integrative autonomic control of pacemaker function. *Am. J. Physiol. - Hear. Circ. Physiol.* 311, H676–H688. doi:10.1152/ajpheart.00330.2016.

Tessadori, F., van Weerd, J. H., Burkhard, S. B., Verkerk, A. O., de Pater, E., Boukens, B. J., et al. (2012). Identification and functional characterization of cardiac pacemaker cells in zebrafish. *PLoS One* 7, 1–9. doi:10.1371/journal.pone.0047644.

Torrente, A. G., Mesirca, P., Neco, P., Rizzetto, R., Dubel, S., Barrere, C., et al. (2016). L-type Cav1.3 channels regulate ryanodine receptor-dependent Ca^{2+} release during sino-atrial node pacemaker activity. *Cardiovasc. Res.* 109, 451–461. doi:10.1093/cvr/cvw006.

Trayanova, N. A., O'Hara, T., Bayer, J. D., Boyle, P. M., McDowell, K. S., Constantino, J., et al. (2012). Computational cardiology: how computer simulations could be used to develop new therapies and advance existing ones. *Europace* 14, v82–v89. doi:10.1093/europace/eus277.

Tsalikakis, D. G., Fotiadis, D. I., Michalis, L. K., and Kremmydas, G. P. (2007a). Phase resetting in one-dimensional model of the sinoatrial node. *IEEE Trans. Biomed. Eng.* 54, 1710–1714. doi:10.1109/TBME.2007.902606.

Tsalikakis, D. G., Zhang, H. G., Fotiadis, D. I., Kremmydas, G. P., and Michalis, K. (2007b). Phase response characteristics of sinoatrial node cells. *Comput. Biol. Med.* 37, 8–20. doi:10.1016/j.compbiomed.2005.09.011.

Unudurthi, S. D., Wu, X., Qian, L., Amari, F., Onal, B., Li, N., et al. (2016). Two-Pore K^+ channel TREK-1 regulates sinoatrial node membrane excitability. *J. Am. Heart Assoc.* 5. doi:10.1161/JAHA.115.002865.

Ushiyama, J., and Brooks, C. M. C. (1977). Interaction of oscillators: Effect of sinusoidal stretching of the sinoatrial node on nodal rhythm. *J. Electrocardiol.* 10, 39–44. doi:10.1016/S0022-0736(77)80029-0.

Vaidyanathan, R., O'Connell, R. P., Deo, M., Milstein, M. L., Furspan, P., Herron, T. J., et al. (2013). The ionic bases of the action potential in isolated mouse cardiac Purkinje cell. *Hear. Rhythm* 10, 80–87. doi:10.1016/j.hrthm.2012.10.002.

van Opbergen, C. J. M., Koopman, C. D., Kok, B. J. M., Knöpfel, T., Renninger, S. L., Orger, M. B., et al. (2018a). Optogenetic sensors in the zebrafish heart: A novel in vivo electrophysiological tool to study cardiac arrhythmogenesis. *Theranostics* 8, 4750–4764. doi:10.7150/thno.26108.

van Opbergen, C. J. M., van der Voorn, S. M., Vos, M. A., de Boer, T. P., and van Veen, T. A. B. (2018b). Cardiac Ca^{2+} signalling in zebrafish: Translation of findings to man. *Prog. Biophys. Mol. Biol.* 138, 45–58. doi:10.1016/j.pbiomolbio.2018.05.002.

Verheijck, E. E., Van Kempen, M. J. A., Veereschild, M., Lurvink, J., Jongsma, H. J., and Bouman, L. N. (2001). Electrophysiological features of the mouse sinoatrial node in relation to connexin distribution. *Cardiovasc. Res.* 52, 40–50. doi:10.1016/S0008-6363(01)00364-9.

Verheijck, E. E., Wessels, A., Van Ginneken, A. C. G., Bourier, J., Markman, M. W. M., Vermeulen, J. L. M., et al. (1998a). Distribution of atrial and nodal cells within the rabbit sinoatrial node: Models of sinoatrial transition. *Circulation* 97, 1623–1631. doi:10.1161/01.CIR.97.16.1623.

Verheijck, E. E., Wilders, R., Joyner, R. W., Golod, D. A., Kumar, R., Jongsma, H. J., et al. (1998b). Pacemaker synchronization of electrically coupled rabbit sinoatrial node cells. *J. Gen. Physiol.* 111, 95–112. doi:10.1085/jgp.111.1.95.

Vornanen, M., and Hassinen, M. (2016). Zebrafish heart as a model for human cardiac electrophysiology. *Channels* 10, 101–110. doi:10.1080/19336950.2015.1121335.

Warren, K. S., Baker, K., and Fishman, M. C. (2001). The slow mo mutation reduces pacemaker current and heart rate in adult zebrafish. *Am. J. Physiol. - Hear. Circ. Physiol.* 281, 1711–1719. doi:10.1152/ajpheart.2001.281.4.h1711.

Weisbrod, D., Khun, S. H., Bueno, H., Peretz, A., and Attali, B. (2016). Mechanisms underlying the cardiac pacemaker: The role of SK4 calcium-activated potassium channels. *Acta Pharmacol. Sin.* 37, 82–97. doi:10.1038/aps.2015.135.

Werdich, A. A., Brzezinski, A., Jeyaraj, D., Khaled Sabeh, M., Ficker, E., Wan, X., et al. (2012). The zebrafish as a novel animal model to study the molecular mechanisms of mechano-electrical feedback in the heart. *Prog. Biophys. Mol. Biol.* 110, 154–165. doi:10.1016/j.pbiomolbio.2012.07.006.

Wilders, R. (2007). Computer modelling of the sinoatrial node. *Med. Biol. Eng. Comput.* 45, 189–207. doi:10.1007/s11517-006-0127-0.

Wilson, S. J., and Bolter, C. P. (2001). Interaction of the autonomic nervous system with intrinsic cardiac rate regulation in the guinea-pig, Cavia porcellus. *Comp. Biochem. Physiol. A. Mol. Integr. Physiol.* 130, 723–30. doi:10.1016/s1095-6433(01)00404-4.

Wilson, S. J., and Bolter, C. P. (2002). Do cardiac neurons play a role in the intrinsic control of heart rate in the rat? *Exp. Physiol.* 87, 675–682. doi:10.1113/eph8702364.

Yasuma, F., and Hayano, J. I. (2004). Respiratory sinus arrhythmia: why does the heartbeat synchronize with respiratory rhythm? *Chest* 125, 683–690. doi:10.1378/chest.125.2.683.

Ypey, D. L., Van Meerwijk, W. P. M., and de Bruin, G. (1982). Suppression of pacemaker activity by rapid repetitive phase delay. *Biol. Cybern.* 45, 187–194. doi:10.1007/BF00336191.

Zhang, H., Holden, A. V., and Boyett, M. R. (2002). Sustained inward current and pacemaker activity of mammalian sinoatrial node. *J. Cardiovasc. Electrophysiol.* 13, 809–812. doi:10.1046/j.1540-8167.2002.00809.x.

APPENDIX – COPYRIGHT PERMISSIONS

Figure 1.2: This figure was previously published and is used with permission from John Wiley and Sons. Citation: Bainbridge, F. A. (1915). The influence of venous filling upon the rate of the heart. J. Physiol. 50, 65–84. doi:10.1113/jphysiol.1915.sp001736. Figure 1.

JOHN WILEY AND SONS LICENSE
TERMS AND CONDITIONS

Mar 27, 2020

This Agreement between Eilidh MacDonald ("You") and John Wiley and Sons ("John Wiley and Sons") consists of your license details and the terms and conditions provided by John Wiley and Sons and Copyright Clearance Center.

License Number	4797121227161
License date	Mar 27, 2020
Licensed Content Publisher	John Wiley and Sons
Licensed Content Publication	Journal of Physiology
Licensed Content Title	The influence of venous filling upon the rate of the heart
Licensed Content Author	F. A. Bainbridge
Licensed Content Date	Dec 24, 1915
Licensed Content Volume	50
Licensed Content Issue	2
Licensed Content Pages	20
Type of use	Dissertation/Thesis
Requestor type	University/Academic
Format	Print and electronic

Portion	Figure/table
Number of figures/tables	1
Original Wiley figure/table number(s)	Figure 1
Will you be translating?	No
Title of your thesis / dissertation	PhD thesis
Expected completion date	Jun 2020
Expected size (number of pages)	1
Requestor Location	Eilidh MacDonald 5850 College Street Halifax, NS B3H4H7 Canada Attn: Eilidh MacDonald
Publisher Tax ID	EU826007151
Total	0.00 USD

Terms and Conditions

TERMS AND CONDITIONS

This copyrighted material is owned by or exclusively licensed to John Wiley & Sons, Inc. or one of its group companies (each a"Wiley Company") or handled on behalf of a society with which a Wiley Company has exclusive publishing rights in relation to a particular work (collectively "WILEY"). By clicking "accept" in connection with completing this licensing transaction, you agree that the following terms and conditions apply to this transaction (along with the billing and payment terms and conditions established by the Copyright Clearance Center Inc., ("CCC's Billing and Payment terms and conditions"), at the time that you opened your RightsLink account (these are available at any time at http://myaccount.copyright.com).

Terms and Conditions

- The materials you have requested permission to reproduce or reuse (the "Wiley Materials") are protected by copyright.

- You are hereby granted a personal, non-exclusive, non-sub licensable (on a stand-alone basis), non-transferable, worldwide, limited license to reproduce the Wiley Materials for the purpose specified in the licensing process. This license, **and any CONTENT (PDF or image file) purchased as part of your order,** is for a one-time use only and limited to any maximum distribution number specified in the license. The first instance of republication or reuse granted by this license must be completed within two years of the date of the grant of this license (although copies prepared before the end date may be distributed thereafter). The Wiley Materials shall not be used in any other manner or for any other purpose, beyond what is granted in the license. Permission is granted subject to an appropriate acknowledgement given to the author, title of the material/book/journal and the publisher. You shall also duplicate the copyright notice that appears in the Wiley publication in your use of the Wiley Material. Permission is also granted on the understanding that nowhere in the text is a previously published source acknowledged for all or part of this Wiley Material. Any third party content is expressly excluded from this permission.

- With respect to the Wiley Materials, all rights are reserved. Except as expressly granted by the terms of the license, no part of the Wiley Materials may be copied, modified, adapted (except for minor reformatting required by the new Publication), translated, reproduced, transferred or distributed, in any form or by any means, and no derivative works may be made based on the Wiley Materials without the prior permission of the respective copyright owner.**For STM Signatory Publishers clearing permission under the terms of the STM Permissions Guidelines only, the terms of the license are extended to include subsequent editions and for editions in other languages, provided such editions are for the work as a whole in situ and does not involve the separate exploitation of the permitted figures or extracts,** You may not alter, remove or suppress in any manner any copyright, trademark or other notices displayed by the Wiley Materials. You may not license, rent, sell, loan, lease, pledge, offer as security, transfer or assign the Wiley Materials on a stand-alone basis, or any of the rights granted to you hereunder to any other person.

- The Wiley Materials and all of the intellectual property rights therein shall at all times remain the exclusive property of John Wiley & Sons Inc, the Wiley Companies, or their respective licensors, and your interest therein is only that of having possession of and the right to reproduce the Wiley Materials pursuant to Section 2 herein during the continuance of this Agreement. You agree that you own no right, title or interest in or to the Wiley Materials or any of the intellectual property rights therein. You shall have no rights hereunder other than the license as provided for above in Section 2. No right, license or interest to any trademark, trade name, service mark or other branding ("Marks") of WILEY or its licensors is granted hereunder, and you agree that you shall not assert any such right, license or interest with respect thereto

- NEITHER WILEY NOR ITS LICENSORS MAKES ANY WARRANTY OR REPRESENTATION OF ANY KIND TO YOU OR ANY THIRD PARTY, EXPRESS, IMPLIED OR STATUTORY, WITH RESPECT TO THE MATERIALS OR THE ACCURACY OF ANY INFORMATION CONTAINED IN THE MATERIALS, INCLUDING, WITHOUT LIMITATION, ANY IMPLIED WARRANTY OF MERCHANTABILITY, ACCURACY, SATISFACTORY

QUALITY, FITNESS FOR A PARTICULAR PURPOSE, USABILITY, INTEGRATION OR NON-INFRINGEMENT AND ALL SUCH WARRANTIES ARE HEREBY EXCLUDED BY WILEY AND ITS LICENSORS AND WAIVED BY YOU.

- WILEY shall have the right to terminate this Agreement immediately upon breach of this Agreement by you.
- You shall indemnify, defend and hold harmless WILEY, its Licensors and their respective directors, officers, agents and employees, from and against any actual or threatened claims, demands, causes of action or proceedings arising from any breach of this Agreement by you.
- IN NO EVENT SHALL WILEY OR ITS LICENSORS BE LIABLE TO YOU OR ANY OTHER PARTY OR ANY OTHER PERSON OR ENTITY FOR ANY SPECIAL, CONSEQUENTIAL, INCIDENTAL, INDIRECT, EXEMPLARY OR PUNITIVE DAMAGES, HOWEVER CAUSED, ARISING OUT OF OR IN CONNECTION WITH THE DOWNLOADING, PROVISIONING, VIEWING OR USE OF THE MATERIALS REGARDLESS OF THE FORM OF ACTION, WHETHER FOR BREACH OF CONTRACT, BREACH OF WARRANTY, TORT, NEGLIGENCE, INFRINGEMENT OR OTHERWISE (INCLUDING, WITHOUT LIMITATION, DAMAGES BASED ON LOSS OF PROFITS, DATA, FILES, USE, BUSINESS OPPORTUNITY OR CLAIMS OF THIRD PARTIES), AND WHETHER OR NOT THE PARTY HAS BEEN ADVISED OF THE POSSIBILITY OF SUCH DAMAGES. THIS LIMITATION SHALL APPLY NOTWITHSTANDING ANY FAILURE OF ESSENTIAL PURPOSE OF ANY LIMITED REMEDY PROVIDED HEREIN.
- Should any provision of this Agreement be held by a court of competent jurisdiction to be illegal, invalid, or unenforceable, that provision shall be deemed amended to achieve as nearly as possible the same economic effect as the original provision, and the legality, validity and enforceability of the remaining provisions of this Agreement shall not be affected or impaired thereby.
- The failure of either party to enforce any term or condition of this Agreement shall not constitute a waiver of either party's right to enforce each and every term and condition of this Agreement. No breach under this agreement shall be deemed waived or excused by either party unless such waiver or consent is in writing signed by the party granting such waiver or consent. The waiver by or consent of a party to a breach of any provision of this Agreement shall not operate or be construed as a waiver of or consent to any other or subsequent breach by such other party.
- This Agreement may not be assigned (including by operation of law or otherwise) by you without WILEY's prior written consent.
- Any fee required for this permission shall be non-refundable after thirty (30) days from receipt by the CCC.
- These terms and conditions together with CCC's Billing and Payment terms and conditions (which are incorporated herein) form the entire agreement between you and WILEY concerning this licensing transaction and (in the absence of fraud) supersedes all prior agreements and representations of the parties, oral or written. This Agreement may not be amended except in writing signed by both parties. This Agreement shall be binding upon and inure to the benefit of the parties' successors, legal representatives,

and authorized assigns.

- In the event of any conflict between your obligations established by these terms and conditions and those established by CCC's Billing and Payment terms and conditions, these terms and conditions shall prevail.
- WILEY expressly reserves all rights not specifically granted in the combination of (i) the license details provided by you and accepted in the course of this licensing transaction, (ii) these terms and conditions and (iii) CCC's Billing and Payment terms and conditions.
- This Agreement will be void if the Type of Use, Format, Circulation, or Requestor Type was misrepresented during the licensing process.
- This Agreement shall be governed by and construed in accordance with the laws of the State of New York, USA, without regards to such state's conflict of law rules. Any legal action, suit or proceeding arising out of or relating to these Terms and Conditions or the breach thereof shall be instituted in a court of competent jurisdiction in New York County in the State of New York in the United States of America and each party hereby consents and submits to the personal jurisdiction of such court, waives any objection to venue in such court and consents to service of process by registered or certified mail, return receipt requested, at the last known address of such party.

WILEY OPEN ACCESS TERMS AND CONDITIONS

Wiley Publishes Open Access Articles in fully Open Access Journals and in Subscription journals offering Online Open. Although most of the fully Open Access journals publish open access articles under the terms of the Creative Commons Attribution (CC BY) License only, the subscription journals and a few of the Open Access Journals offer a choice of Creative Commons Licenses. The license type is clearly identified on the article.

The Creative Commons Attribution License

The Creative Commons Attribution License (CC-BY) allows users to copy, distribute and transmit an article, adapt the article and make commercial use of the article. The CC-BY license permits commercial and non-

Creative Commons Attribution Non-Commercial License

The Creative Commons Attribution Non-Commercial (CC-BY-NC)License permits use, distribution and reproduction in any medium, provided the original work is properly cited and is not used for commercial purposes.(see below)

Creative Commons Attribution-Non-Commercial-NoDerivs License

The Creative Commons Attribution Non-Commercial-NoDerivs License (CC-BY-NC-ND) permits use, distribution and reproduction in any medium, provided the original work is properly cited, is not used for commercial purposes and no modifications or adaptations are made. (see below)

Use by commercial "for-profit" organizations

Use of Wiley Open Access articles for commercial, promotional, or marketing purposes requires further explicit permission from Wiley and will be subject to a fee.

Further details can be found on Wiley Online Library
http://olabout.wiley.com/WileyCDA/Section/id-410895.html

Other Terms and Conditions:

v1.10 Last updated September 2015

Questions? customercare@copyright.com or +1-855-239-3415 (toll free in the US) or +1-978-646-2777.

Figure 1.3: This figure was previously published and is used with permission from Oxford University Press. Citation: Donald, D. E., and Shepherd, J. T. (1978). Reflexes from the heart and lungs: Physiological curiosities or important regulatory mechanisms. *Cardiovasc. Res.* 12, 449–469. doi:10.1093/cvr/12.8.449. Figure 11.

OXFORD UNIVERSITY PRESS LICENSE TERMS AND CONDITIONS

Mar 27, 2020

This Agreement between Eilidh MacDonald ("You") and Oxford University Press ("Oxford University Press") consists of your license details and the terms and conditions provided by Oxford University Press and Copyright Clearance Center.

License Number	4797110497995
License date	Mar 27, 2020
Licensed Content Publisher	Oxford University Press
Licensed Content Publication	Cardiovascular Research
Licensed Content Title	Reflexes from the heart and lungs: physiological curiosities or important regulatory mechanisms[1]
Licensed Content Author	DONALD, DAVID E.; SHEPHERD, JOHN T.
Licensed Content Date	Aug 1, 1978
Type of Use	Thesis/Dissertation
Institution name	
Title of your work	PhD thesis
Publisher of your work	Dalhousie University
Expected publication date	Jun 2020
Permissions cost	0.00 USD
Value added tax	0.00 USD
Total	**0.00 USD**
Title	PhD thesis
Institution name	Dalhousie University
Expected presentation date	Jun 2020
Portions	Figure 11
Requestor Location	Eilidh MacDonald 5850 College Street Halifax, NS B3H4H7 Canada Attn: Eilidh MacDonald
Publisher Tax ID	GB125506730
Total	**0.00 USD**
Terms and Conditions	

STANDARD TERMS AND CONDITIONS FOR REPRODUCTION OF MATERIAL FROM AN OXFORD UNIVERSITY PRESS JOURNAL

1. Use of the material is restricted to the type of use specified in your order details.
2. This permission covers the use of the material in the English language in the following territory: world. If you have requested additional permission to translate this material, the terms and conditions of this reuse will be set out in clause 12.
3. This permission is limited to the particular use authorized in (1) above and does not allow you to sanction its use elsewhere in any other format other than specified above, nor does it apply to quotations, images, artistic works etc that have been reproduced from other sources which may be part of the material to be used.
4. No alteration, omission or addition is made to the material without our written consent. Permission must be re-cleared with Oxford University Press if/when you decide to reprint.
5. The following credit line appears wherever the material is used: author, title, journal, year, volume, issue number, pagination, by permission of Oxford University Press or the sponsoring society if the journal is a society journal. Where a journal is being published

on behalf of a learned society, the details of that society must be included in the credit line.
6. For the reproduction of a full article from an Oxford University Press journal for whatever purpose, the corresponding author of the material concerned should be informed of the proposed use. Contact details for the corresponding authors of all Oxford University Press journal contact can be found alongside either the abstract or full text of the article concerned, accessible from www.oxfordjournals.org Should there be a problem clearing these rights, please contact journals.permissions@oup.com
7. If the credit line or acknowledgement in our publication indicates that any of the figures, images or photos was reproduced, drawn or modified from an earlier source it will be necessary for you to clear this permission with the original publisher as well. If this permission has not been obtained, please note that this material cannot be included in your publication/photocopies.
8. While you may exercise the rights licensed immediately upon issuance of the license at the end of the licensing process for the transaction, provided that you have disclosed complete and accurate details of your proposed use, no license is finally effective unless and until full payment is received from you (either by Oxford University Press or by Copyright Clearance Center (CCC)) as provided in CCC's Billing and Payment terms and conditions. If full payment is not received on a timely basis, then any license preliminarily granted shall be deemed automatically revoked and shall be void as if never granted. Further, in the event that you breach any of these terms and conditions or any of CCC's Billing and Payment terms and conditions, the license is automatically revoked and shall be void as if never granted. Use of materials as described in a revoked license, as well as any use of the materials beyond the scope of an unrevoked license, may constitute copyright infringement and Oxford University Press reserves the right to take any and all action to protect its copyright in the materials.
9. This license is personal to you and may not be sublicensed, assigned or transferred by you to any other person without Oxford University Press's written permission.
10. Oxford University Press reserves all rights not specifically granted in the combination of (i) the license details provided by you and accepted in the course of this licensing transaction, (ii) these terms and conditions and (iii) CCC's Billing and Payment terms and conditions.
11. You hereby indemnify and agree to hold harmless Oxford University Press and CCC, and their respective officers, directors, employs and agents, from and against any and all claims arising out of your use of the licensed material other than as specifically authorized pursuant to this license.
12. Other Terms and Conditions:
v1.4

Questions? customercare@copyright.com or +1-855-239-3415 (toll free in the US) or +1-978-646-2777.

Figure 1.4: This figure was previously published and is used with permission from The American Physiological Society. Citation: Pathak, C. L. (1958). Effects of changes in intraluminal pressure on inotropic and chronotropic responses of isolated mammalian hearts. *Am. J. Physiol*. 194, 197–9. doi:10.1152/ajplegacy.1958.194.1.197. Figure 2.

THE AMERICAN PHYSIOLOGICAL SOCIETY LICENSE
TERMS AND CONDITIONS

Mar 30, 2020

This Agreement between Eilidh MacDonald ("You") and The American Physiological Society ("The American Physiological Society") consists of your license details and the terms and conditions provided by The American Physiological Society and Copyright Clearance Center.

License Number	4798901030506
License date	Mar 30, 2020
Licensed Content Publisher	The American Physiological Society
Licensed Content Publication	American Journal of Physiology, Consolidated
Licensed Content Title	Effects of Changes in Intraluminal Pressure on Inotropic and Chronotropic Responses of Isolated Mammalian Hearts
Licensed Content Author	C. L. Pathak
Licensed Content Date	Jul 1, 1958
Licensed Content Volume	194
Licensed Content Issue	1
Type of Use	Thesis/Dissertation
Requestor type	non-profit academic/educational

Readers being charged a fee for this work	No
Format	print and electronic
Portion	figures/tables/images
Number of figures/tables/images	1
Will you be translating?	no
World Rights	no
Order reference number	
Title	PhD thesis
Institution name	Dalhousie University
Expected presentation date	Jun 2020
Portions	Figure 2.
Requestor Location	Eilidh MacDonald 5850 College Street Halifax, NS B3H4H7 Canada Attn: Eilidh MacDonald
Billing Type	Invoice
Billing Address	Eilidh MacDonald 5850 College Street Halifax, NS B3H4H7

Canada
Attn: Eilidh MacDonald

Total 0.00 USD

Terms and Conditions

Terms and Conditions:

Figures/Tables/Images are available to the requestor from the APS journals website at http://www.the-aps.org/publications/journals/. The obtaining of content is a separate transaction and does not involve Rightslink or CCC, and is the responsibility of the permission seeker. Higher resolution images are available at additional charge from APS; please contact cvillemez@the-aps.org

Original Authors of Published Works: To see a full list of original authors rights concerning their own published work http://www.the-aps.org/publications/authorinfo/copyright.htm

Content reuse rights awarded by the APS may be exercised immediately upon issuance of this license, provided full disclosure and complete and accurate details of the proposed reuse have been made; no license is finally granted unless and until full payment is received either by the publisher or by CCC as provided in CCC's Billing and Payment Terms and Conditions. If full payment is not received on a timely basis, then any license preliminarily granted shall be deemed automatically revoked and shall be void as if never granted. Further, in the event that you breach any of these Terms and Conditions or any of CCC's Billing and Payment Terms and Conditions, the license is automatically revoked and shall be void as if never granted. Use of materials as described in a revoked license, as well as any use of the materials beyond the scope of the license, may constitute copyright infringement and the Publisher reserves the right to take action to protect its copyright of its materials.

The APS makes no representations or warranties with respect to the licensed material. You hereby indemnify and agree to hold harmless the publisher and CCC, and their respective officers, directors, employees and agents, from and against any and all claims arising out of your use of the licensed material other than as specifically authorized pursuant to this license.

This license is personal to you /your organization and may not be sublicensed, assigned, or transferred by you /your organization to another person /organization without the publisher's permission.This license may not be amended except in writing signed by both parties, or in the case of the publisher, by CCC on the publisher's behalf.

The APS reserves all rights not specifically granted in the combination of (i) the license details provided by you and accepted in the course of this licensing transaction, (ii) these Terms and Conditions and (iii) CCC's Billing and Payment Terms and Conditions.

v1.0

Questions? customercare@copyright.com or +1-855-239-3415 (toll free in the US) or +1-978-646-2777.

Figure 1.5: This figure was previously published and is used with permission from John Wiley and Sons. Citation: Cooper, P. J., and Kohl, P. (2005). Species- and preparation-dependence of stretch effects on sino-atrial node pacemaking. *Ann. N. Y. Acad. Sci*. 1047, 324–335. doi:10.1196/annals.1341.029. Figure 4.

JOHN WILEY AND SONS LICENSE
TERMS AND CONDITIONS

Oct 07, 2020

This Agreement between Eilidh MacDonald ("You") and John Wiley and Sons ("John Wiley and Sons") consists of your license details and the terms and conditions provided by John Wiley and Sons and Copyright Clearance Center.

License Number	4923601083192
License date	Oct 07, 2020
Licensed Content Publisher	John Wiley and Sons
Licensed Content Publication	Annals of the New York Academy of Sciences
Licensed Content Title	Species− and Preparation−Dependence of Stretch Effects on Sino−Atrial Node Pacemaking
Licensed Content Author	PETER KOHL, PATRICIA J. COOPER
Licensed Content Date	Jan 9, 2006
Licensed Content Volume	1047
Licensed Content Issue	1
Licensed Content Pages	12

Type of use	Dissertation/Thesis
Requestor type	University/Academic
Format	Print and electronic
Portion	Figure/table
Number of figures/tables	1
Will you be translating?	No
Title	PhD thesis
Institution name	Dalhousie University
Expected presentation date	Dec 2020
Order reference number	4798731081298
Portions	Figure 4
Requestor Location	Eilidh MacDonald 5850 College Street Halifax, NS B3H4H7 Canada Attn: Eilidh MacDonald
Publisher Tax ID	EU826007151
Total	0.00 USD

Terms and Conditions

TERMS AND CONDITIONS

This copyrighted material is owned by or exclusively licensed to John Wiley & Sons, Inc. or one of its group companies (each a"Wiley Company") or handled on behalf of a society with which a Wiley Company has exclusive publishing rights in relation to a particular work (collectively "WILEY"). By clicking "accept" in connection with completing this licensing transaction, you agree that the following terms and conditions apply to this transaction (along with the billing and payment terms and conditions established by the Copyright Clearance Center Inc., ("CCC's Billing and Payment terms and conditions"), at the time that you opened your RightsLink account (these are available at any time at http://myaccount.copyright.com).

Terms and Conditions

- The materials you have requested permission to reproduce or reuse (the "Wiley Materials") are protected by copyright.
- You are hereby granted a personal, non-exclusive, non-sub licensable (on a stand-alone basis), non-transferable, worldwide, limited license to reproduce the Wiley Materials for the purpose specified in the licensing process. This license, **and any CONTENT (PDF or image file) purchased as part of your order,** is for a one-time use only and limited to any maximum distribution number specified in the license. The first instance of republication or reuse granted by this license must be completed within two years of the date of the grant of this license (although copies prepared before the end date may be distributed thereafter). The Wiley Materials shall not be used in any other manner or for any other purpose, beyond what is granted in the license. Permission is granted subject to an appropriate acknowledgement given to the author, title of the material/book/journal and the publisher. You shall also duplicate the copyright notice that appears in the Wiley publication in your use of the Wiley Material. Permission is also granted on the understanding that nowhere in the text is a previously published source acknowledged for all or part of this Wiley Material. Any third party content is expressly excluded from this permission.
- With respect to the Wiley Materials, all rights are reserved. Except as expressly granted by the terms of the license, no part of the Wiley Materials may be copied, modified, adapted (except for minor reformatting required by the new Publication), translated, reproduced, transferred or distributed, in any form or by any means, and no derivative works may be made based on the Wiley Materials without the prior permission of the respective copyright owner.**For STM Signatory Publishers clearing permission under the terms of the STM Permissions Guidelines only, the terms of the license are extended to include subsequent editions and for editions in other languages, provided such editions are for the work as a whole in situ and does not involve the separate exploitation of the permitted figures or extracts,** You may not alter, remove or suppress in any manner any copyright, trademark or other notices displayed by the Wiley Materials. You may not license, rent, sell, loan, lease, pledge, offer as security, transfer or assign the Wiley Materials on a stand-alone basis, or any of the rights granted to you hereunder to any other person.
- The Wiley Materials and all of the intellectual property rights therein shall at all times remain the exclusive property of John Wiley & Sons Inc, the Wiley Companies, or their respective licensors, and your interest therein is only that of having possession of and the right to reproduce the Wiley Materials pursuant to Section 2 herein during the continuance of this Agreement. You agree that you own no right, title or interest in or

to the Wiley Materials or any of the intellectual property rights therein. You shall have no rights hereunder other than the license as provided for above in Section 2. No right, license or interest to any trademark, trade name, service mark or other branding ("Marks") of WILEY or its licensors is granted hereunder, and you agree that you shall not assert any such right, license or interest with respect thereto

- NEITHER WILEY NOR ITS LICENSORS MAKES ANY WARRANTY OR REPRESENTATION OF ANY KIND TO YOU OR ANY THIRD PARTY, EXPRESS, IMPLIED OR STATUTORY, WITH RESPECT TO THE MATERIALS OR THE ACCURACY OF ANY INFORMATION CONTAINED IN THE MATERIALS, INCLUDING, WITHOUT LIMITATION, ANY IMPLIED WARRANTY OF MERCHANTABILITY, ACCURACY, SATISFACTORY QUALITY, FITNESS FOR A PARTICULAR PURPOSE, USABILITY, INTEGRATION OR NON-INFRINGEMENT AND ALL SUCH WARRANTIES ARE HEREBY EXCLUDED BY WILEY AND ITS LICENSORS AND WAIVED BY YOU.

- WILEY shall have the right to terminate this Agreement immediately upon breach of this Agreement by you.

- You shall indemnify, defend and hold harmless WILEY, its Licensors and their respective directors, officers, agents and employees, from and against any actual or threatened claims, demands, causes of action or proceedings arising from any breach of this Agreement by you.

- IN NO EVENT SHALL WILEY OR ITS LICENSORS BE LIABLE TO YOU OR ANY OTHER PARTY OR ANY OTHER PERSON OR ENTITY FOR ANY SPECIAL, CONSEQUENTIAL, INCIDENTAL, INDIRECT, EXEMPLARY OR PUNITIVE DAMAGES, HOWEVER CAUSED, ARISING OUT OF OR IN CONNECTION WITH THE DOWNLOADING, PROVISIONING, VIEWING OR USE OF THE MATERIALS REGARDLESS OF THE FORM OF ACTION, WHETHER FOR BREACH OF CONTRACT, BREACH OF WARRANTY, TORT, NEGLIGENCE, INFRINGEMENT OR OTHERWISE (INCLUDING, WITHOUT LIMITATION, DAMAGES BASED ON LOSS OF PROFITS, DATA, FILES, USE, BUSINESS OPPORTUNITY OR CLAIMS OF THIRD PARTIES), AND WHETHER OR NOT THE PARTY HAS BEEN ADVISED OF THE POSSIBILITY OF SUCH DAMAGES. THIS LIMITATION SHALL APPLY NOTWITHSTANDING ANY FAILURE OF ESSENTIAL PURPOSE OF ANY LIMITED REMEDY PROVIDED HEREIN.

- Should any provision of this Agreement be held by a court of competent jurisdiction to be illegal, invalid, or unenforceable, that provision shall be deemed amended to achieve as nearly as possible the same economic effect as the original provision, and the legality, validity and enforceability of the remaining provisions of this Agreement shall not be affected or impaired thereby.

- The failure of either party to enforce any term or condition of this Agreement shall not constitute a waiver of either party's right to enforce each and every term and condition of this Agreement. No breach under this agreement shall be deemed waived or excused by either party unless such waiver or consent is in writing signed by the party granting such waiver or consent. The waiver by or consent of a party to a breach of any provision of this Agreement shall not operate or be construed as a waiver of or consent to any other or subsequent breach by such other party.

- This Agreement may not be assigned (including by operation of law or otherwise) by you without WILEY's prior written consent.
- Any fee required for this permission shall be non-refundable after thirty (30) days from receipt by the CCC.
- These terms and conditions together with CCC's Billing and Payment terms and conditions (which are incorporated herein) form the entire agreement between you and WILEY concerning this licensing transaction and (in the absence of fraud) supersedes all prior agreements and representations of the parties, oral or written. This Agreement may not be amended except in writing signed by both parties. This Agreement shall be binding upon and inure to the benefit of the parties' successors, legal representatives, and authorized assigns.
- In the event of any conflict between your obligations established by these terms and conditions and those established by CCC's Billing and Payment terms and conditions, these terms and conditions shall prevail.
- WILEY expressly reserves all rights not specifically granted in the combination of (i) the license details provided by you and accepted in the course of this licensing transaction, (ii) these terms and conditions and (iii) CCC's Billing and Payment terms and conditions.
- This Agreement will be void if the Type of Use, Format, Circulation, or Requestor Type was misrepresented during the licensing process.
- This Agreement shall be governed by and construed in accordance with the laws of the State of New York, USA, without regards to such state's conflict of law rules. Any legal action, suit or proceeding arising out of or relating to these Terms and Conditions or the breach thereof shall be instituted in a court of competent jurisdiction in New York County in the State of New York in the United States of America and each party hereby consents and submits to the personal jurisdiction of such court, waives any objection to venue in such court and consents to service of process by registered or certified mail, return receipt requested, at the last known address of such party.

WILEY OPEN ACCESS TERMS AND CONDITIONS

Wiley Publishes Open Access Articles in fully Open Access Journals and in Subscription journals offering Online Open. Although most of the fully Open Access journals publish open access articles under the terms of the Creative Commons Attribution (CC BY) License only, the subscription journals and a few of the Open Access Journals offer a choice of Creative Commons Licenses. The license type is clearly identified on the article.

The Creative Commons Attribution License

The Creative Commons Attribution License (CC-BY) allows users to copy, distribute and transmit an article, adapt the article and make commercial use of the article. The CC-BY license permits commercial and non-

Creative Commons Attribution Non-Commercial License

The Creative Commons Attribution Non-Commercial (CC-BY-NC)License permits use, distribution and reproduction in any medium, provided the original work is properly cited

and is not used for commercial purposes.(see below)

Creative Commons Attribution-Non-Commercial-NoDerivs License

The Creative Commons Attribution Non-Commercial-NoDerivs License (CC-BY-NC-ND) permits use, distribution and reproduction in any medium, provided the original work is properly cited, is not used for commercial purposes and no modifications or adaptations are made. (see below)

Use by commercial "for-profit" organizations

Use of Wiley Open Access articles for commercial, promotional, or marketing purposes requires further explicit permission from Wiley and will be subject to a fee.

Further details can be found on Wiley Online Library
http://olabout.wiley.com/WileyCDA/Section/id-410895.html

Other Terms and Conditions:

v1.10 Last updated September 2015

Questions? customercare@copyright.com or +1-855-239-3415 (toll free in the US) or +1-978-646-2777.

Figure 1.6: This figure was previously published and is used with permission from Springer Nature. Citation: Deck, K. A. (1964). Dehnungseffekte am spontanschlagenden, isolierten Sinusknoten. *Pflugers Arch. Gesamte Physiol. Menschen Tiere* 280, 120–130. doi:10.1007/BF00363751.Figure 2.

SPRINGER NATURE LICENSE TERMS AND CONDITIONS

Mar 27, 2020

This Agreement between Eilidh MacDonald ("You") and Springer Nature ("Springer Nature") consists of your license details and the terms and conditions provided by Springer Nature and Copyright Clearance Center.

License Number	4797090309980
License date	Mar 27, 2020
Licensed Content Publisher	Springer Nature
Licensed Content Publication	Pflüger's Archiv für die gesamte Physiologie des Menschen und der Tiere
Licensed Content Title	Dehnungseffekte am spontanschlagenden, isolierten Sinusknoten
Licensed Content Author	Klaus A. Deck
Licensed Content Date	Jan 1, 1964
Type of Use	Thesis/Dissertation
Requestor type	non-commercial (non-profit)
Format	print and electronic
Portion	figures/tables/illustrations
Number of figures/tables/illustrations	1
Will you be translating?	no
Circulation/distribution	1 - 29
Author of this Springer Nature content	no
Title	PhD thesis
Institution name	Dalhousie University
Expected presentation date	Jun 2020
Portions	Figure 2: Spontanschlagendes Sinuspräparat der Katze.
Requestor Location	Eilidh MacDonald 5850 College Street Halifax, NS B3H4H7 Canada Attn: Eilidh MacDonald
Total	**0.00 CAD**
Terms and Conditions	

Springer Nature Customer Service Centre GmbH
Terms and Conditions

This agreement sets out the terms and conditions of the licence (the **Licence**) between you and **Springer Nature Customer Service Centre GmbH** (the **Licensor**). By clicking 'accept' and completing the transaction for the material (**Licensed Material**), you also confirm your acceptance of these terms and conditions.

1. Grant of License

1. 1. The Licensor grants you a personal, non-exclusive, non-transferable, world-wide licence to reproduce the Licensed Material for the purpose specified in your order only. Licences are granted for the specific use requested in the order and for no other use, subject to the conditions below.

1. 2. The Licensor warrants that it has, to the best of its knowledge, the rights to license reuse of the Licensed Material. However, you should ensure that the material you are requesting is original to the Licensor and does not carry the copyright of another entity (as credited in the published version).

1. 3. If the credit line on any part of the material you have requested indicates that it was reprinted or adapted with permission from another source, then you should also seek permission from that source to reuse the material.

2. Scope of Licence

2. 1. You may only use the Licensed Content in the manner and to the extent permitted by these Ts&Cs and any applicable laws.

2. 2. A separate licence may be required for any additional use of the Licensed Material, e.g. where a licence has been purchased for print only use, separate permission must be obtained for electronic re-use. Similarly, a licence is only valid in the language selected and does not apply for editions in other languages unless additional translation rights have been granted separately in the licence. Any content owned by third parties are expressly excluded from the licence.

2. 3. Similarly, rights for additional components such as custom editions and derivatives require additional permission and may be subject to an additional fee. Please apply to Journalpermissions@springernature.com/bookpermissions@springernature.com for these rights.

2. 4. Where permission has been granted **free of charge** for material in print, permission may also be granted for any electronic version of that work, provided that the material is incidental to your work as a whole and that the electronic version is essentially equivalent to, or substitutes for, the print version.

2. 5. An alternative scope of licence may apply to signatories of the STM Permissions Guidelines, as amended from time to time.

3. Duration of Licence

3. 1. A licence for is valid from the date of purchase ('Licence Date') at the end of the relevant period in the below table:

Scope of Licence	Duration of Licence
Post on a website	12 months
Presentations	12 months
Books and journals	Lifetime of the edition in the language purchased

4. Acknowledgement

4. 1. The Licensor's permission must be acknowledged next to the Licenced Material in print. In electronic form, this acknowledgement must be visible at the same time as the figures/tables/illustrations or abstract, and must be hyperlinked to the journal/book's homepage. Our required acknowledgement format is in the Appendix below.

5. Restrictions on use

5. 1. Use of the Licensed Material may be permitted for incidental promotional use and minor editing privileges e.g. minor adaptations of single figures, changes of format, colour and/or style where the adaptation is credited as set out in Appendix 1 below. Any other changes including but not limited to, cropping, adapting, omitting material that affect the meaning, intention or moral rights of the author are strictly prohibited.

5. 2. You must not use any Licensed Material as part of any design or trademark.

5. 3. Licensed Material may be used in Open Access Publications (OAP) before publication by Springer Nature, but any Licensed Material must be removed from OAP sites prior to final publication.

6. Ownership of Rights

6. 1. Licensed Material remains the property of either Licensor or the relevant third party and any rights not explicitly granted herein are expressly reserved.

7. Warranty

IN NO EVENT SHALL LICENSOR BE LIABLE TO YOU OR ANY OTHER PARTY OR ANY OTHER PERSON OR FOR ANY SPECIAL, CONSEQUENTIAL, INCIDENTAL OR INDIRECT DAMAGES, HOWEVER CAUSED, ARISING OUT OF OR IN CONNECTION WITH THE DOWNLOADING, VIEWING OR USE OF THE MATERIALS REGARDLESS OF THE FORM OF ACTION, WHETHER FOR BREACH OF CONTRACT, BREACH OF WARRANTY, TORT, NEGLIGENCE, INFRINGEMENT OR OTHERWISE (INCLUDING, WITHOUT LIMITATION, DAMAGES BASED ON LOSS OF PROFITS, DATA, FILES, USE, BUSINESS OPPORTUNITY OR CLAIMS OF THIRD PARTIES), AND
WHETHER OR NOT THE PARTY HAS BEEN ADVISED OF THE POSSIBILITY OF SUCH DAMAGES. THIS LIMITATION SHALL APPLY NOTWITHSTANDING ANY FAILURE OF ESSENTIAL PURPOSE OF ANY LIMITED REMEDY PROVIDED HEREIN.

8. Limitations

8. 1. ***BOOKS ONLY:***Where **'reuse in a dissertation/thesis'** has been selected the following terms apply: Print rights of the final author's accepted manuscript (for clarity, NOT the published version) for up to 100 copies, electronic rights for use only on a personal website or institutional repository as defined by the Sherpa guideline (www.sherpa.ac.uk/romeo/).

9. Termination and Cancellation

9. 1. Licences will expire after the period shown in Clause 3 (above).

9. 2. Licensee reserves the right to terminate the Licence in the event that payment is not received in full or if there has been a breach of this agreement by you.

Appendix 1 — Acknowledgements:

For Journal Content:
Reprinted by permission from [**the Licensor**]: [**Journal Publisher** (e.g. Nature/Springer/Palgrave)] [**JOURNAL NAME**] [**REFERENCE CITATION** (Article name, Author(s) Name), [**COPYRIGHT**] (year of publication)

For **Advance Online Publication papers:**
Reprinted by permission from [**the Licensor**]: [**Journal Publisher** (e.g. Nature/Springer/Palgrave)] [**JOURNAL NAME**] [**REFERENCE CITATION** (Article name, Author(s) Name), [**COPYRIGHT**] (year of publication), advance online publication, day month year (doi: 10.1038/sj.[JOURNAL ACRONYM].)

For Adaptations/Translations:
Adapted/Translated by permission from [**the Licensor**]: [**Journal Publisher** (e.g. Nature/Springer/Palgrave)] [**JOURNAL NAME**] [**REFERENCE CITATION** (Article name, Author(s) Name), [**COPYRIGHT**] (year of publication)

Note: For any republication from the British Journal of Cancer, the following credit line style applies:

Reprinted/adapted/translated by permission from [**the Licensor**]: on behalf of Cancer Research UK: : [**Journal Publisher** (e.g. Nature/Springer/Palgrave)] [**JOURNAL NAME**] [**REFERENCE CITATION** (Article name, Author(s) Name), [**COPYRIGHT**] (year of publication)

For **Advance Online Publication** papers:
Reprinted by permission from The [**the Licensor**]: on behalf of Cancer Research UK: [**Journal Publisher** (e.g. Nature/Springer/Palgrave)] [**JOURNAL NAME**] [**REFERENCE CITATION** (Article name, Author(s) Name), [**COPYRIGHT**] (year of publication), advance online publication, day month year (doi: 10.1038/sj.[JOURNAL ACRONYM])

For Book content:
Reprinted/adapted by permission from [**the Licensor**]: [**Book Publisher** (e.g. Palgrave Macmillan, Springer etc) [**Book Title**] by [**Book author**(s)] [**COPYRIGHT**] (year of publication)

Other Conditions:

Version 1.2

Questions? customercare@copyright.com or +1-855-239-3415 (toll free in the US) or +1-978-646-2777.

Figure 1.7: This figure was previously published and is used with permission from The American Physiological Society. Citation: Cooper, P. J., Lei, M., Cheng, L. X., and Kohl, P. (2000). Selected contribution: axial stretch increases spontaneous pacemaker activity in rabbit isolated sinoatrial node cells. *J. Appl. Physiol*. 89, 2099–104. doi:10.1152/jappl.2000.89.5.2099. Figure 1.

THE AMERICAN PHYSIOLOGICAL SOCIETY LICENSE
TERMS AND CONDITIONS

Oct 07, 2020

This Agreement between Eilidh MacDonald ("You") and The American Physiological Society ("The American Physiological Society") consists of your license details and the terms and conditions provided by The American Physiological Society and Copyright Clearance Center.

License Number	4798901460171
License date	Mar 30, 2020
Licensed Content Publisher	The American Physiological Society
Licensed Content Publication	Journal of Applied Physiology
Licensed Content Title	Selected Contribution: Axial stretch increases spontaneous pacemaker activity in rabbit isolated sinoatrial node cells
Licensed Content Author	Patricia J. Cooper, Ming Lei, Long-Xian Cheng, et al
Licensed Content Date	Nov 1, 2000
Licensed Content Volume	89
Licensed Content Issue	5
Type of Use	Thesis/Dissertation
Requestor type	non-profit academic/educational

Readers being charged a fee for this work	No
Format	print and electronic
Portion	figures/tables/images
Number of figures/tables/images	1
Will you be translating?	no
World Rights	no
Order reference number	
Title	PhD thesis
Institution name	Dalhousie University
Expected presentation date	Jun 2020
Portions	Figure 1
Requestor Location	Eilidh MacDonald 5850 College Street Halifax, NS B3H4H7 Canada Attn: Eilidh MacDonald
Billing Type	Invoice
Billing Address	Eilidh MacDonald 5850 College Street Halifax, NS B3H4H7

Canada
Attn: Eilidh MacDonald

Total 0.00 USD

Terms and Conditions

Terms and Conditions:

Figures/Tables/Images are available to the requestor from the APS journals website at http://www.the-aps.org/publications/journals/. The obtaining of content is a separate transaction and does not involve Rightslink or CCC, and is the responsibility of the permission seeker. Higher resolution images are available at additional charge from APS; please contact cvillemez@the-aps.org

Original Authors of Published Works: To see a full list of original authors rights concerning their own published work http://www.the-aps.org/publications/authorinfo/copyright.htm

Content reuse rights awarded by the APS may be exercised immediately upon issuance of this license, provided full disclosure and complete and accurate details of the proposed reuse have been made; no license is finally granted unless and until full payment is received either by the publisher or by CCC as provided in CCC's Billing and Payment Terms and Conditions. If full payment is not received on a timely basis, then any license preliminarily granted shall be deemed automatically revoked and shall be void as if never granted. Further, in the event that you breach any of these Terms and Conditions or any of CCC's Billing and Payment Terms and Conditions, the license is automatically revoked and shall be void as if never granted. Use of materials as described in a revoked license, as well as any use of the materials beyond the scope of the license, may constitute copyright infringement and the Publisher reserves the right to take action to protect its copyright of its materials.

The APS makes no representations or warranties with respect to the licensed material. You hereby indemnify and agree to hold harmless the publisher and CCC, and their respective officers, directors, employees and agents, from and against any and all claims arising out of your use of the licensed material other than as specifically authorized pursuant to this license.

This license is personal to you /your organization and may not be sublicensed, assigned, or transferred by you /your organization to another person /organization without the publisher's permission.This license may not be amended except in writing signed by both parties, or in the case of the publisher, by CCC on the publisher's behalf.

The APS reserves all rights not specifically granted in the combination of (i) the license details provided by you and accepted in the course of this licensing transaction, (ii) these Terms and Conditions and (iii) CCC's Billing and Payment Terms and Conditions.

v1.0

Questions? customercare@copyright.com or +1-855-239-3415 (toll free in the US) or +1-978-646-2777.

Figures 2.1 – 3.1: These figures were previously published and are used with permission from Elsevier. Citation: MacDonald, E. A., Stoyek, M. R., Rose, R. A., and Quinn, T. A. (2017). Intrinsic regulation of sinoatrial node function and the zebrafish as a model of stretch effects on pacemaking. *Prog. Biophys. Mol. Biol.* 130, 198–211. doi:10.1016/j.pbiomolbio.2017.07.012. Figures 1 – 9.

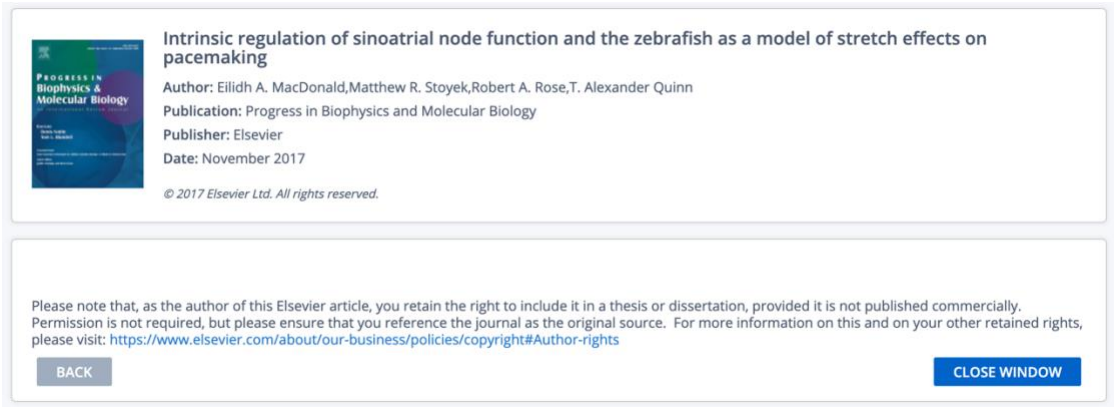

Figure 2.9: This figure was previously published and is used with permission from John Wiley and Sons. Citation: Cooper, P. J., and Kohl, P. (2005). Species- and preparation-dependence of stretch effects on sino-atrial node pacemaking. *Ann. N. Y. Acad. Sci*. 1047, 324–335. doi:10.1196/annals.1341.029. Figure 1.

JOHN WILEY AND SONS LICENSE
TERMS AND CONDITIONS

Mar 30, 2020

This Agreement between Eilidh MacDonald ("You") and John Wiley and Sons ("John Wiley and Sons") consists of your license details and the terms and conditions provided by John Wiley and Sons and Copyright Clearance Center.

License Number	4798731081298
License date	Mar 30, 2020
Licensed Content Publisher	John Wiley and Sons
Licensed Content Publication	Annals of the New York Academy of Sciences
Licensed Content Title	Species− and Preparation−Dependence of Stretch Effects on Sino−Atrial Node Pacemaking
Licensed Content Author	PETER KOHL, PATRICIA J. COOPER
Licensed Content Date	Jan 9, 2006
Licensed Content Volume	1047
Licensed Content Issue	1
Licensed Content Pages	12

Type of use	Dissertation/Thesis
Requestor type	University/Academic
Format	Print and electronic
Portion	Figure/table
Number of figures/tables	1
Will you be translating?	No
Title	PhD thesis
Institution name	Dalhousie University
Expected presentation date	Jun 2020
Portions	Figure 1
Requestor Location	Eilidh MacDonald 5850 College Street Halifax, NS B3H4H7 Canada Attn: Eilidh MacDonald
Publisher Tax ID	EU826007151
Total	0.00 USD

Terms and Conditions

TERMS AND CONDITIONS

This copyrighted material is owned by or exclusively licensed to John Wiley & Sons, Inc. or one of its group companies (each a"Wiley Company") or handled on behalf of a society with which a Wiley Company has exclusive publishing rights in relation to a particular work (collectively "WILEY"). By clicking "accept" in connection with completing this licensing transaction, you agree that the following terms and conditions apply to this transaction (along with the billing and payment terms and conditions established by the Copyright Clearance Center Inc., ("CCC's Billing and Payment terms and conditions"), at the time that you opened your RightsLink account (these are available at any time at http://myaccount.copyright.com).

Terms and Conditions

- The materials you have requested permission to reproduce or reuse (the "Wiley Materials") are protected by copyright.

- You are hereby granted a personal, non-exclusive, non-sub licensable (on a stand-alone basis), non-transferable, worldwide, limited license to reproduce the Wiley Materials for the purpose specified in the licensing process. This license, **and any CONTENT (PDF or image file) purchased as part of your order,** is for a one-time use only and limited to any maximum distribution number specified in the license. The first instance of republication or reuse granted by this license must be completed within two years of the date of the grant of this license (although copies prepared before the end date may be distributed thereafter). The Wiley Materials shall not be used in any other manner or for any other purpose, beyond what is granted in the license. Permission is granted subject to an appropriate acknowledgement given to the author, title of the material/book/journal and the publisher. You shall also duplicate the copyright notice that appears in the Wiley publication in your use of the Wiley Material. Permission is also granted on the understanding that nowhere in the text is a previously published source acknowledged for all or part of this Wiley Material. Any third party content is expressly excluded from this permission.

- With respect to the Wiley Materials, all rights are reserved. Except as expressly granted by the terms of the license, no part of the Wiley Materials may be copied, modified, adapted (except for minor reformatting required by the new Publication), translated, reproduced, transferred or distributed, in any form or by any means, and no derivative works may be made based on the Wiley Materials without the prior permission of the respective copyright owner.**For STM Signatory Publishers clearing permission under the terms of the STM Permissions Guidelines only, the terms of the license are extended to include subsequent editions and for editions in other languages, provided such editions are for the work as a whole in situ and does not involve the separate exploitation of the permitted figures or extracts,** You may not alter, remove or suppress in any manner any copyright, trademark or other notices displayed by the Wiley Materials. You may not license, rent, sell, loan, lease, pledge, offer as security, transfer or assign the Wiley Materials on a stand-alone basis, or any of the rights granted to you hereunder to any other person.

- The Wiley Materials and all of the intellectual property rights therein shall at all times remain the exclusive property of John Wiley & Sons Inc, the Wiley Companies, or their respective licensors, and your interest therein is only that of having possession of and the right to reproduce the Wiley Materials pursuant to Section 2 herein during the continuance of this Agreement. You agree that you own no right, title or interest in or to the Wiley Materials or any of the intellectual property rights therein. You shall have no rights hereunder other than the license as provided for above in Section 2. No right,

license or interest to any trademark, trade name, service mark or other branding ("Marks") of WILEY or its licensors is granted hereunder, and you agree that you shall not assert any such right, license or interest with respect thereto

- NEITHER WILEY NOR ITS LICENSORS MAKES ANY WARRANTY OR REPRESENTATION OF ANY KIND TO YOU OR ANY THIRD PARTY, EXPRESS, IMPLIED OR STATUTORY, WITH RESPECT TO THE MATERIALS OR THE ACCURACY OF ANY INFORMATION CONTAINED IN THE MATERIALS, INCLUDING, WITHOUT LIMITATION, ANY IMPLIED WARRANTY OF MERCHANTABILITY, ACCURACY, SATISFACTORY QUALITY, FITNESS FOR A PARTICULAR PURPOSE, USABILITY, INTEGRATION OR NON-INFRINGEMENT AND ALL SUCH WARRANTIES ARE HEREBY EXCLUDED BY WILEY AND ITS LICENSORS AND WAIVED BY YOU.

- WILEY shall have the right to terminate this Agreement immediately upon breach of this Agreement by you.

- You shall indemnify, defend and hold harmless WILEY, its Licensors and their respective directors, officers, agents and employees, from and against any actual or threatened claims, demands, causes of action or proceedings arising from any breach of this Agreement by you.

- IN NO EVENT SHALL WILEY OR ITS LICENSORS BE LIABLE TO YOU OR ANY OTHER PARTY OR ANY OTHER PERSON OR ENTITY FOR ANY SPECIAL, CONSEQUENTIAL, INCIDENTAL, INDIRECT, EXEMPLARY OR PUNITIVE DAMAGES, HOWEVER CAUSED, ARISING OUT OF OR IN CONNECTION WITH THE DOWNLOADING, PROVISIONING, VIEWING OR USE OF THE MATERIALS REGARDLESS OF THE FORM OF ACTION, WHETHER FOR BREACH OF CONTRACT, BREACH OF WARRANTY, TORT, NEGLIGENCE, INFRINGEMENT OR OTHERWISE (INCLUDING, WITHOUT LIMITATION, DAMAGES BASED ON LOSS OF PROFITS, DATA, FILES, USE, BUSINESS OPPORTUNITY OR CLAIMS OF THIRD PARTIES), AND WHETHER OR NOT THE PARTY HAS BEEN ADVISED OF THE POSSIBILITY OF SUCH DAMAGES. THIS LIMITATION SHALL APPLY NOTWITHSTANDING ANY FAILURE OF ESSENTIAL PURPOSE OF ANY LIMITED REMEDY PROVIDED HEREIN.

- Should any provision of this Agreement be held by a court of competent jurisdiction to be illegal, invalid, or unenforceable, that provision shall be deemed amended to achieve as nearly as possible the same economic effect as the original provision, and the legality, validity and enforceability of the remaining provisions of this Agreement shall not be affected or impaired thereby.

- The failure of either party to enforce any term or condition of this Agreement shall not constitute a waiver of either party's right to enforce each and every term and condition of this Agreement. No breach under this agreement shall be deemed waived or excused by either party unless such waiver or consent is in writing signed by the party granting such waiver or consent. The waiver by or consent of a party to a breach of any provision of this Agreement shall not operate or be construed as a waiver of or consent to any other or subsequent breach by such other party.

- This Agreement may not be assigned (including by operation of law or otherwise) by you without WILEY's prior written consent.

- Any fee required for this permission shall be non-refundable after thirty (30) days from receipt by the CCC.
- These terms and conditions together with CCC's Billing and Payment terms and conditions (which are incorporated herein) form the entire agreement between you and WILEY concerning this licensing transaction and (in the absence of fraud) supersedes all prior agreements and representations of the parties, oral or written. This Agreement may not be amended except in writing signed by both parties. This Agreement shall be binding upon and inure to the benefit of the parties' successors, legal representatives, and authorized assigns.
- In the event of any conflict between your obligations established by these terms and conditions and those established by CCC's Billing and Payment terms and conditions, these terms and conditions shall prevail.
- WILEY expressly reserves all rights not specifically granted in the combination of (i) the license details provided by you and accepted in the course of this licensing transaction, (ii) these terms and conditions and (iii) CCC's Billing and Payment terms and conditions.
- This Agreement will be void if the Type of Use, Format, Circulation, or Requestor Type was misrepresented during the licensing process.
- This Agreement shall be governed by and construed in accordance with the laws of the State of New York, USA, without regards to such state's conflict of law rules. Any legal action, suit or proceeding arising out of or relating to these Terms and Conditions or the breach thereof shall be instituted in a court of competent jurisdiction in New York County in the State of New York in the United States of America and each party hereby consents and submits to the personal jurisdiction of such court, waives any objection to venue in such court and consents to service of process by registered or certified mail, return receipt requested, at the last known address of such party.

WILEY OPEN ACCESS TERMS AND CONDITIONS

Wiley Publishes Open Access Articles in fully Open Access Journals and in Subscription journals offering Online Open. Although most of the fully Open Access journals publish open access articles under the terms of the Creative Commons Attribution (CC BY) License only, the subscription journals and a few of the Open Access Journals offer a choice of Creative Commons Licenses. The license type is clearly identified on the article.

The Creative Commons Attribution License

The Creative Commons Attribution License (CC-BY) allows users to copy, distribute and transmit an article, adapt the article and make commercial use of the article. The CC-BY license permits commercial and non-

Creative Commons Attribution Non-Commercial License

The Creative Commons Attribution Non-Commercial (CC-BY-NC)License permits use, distribution and reproduction in any medium, provided the original work is properly cited and is not used for commercial purposes.(see below)

Creative Commons Attribution-Non-Commercial-NoDerivs License

The Creative Commons Attribution Non-Commercial-NoDerivs License (CC-BY-NC-ND) permits use, distribution and reproduction in any medium, provided the original work is properly cited, is not used for commercial purposes and no modifications or adaptations are made. (see below)

Use by commercial "for-profit" organizations

Use of Wiley Open Access articles for commercial, promotional, or marketing purposes requires further explicit permission from Wiley and will be subject to a fee.

Further details can be found on Wiley Online Library
http://olabout.wiley.com/WileyCDA/Section/id-410895.html

Other Terms and Conditions:

v1.10 Last updated September 2015

Questions? customercare@copyright.com or +1-855-239-3415 (toll free in the US) or +1-978-646-2777.

Figure 3.2: This figure was previously published and is used with permission from Springer Nature and The American Physiological Society. Citations: Cooper, P. J., Lei, M., Cheng, L. X., and Kohl, P. (2000). Selected contribution: axial stretch increases spontaneous pacemaker activity in rabbit isolated sinoatrial node cells. J. Appl. Physiol. 89, 2099–104. doi:10.1152/jappl.2000.89.5.2099. Figure 3D.
Bruegmann, T., Malan, D., Hesse, M., Beiert, T., Fuegemann, C. J., Fleischmann, B. K., et al. (2010). Optogenetic control of heart muscle in vitro and in vivo. Nat. Methods. 7, 897–900. doi:10.1038/nmeth.1512. Figure 2D.

THE AMERICAN PHYSIOLOGICAL SOCIETY LICENSE
TERMS AND CONDITIONS

Apr 13, 2020

This Agreement between Eilidh MacDonald ("You") and The American Physiological Society ("The American Physiological Society") consists of your license details and the terms and conditions provided by The American Physiological Society and Copyright Clearance Center.

License Number	4807050918564
License date	Apr 13, 2020
Licensed Content Publisher	The American Physiological Society
Licensed Content Publication	Journal of Applied Physiology
Licensed Content Title	Selected Contribution: Axial stretch increases spontaneous pacemaker activity in rabbit isolated sinoatrial node cells
Licensed Content Author	Patricia J. Cooper, Ming Lei, Long-Xian Cheng, et al
Licensed Content Date	Nov 1, 2000
Licensed Content Volume	89
Licensed Content Issue	5
Type of Use	Thesis/Dissertation
Requestor type	non-profit academic/educational

Readers being charged a fee for this work	No
Format	print and electronic
Portion	figures/tables/images
Number of figures/tables/images	1
Will you be translating?	no
World Rights	no
Order reference number	
Title	PhD thesis
Institution name	Dalhousie University
Expected presentation date	Jun 2020
Portions	Figure 3d
Requestor Location	Eilidh MacDonald 5850 College Street Halifax, NS B3H4H7 Canada Attn: Eilidh MacDonald
Billing Type	Invoice
Billing Address	Eilidh MacDonald 5850 College Street Halifax, NS B3H4H7

Canada
Attn: Eilidh MacDonald

Total 0.00 USD

Terms and Conditions

Terms and Conditions:

Figures/Tables/Images are available to the requestor from the APS journals website at http://www.the-aps.org/publications/journals/. The obtaining of content is a separate transaction and does not involve Rightslink or CCC, and is the responsibility of the permission seeker. Higher resolution images are available at additional charge from APS; please contact cvillemez@the-aps.org

Original Authors of Published Works: To see a full list of original authors rights concerning their own published work http://www.the-aps.org/publications/authorinfo/copyright.htm

Content reuse rights awarded by the APS may be exercised immediately upon issuance of this license, provided full disclosure and complete and accurate details of the proposed reuse have been made; no license is finally granted unless and until full payment is received either by the publisher or by CCC as provided in CCC's Billing and Payment Terms and Conditions. If full payment is not received on a timely basis, then any license preliminarily granted shall be deemed automatically revoked and shall be void as if never granted. Further, in the event that you breach any of these Terms and Conditions or any of CCC's Billing and Payment Terms and Conditions, the license is automatically revoked and shall be void as if never granted. Use of materials as described in a revoked license, as well as any use of the materials beyond the scope of the license, may constitute copyright infringement and the Publisher reserves the right to take action to protect its copyright of its materials.

The APS makes no representations or warranties with respect to the licensed material. You hereby indemnify and agree to hold harmless the publisher and CCC, and their respective officers, directors, employees and agents, from and against any and all claims arising out of your use of the licensed material other than as specifically authorized pursuant to this license.

This license is personal to you /your organization and may not be sublicensed, assigned, or transferred by you /your organization to another person /organization without the publisher's permission.This license may not be amended except in writing signed by both parties, or in the case of the publisher, by CCC on the publisher's behalf.

The APS reserves all rights not specifically granted in the combination of (i) the license details provided by you and accepted in the course of this licensing transaction, (ii) these Terms and Conditions and (iii) CCC's Billing and Payment Terms and Conditions.

v1.0

Questions? customercare@copyright.com or +1-855-239-3415 (toll free in the US) or +1-978-646-2777.

SPRINGER NATURE LICENSE
TERMS AND CONDITIONS

Mar 30, 2020

This Agreement between Eilidh MacDonald ("You") and Springer Nature ("Springer Nature") consists of your license details and the terms and conditions provided by Springer Nature and Copyright Clearance Center.

License Number	4798880464378
License date	Mar 30, 2020
Licensed Content Publisher	Springer Nature
Licensed Content Publication	Nature Methods
Licensed Content Title	Optogenetic control of heart muscle in vitro and in vivo
Licensed Content Author	Tobias Bruegmann et al
Licensed Content Date	Oct 3, 2010
Type of Use	Thesis/Dissertation
Requestor type	non-commercial (non-profit)
Format	print and electronic
Portion	figures/tables/illustrations
Number of figures/tables/illustrations	1
High-res required	no

Will you be translating?	no
Circulation/distribution	1 - 29
Author of this Springer Nature content	no
Title	PhD thesis
Institution name	Dalhousie University
Expected presentation date	Jun 2020
Portions	Figure 2d
Requestor Location	Eilidh MacDonald 5850 College Street Halifax, NS B3H4H7 Canada Attn: Eilidh MacDonald
Total	0.00 USD

Terms and Conditions

Springer Nature Customer Service Centre GmbH
Terms and Conditions

This agreement sets out the terms and conditions of the licence (the **Licence**) between you and **Springer Nature Customer Service Centre GmbH** (the **Licensor**). By clicking 'accept' and completing the transaction for the material (**Licensed Material**), you also confirm your acceptance of these terms and conditions.

1. Grant of License

1. 1. The Licensor grants you a personal, non-exclusive, non-transferable, world-wide licence to reproduce the Licensed Material for the purpose specified in your order only. Licences are granted for the specific use requested in the order and for no other use, subject to the conditions below.

1. 2. The Licensor warrants that it has, to the best of its knowledge, the rights to license reuse of the Licensed Material. However, you should ensure that the material you are requesting is original to the Licensor and does not carry the copyright of another entity (as credited in the published version).

1. 3. If the credit line on any part of the material you have requested indicates that it was reprinted or adapted with permission from another source, then you should also seek permission from that source to reuse the material.

2. Scope of Licence

2. 1. You may only use the Licensed Content in the manner and to the extent permitted by these Ts&Cs and any applicable laws.

2. 2. A separate licence may be required for any additional use of the Licensed Material, e.g. where a licence has been purchased for print only use, separate permission must be obtained for electronic re-use. Similarly, a licence is only valid in the language selected and does not apply for editions in other languages unless additional translation rights have been granted separately in the licence. Any content owned by third parties are expressly excluded from the licence.

2. 3. Similarly, rights for additional components such as custom editions and derivatives require additional permission and may be subject to an additional fee. Please apply to Journalpermissions@springernature.com/bookpermissions@springernature.com for these rights.

2. 4. Where permission has been granted **free of charge** for material in print, permission may also be granted for any electronic version of that work, provided that the material is incidental to your work as a whole and that the electronic version is essentially equivalent to, or substitutes for, the print version.

2. 5. An alternative scope of licence may apply to signatories of the STM Permissions Guidelines, as amended from time to time.

3. Duration of Licence

3. 1. A licence for is valid from the date of purchase ('Licence Date') at the end of the relevant period in the below table:

Scope of Licence	Duration of Licence
Post on a website	12 months
Presentations	12 months
Books and journals	Lifetime of the edition in the language purchased

4. Acknowledgement

4. 1. The Licensor's permission must be acknowledged next to the Licenced Material in print. In electronic form, this acknowledgement must be visible at the same time as the figures/tables/illustrations or abstract, and must be hyperlinked to the journal/book's

homepage. Our required acknowledgement format is in the Appendix below.

5. Restrictions on use

5. 1. Use of the Licensed Material may be permitted for incidental promotional use and minor editing privileges e.g. minor adaptations of single figures, changes of format, colour and/or style where the adaptation is credited as set out in Appendix 1 below. Any other changes including but not limited to, cropping, adapting, omitting material that affect the meaning, intention or moral rights of the author are strictly prohibited.

5. 2. You must not use any Licensed Material as part of any design or trademark.

5. 3. Licensed Material may be used in Open Access Publications (OAP) before publication by Springer Nature, but any Licensed Material must be removed from OAP sites prior to final publication.

6. Ownership of Rights

6. 1. Licensed Material remains the property of either Licensor or the relevant third party and any rights not explicitly granted herein are expressly reserved.

7. Warranty

IN NO EVENT SHALL LICENSOR BE LIABLE TO YOU OR ANY OTHER PARTY OR ANY OTHER PERSON OR FOR ANY SPECIAL, CONSEQUENTIAL, INCIDENTAL OR INDIRECT DAMAGES, HOWEVER CAUSED, ARISING OUT OF OR IN CONNECTION WITH THE DOWNLOADING, VIEWING OR USE OF THE MATERIALS REGARDLESS OF THE FORM OF ACTION, WHETHER FOR BREACH OF CONTRACT, BREACH OF WARRANTY, TORT, NEGLIGENCE, INFRINGEMENT OR OTHERWISE (INCLUDING, WITHOUT LIMITATION, DAMAGES BASED ON LOSS OF PROFITS, DATA, FILES, USE, BUSINESS OPPORTUNITY OR CLAIMS OF THIRD PARTIES), AND
WHETHER OR NOT THE PARTY HAS BEEN ADVISED OF THE POSSIBILITY OF SUCH DAMAGES. THIS LIMITATION SHALL APPLY NOTWITHSTANDING ANY FAILURE OF ESSENTIAL PURPOSE OF ANY LIMITED REMEDY PROVIDED HEREIN.

8. Limitations

8. 1. ***BOOKS ONLY:*** Where **'reuse in a dissertation/thesis'** has been selected the following terms apply: Print rights of the final author's accepted manuscript (for clarity, NOT the published version) for up to 100 copies, electronic rights for use only on a personal website or institutional repository as defined by the Sherpa guideline (www.sherpa.ac.uk/romeo/).

9. Termination and Cancellation

9. 1. Licences will expire after the period shown in Clause 3 (above).

9. 2. Licensee reserves the right to terminate the Licence in the event that payment is not received in full or if there has been a breach of this agreement by you.

Appendix 1 — Acknowledgements:

For Journal Content:
Reprinted by permission from [**the Licensor**]: [**Journal Publisher** (e.g. Nature/Springer/Palgrave)] [**JOURNAL NAME**] [**REFERENCE CITATION** (Article name, Author(s) Name), [**COPYRIGHT**] (year of publication)

For **Advance Online Publication papers:**
Reprinted by permission from [**the Licensor**]: [**Journal Publisher** (e.g. Nature/Springer/Palgrave)] [**JOURNAL NAME**] [**REFERENCE CITATION** (Article name, Author(s) Name), [**COPYRIGHT**] (year of publication), advance online publication, day month year (doi: 10.1038/sj.[JOURNAL ACRONYM].)

For Adaptations/Translations:
Adapted/Translated by permission from [**the Licensor**]: [**Journal Publisher** (e.g. Nature/Springer/Palgrave)] [**JOURNAL NAME**] [**REFERENCE CITATION** (Article name, Author(s) Name), [**COPYRIGHT**] (year of publication)

Note: For any republication from the British Journal of Cancer, the following credit line style applies:

Reprinted/adapted/translated by permission from [**the Licensor**]: on behalf of Cancer Research UK: : [**Journal Publisher** (e.g. Nature/Springer/Palgrave)] [**JOURNAL NAME**] [**REFERENCE CITATION** (Article name, Author(s) Name), [**COPYRIGHT**] (year of publication)

For **Advance Online Publication** papers:
Reprinted by permission from The [**the Licensor**]: on behalf of Cancer Research UK: [**Journal Publisher** (e.g. Nature/Springer/Palgrave)] [**JOURNAL NAME**] [**REFERENCE CITATION** (Article name, Author(s) Name), [**COPYRIGHT**] (year of publication), advance online publication, day month year (doi: 10.1038/sj.[JOURNAL ACRONYM])

For Book content:
Reprinted/adapted by permission from [**the Licensor**]: [**Book Publisher** (e.g. Palgrave Macmillan, Springer etc) [**Book Title**] by [**Book author**(s)] [**COPYRIGHT**] (year of publication)

Other Conditions:

Version 1.2

Figures 3.21, 4.2, 4.6 – 4.14: These figures were previously published and are used under the terms of the Creative Commons Attribution License (CC BY). Citation: MacDonald, E. A., Madl, J., Greiner, J., Ramadan, A. F., Wells, S. M., Torrente, A. G., et al. (2020a). Sinoatrial Node Structure, Mechanics, Electrophysiology and the Chronotropic Response to Stretch in Rabbit and Mouse. Front. Physiol. 11, 1–15. doi:10.3389/fphys.2020.00809.. Figures 1 – 4.

Figure 5.1: This figure was previously published and is used with permission from The American Physiological Society. Citation: Lange, G., Lu, H. H., Chang, A., and Brooks, C. M. (1966). Effect of stretch on the isolated cat sinoatrial node. *Am. J. Physiol*. 211, 1192–1196. doi:10.1152/ajplegacy.1966.211.5.1192. Figure 5.

THE AMERICAN PHYSIOLOGICAL SOCIETY LICENSE
TERMS AND CONDITIONS

Apr 13, 2020

This Agreement between Eilidh MacDonald ("You") and The American Physiological Society ("The American Physiological Society") consists of your license details and the terms and conditions provided by The American Physiological Society and Copyright Clearance Center.

License Number	4807070167889
License date	Apr 13, 2020
Licensed Content Publisher	The American Physiological Society
Licensed Content Publication	American Journal of Physiology, Consolidated
Licensed Content Title	Effect of stretch on the isolated cat sinoatrial node
Licensed Content Author	G Lange, HH Lu, A Chang, et al
Licensed Content Date	Nov 1, 1966
Licensed Content Volume	211
Licensed Content Issue	5
Type of Use	Thesis/Dissertation
Requestor type	non-profit academic/educational
Readers being charged a fee for this work	No
Format	print and electronic

Portion	figures/tables/images
Number of figures/tables/images	1
Will you be translating?	no
World Rights	no
Order reference number	
Title	PhD thesis
Institution name	Dalhousie University
Expected presentation date	Jun 2020
Portions	Figure 5
Requestor Location	Eilidh MacDonald 5850 College Street Halifax, NS B3H4H7 Canada Attn: Eilidh MacDonald
Billing Type	Invoice
Billing Address	Eilidh MacDonald 5850 College Street Halifax, NS B3H4H7 Canada Attn: Eilidh MacDonald
Total	0.00 USD
Terms and Conditions	

Terms and Conditions:

have been made; no license is finally granted unless and until full payment is received either by the publisher or by CCC as provided in CCC's Billing and Payment Terms and Conditions. If full payment is not received on a timely basis, then any license preliminarily granted shall be deemed automatically revoked and shall be void as if never granted. Further, in the event that you breach any of these Terms and Conditions or any of CCC's Billing and Payment Terms and Conditions, the license is automatically revoked and shall be void as if never granted. Use of materials as described in a revoked license, as well as any use of the materials beyond the scope of the license, may constitute copyright infringement and the Publisher reserves the right to take action to protect its copyright of its materials.

The APS makes no representations or warranties with respect to the licensed material. You hereby indemnify and agree to hold harmless the publisher and CCC, and their respective officers, directors, employees and agents, from and against any and all claims arising out of your use of the licensed material other than as specifically authorized pursuant to this license.

This license is personal to you /your organization and may not be sublicensed, assigned, or transferred by you /your organization to another person /organization without the publisher's permission.This license may not be amended except in writing signed by both parties, or in the case of the publisher, by CCC on the publisher's behalf.

The APS reserves all rights not specifically granted in the combination of (i) the license details provided by you and accepted in the course of this licensing transaction, (ii) these Terms and Conditions and (iii) CCC's Billing and Payment Terms and Conditions.

v1.0

Questions? customercare@copyright.com or +1-855-239-3415 (toll free in the US) or +1-978-646-2777.